THE UNIVERSITY
OF BIRMINGHAM

Membrane Emulsification to Produce Perfume Microcapsules

By

Xuemiao Pan

A thesis submitted to

The University of Birmingham

For the Degree of

DOCTOR OF PHILOSOPHY

School of Chemical Engineering

The University of Birmingham

United Kingdom

July 2013

Abstract

Microencapsulation is an efficient technology to deliver perfume oils from consumer products onto the surface of fabrics. The work presented in this thesis aims to prepare perfume microcapsules with different shell and core materials using membrane emulsification to achieve uniform microcapsule size/mechanical strength, which may provide better end-use performance than those currently produced in industry. Membrane emulsification in a dispersion cell followed by *in-situ* polymerization was used to prepare melamine-formaldehyde (MF) microcapsules with narrow size distribution, which contained several types of oil-based fragrances or ingredients. Investigated in this study are the parameters impacting on the size and size distribution of the droplets and final MF microcapsules, and the optimum conditions to produce the microcapsules with narrowest size distribution have been identifies. A pilot plant-scale cross-flow membrane system was also used to produce MF microcapsules, demonstrating that the membrane emulsification process has potential to be scaled up for industrial applications. The mechanical strength of the formed MF microcapsules was measured using a micromanipulation technique. It has been found that microcapsules with narrower size distribution also had narrower distribution in mechanical strength parameters.

Moreover, user- and environmentally- friendly poly (methyl methacrylate) (PMMA) microcapsules with narrow size distribution were prepared for the first time using the dispersion cell membrane emulsification system.

Several newly developed techniques have been applied to PMMA microcapsules, in order to determine their various properties. Confocal laser scanning microscopy (CLSM) was used to determine the shell thickness of PMMA microcapsules labelled with a fluorescence dye instead of transmission electron microscopy (TEM). Characterization methods previously used for thin-shell MF microcapsules were expanded to analyse PMMA microcapsules with thick shells. The intrinsic mechanical properties of PMMA with thick shells were determined using a micromanipulation technique and finite element analysis (FEM). The structure of MF and PMMA microcapsules was also characterised in the determination of the permeability and diffusivity of the perfume oils in the shell of microcapsules.

Acknowledgements

I will begin by thanking my supervisors, Prof. Zhibing Zhang, Prof. Jon Preece and Prof. David York, for their excellent supervision, and the past and present members of Micromanipulation Group for their support throughout these years. Their experience and help have been important for my research and they have always been ready to help me when I needed. .

A special thank goes to Dr Theresa Morris, Dr James Bowen and Dr Paul Young for their technical support on using technical equipment; thanks also go to Dr Stephen Collins (University of Leeds) for his support to run the cross-flow membrane system experiment; I also acknowledge Prof. H. Chen (Department of Chemical and Materials Engineering, National Central University, Jhongli City, Taiwan), Dr Raul Rodrigo Gomez (Procter & Gamble, Brussels) and Dr Y. Long (Chinese Academy of Sciences, Beijing) for technical discussions; I am very grateful to Dr. Johan Smets, Ms Susana Fernandez Prieto, Dr Carols Amador from Procter & Gamble for their support on this project; I am very grateful to all the people from inprotec Germany; I would like to convey my deepest thanks to all the people in the Department of Chemical Engineering.

I would like to thank School of Chemical Engineering, University of Birmingham for administrative support and providing laboratory facilities, as well as China Scholarship Council and Procter and Gamble for the financial support.

I would like to mention my family and friends in China and Spain, because they were distant only in geographical terms, and they were all by my side, throughout my troubles and glory; I would like to thank all my friends in Birmingham because life is more than engineering and they were always ready for supporting me!

Last but not least, I would like to thank Prof. Ruben Mercadé Prieto not only for his support to my PhD study but also for his encourage and motivation. I couldn't have done it without him.

Table of Contents

Abstract.....I

Acknowledgements.....III

Table of Contents.....V

List of Figures.....XIV

List of Tables.....XXVI

Nomenclature.....XXVIII

Greek Symbol.....XXXIV

Abbreviations.....XXXVI

List of Publications.....XXXVIII

Chapter 1 Introduction 1

Chapter 2 Literature work.....7

2.1 Introduction.....7

2.2 Microencapsulation 8

2.2.1 Introduction.....8

2.2.2 Perfumes used in detergents.....9

2.2.3 Perfume microcapsules….....11

2.3 Emulsification.....16

2.3.1 Emulsion and emulsion stability.....16

2.3.2 Emulsification methods.....17

2.3.2.1 Homogenization.....17

2.3.2.2 Other emulsification methods.....19

2.3.3 Membrane emulsification.....21

2.3.3.1 Introduction of membrane emulsification.....21

2.3.3.2 Flat membrane combined with a stirrer system (Dispersion cell) ...23

2.3.4 Theoretical models to describe droplet formation at the membrane surface.....25

2.4 Encapsulation techniques.....34

2.4.1 Chemical processes.....34

2.4.2 Physico-chemical processes.....37

2.4.3 Mechanical processes.....37

2.5 Shell materials.....38

2.5.1 Melamine formaldehyde.....38

2.5.1.1 Chemical structure of melamine-formaldehyde precondensate.....39

2.5.1.2 Application of melamine-formaldehyde microcapsules.....42

2.5.1.3 Limitation of melamine-formaldehyde.....47

2.5.1.4 Poly (methyl methacrylate) (PMMA) 49

2.6 Characterization of microcapsules.....53

2.6.1 Characterisation of size and size distribution.....54

2.6.2 Measurement of the mechanical strength of single microcapsules.....57

2.6.2.1 Control of microcapsule size and strength distribution.....61

2.6.3 Release test and shell permeability.....64

2.6.4 Morphology, microstructure and shell thickness 72

2.7 Conclusions.....74

Chapter 3 Materials and experimental techniques.....77

3.1 Introduction.....77

3.2 Materials.....78

3.2.1 Materials used to prepare melamine formaldehyde (MF) Microcapsule….....78

3.2.2 Materials used to prepare poly (methyl methacrylate) (PMMA) microcapsules.....79

3.3 Technique to prepare microcapsules.....79

3.3.1 Dispersion cell system.....79

3.3.1.1 Cell system.....79

3.3.1.2 The membrane.....82

3.3.2 Cross flow membrane system 86

3.3.2.1 Cross flow membrane system 86

3.3.2.2 Membrane Tube.....90

3.4 Technique to characterise microcapsules.....92

3.4.1 Malvern size analyzer - laser diffraction 92

3.4.1.1 Typical data generated 95

3.4.2 Micromanipulation technique.....97

3.4.2.1 Typical data generated 101

3.4.3 Ultraviolet-Visible spectrophotometery (UV-Vis) 104

3.4.3.1 Typical data generated 106

3.4.4 Environmental scanning electron microscopy (ESEM) 107

3.4.4.1 Typical ESEM image.....109

3.4.5 Transmission electron microscopy (TEM).....110

3.4.5.1 Typical TEM image….....111

3.4.6 Confocal laser scanning microscopy (CLSM) 112

3.4.6.1 Typical CLSM image.....114

3.4.7 Contact angle measurement device.....114

3.4.8 Tensiometer.....115

3.4.8.1 Typical data generated 118

3.4.9 Rheometer.....119

3.4.9.1 Typical data obtained.....120

Chapter 4 Size and Strength Distributions of Melamine-formaldehyde Microcapsules Prepared by Membrane Emulsification.....121

4.1 Introduction.....121

4.2 Experimental section.....122

4.2.1 Preparation of microcapsules.....122

4.2.1.1 Preparation of microcapsules using membrane emulsification.....122

4.2.1.2 Preparation of microcapsules using conventional homogenization……123

4.2.1.3 Preparation of microcapsules with fluorescent dye.....124

4.2.2 Morphology and shell thickness of microcapsule.....124

4.2.3 Size analysis.....125

4.2.4 Measurement of the mechanical strength of single microcapsules.....126

4.3 Results and discussion.....127

4.3.1 The effect of membrane surface hydrophilicity on the mean size and size distribution of oil droplets.....127

4.3.2 Stability of the oil/water emulsion.....132

4.3.3 Effects of process conditions on the mean size and size distribution of

oil droplets.....134

4.3.4 Effects of reaction temperature on the mean size and size distribution of microcapsules.....139

4.3.5 Morphology.....140

4.3.6 Shell thickness.....142

4.3.7 Size analysis of microcapsules.....145

4.3.8 Mechanical properties of microcapsules 147

4.4 Conclusions.....153

Chapter 5 Scale-up of Membrane Emulsification to Prepare Melamine-formaldehyde Microcapsules and Microencapsulation of Different Oils……...154

5.1 Introduction.....154

5.2 Experimental methods.....155

5.2.1 Scale up experiment with cross-flow membrane emulsification.....155

5.2.2 Preparation of microcapsules with different core oils using a dispersion cell.....157

5.2.3 Characterization of MF microcapsules.....157

5.3 Results and discussion.....160

5.3.1 Cross-flow membrane system.....160

5.3.1.1 Stability of the oil/water emulsion.....160

5.3.1.2 Effect of the processing conditions on the mean size and size distribution of oil droplets.....162

5.3.2 Preparation of MF microcapsules with different core oils using a dispersion cell.....166

5.3.2.1 The effect of membrane configurations on the size distribution of

droplets in emulsion.....167

5.3.2.2 Effect of the two phases physical properties on the size distribution of droplets of different oils.....168

5.3.2.3 The effects of processing conditions on size distribution of droplets with different oils. 172

5.3.2.3.1 Impeller agitation speed.....172

5.3.2.3.2 Dispersed phase flux.....175

5.3.3 Morphology of emulsion droplets and microcapsules.....179

5.3.4 Shell thickness of MF microcapsules 182

5.4 Conclusions.....185

Chapter 6 Structure and Mechanical Properties of Consumer-friendly PMMA Microcapsules.....186

6.1 Introduction.....186

6.2 Experimental section.....188

6.2.1 Preparation of microcapsules.....188

6.2.1.1 Preparation of PMMA precondensate.....188

6.2.1.2 Preparation of emulsion using conventional homogenization…...188

6.2.1.3 Preparation of double emulsions using the dispersion cell.....189

6.2.1.4 Preparation of PMMA microcapsules.....189

6.2.2 Morphology and shell thickness of microcapsules.....189

6.2.2.1 Morphology.....189

6.2.2.2 Determination shell thickness of microcapsules.....190

6.2.2.3 Shell thickness and radius corrections from CSLM measurements……...191

6.2.3 Size analysis.....193

6.2.4 Determination of the mechanical properties of PMMA microcapsules.....194
6.3 Results and discussion.....195
6.3.1 Stability of the oil/water emulsion.....195
6.3.2 Size and size distribution of oil droplets and microcapsules.....197
6.3.3 Morphology.....200
6.3.4 Determination of the shell thickness using CLSM.....201
6.3.5 Experimental determination of the mechanical properties of PMMA microcapsules.....205
6.3.5.1 Fractional deformation at the elastic limit ε_{LE}.....212
6.3.5.2 Elastic modulus E.....218
6.3.5.3 Failure force F_{LE}.....221
6.3.5.4 Failure stresses σp.....223
6.3.5.5 Weibull distribution analysis for failure stress.....227
6.4 Conclusion.....232

Chapter 7 Determination of Perfume Release Rate and the Shell Permeability of Microcapsules.....234

7.1 Introduction.....234
7.2 Experimental methods.....236
7.2.1 Formation of MF and PMMA microcapsules.....236
7.2.2 Perfume oil calibration using UV-Vis spectrophotometry.....237
7.2.3 Solubility Measurements.....238
7.2.4 Encapsulation efficiency measurement.....239
7.2.5 Continuous release experiment.....240
7.2.6 Perfume solubility in PMMA microspheres.....242

7.3 Release models for spherical microcapsules.....244

7.3.1 Oil release from a thin-shell microcapsule.....244

7.3.2 Oil release from a homogenous microsphere.....245

7.3.3 Oil release from a thick shell microcapsule.....247

7.4 Results and discussion.....248

7.4.1 Co-solvent selection and solubility measurements.....248

7.4.2 Encapsulation efficiency.....253

7.4.3 Determination of permeability of thin shell microcapsules from release data.....255

7.4.4 Oil release from full microspheres.....262

7.4.5 Oil release from a thick shell microcapsule.....264

7.5 Conclusions.....268

Chapter 8 Overall Conclusions and Future Plan.....270

8.1 Overall Conclusions.....270

8.1.1 Membrane emulsification process 275

8.1.2 Preparation of PMMA microcapsules.....276

8.1.3 Novel methodology development 276

8.1.3.1 Determination of shell thickness using CLSM.....276

8.1.3.2 Investigation of intrinsic mechanical properties of microcapsules with different shell thickness.....277

8.1.3.3 Investigation of intrinsic mass transfer parameters of microcapsules shell with different shell material and thickness.....278

8.2 Future work.....279

Appendix A.....283

Finite Element Modelling (FEM) of the compression of thick shell microcapsules

Appendix B.....294

MATLAB code for calculating shell permeability of PMMA microcapsules

References.....311

List of Figures

Figure 2-1. Environmental factors that can cause perfume loss during manufacturing and storage.....10

Figure 2-2 (a) SEM and (b) TEM image of core/shell perfume oil microcapsules with a melamine -formaldehyde shell…….....12

Figure 2-3 Schematic graph of basic steps of microencapsulation process.....13

Figure 2-4. Release of perfumery ingredient Doremox® in (a) free form and (b) encapsulated form in a fabric softener.....15

Figure 2-5 Different mechanisms that induce emulsion instability.....17

Figure 2-6 Schematic graph and picture of a rotor-stator high shear homogenizer.....18

Figure 2-7 Schematic illustration of dispersion cell, which has a two-blade paddle impeller above a membrane with pores.....24

Figure 2-8 Schematic of a droplet formation.....26

Figure 2-9 Schematic microencapsulation process based on *in situ* polymerization...35

Figure 2-10 The schematic diagram showing an *in situ* MF polymerization process to encapsulate a perfume oil.....36

Figure 2-11 Chemical structures of melamine and formaldehyde.....40

Figure 2-12 Schematic representation of classical MF precondensate products from the condensation of MF reaction with different M/F ratios.....41

Figure 2-13 Mechanism of polymerization to form melamine formaldehyde resin in acid condition.....42

Figure 2-14 Mechanism of MMA free radical polymerization.....52

Figure 2-15 A typical schematic diagram of the mechanical measurement using micromanipulation rig.....59

Figure 2-16 The relationship between the rupture force and diameter for microcapsules.....61

Figure 2-17 Examples of perfume microcapsules applied in papers.....63

Figure 2-18 Release experiments for perfume microcapsules.....65

Figure 2-19 A schematic diagram of encapsulated perfume oil release through MF shell.....68

Figure 2-20 Typical release curve from thin-shell microcapsules.....69

Figure 2-21 Example of the use of CLSM for the observation of the microcapsules shell cross section.....73

Figure 3-1 Illustration of the dispersion cell system.....80

Figure 3-2 The set-up diagram of membrane emulsification process.....81

Figure 3-3 Agitation speed of the stirrer in continuous phase vs voltage of the DC motor driving the paddle stirrer.....82

Figure 3-4 The schematic diagrams and the SEM micrographs of representative flat membrane used.....83

Figure 3-5 Pilot plant-scale cross-flow membrane apparatus (from the rear).....87

Figure 3-6 Front view of the control panel.....88

Figure 3-7 Disperse phase tank lid showing the gas pressure dial (12) and gas release valve (13), enlargement of (1) in Figure 3-5.....89

Figure 3-8 Schematic diagram showing emulsification of oil in water in the membrane system.....89

Figure 3-9 Photo showing the cross-section of the membrane tube with seven star-shaped channels…….....90

Figure 3-10 SEM images of the substrate material of 0.2 μm cross-flow membrane tube…….....91

Figure 3-11 SEM images of the cross-flow membrane tube channel from inside. The rough porous inside surface of the channel, has pores with the average size of 0.2μm…….....92

Figure 3-12 Schematic diagram of laser light rays interacting with a solid particle....94

Figure 3-13 Schematic diagram of laser light rays interacting with particles of different sizes.....94

Figure 3-14 Schematic representation of laser diffraction instrument.....95

Figure 3-15 A typical size distribution curve of MF microcapsules obtained from laser diffraction measurement.....96

Figure 3-16 Schematic diagram of the micromanipulation rig.....99

Figure 3-17 Photographs of a micromanipulation rig to compress single microcapsules……..100

Figure 3-18 Typical curve of compressing a single microcapsule.....103

Figure 3-19 Example to calculate the extinction coefficients using calibration plats.....105

Figure 3-20 A typical curve showing perfume oil released from MF microcapsules in

60% v/v glycerol obtained using the UV-Vis spectrophotometry.....107

Figure 3-21 Schematic representation of environmental scanning electron microscopy (ESEM).....108

Figure 3-22 Schematic representation of the environmental secondary detector with gas.....109

Figure 3-23 A typical image of MF microcapsules obtained by ESEM in wet mode at an accelerating voltage of 10.0 kV.....110

Figure 3-24 A TEM image of the cross section of MF microcapsules.....112

Figure 3-25 Schematic representation of confocal laser scanning microscopy (CLSM).....113

Figure 3-26 A CLSM micro-image of the cross-section of PMMA microcapsules...114

Figure 3-27 Schematic diagram of the device for measuring the contact angle.....115

Figure 3-28 Photography of the tensiometer K100 used in this study.....116

Figure 3-29 Schematic of the Wilhelmy plate method applied to an interface of two liquid phases.....117

Figure 3-30 A interfacial tension versus time curve obtained through a Tensiometer.....118

Figure 3-31 Photo of the rheometer AR1000 used in this study.....119

Figure 3-32 Viscosity of peppermint oil tested with the rheometer.....120

Figure 4-1 Schematic diagram of preparing MF microcapsules using a flat membrane combined with a stirred system.....123

Figure 4-2. Effect of concentration of the wetting agent on (a) the size distribution of

the droplets in the emulsion and (b) the size of the droplets in the emulsion and contact angle of water on membrane surface, prepared using an agitation speed of 1080 rpm, dispersed phase flux of 1.6×10^{-5} m s^{-1}, and a membrane "15 rcia A".....129

Figure 4-3. Size distribution of droplets in emulsions generated by different membrane materials.....131

Figure 4-4. The (a) mean diameter ($D_{4,3}$) and (b) *CV and SPAN* values of the oil emulsions measured at different times after their formation at 25°C. Emulsions were prepared using an agitation speed of 1080 rpm, dispersed phase flux of 1.6×10^{-5} m s^{-1} and a "15rcia A" membrane.....133

Figure 4-5. The effect of agitation speed in the dispersion cell on the (a) size and (b) size distribution of the droplets in emulsion, prepared with a dispersed phase flux of 1.6×10^{-5} m s^{-1}, and "15 rcia A" membrane. Some of the error bars are smaller than the symbols used.…….....135

Figure 4-6. The influence of the flux of the dispersed phase pumped through the membrane on (a) the size and (b) size distribution of the droplets in emulsion prepared using an agitation speed of 1080 rpm and a membrane "15 rcia A".…….....137

Figure 4-7. Size distributions of the emulsion droplets and the formed microcapsules, prepared by membrane emulsification using an agitation speed of 1080 rpm, dispersed phase flux of 1.6×10^{-5} m s^{-1} and a membrane "15 rcia A".....138

Figure 4-8. Size distribution of the microcapsules prepared at different temperature by membrane emulsification (with an agitation speed of 1080 rpm, dispersed phase flux of 1.6×10^{-5} m s^{-1} and a "15rcia A" membrane).……140

Figure 4-9. Micrographs of the microcapsules obtained using (a) optical microscopy, (b) and (c) ESEM.…….……..…141

Figure 4-10. TEM micrographs of microcapsules prepared using the membrane emulsification and homogenization methods.……....143

Figure 4-11. CLSM micrographs of microcapsules prepared using the membrane emulsification and homogenization methods.……...….144

Figure 4-12. Size distribution of the microcapsules prepared by two different methods: homogenization (at 600 rpm) and membrane emulsification (with an agitation speed of 1080 rpm, dispersed phase flux of 1.6×10^{-5} m s^{-1} , a "15 rcia A" membrane wetted with an agent concentration of 0.5% (v/v)).……...145

Figure 4-13. Double logarithmic representation of the effect of the agitation speed on $D_{3,2}$ for MF microcapsules prepared using homogenization.…….146

Figure 4-14. Typical profiles of force divided by diameter of microcapsules versus fractional deformation at rupture ε_B.……..…….147

Figure 4-15. Strength parameter distributions of the microcapsules prepared by two different methods.……...…151

Figure 5-1 The (a) mean diameter ($D_{4,3}$) and (b) size distribution (*CV* and *SPAN* values) of the oil droplets measured at different storage times without agitation at room temperature.…….….161

Figure 5-2 The effect of oil pressure on the (a) size and (b) size distribution of the emulsions droplets, prepared with a circulation flow rate of 1.1×10^{-4} $m^3\cdot s^{-1}$ and a dispersed phase pressure of 0.3×10^5Pa.……163

Figure 5-3 Size distribution of the emulsion droplets and the formed MF microcapsules, prepared using a circulation flow rate of 1.1×10^{-4} m^3 s^{-1} and an oil pressure of 0.3×10^5Pa.……...…….164

Figure 5-4. Size distributions of microcapsules prepared by three different methods: lab- scale membrane emulsification (with an agitation speed of 1080 rpm and dispersed phase flux of 1.6×10^{-5} m s^{-1}), pilot plant-scale membrane emulsification (using a flow rate of 1.1×10^{-4} m^3 s^{-1} and oil pressure of 0.3×10^5Pa) and lab-scale homogenization (600 rpm).…….…….165

Figure 5-5. Size distributions of droplets in the emulsions generated using membranes with different pore locations. "15 rcia A" (square) and "15 cia" (circle).…….…..168

Figure 5-6. Experimental measurements and theoretical predictions of droplets sizes in the emulsions with varying physical properties.……171

Figure 5-7. The model predictions and experimental measurements of droplet size in the emulsions versus agitation speed in the dispersion cell.……..…174

Figure 5-8 The effect of agitation speed in the dispersion cell on size distribution of droplets of different oils in emulsions.……...……175

Figure 5-9 The influence of the flux of the dispersed phase pumped through the membrane on the (a) size and (b) size distribution of the droplets in emulsion.…...178

Figure. 5-10. Images of the oil droplets in emulsion and microcapsules obtained by

optical microscopy.……180

Figure. 5-11. Micrographs of MF microcapsules with different core oils obtained by ESEM..……..181

Figure. 5-12. Typical TEM micro-images of MF microcapsules with different core oils prepared using the dispersion cell.……..184

Figure 6-1. Schematic diagram of a cross section measurement plane at a distance αr from the equatorial plane.……192

Figure 6-2. Correction factor of the measured shell thickness ratio from simulations with different maximum measurement planes away from the equator, parameter α as described in Figure 6-1..……193

Figure 6-3 The mean diameter ($D_{4,3}$) and *CV* values of the oil droplets measured at different times after their formation, which were prepared by membrane emulsification using an agitation speed of 1080rpm and dispersed phase flux of 1.6×10^{-5} m s^{-1}……..……...……196

Figure 6-4. Effect of the process parameters: agitation speed (diamonds) and dispersed phase flux (squares) on the mean size and the size distribution of the resultant emulsion droplets.……..197

Figure 6-5. Size distributions of the emulsion droplets and microcapsules with reaction time 4 h, prepared by two different methods: membrane emulsification (with an agitation speed of 1080 rpm and dispersed phase flux of 1.6×10-5 m s-1) and homogenization (800 rpm).……...…….198

Figure 6-6. Micrographs of PMMA microcapsules with reaction time 4 h, obtained using (a) optical microscopy and (b-c) ESEM.……....….200

Figure 6-7. CLSM micrographs of oil droplets and PMMA microcapsules at different stages of polymerization.……..……..…202

Figure 6-8. CLSM micrograph (inset) and fluorescence intensity profiles of a microcapsule (52 μm) measured at four different directions.……....203

Figure 6-9. Shell thickness h measured with CSLM for microcapsules larger than 40 μm prepared by membrane emulsification (empty points) and homogenization (filled points), after a reaction time of 1 h (circles) and 4 h (triangles).……..….205

Figure 6-10. Typical normalized compression force profiles of 1 h, 4 h and 24 h PMMA microcapsules, together with that of a MF microcapsule…….208

Figure 6-11. Force versus $\varepsilon_m^{1.5}$ data for compression of a PMMA capsule (47 μm in diameter) formed after a reaction time of 24 h. The straight line in red represents the fitting by Hertz model. The Young's modulus value estimated by Hertz model is 423 MPa.…….209

Figure 6-12. Experimental compression results of single PMMA microcapsules made of different reaction time and simulation profiles of the initial elastic regime.…….211

Figure 6-13. Fractional deformation at the elastic limit ε_{LE} of individual microcapsules larger than 40 μm prepared by both emulsification methods, which were determined using two different models: 1 h (thin-shell model : triangles), 4 h (linear model: filled diamonds and power law model: empty diamonds) and 24 h (power law model: circles) PMMA microcapsules.……..…….214

Figure 6-14. Fractional deformation at bursting point ε_B (squares) and fractional deformation at the elastic limit ε_{LE} (triangles) versus diameter for 1 h PMMA microcapsules prepared by membrane emulsification (filled points) and homogenization (empty points).……...……..215

Figure 6-15. (a) Elastic limit, (b) elastic modulus and (c) force at the elastic limit of individual 4 h PMMA microcapsules prepared by membrane emulsification (filled points) and homogenization (empty points) determined using different methodologies: power law model (diamonds) and linear model (circles)….……...216

Figure 6-16. Comparison between experimental compression data (points) and the best fit profiles of elastic regime from FEM simulations (lines) of individual PMMA microcapsules produced with different reaction times: 1 h (thin-shell model), 4 h (continuous line - linear model; dashed line - power law model), and 24 h (power law model) PMMA microcapsules. The *E* and $\boldsymbol{\varepsilon_{LE}}$ values determined from the best fitting curves are shown in the legend (for 4 h PMMA microcapsules, average of the two models is given).……..…..217

Figure 6-17. Compression profiles of four different PMMA microcapsules 4h with two different sizes, < 30 µm and > 60 µm……...…….219

Figure 6-18. (a) Elastic modulus and (b) force at the elastic limit determined for individual PMMA microcapsules prepared at different reaction times: PMMA 1 h (thin-shell model : triangles), 4 h (linear model: filled diamonds and power law model: empty diamonds) and 24 h (power law model: circles).…….…….220

Figure 6-19. Bursting force F_B (squares) and force at elastic limited F_{LE} (triangles) versus diameter for 1 h PMMA microcapsules prepared by membrane emulsification (filled points) and homogenization (empty points).……...223

Figure 6-20. Largest tensile (empty points) and compressive (filled points) principal stress determined for individual PMMA microcapsules at ε_{LE} prepared at different reaction times: PMMA 1 h (triangles), 4 h (diamonds) and 24 h (circles)……...227

Figure 6-21. Three- parameter Weibull distribution using the median ranks method fitting with experimental compressive stress data of 4 h (d > 40μm) PMMA microcapsules…….229

Figure 6-22. Cumulative failure probability using a compressive stress failure criterion of 1 h (a), 4 h (d > 40μm) (b) and 24 h (c) PMMA microcapsules.…….230

Figure 7-1 Schematic diagram of the device used to conduct continuous release experiments.……...242

Figure 7-2 Schematic diagram of PMMA perfume microcapsules with different shell thicknesses.……...244

Figure 7-3 Determination of P using the thin-shell method. The red line is the best fitting of the linear regime for R <0.6 and $R > W_{oil}$.……...…255

Figure 7-4 Comparison of the release profiles of MF microcapsules prepared with different methods in 60% v/v glycerol aqueous solution: membrane (Sample No.1 in Table 7-1) and homogenization (Sample No.2).……257

Figure 7-5 Comparison of release profiles of MF microcapsules containing same core oil A exposed to different co-solvents……..……..258

Figure 7-6 Modified permeability results of MF microcapsules prepared with same process conditions but with two different kinds of core oil; the microcapsules were tested using different co-solvents, given in the legend……..……...……..260

Figure 7-7 Comparison of the release profiles of MF microcapsules (Sample No.1) and 1 h PMMA microcapsules (Sample No.5).……..262

Figure 7-8 Experimental and best-fitted release profile for 24 h PMMA microspheres (Sample No. 7) tested in 60% (v/v) glycerol aqueous solution. The best fitted diffusion coefficient value is $D = 3.2 \times 10^{-13} \mathrm{m}^2\ \mathrm{s}^{-1}$ using the homogenous sphere model for $R\ (t)$<0.8 (Section 7.3.2), the continuous line shows all the predicted release.....264

Figure 7-9 Release profiles of 4 h PMMA microcapsules analysed using the sphere and hollow sphere models.……..……...……...……..266

Figure 7-10 Experimental release profile of 1 h PMMA microcapsules (Sample No.5) tested in 60% (v/v) glycerol aqueous solution. The blue line shows the best fits using the hollow sphere model.……...……267

List of Tables

Table 2-1 Patented manufacturing processes on the microencapsulation of fragrances using MF for consumer product applications.....44

Table 2-2 Techniques for characterizing size and size distribution of particles.....56

Table 3-1 Summary of membrane area (A_m), porosity φ, pore active membrane area ($Aac = Am \times \varphi$), the inner radium (*Rin*), the outer radium (*Rout*), pore distance *L*, pore diameter *dp*, number of pores of the membranes *N* studied.....85

Table 4-1. Summary of the mechanical property data of the microcapsules prepared by membrane emulsification and homogenization. Confidence intervals represent the standard error of the mean, with 50 microcapsules for each group.…….…….152

Table 5-1. Refractive indexes of the materials used in the study on encapsulation of different core oils by MF…….……...…159

Table 5-2. Physical properties of the dispersed and continuous phases: viscosity, density and interfacial tension between the two phases. Error represents the standard error of the mean.……..….169

Table 5-3 Summary of sizes of the droplets and microcapsules as well as shell thickness obtained through laser diffraction and TEM.…….……...183

Table 7-1 Formulations and operation conditions used for preparation of microcapsules in this study...…….237

Table 7-2. The wavelength where absorbance is maximum (λ_{max}), extinction coefficients (ε) as well as the saturation concentration (C_s) of oil A and oil HS in water and in aqueous co-solvent solutions. The viscosities (μ_{cs}) of the pure compounds and aqueous solutions at room temperature 25 ± 1 ºC are taken from the literature.……..…...……..….252

Table 7-3. The list of encapsulation efficiency s *EE %*, the total amount of perfume oil in the slurry ϕ_{slurry} *%* and waste oil in slurry *Woil %* of MF and PMMA microcapsules.……....254

Table 8-1. Overview summary of shell materials, reaction conditions, encapsulation efficiency, size and size distribution, mechanical properties and permeability data of microcapsules.……..…..272

Nomenclature

A Absorbance of sample

Aac Pore active membrane area (m^2)

A_h Proportionality constants for equation $D_{3,2} = A_h \omega_m^{\ B}$

B Proportionality constants for equation $D_{3,2} = A_h \omega_m^{\ B}$

b Width of the paddle (m)

C Concentration of the sample (g ml^{-1})

Cs Perfume oil solubility in the solvent (g ml^{-1})

$C_{s-shell}$ Saturation solubility of the core oil in the shell material (g ml^{-1})

C_{sus} Concentration of perfume oil in suspension (g ml^{-1})

$C_{in(s)}$ and $C_{out(s)}$ Oil concentrations (w/v) at the inner and outer side of the shell-fluid interface (g ml^{-1})

C_{in} and C_{out} Oil concentrations in the solvent inside and outside the microcapsule (g ml^{-1})

$C_{in\infty}$ Concentration inside the particle at the end of release (g ml^{-1})

$C_{out\infty}$ Concentration outside the particle at the end of release (g ml^{-1})

C_{in0} Initial concentration inside the particle (g ml^{-1})

D Diffusivity of microcapsules shell (m^2 s^{-1})

D_{90} Diameter under which the cumulative volume of the droplets/microcapsules is 90% (m)

D_{10} Diameter under which the cumulative volume of the droplets/microcapsules is 10% (m)

D_{50} Diameter under which the cumulative volume of the droplets/microcapsules is 50% (m)

Dp Diameter of paddle impeller (m)

$D_{4,3}$ Volume mean diameter (m)

$D_{3,2}$ Sauter mean diameter (m)

d_{lsa} Particle size to test using laser diffraction (m)

d_c Droplet diameter before detachment, varies with time, $d_p \leq dc \leq d_d$ (m)

d_d Droplet diameter during detachment (m)

d_N Diameter of "neck" at the membrane pore surface (m)

d_p Diameter of the pore on the membrane (m)

d_i Diameter of single droplets/microcapsules (m)

$\bar{d}$ Number- based mean diameter (m)

E Young's modulus of microcapsules (MPa)

EE Encapsulation efficiency (% w/w)

F_{BG} Buoyancy force when droplets forming on the membrane surface (N)

F_B Force at the bursting point (mN)

F_d Drag force (N)

F_{dl} Dynamic lift force (N)

F_l Linear momentum force (N)

F_{LE} Force at ε_{LE} (mN)

$F_{LE,P}$ Force at ε_{LE} using power law model (mN)

$F_{LE,P}$ Force at ε_{LE} using linear model (mN)

F_{push} Push off force (N)

F_{γ} Interfacial tension force (N)

F_s Force generated by shear stress (N)

F_{stat} Force due to a static pressure difference between the two phases (N)

$F_{tension}$ Force on the Wilhelmy plate during the measurement (N)

g Acceleration of gravity (m s^{-2})

h Shell thickness (m)

h_m Measured shell thickness (m)

H Height of the continuous phase

I_{sc} Intensity of scattered light (w m^{-2})

I_{in} Intensity of laser light (w m^{-2})

I_t Intensity of the transmitted light (w m^{-2})

I_0 Intensity of the incident light (w m^{-2})

J Perfume oil flux passing through the microcapsule shell (m s^{-1})

J_d Flux of dispersed phase (m s^{-1})

k_B Boltzmann's constant

k_{wl} Viscosity modification factor for the dispersed phase

K Partition coefficients

$K_p = \frac{C_{in\infty}}{C_{out\infty}}$ Partition coefficient

l Optical path length (cm), in this study, it could be dimension of the cuvette, which is 1cm

lw Length of the wetted area of the Wilhelmy plate (m)

L Gap between pores (m)

m Linear slope used to estimate the elastic modulus of microcapsule

m_{slurry} Weight of slurry (g)

M_{cz} Torque when droplets forming on the membrane surface (N m)

N Number of pores of the membranes

n Number of root of equation

n_b Number of paddle

n_i Number of droplets/microcapsules measured

n_{index} Relative refraction index of the particle and the medium

P Permeability of microcapsules shell (m^2 s^{-1})

$\bar{P}_m$ Modified shell permeability of microcapsules, $\bar{P}_{ma}$ for $\tau = 2/3$, $\bar{P}_{mb}$ for $\tau = 1$

$\overline{P/h}$ Mean permeability of a microcapsule shell divided by its shell thickness (m s^{-1})

Q Actual flow rate of the dispersed phase through the pore (m^3 s^{-1})

q_n Non-zero positive roots of the transcendent equation $q_n = \frac{3q_n}{3+\alpha {q_n}^2}$

r Radius of microcapsules (m)

r_{inner} Inner radius of thick shell microcapsules (m)

r_m Measured radius of microcapsules (m)

r_p Radius of the pore (m)

r_{trans} Transitional radius (m)

r_r Distance from the centre of particle/microcapsule to the location where parameters are simulated in the equations (m)

r_{solute} Radius of the solute particle (m)

R_{in} Inner radius of membrane's ring area (m)

R_{out} Outer radius of membrane's ring area(m)

$R(t)$ Relative oil release by weight (s^{-1})

Re Reynolds number

$\overline{dR/dt}$ Mean slope release profile for thin-shell microcapsules (s^{-1})

t_r Microcapsules release time (s)

t_{end} End of microcapsules release time (s)

t_d Duration of detachment period (s)

T Diameter of the vessel with the membrane fixed at the bottom (m)

T_{ab} Absolute temperature (K)

T_B Nominal wall tension, defined as the rupture force normalized by the circumference of the uncompressed microcapsule (MPa)

u_d Velocity of dispersions phase (m s^{-1})

v_c Velocity of the continuous phase is (m s^{-1})

ν Poisson ratio

V Co-solvent aqueous solution (ml)

V_a Voltage of the DC motor (v)

V_d Volume of droplet (m^3)

V_f Final volume of a droplet (m^3)

V_g Initial volume of the droplet (m^3)

Vs Volume of the particle released in co-solvent solution (ml)

V_{sus} Volume of microcapsule suspension (ml)

$Woil$ Percentage of waste oil in slurry (% w/w)

x Compressive stress of microcapsules for three- parameter Weibull distribution

x_0 Location parameter, (x_c+x_0) is about the median value for three- parameter Weibull distribution

Greek Symbol

α Radius corrections factor

$\alpha_r = V/V_S\,K_p$ Ratio of oil released to that remaining in the particle at equilibrium

β Shape parameter of microcapsules for three- parameter Weibull distribution

ε Extinction coefficients of the concentration calibration curve (ml g^{-1} cm^{-1})

ε_B Fractional deformation at rupture

ε_{LE} Fractional deformation above which there is a continuously increasing difference between the experimental force profile and the theoretical elastic profile

$\varepsilon_{LE,P}$ ε_{LE} using power law model

$\varepsilon_{LE,P}$ ε_{LE} using linear model

ε_m Fractional deformation of microcapsules

λ_{max} Maximum absorbance wavelength (nm)

λ_{lsa} Wavelength of the laser light (nm)

ϕ_{oil0} Initial concentration of perfume oil used in slurry(g g^{-1})

ϕ_{slurry} Total amount of perfume oil in the slurry (% w/w)

φ Porosity of the membrane

θ Contact angle between membrane and pure water (°)

θ_{lsa} Light scattering angle of the laser diffraction instrument (°)

θp Contact angle between the heavier phase and the Wilhelmy plate (°)

ρ_C Density of continuous phase (kg m^{-3})

ρ_d Density of dispersions phase (kg m^{-3})

γ Interfacial tension of the two phases (N/m)

τ Fitted constant for equation $D \propto \mu_{cs}{}^{-\tau}$

τ_w Shear stress at the membrane surface (Pa)

τ_{max} Maximum shear stress at the membrane surface (Pa)

τ_{av} Average shear stress of the whole membrane at the membrane surface (Pa)

τ_{avRing} Average shear stress of the ring area where the pores located (Pa)

σp Microcapsules failure stress (MPa)

$\sigma_{P,T}$ Principle tensile stresses of microcapsules (MPa)

$\sigma_{P,C}$ Principle compressive stresses of microcapsules (MPa)

δ Boundary layer thickness (m).

δ_B Nominal rupture stress, defined by the ratio of the rupture force to the initial cross sectional area of the microcapsule (MPa)

μ_c Viscosity of continuous phase (Pa s)

μ_{cs} Viscosity of co-solvent for oil release (Pa s)

μ_d Dispersed phase viscosity (Pa s)

ω Angular velocity of the stirred impeller (rad s^{-1})

ω_m Agitation speed (rpm)

Abbreviations

AIBN 2,20-azobisisobutyronitril

CDF(x) Cumulative distribution function

CFD Computational fluid dynamics

CLSM Confocal laser scanning microscopy

CV Coefficient of variation

EGDMA Ethylene glycol dimethacrylate

ESEM Environmental scanning electron microscopy

FEM Finite Element Modelling

HG Homogenization

HS Hexyl salicylate

LALLS Low angle laser light scattering

ME Membrane emulsification

MF Melamine formaldehyde

MMA Methyl methacrylate

NaCl Sodium chloride

P Peppermint

P&G Procter & Gamble

PMMA Poly (methyl methacrylate)

PVA Polyvinyl alcohol 18-88

RB Rhodamine B

S Sunflower

SD Standard deviation

SE Standard error

SEM Scanning electron microscopy

TEM Transmission electron microscopy

UF Urea-formaldehyde

UV-Vis Ultraviolet-visible spectrophotometry

List of Publications

Xuemiao. Pan, R. Mercadé-Prieto, J. A. Preece, D. York, and Z. Zhang. "Preparation and Characterisation of User-friendly PMMA Microcapsules for Consumer Care". *Powders & Grains*. University of New South Wales (UNSW), Australia, 8-12 July 2013.

Xuemiao. Pan, R. Mercadé-Prieto, J. A. Preece, D. York, and Z. Zhang. "Structure and Mechanical Properties of Consumer-friendly PMMA Microcapsules". 2013. accepted by *Industrial & Engineering Chemistry Research*.

R. Mercadé-Prieto, **Xuemiao. Pan**, A. Fernández-González, Z. Zhang, S. Bakalis. "Quantification of perfume microcapsules deposited in cotton fabrics before and after abrasion using fluorescence microscopy". *Industrial & Engineering Chemistry Research*. 2012. (51): 16741–16749

Xuemiao. Pan, J. A. Preece, D. York, and Z. Zhang. "Size and Strength Distribution of Melamine-formaldehyde Microcapsules Prepared by Membrane Emulsification". *Powder Technology*, 2012(227): 43-50.

Xuemiao. Pan, R. Mercadé-Prieto, J. A. Preece, D. York, and Z. Zhang, "Preparation and Characterization of Consumer-friendly PMMA Microcapsules for Liquid Detergents". *The 19th Joint Annual Conference of CSCST-UK and SCI-CS*, University of Reading, 15 Sept. 2012.

R. Mercadé-Prieto, **Xuemiao. Pan**, A. Fernández-González, Z. Zhang, S. Bakalis. "Effect of drying on the survival of microcapsules deposited in cotton fabrics during abrasion." *18th international drying symposium*, Xiamen, 11 Nov. 2012.

Xuemiao. Pan, J. A. Preece, D. York, and Z. Zhang. "Factors Influencing the Size and Size Distribution of Oil-filled Melamine-formaldehyde Microcapsules Prepared using Membrane Emulsification". *3rd UK-China Particle Technology Forum*, Birmingham, 4-6 July 2011.

Xuemiao. Pan, J. A. Preece, D. York, and Z. Zhang, "Preparation of Uniform-sized Melamine-formaldehyde Microcapsules by Membrane Emulsification".*2nd UK-China Particle Technology Forum*, Guiyang, 1-3 Sept. 2009.

Xuemiao. Pan, J. A. Preece, D. York, and Z. Zhang, "Using Membrane Emulsification to Prepare Microcapsules with Narrow Strength Distribution". *10th UK Particle Technology Forum*, Birmingham, 1 July 2009.

Chapter 1 Introduction

There is a rising need to deliver and deposit “active ingredients” on solid surfaces, covering a wide range of applications, from consumer products (Vladisavljevic and Williams, 2005) to pharmaceuticals (Fukumori et al., 1991). Of special interest in the present study is the controlled release of functional oils to fabric surfaces. Unfortunately, many active components, particularly functional oils, are sensitive and volatile. They can be susceptible to environmental conditions, such as changes in the pH value or temperature, and they can lose their activity during storage due to oxidation, evaporation, and even reaction with outside agents (Hsieh *et al.*, 2006). For this purpose, microencapsulation techniques have been used in the past to preserve aromas for laundry applications for long periods (Long *et al.*, 2009), and in addition they may also provide special functions to textiles, such as temperature control or colour maintenance (Nelson, 2002).

Microencapsulation is one of suitable solution to stabilize active ingredients during storage, but it can also be used to control the release of the encapsulated functional oils. One shell material that is commonly used for coating functional oils in industry and for research purposes is melamine formaldehyde (MF) (Zhu *et al.*, 2012). MF is fairly inexpensive, highly stable and has ample applications in consumer products

(Hwang *et al.*, 2006a, Hwang *et al.*, 2006b, Long *et al.*, 2009). MF perfume oil microcapsules used in laundry applications should deposit onto fabrics and be stable during the production, transportation, storage and laundry process. In addition, they should provide a long lasting perfume release after laundry washing. In this case, it is crucial to formulate microcapsules that possess a number of desirable properties, including high active content and controllable barrier properties of the shell.

A second desirable characteristic of some perfume-filled microcapsules is that they should be able to break when customers caress clothes, thus releasing a sudden burst of pleasant perfume. At present, the breakage of microcapsules due to human contact or due to fabric abrasion is poorly understood, yet it is typically desired that the mechanical rupture of a batch of microcapsules to be narrowly dispersed to assure a homogeneous bursting behaviour. For the case of MF microcapsules, it has been reported in the literature that there is a strong relationship between the mechanical strength and the microcapsules size (Hu *et al.*, 2009, Sun and Zhang, 2001). Hence, a potential way to obtain batches of microcapsules with well-defined rupture properties would be to obtain microcapsules with narrow size distributions. However, little has been done on the study of factors which control the size, and thus the strength, distributions of MF microcapsules. Membrane emulsification is one of the techniques which can generate mono-dispersed emulsion droplets, and therefore it could be used to produce microcapsules of narrower size distribution (Renken and Hunkeler, 1998, Vladisavljevic and Williams, 2005). In the present work, melamine formaldehyde

microcapsules with an oil-based active ingredient have been prepared using one lab-scale membrane emulsification technique, a dispersion cell system (Holdich *et al.*, 2010), and one pilot plant-scale membrane emulsification system, a cross-flow membrane system (Yuan *et al.*, 2008a). Different core materials were used during membrane emulsification in order to explore its manufacturing capability. For this reason, the effect of processing conditions on the size and size distribution of microcapsules has been investigated thoroughly in the present work.

The manufacturing of MF microcapsules results in small amounts of free formaldehyde in the solutions, which due to its high toxicity is a key concern for consumer product applications. For this reason, a new shell material should be developed for future manufacturing. The potential of polymethylmethacrylate (PMMA), an environmentally friendly material, to encapsulate perfume oil is a second area of study in the present dissertation. The properties of the new PMMA microcapsules created have been extensively characterised in order to evaluate their potential applications.

Some mechanical strength parameters such as the rupture force, and the displacement at rupture can be determined directly using a micromanipulation technique (Sun and Zhang, 2001, Sun and Zhang, 2002). Intrinsic mechanical properties of thin shell microcapsules (*eg.* MF microcapsules), such as Young's modulus and the rupture

stress were addressed and calculated in literature (Mercade-Prieto *et al.*, 2011a, Mercade-Prieto *et al.*, 2011b). However, little has been done for thick-shell microcapsules. In this project, the mechanical properties of PMMA microcapsules with different thicknesses were determined using the micromanipulation technique and finite element analysis.

Recently, Mercadé-Prieto *et al.* (2012b) has developed a methodology to determine the shell permeability of thin-shell MF microcapsules with a single fragrance compound. However, there is not much work done on the shell permeability of microcapsules with real perfume oils, which are complex mixtures of many chemicals with various functionalities. In this project, a methodology was developed to determine the permeability of MF microcapsules with real complex perfume oils and this methodology was applied to PMMA microcapsules with a wide range of shell thicknesses, in order to better understand the effects of formulation and processing conditions on the microcapsules wall properties.

A summary of this thesis is given as below:

In Chapter 2, a literature review on membrane emulsification and encapsulation methods is provided. This chapter provides an overview of how encapsulation processes affect the size of liquid droplets in emulsions and the corresponding microcapsules. Industrial applications of microcapsules, especially those with MF or

PMMA shell materials are then presented. A general survey on characterization methods for microcapsules is also presented.

In Chapter 3, the materials, methods and equipment used in this study are described in detail.

Chapter 4 describes the encapsulation of perfume oils by membrane emulsification using MF as a shell material. The experimental conditions and procedures are also described in detail. The effects of process conditions and membrane surface properties on the size and size distribution of the oil droplets produced in the emulsification stage and of the final microcapsules are reported. The physical and mechanical properties of the resulting microcapsules are characterized.

Chapter 5 examines the feasibility to scale up the encapsulation of perfume oils with membranes by using a cross-flow membrane system. Lab-scale results from Chapter 4 are compared with those from a pilot plant-scale membrane system. Different core oils are encapsulated with MF in order to study the effect of different liquids properties, such as the interfacial tension and viscosities of two phases, on the size and size distribution of microcapsules.

Chapter 6 focuses on the formulation and encapsulation process using PMMA as a shell material. The size and the shell thickness of resulting PMMA microcapsules are studied with confocal laser scanning microscopy (CLSM). The intrinsic mechanical properties of the PMMA shells, such as the elastic modulus and the rupture stress, are determined using the micromanipulation technique and finite element modelling (FEM).

In Chapter 7 results are reported on the release of perfume oils from the MF and PMMA microcapsules described in Chapters 4 and 6. Further investigation of the shell structural properties, such as the shell permeability and diffusivity are reported.

Chapter 8 presents an overall summary of the work presented in this thesis, followed by recommendations for further work.

Chapter 2 Literature Review

2.1 Introduction

In this chapter previous literature on theoretical models, experimental techniques and industrial applications of microencapsulation are reviewed. The literature review is divided into five sections. The first section provides a general introduction on emulsions and encapsulation techniques for perfume oils. In the second section a literature review is provided on emulsion and emulsification, with emphasis on membrane emulsification. A brief introduction is provided of theoretical models that describe droplet formation during membrane emulsification. In the third section a literature survey is given on encapsulation methods which are commonly used for perfume microcapsules. In the forth section, the current industrial applications of the shell materials melamine formaldehyde (MF) and poly (methyl methacrylate) (PMMA) are introduced. The last section deals with experimental techniques used to characterize microcapsules.

2.2 Microencapsulation

2.2.1 Introduction

Microencapsulation is the process to produce individual capsules in the micron size range with a core that can be a solid (Fukumori *et al.*, 1991), a liquid (Sohn *et al.*, 2007) or a gas (Madene *et al.*, 2006), surrounded by a shell made of natural (Lan *et al.*, 2011) or synthetic materials (Su *et al.*, 2012). Since this technique was first applied to carbonless copying papers in the 1930's by the National Cash Register Co. (NCR) from USA (Green, 1957), it has now been introduced into diverse industry sectors. For example it is used to encapsulate cells (Murua *et al.*, 2008, Renken and Hunkeler, 1998) and enzymes (Inomata *et al.*, 1995) for pharmaceutical and biomedical applications. It is applied to stabilise flavours or to mask tastes in food manufacturing (Charcosset, 2009), to deliver fine fragrances in consumer products (Anton *et al.*, 2008, Hong and Park, 1999a), as well as for coating pressure - sensitive materials or inks for the paper industry (Schmidt *et al.*, 2000). In addition, the solid final capsules are commonly easier to handle than their liquid cores, as in the case of pesticides for agriculture (Liu *et al.*, 2006), which facilitates the deposition of functional ingredients in added-value textiles for example (Rodrigues *et al.*, 2008, Teixeira *et al.*, 2012a, Zuckerman *et al.*, 2003). The main advantages of encapsulating active ingredients, as opposed to deliver them in free form, are to

- enhance the stability (Sotoyama *et al.*, 1999);

- allow control release applications (Madene *et al.*, 2006, Sun and Zhang, 2001), for example using temperature as a trigger parameter (An *et al.*, 2010, Katagiri *et al.*, 2011), light (Volodkin *et al.*, 2009), pH (Ma *et al.*, 2012, Song *et al.*, 2012, Yuan *et al.*, 2010a), or mechanical rupture (Moira, 1986, Okada and Igarashi, 1984, Okada and Igarashi, 1985, Sinclair, 1981);
- allow targeting delivery (Ghosh, 2006b);
- reduce chemical hazards which may damage the environment or human health (Li *et al.*, 2009);
- shield undesirable odour or taste (Balentine *et al.*, 1997, Madene *et al.*, 2006);
- separate the reactive components in a product (Madene *et al.*, 2006);
- facilitate handling , as well as improve mixing (Ghosh, 2006b, Hwang *et al.*, 2006a), solubility (Ghosh, 2006b, Hwang *et al.*, 2006a), dispensability (Ghosh, 2006b, Hwang *et al.*, 2006a), and flow-ability (Berry *et al.*, 1995, Ghosh, 2006a).

2.2.2 Perfumes used in detergents

Perfume oils, such as those used in detergents, can be highly complex mixtures, including aliphatic compounds, acyclic terpenes, cyclic terpenes, alcohols, ethers, aldehydes and ketones (Bauer *et al.*, 2001). The pleasant fragrance of fabrics washed with perfume-containing detergents is considered a key purchase factor in customers

(Happi, 2009). Perfume oils also provide other special functions to detergents, such as helping to release consumers stress (Gobel *et al.*, 1994, Salari *et al.*, 2006). They are associated with specific images and emotional benefits in the consumer's mind, enhancing the product value (Retiveau, 2012). Importantly, perfumes are one of the most expensive ingredients in detergents (Retiveau, 2012), hence there is a commercial desire to minimize its loss and to enhance its delivery.

The loss of fragrance compounds during detergent manufacturing, packaging, storage and transport can vary from several percent up to 50% before going on sale (Gimenez-Arnau *et al.*, 2002, Ho, 2000, Jellinek, 1975), see Figure 2-1. It is typically caused by evaporation or oxidation reactions, due to environmental conditions, such as light, heat, oxygen, humidity, or by changes in the pH value. In addition, perfumes can react with extraneous organic materials or ingredients in the detergents, such enzymes or proteins (Specos et al., 2010, Teixeira et al., 2012a, Teixeira et al., 2012b).

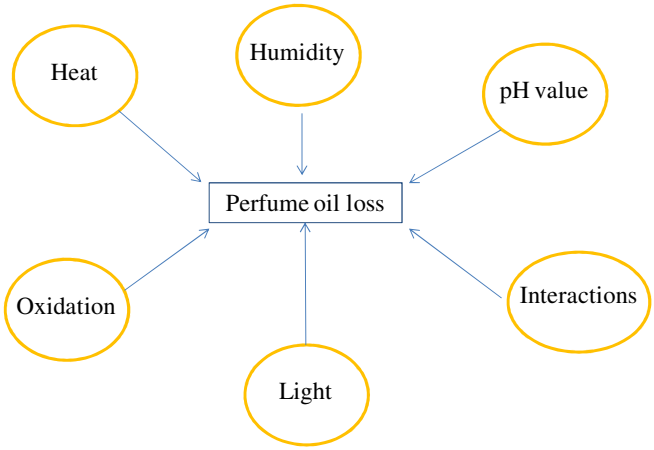

Figure 2-1. Environmental factors that can cause perfume loss during manufacturing and storage.

Perfume oils may be washed away by the surfactants inside the detergents during laundry processes, especially when they are highly water soluble, as discussed by Haefliger *et al.* (2010). They may also evaporate during the drying process after washing (Haefliger *et al.*, 2010). In addition, it is difficult to deposit perfume oil onto the fibre surface (Haefliger *et al.*, 2010) and to release perfume oil at the right moment (after the wash) (Mercadé-Prieto *et al.*, 2012a).

2.2.3 Perfume microcapsules

Microcapsules containing fragrances are commonly employed in detergents, fabric softeners and functional fabrics (Hu *et al.*, 2012, Hu *et al.*, 2011, Mihranyan *et al.*, 2012, Teixeira *et al.*, 2012b, Tzhayik *et al.*, 2012). Most of the perfume oil microcapsules used in laundry applications have a core/shell structure, as shown in Figure 2-2 (Hwang *et al.*, 2006b, Long *et al.*, 2009). In order to make perfume microcapsules, the perfume oil is first well dispersed into a media (it can be aqueous or oil phase (Zhang and Rochefort, 2012)) to form emulsion droplets as a soft template. Then, a shell is formed to coat the droplets (Figure 2-3). Chemical or physical methods are used to form the solid shell, providing a mechanical strength to the microcapsules that will be crucial for their subsequent survival.

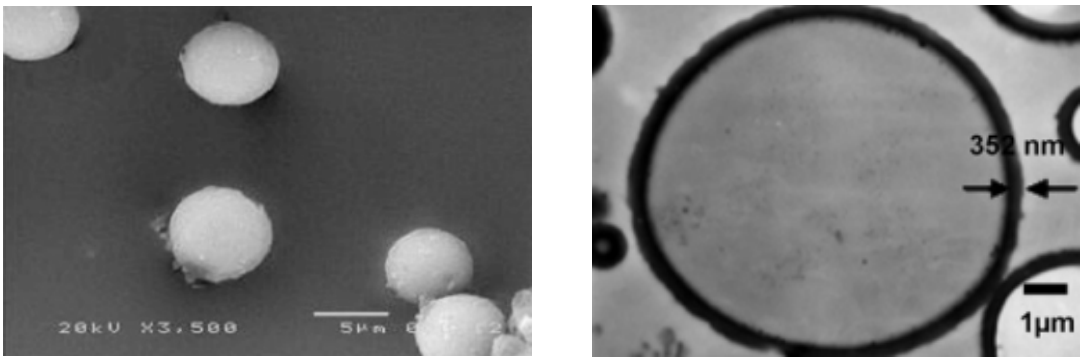

(a) (b)

Figure 2-2 (a) SEM and (b) TEM image of core/shell perfume oil microcapsules with a melamine -formaldehyde shell (Hwang *et al.*, 2006b, Long *et al.*, 2009).

Melamine-formaldehyde (MF) is one of the most common materials used in industry to produce perfume microcapsules. As introduced above, MF microcapsules are typically made from an oil emulsion in an aqueous MF precondensate, followed by *in situ* polymerisation of the MF precondensate on the surface of oil droplets. The emulsification process determines the size distribution of the droplets formed, which largely controls the size distribution of the final microcapsules if the emulsions is stable. The typical technique used to generate the emulsion in industry is homogenisation or agitation. Recently, membrane emulsification has also been used to generate the emulsions (Aryanti *et al.*, 2009, Yuan *et al.*, 2010b).

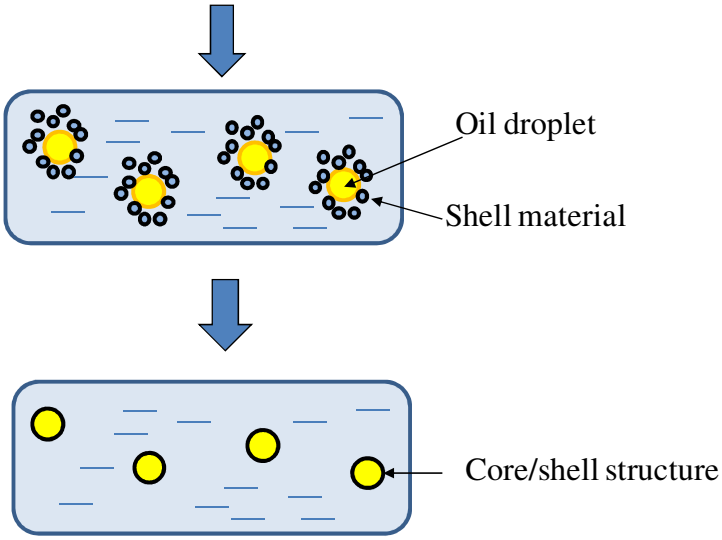

Figure 2-3 Schematic graph of basic steps of microencapsulation process.

The improved performance and delivery of perfume microcapsules for laundry applications has been shown at length in the past (Bone et al., 2011, Hu et al., 2011, Pena et al., 2011, Pena et al., 2012, Zhang and Rochefort, 2012). As discussed previously to microcapsules in general, the encapsulated perfumes have improved stability and durability during prolonged storage (Specos et al., 2010, Teixeira et al., 2012a, Teixeira et al., 2012b); increase the perfume oil content in detergents (Zhang and Rochefort, 2012); increase the total oil deposited on fabrics (Monllor et al., 2007); and reduce perfume dermatitis due to the contact of perfume in detergents (Ezendam et al., 2009).

The perfume release from microcapsules can be designed to be long lasting, or to occur suddenly if microcapsules are burst, for example by friction (Mercadé-Prieto *et al.*, 2012a). Haefliger *et al.* (2010) developed a new technique to monitor the real time perfume release in air with a headspace setup and a gas chromatography. The new technique was used to compare the release of perfume oils used in free form, shown in Figure 2-4(a), with the long term release that is possible using perfume microcapsules, Figure 2-4(b) for the case of ~21 μm MF microcapsules. Note that the release rate, given in the y axis, is about one order of magnitude lower when using encapsulated perfume. Figure 2-4(c) shows the perfume release from microcapsules deposited in a towel after the fabric is rubbed at different intervals. This study provided the first scientific evidence of the mechanical trigger release of perfume microcapsules used in many commercial products. The actual release rate of the perfume is different for the different compounds.

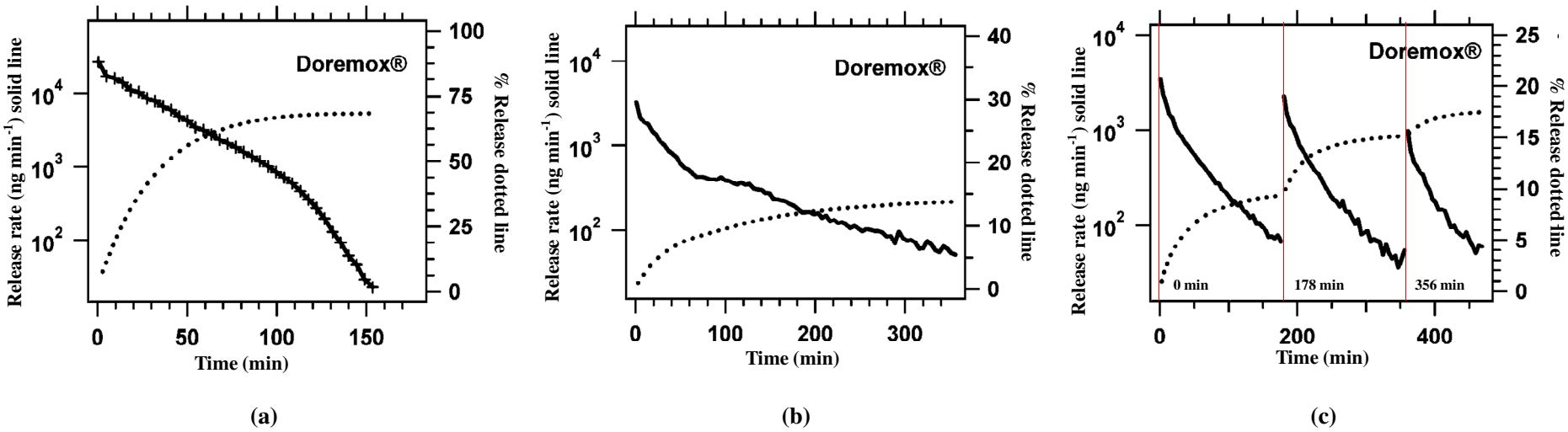

Figure 2-4. Release of perfumery ingredient Doremox® in (a) free form and (b) encapsulated form in a fabric softener (Haefliger *et al.*, 2010). A wet cotton towel with perfume was dried in an air stream from which the perfume oil release was determined using low thermal mass gas chromatography. (c) The experiment (b) was repeated, but here the towel with microcapsules was suddenly rubbed for 0, 178, and 356 min (as shown by the red solid line in the figure) to rupture the microcapsules and release the perfume oils.

2.3 Emulsification

2.3.1 Emulsion and emulsion stability

An emulsion is normally created by inputting energy to a system with two or more immiscible phases, although the resultant droplets tend to be unstable (Sotoyama *et al.*, 1999). There are several reasons that lead to unstable emulsions: droplet rising, flocculation, coalescence and Ostwald ripening, illustrated in Figure 2-5 (Xu *et al.*, 2006). Surfactants (Leal-Calderon et al., 2007) or copolymers (Long *et al.*, 2009) are commonly added before emulsification in order to increase the stability of the emulsion. In a recent study (Long et al., 2009), poly (acrylamide-acylic acid, sodium salt) was utilized to stabilize the perfume oil droplets formed in a MF precondensate aqueous solution.

Emulsions can also be stabilized using small insoluble particles, called Pickering emulsions (Fletcher *et al.*, 2010, Holdich *et al.*, 2012, Salari *et al.*, 2011, Yuan *et al.*, 2010b). The particles used for Pickering emulsions are mainly hydrophobic or amphiphilic (Janus particles) (Binks and Fletcher, 2001) nano-particles, such as colloidal silica (Fletcher *et al.*, 2010), latex particles (Manga *et al.*, 2012) and proteins (Okubo and Hattori, 1993). In addition to the stabilizers described above, temperature and pH are also important factors to maintain the stability of emulsions (Kentepozidou and Kiparissides, 1995, Xu *et al.*, 2006).

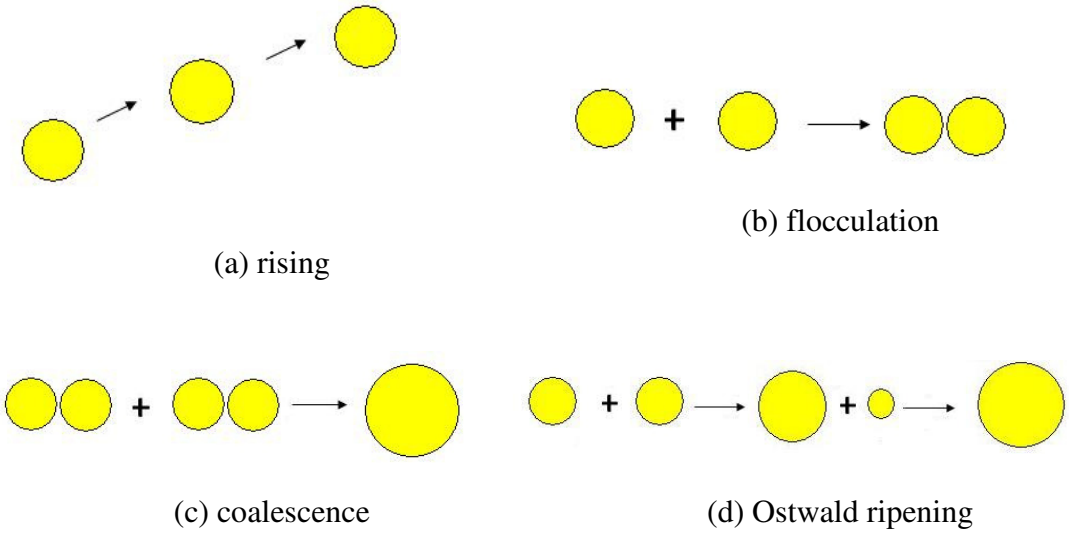

Figure 2-5 Different mechanisms that induce emulsion instability

There are many different techniques to add the energy required to create emulsion, as spontaneous emulsions are rare (Capek, 1999). The most common techniques include homogenisation (Turchiuli *et al.*, 2013), agitation (Choi and Lee, 2010) and membrane emulsification (Peng and Williams, 1998a).

2.3.2 Emulsification methods

2.3.2.1 Homogenization

Homogenization is one of the most frequent technique to generate emulsions in industry. There are two types of conventional homogenizers which are regularly used:

high pressure homogenizer and rotor-stator high shear homogenizer (Turchiuli *et al.*, 2013). The high pressure homogenizer is mainly used to generate nano-emulsions (Turchiuli *et al.*, 2013), whereas the high shear homogenizer is used for micron-sized emulsions (Rueger and Calabrese). Compared with conventional agitators, a rotor-stator high shear homogenizer has an extra membrane tube surrounding the rotor blades, as shown in Figure 2-6. During emulsification, the high speed rotation of the blades mixes well of the two phases, forming a coarse emulsion, which is subsequently broken down and refined when it is pushed through the membrane tube by centrifugal forces. This process occurs continuously until an emulsion with a constant size is formed (Turchiuli *et al.*, 2013).

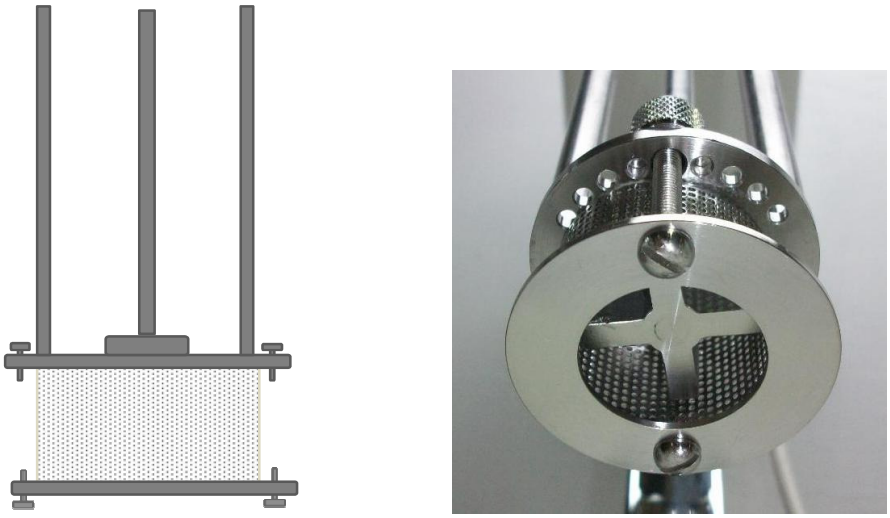

Figure 2-6 Schematic graph and picture of a rotor-stator high shear homogenizer. The homogenizer has a 4 blade impeller (Φ 30 mm) in the middle, surrounded by metal cylinder (Φ 35 mm) with regular round pores (Model L4RT, Silverson Machines Ltd., UK).

The size of the emulsion droplets generated by an homogenizer highly depends on the agitation speed. Calabrese *et al.* (1986b) described the relationship between the Sauter mean diameter $D_{3,2}$ of droplets in an emulsion and the agitation speed in a stirred vessel, Equation 2.1. This equation was later applied to describe the effect of a homogenizer on MF microcapsules (Hu *et al.*, 2009).

$$D_{3,2} = A_h \omega_m^{\ B} \qquad \text{(Equation 2.1)}$$

where A_h and B are proportionality constants and ω_m is the agitation speed (rpm).

Homogenization is easy to scale up and not expensive process compared with membrane emulsification, which provides a convenient method to generate the emulsion with reasonable size distributions. The coefficient of variation (*CV* value) that quantifies the size distribution of emulsions (Section 4.3) is typically around 30% to 40% in the lab (Long *et al.*, 2009) and in the pilot scale (Turchiuli *et al.*, 2013).

2.3.2.2 Other emulsification methods

Some innovative approaches have been proposed recently to generate uniform emulsions, such as emulsification in a micro-channel (Kawakatsu et al., 2001,

Vladisavljevic et al., 2008), using a micropipette (Kamat et al., 2011), using microchips (van Dijke et al., 2010), micro-fluidics (Zhao and Middelberg, 2011) or a flow focusing (co-extrusion) device (Anna et al., 2003, Martin-Banderas et al., 2005, Sakai et al., 2011, Ward et al., 2005). They may generate an emulsion with highly uniform oil droplets, with coefficient of variation (*CV* value) lower than 15%, even 2-5% in some cases (Kawakatsu *et al.*, 2001, Kuroiwa *et al.*, 2009, Li, 2010, Stoffel *et al.*, 2012, Vladisavljevic *et al.*, 2008). However, most of the devices are still in the development phase, they are difficult to scale up, or they can be costly (Charcosset et al., 2004).

Previous literature work (Nazir *et al.*, 2010) has mentioned a "premix" technique based on a direct cross-flow membrane emulsification system. Emulsions are circulated in the system several times in order to narrow the size distribution of the initial emulsion (Nazir *et al.*, 2010). This technique can provide much narrower distributions compared to single-pass cross-flow systems (Joseph and Bunjes, 2012, Kou *et al.*, 2012, Vladisavljevic *et al.*, 2004), although it presents some limitations: membrane fouling or even membrane blocking in some cases (Nazir *et al.*, 2010).

2.3.3 Membrane emulsification

2.3.3.1 Introduction of membrane emulsification

Membrane emulsification was reported for the first time in 1988 at the Autumn Conference of the Society of Chemical Engineering in Japan (Nakashima and Shimizu, 1988, Nakashima *et al.*, 1991). Since then, membrane emulsification has become a widely used method to produce emulsions. In membrane emulsification the dispersed phase liquid is pumped through a membrane with uniform pores, in most cases, into the continuous phase, to form a emulsion. Droplets are formed one by one at the pore openings at the membrane surface. Compared with common industrial equipment, such as, homogenizers or stirrer vessels, a membrane system is a promising technique to provide emulsion droplets with a narrower size distribution, and without high energy consumption (Aryanti et al., 2009, Yuan et al., 2010b). Membrane emulsification systems have been demonstrated with different kinds of membrane materials: ceramic (Schroder *et al.*, 1998, Schroder and Schubert, 1999), glass (Omi *et al.*, 2001), polytetrafluoroethene (Ribeiro *et al.*, 2005) or metal (Holdich *et al.*, 2010, Kosvintsev *et al.*, 2008, Kosvintsev *et al.*, 2005).

There are mainly three types of membrane systems for emulsification: cross flow membranes, vibrating (or rotating) membranes and flat membranes in conjunction

with a mechanical stirrer (also called a dispersion cell) (Dragosavac *et al.*, 2008, Manga *et al.*, 2012, Vladisavljevic and Williams, 2005). The vibrating (or rotating) membrane can be used to control the size and size distribution of the droplets, but it is relatively expensive to operate (Aryanti *et al.*, 2009, Aryanti *et al.*, 2006, Holdich *et al.*, 2010, Yuan *et al.*, 2009b).

Cross flow membranes are one of the most widely used membrane systems (Peng and Williams, 1998a, Peng and Williams, 1998b, Williams *et al.*, 1998). The dispersed phase was forced through the membrane pores using pressurized gas. The flowing continuous phase at the other size of the membrane provides constant shear that will help to break the forming droplets from the pores (Nazir *et al.*, 2010). It is a simple device that is scaled up in many applications (Yuan *et al.*, 2009a, Yuan *et al.*, 2009c). However, it needs a long operation time, during which the droplets generated may change their size due to breakage or coalescence. In addition, the system may also be difficult to clean (Charcosset et al., 2004).

Membrane emulsification is a simple method to produce oil droplets with a narrow size distribution (Nakashima *et al.*, 1991), which could scale up easily. Cross-flow membrane system (Charcosset, 2009) or vibration membrane system, such as oscillating membrane system (Holdich *et al.*, 2010) and pulsed flow membrane

(Holdich *et al.*, 2013) *etc.* are techniques that have great potential for industrial manufacturing.

2.3.3.2 Flat membrane combined with a stirrer system (Dispersion cell)

The dispersion cell, pioneered by Kosvintsev *et al.* (2005), is based on a flat membrane with an overhead stirrer (Figure 2-7). Compared to other more complex membrane systems, it is relatively cheap to own and operate. The dispersion cell has been used in research studies to investigate the influence of different parameters on the sizes and size distributions of emulsions. The different parameters studied include: membrane properties (Bromley *et al.*, 2002, Egidi *et al.*, 2008, Ullah *et al.*, 2012a, Ullah *et al.*, 2012b), physical properties of the dispersed and continuous phases (Dragosavac *et al.*, 2008, Kosvintsev *et al.*, 2005), and process conditions, such as dispersed phase flux and agitation speed of continuous phase (Dragosavac *et al.*, 2008, Gasparini *et al.*, 2010, Kosvintsev *et al.*, 2008). The dispersion cell has been successfully used to generate oil in water emulsions (O/W) (Dragosavac *et al.*, 2008, Kosvintsev *et al.*, 2005) and water in oil in water double emulsions (W/O/W) (Dragosavac *et al.*, 2012a, Gasparini *et al.*, 2010) with narrow size distribution. It has also used to produce mono-dispersed silica particles (Dragosavac *et al.*, 2012b, Vladisavljevic and Williams, 2005) and PLGA microcapsules (Gasparini *et al.*, 2010, Gasparini *et al.*, 2008).

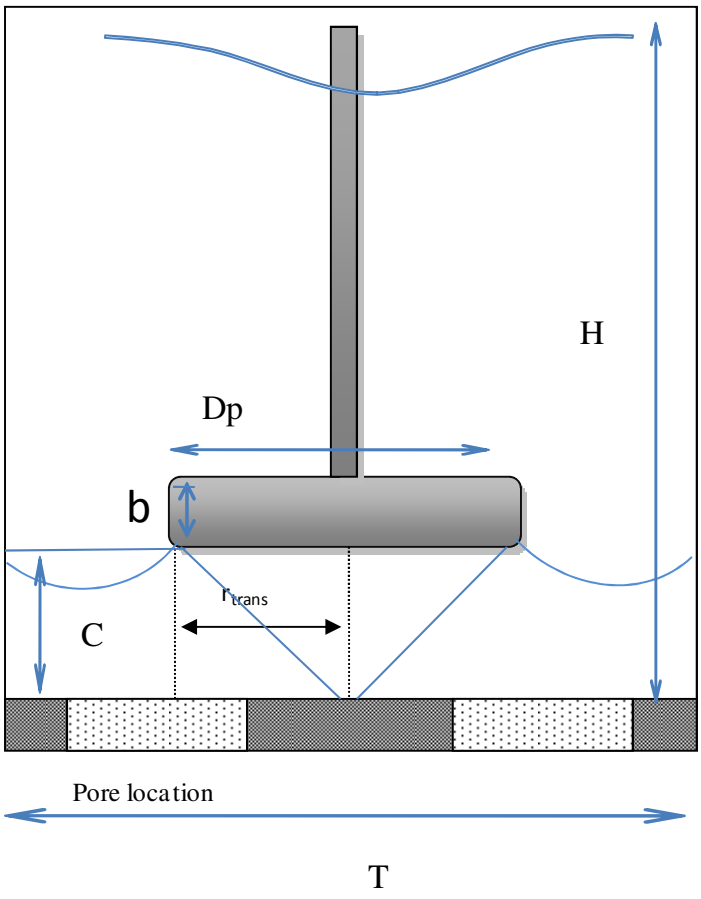

Figure 2-7 Schematic illustration of dispersion cell, which has a two-blade paddle impeller above a membrane with pores. *Dp* is the diameter of paddle impeller (m) , *T* is the diameter of the vessel with the membrane fixed at the bottom (m), *b* is the depth of the paddle (m) and *H* is the height of the continuous phase, n_b is the number of paddles, r_{trans} is the transitional radius where the shear stress on the membrane is maximum.

2.3.4 Theoretical models to describe droplet formation at the membrane surface

There have been a number of studies on the formation of droplets using membranes in order to understand the emulsification process better and to design improved systems. Imaging devices have been applied to observe the formation of droplets at the membrane surface (Xu *et al.*, 2005, Zhu and Barrow, 2005), which has allowed the development of numerical models for the formation of single droplets. Several common methodologies have been used in the previous literature work to numerically analyze droplet formation. At the microscopic level, work has been performed using computational fluid dynamics (CFD) modelling (Abrahamse *et al.*, 2001, Kobayashi *et al.*, 2007, Timgren *et al.*, 2010), Rayner *et al.'s* (2005, 2004) work using surface evolver (surface evolver is an interactive program for the study of surfaces shaped by surface tension and other energies, and subject to various constraints), lattice Boltzmann simulations (De Luca *et al.*, 2008, van der Graaf *et al.*, 2006). At macroscopic level studies have used force balances (De Luca and Drioli, 2006) or torque balances (Charcosset *et al.*, 2004, De Luca *et al.*, 2008) to understand droplet formation. Among all these models, the one based on torque balances was frequently applied on various membrane system (Charcosset *et al.*, 2004). Torque balance models have been developed for the dispersion cell membrane system, showing good agreement with the experimental data (Kosvintsev *et al.*, 2005). In this section, a brief

overview is provided on the different theoretical analysis in the literature for droplet formation using torque balances.

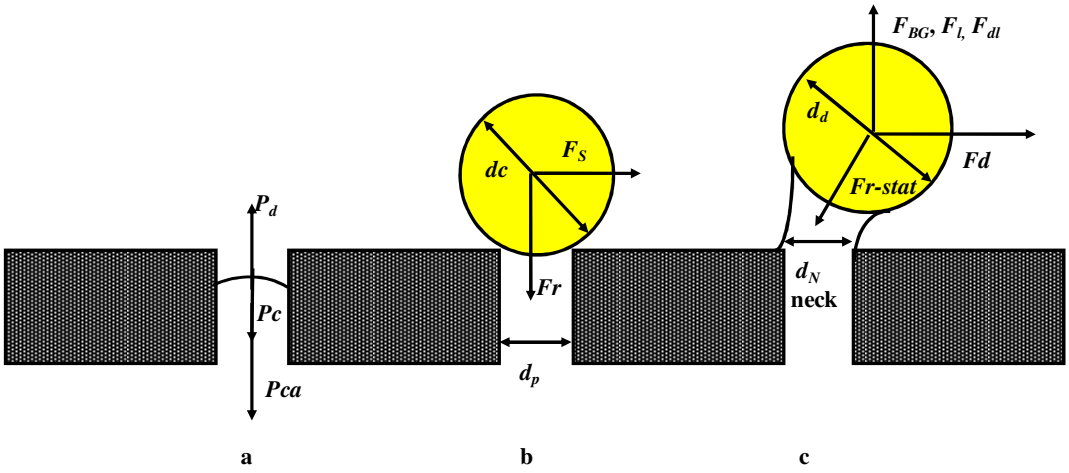

Figure 2-8 Schematic of droplet formation (Charcosset *et al.*, 2004, Xu *et al.*, 2005). (**a)** Initial stage of droplet formation in a pore membrane, where P_d is the pressure of the dispersed phase (Pa), P_c is the pressure of the continuous phase (Pa), P_{ca} is the pressure of the capillary (Pa). (**b**) Torque balance in a droplet formed without a neck, where d_c is the droplet diameter before detachment (m), d_p is diameter of the pore on the membrane (m), F_s is the he force generated by shear stress (N) and F_γ is the interfacial tension force (N). (**c**) Torque balance in a droplet considering neck formation, where d_d is the droplet diameter during detachment, d_N is diameter of the "neck" (m), F_{BG} is the buoyancy force when droplets forming on the membrane surface (N), F_d is the drag force (N), F_{dl} is the dynamic lift force (N), F_l is the linear momentum force (N), F_{stat} is the force due to a static pressure difference between the two phases (N), $F_{\gamma-stat} = F_\gamma - F_{stat}$ (N).

The torque balance model for the droplet formation from a single pore at a cross-flow membrane surface was developed by Williams and co-workers in 1998, shown schematically in Figure 2-8 (Peng and Williams, 1998b). Droplets are considered as spherical subjects, and the model predicts the resultant droplet size and the production rate. The initial model has been further extended in many other subsequent studies (Charcosset *et al.*, 2004, De Luca *et al.*, 2008, De Luca *et al.*, 2006, De Luca *et al.*, 2004, Schroder *et al.*, 1998, Schroder and Schubert, 1999).

An analogous torque balance analysis was then applied by Holdich *et al.* (2005) to study emulsification in a dispersion cell. For the initial simple scenario where a droplet is formed without a neck, the schematic diagram shown in Figure 2-8(b), the torque balance when a droplet is formed is (Dragosavac *et al.*, 2008, Stillwell *et al.*, 2007) :

$$M_{cz} = 2\pi r_p^2 \gamma \qquad \text{(Equation 2.2)}$$

$$M_{cz} = F_s \frac{d_c}{2} \qquad \text{(Equation 2.3)}$$

where M_{cz} is torque on the droplets during detachment, r_p is the radius of the pore (m), γ is the interfacial tension of the two phases (N m^{-1}), d_c is the droplet diameter before detachment (m) and F_s is the force generated by shear stress (N) defined as

$$F_s = k_{wl}\pi\tau_w d_d \sqrt{(d_c/2)^2 - \left(d_p/2\right)^2} \qquad \text{(Equation2.4)}$$

where the parameter k_{wl} is a viscosity-related factor for the dispersed phase, depends on the viscosity difference between two phases (Keh and Chen, 2001), τ_{w} is the shear stress (Pa) at the membrane surface, d_d is the droplet diameter during detachment (m), d_p is diameter of the pore (m), d_c varies with time but it is limited to $d_p \leq d_c \leq d_d$. From Equations 2.2, 2.3 and 2.4, it is found that:

$$d_c = \frac{\sqrt{18\tau_w{}^2 r_p^2 + 2\sqrt{81\tau_w{}^4 r_p^4 + 4\gamma^2 \tau_w{}^2 r_p^2}}}{3\tau_w} \qquad \text{(Equation 2.5)}$$

The shear stress at the membrane surface is considered to follow Yamamoto's equation (Nagata, 1975), which basically considers different shear regimes in the dispersion cell system shown in Figure 2-7.

$$\tau_w = \begin{cases} 0.825\mu_c \omega r_r \frac{1}{\delta} & , \ r_r < r_{trans} \\ 0.825\mu_c \omega r_{trans} \left(\frac{r_{trans}}{r_r}\right)^{0.6} \frac{1}{\delta}, & r_r \geq r_{trans} \end{cases} \qquad \text{(Equation 2.6)}$$

where μ_c is the viscosity of continuous phase (Pa s), considered constant during the emulsification process, ω is the angular velocity of the stirred impeller (rad s^{-1}), r_{trans} is the transitional radius (m), r_r is the radius from the centre to the point where the shear stress was calculated (m), δ is boundary layer thickness (m).

The transitional radius where the shear stress on the membrane is maximum, as shown in Figure 2-7, was found using (Kosvintsev *et al.*, 2005, Nagata, 1975):

$$r_{trans} = 1.23\frac{Dp}{2}\left(0.57 + 0.35\frac{Dp}{T}\right)\left(\frac{b}{T}\right)^{0.036} n_b^{0.116}\frac{R_e}{1000+1.43R_e} \quad \text{(Equation2.7)}$$

where the Reynolds (*Re*) number and the boundary layer thickness δ are defined as (Kosvintsev *et al.*, 2005):

$$Re = \frac{\rho_C \omega D_p^2}{2\pi\eta_C} \quad \text{(Equation 2.8)}$$

$$\delta = \sqrt{\frac{\eta_C}{\omega\rho_C}} \quad \text{(Equation 2.9)}$$

where ρ_C is the density of continuous phase (kg m^{-3}), *b* is the width of the paddle (m), shown in Figure 2-7.

Several models are considered to simplify the applicable shear stress for the whole dispersion cell setup, following that the local τ_w depends on the individual radial position of each pore.

Model A (Holdich et al., 2010)

This model considers that shear stress along the whole membrane is the maximum possible, corresponding to that at the transitional radius:

$$\tau_w = \tau_{max} = 0.825\mu_c \omega r_{trans}\frac{1}{\delta} \quad \text{(Equation 2.10)}$$

Model B (Holdich *et al.*, 2010)

Model B considers the average shear stress of the whole membrane surface, as follows:

$$\tau_{av} = \frac{6.6}{D_p^2}\mu\omega\frac{1}{\delta}\left\{\frac{r_{trans}^3}{3} + \frac{r_{trans}^{1.6}}{1.4}\left[\left(\frac{Dp}{2}\right)^{1.4} - r_{trans}^{1.4}\right]\right\} \qquad \text{(Equation 2.11)}$$

Model C (Kosvintsev *et al.*, 2005)

Model C, on the other hand, realizes that there are pores in only narrow ring of the membrane, hence it considers for the torque balance equations the average shear stress in the ring area with pores:

$$\tau_{avRING} = \frac{1.65}{R_{out}^2 - R_{in}^2}\mu\omega\frac{1}{\delta}\left[\frac{r_{trans}^3 - R_{in}^3}{3} + \frac{r_{trans}^{1.6}}{1.4}\left(R_{out}^{1.4} - r_{trans}^{1.4}\right)\right] \qquad \text{(Equation 2.12)}$$

where R_{in} is the inner radius of membrane's ring area (m) and R_{out} is the outer radius of membrane's ring area (m).

Model D (Holdich *et al.*, 2010, Schroder *et al.*, 1998, Xu *et al.*, 2005)

The previous models are based on the assumption that a neck is not formed between the droplet and the liquid inside the pore. However, it is observed experimentally that necks are formed during detachment from the membrane surface (Schroder *et al.*, 1998, Xu *et al.*, 2005). Droplet necking was considered in later modelling research,

and simulation results showed better agreement with experimental data compared to the previous models A, B and C (Egidi *et al.*, 2008). When necking is considered in the formation of droplets in a dispersion cell, shown in Figure 2-8(c), the force balance on a single droplet includes the following forces (Charcosset *et al.*, 2004, Hao *et al.*, 2008, Holdich *et al.*, 2010, Schroder *et al.*, 1998, Xu *et al.*, 2005):

Interfacial tension force F_γ, due to the dispersed phase adhering on the pore opening edge:

$$F_\gamma = \pi \cdot d_N \cdot \gamma \quad \text{(Equation 2.13)}$$

Force due to a static pressure difference between the two phases F_{stat}:

$$F_{stat} = \frac{4\gamma}{d_d}\frac{\pi}{4}d_N^2 = F_\gamma \frac{d_N}{d_d} \quad \text{(Equation 2.14)}$$

where d_N represents the diameter of "neck" (m), which is considered to be equal to the diameter of the pore d_p. The force difference of the previous two forces results

$$F_{\gamma-stat} = F_\gamma - F_{stat} = \pi d_p \gamma \left(1 - \frac{d_p}{d_d}\right) \quad \text{(Equation 2.15)}$$

Buoyancy force F_{BG}, resulting from the density difference between the two phases:

$$F_{BG} = (\rho_C - \rho_d) \cdot g \cdot V_d = \Delta\rho \cdot g \cdot V_d \quad \text{(Equation 2.16)}$$

where ρ_d is the density of the dispersed phase (kg m^{-3}), g is the acceleration of gravity (m s^{-2}), and V_d is the volume of droplet (m^3).

Linear momentum force F_l:

$$F_l = \frac{\pi}{4}\rho_d u_d^2 d_p^2 \quad \text{(Equation 2.17)}$$

where u_d is the velocity of the dispersed phase (m s^{-1}).

Dynamic lift force F_{dl} is:

$$F_{dl} = 0.761\frac{\tau_w^{1.5}\cdot d_d^3\cdot \rho_c^{0.5}}{\eta_C} \quad \text{(Equation 2.18)}$$

The drag force F_d caused by continuous phase flow is calculated according to the Stokes law

$$F_d = 3\pi k_{wl}\eta_c v_c d_d \quad \text{(Equation 2.19)}$$

where the viscosity factor k_{wl} is equal to 2.8 for low viscosity oils (dispersed phase viscosity $\mu_d \approx \mu_c$) and 3.5 for high viscosity oils ($\mu_d \geq 10\mu_c$) (Abrahamse *et al.*, 2002, Keh and Chen, 2001). v_c is the velocity of the continuous phase defined as:

$$v_c = \omega\gamma_{trans}(1 - exp\left(-\frac{d_d}{2\delta}\right)) \quad \text{(Equation 2.20)}$$

The push off force F_{push} for the case when $d_d > L$, is given by

$$F_{push} = \frac{1}{2}\frac{\gamma\pi d_d^3 L\, sin^{-1}\left(\sqrt{d_d^6 - L^6}/d_d^3\right)\left(d_d^6 - 2L^6\right)}{\left(d_d^6 - L^6\right)^{3/2}} + \frac{\gamma\pi L^7 d_d^2}{2\left(d_d^6 - L^6\right)\sqrt{L^6/d_d^2}} - \frac{2\gamma\pi L^2}{3d_d} \quad \text{(Equation 2.21)}$$

where L is the gap between pores (m), d_d is the diameter of droplets during detachment (m).

Finally, the torque balance for a detaching droplet with neck formation is:

$$M_{adhesion} = M_{detach}$$

$$(F_{\gamma-stat} - F_{BG} - F_l - F_{dl} - Fpush)\frac{d_p}{2} = F_d\frac{d_p}{2}$$

Therefore the size of droplets can be calculated using:

$$F_{\gamma-stat} - F_{BG} - F_l - F_{dl} - Fpush = F_d \qquad \text{(Equation 2.22)}$$

When $d_d > L$, the equation is simplified to:

$$\pi d_p \gamma\left(1 - \frac{d_p}{d_d}\right) - \Delta\rho \cdot g \cdot V_d - \frac{\pi}{4}\rho_d u_d^2 d_p^2 - 0.761\frac{\tau_w^{1.5} \cdot d_d^3 \cdot \rho_c^{0.5}}{\eta_c} = 3\pi k_{wl}\eta_c v_c d_d$$

(Equation 2.23)

The size and distribution of the droplets prepared by membrane emulsification are influenced by several parameters, including:

- Membrane configuration: the pore size of the membrane, the gap between the pores, the shape of the pore opening, the membrane surface porosity, the membrane thickness and the membrane surface energy (e.g. as determined from contact angles) (Abrahamse *et al.*, 2002, Boom, 2003, Ma, 2003).

- Process parameters: Trans-membrane pressure of the dispersed phase flux, shear stress (cross flow velocity or stirring speed) and the operation temperature (Ibrahim and Nienow, 2004, Kukizaki, 2009, Peng and Williams, 1998a, Peng and Williams, 1998b).

- Phase parameters: interfacial tension, viscosity (ratio) and density of both phases (Abrahamse *et al.*, 2002, Boom, 2003, Charcosset, 2009, Charcosset *et al.*, 2004).

2.4 Encapsulation techniques

Microcapsules can be prepared using different methods including chemical processes, physico-chemical processes and mechanical processes, which are discussed in the following sections.

2.4.1 Chemical processes

Polymerization and polycondensation processes are the main chemical methods to manufacture microcapsules (Arshady, 1999). Depending on the core materials, emulsion, suspension or dispersion are generated first, followed by polymerization or polycondensation. The polymerization process can be also referred to *in situ* polymerization or interfacial polymerization (Arshady, 1999).

❖ *In situ* polymerization

It is the process in which the microcapsule shell is formed from the chemical precursors (monomers or precondensates) that react at the interface of the emulsion phase. The reactants are initially soluble in the continuous phase, while the core material is contained in the dispersion phase (as droplets). As the polymerization reaction starts, the insoluble oligomers begin to form at the interface between the core

droplets and the continuous phase. As the reaction proceeds, a solid shell forms covering all the core, forming a microcapsule (Figure 2-9).

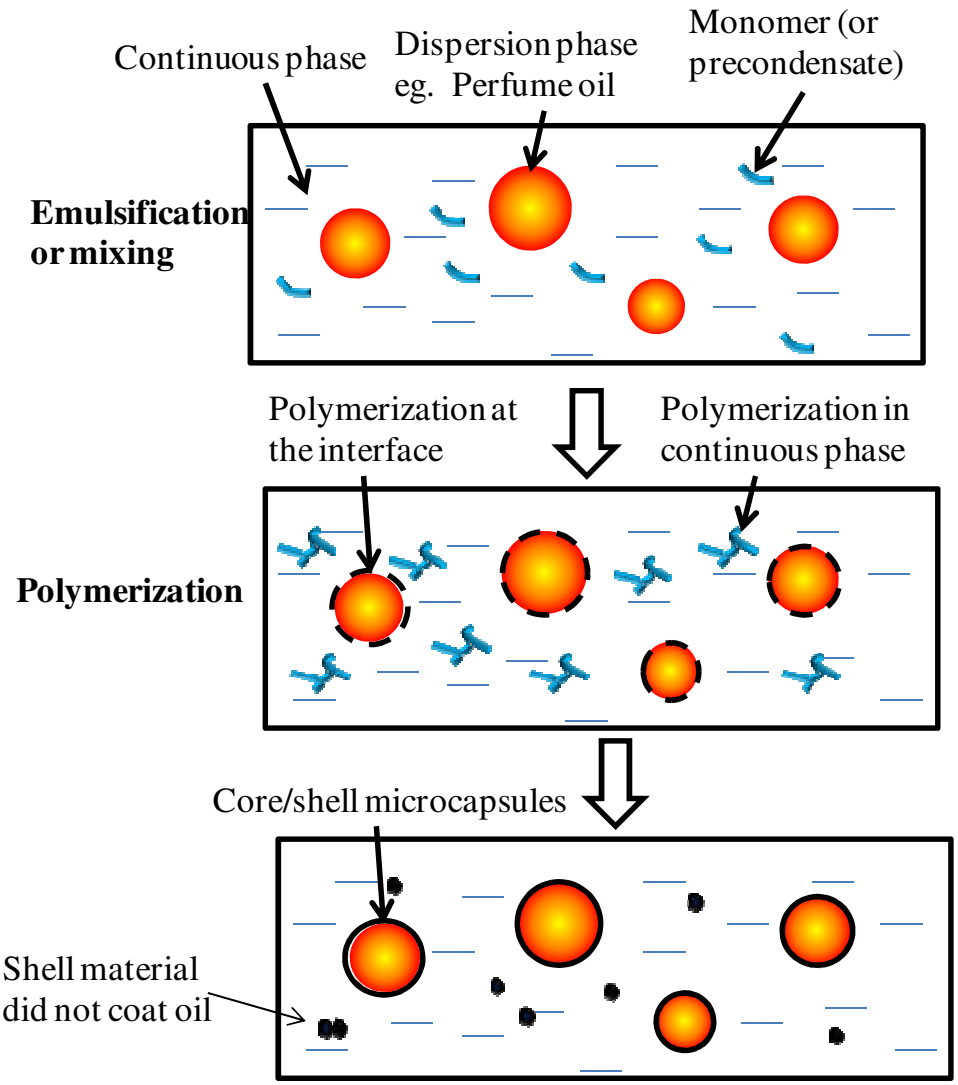

Figure 2-9 Schematic microencapsulation process based on *in situ* polymerization.

In situ polymerization needs a relatively short shell-forming time. In *in situ* polymerization the resultant shell thickness is generally much smaller compared to the capsule diameter (Arshady, 1999, Freiberg and Zhu, 2004), which does not waste the

shell materials (Zhang and Wang, 2009). It is possible to control the size and size distribution of microcapsules by controlling the emulsion droplets. It is a process suitable to prepare various kinds of microcapsules, including the encapsulation of perfume oils (Arshady, 1999, Ghosh, 2006a). Aminoplast based resins are the most common materials used for *in situ* polymerization. Urea-formaldehyde (Jo *et al.*, 2011, Saeki *et al.*, 1981) or melamine-formaldehyde (Hong and Park, 1999b, Long *et al.*, 2009, Sinclair, 1981) systems are examples of encapsulation by *in situ* polymerization. Figure 2-10 shows a typical process to prepare microcapsules consisting of a MF shell and a perfume oil core via *in situ* polymerization (Long *et al.*, 2009).

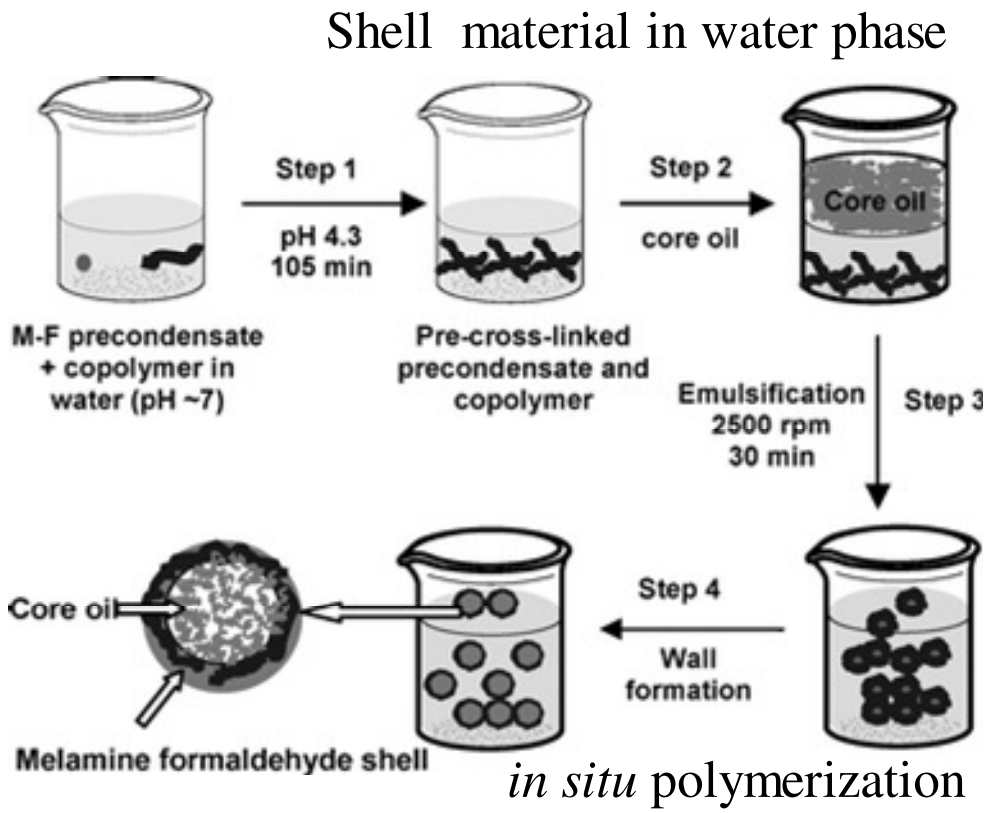

Figure 2-10 The schematic diagram showing an *in situ* MF polymerization process to encapsulate a perfume oil (Long *et al.*, 2009).

2.4.2 Physico-chemical processes

Physico-chemical encapsulation processes involve the formation of the shell materials through heat, changes in pH value or addition of electrolytes (Umer *et al.*, 2011) resulting in:

- Solvent evaporation/phase separation (Zydowicz *et al.*, 2002)
- Coacervation (simple, complex and organic) (Xu *et al.*, 2006, Zuidam and Shimoni, 2010)

2.4.3 Mechanical processes:

Polymeric materials are typically used in these methods where no chemical reactions are involved (Dubey *et al.*, 2009). Typical mechanical encapsulation processes are:

- Fluidized bed coating (Jono *et al.*, 2000, Zuidam and Shimoni, 2010)
- Spray drying, spray cooling/chilling (Edwards and Instone, 2001, Zuidam and Shimoni, 2010)
- Rotational suspension separation (spinning disk) (Gouin, 2004)
- Extrusion/dripping (Barbosa-Cánovas *et al.*, 2005, Xie *et al.*, 2008, Xu *et al.*, 2006)
- Supercritical carbon dioxide processing (Hertz *et al.*, 2006)

2.5 Shell materials

The selection of the shell material is crucial in order to develop a successful microencapsulation process. There are several factors that should be considered in the shell selection process:

- The shell should be compatible with the active ingredients to be encapsulated.
- The shell material has suitable mechanical properties and stability.
- The initial formulation and the final product should be safe and non-toxic.
- The process should be scalable easily and at low cost.

2.5.1 Melamine-formaldehyde

Melamine-formaldehyde (MF) resin is one of the predominant commercial shell materials for the manufacturing of perfume microcapsules (Hunt and O' Neil, 2004, Hwang *et al.*, 2006a, Hwang *et al.*, 2006b, Long *et al.*, 2009, Monllor *et al.*, 2007, Pluyter and Anastasiou, 2006). MF has considerable stability in many consumer products (Li *et al.*, 2007a, Okano and Ogata, 1952) and appropriate strength (Sun and Zhang, 2001, Sun and Zhang, 2002), can resist water, acid and alkaline conditions to

great extents (Li *et al.*, 2007a, Okano and Ogata, 1952) and it is fairly inexpensive for industrial applications (Arshady, 1999, Pretzl *et al.*, 2012).

2.5.1.1 Chemical structure of melamine-formaldehyde precondensate

Since it was first discovered by Liebig in 1834, as mentioned by Bone *et. al* (2011), the MF polymerization reaction has been the focus of many studies (Bauer, 1986, Okano and Ogata, 1952, Sato, 1968, Vo *et al.*, 2008, Wang *et al.*, 2009). The polymerization reaction is controlled by the temperature and pH (Berge *et al.*, 1969, Berge *et al.*, 1970). At a temperature around 65°C, melamine (1,3,5-triamino-2,4,6-triazine) (M) and formaldehyde (F), shown in Figure 2-11, first pre-cross-link to form a MF precondensate.

MF precondensates are commonly used as a starting material for encapsulation applications because monomeric melamine has a low solubility in water (Gattner and Ribka, 1975). In addition, as they are used for many other industrial applications, MF precondensates are commercially available. There are several choices of commercial MF precondensate, such as Hilamin M562® (Dynea, Krems, Austria) (Gindl *et al.*, 2003), Melapret NF70/M® (Kočevje, Slovenia) (Alic *et al.*, 2012), Beetle resin PT336® (BPI, UK) (Hunt and O' Neil, 2004, Long *et al.*, 2009) and Cytec 385® (Cytec, USA) (Bobnock *et al.*, 2010). These MF precondensates have various F/M

molar ratios (Kumar and Katiyar, 1990). Figure 2-12 depicts some examples of typical chemical structures of MF precondensates originating from the condensation step using only high temperatures (Lee *et al.*, 2001, Vo *et al.*, 2008, Yuan *et al.*, 2007). In acid conditions, at pH values of 2-4, the MF precondensates further react to form a MF resin (Lee *et al.*, 2001) (Figure 2-13).

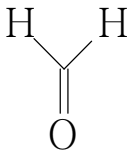

(a) formaldehyde

molecular weight: 30.03

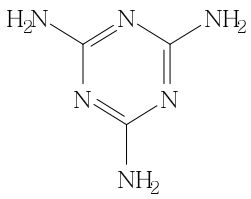

(b) melamine

molecular weight: 126.12

Figure 2-11 Chemical structures of melamine and formaldehyde.

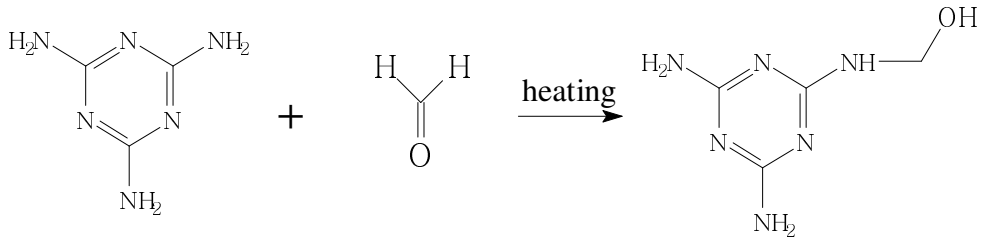

M F methylolmelamine
(molecular weight: 156.15)

M/F = 1:1

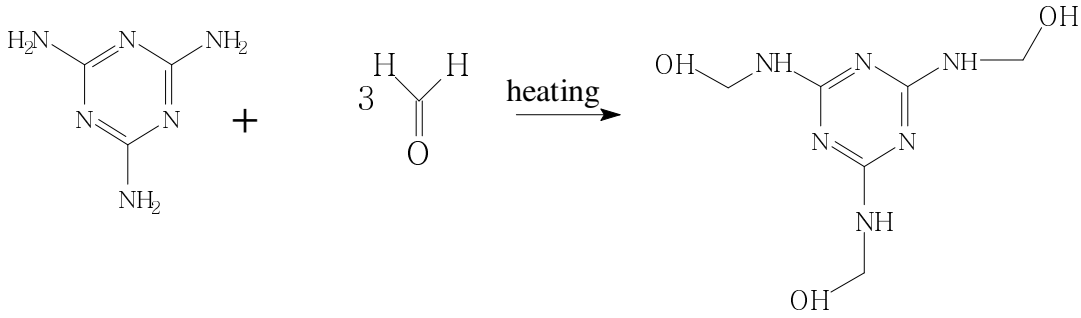

M F tri-methylolmelamine
(molecular weight: 216.20)

M/F = 1:3

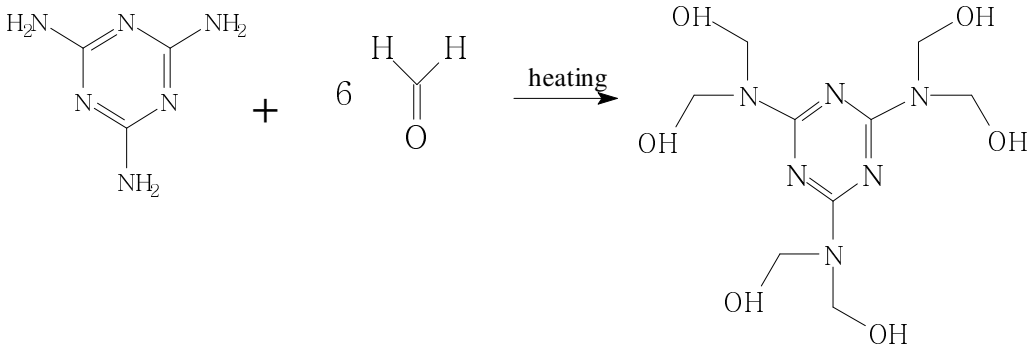

M F Hexamethylolmelamine
(molecular weight: 306.28)

M/F = 1:6

Figure 2-12 Schematic representation of classical MF precondensate products from the condensation of MF reaction with different M/F ratios.

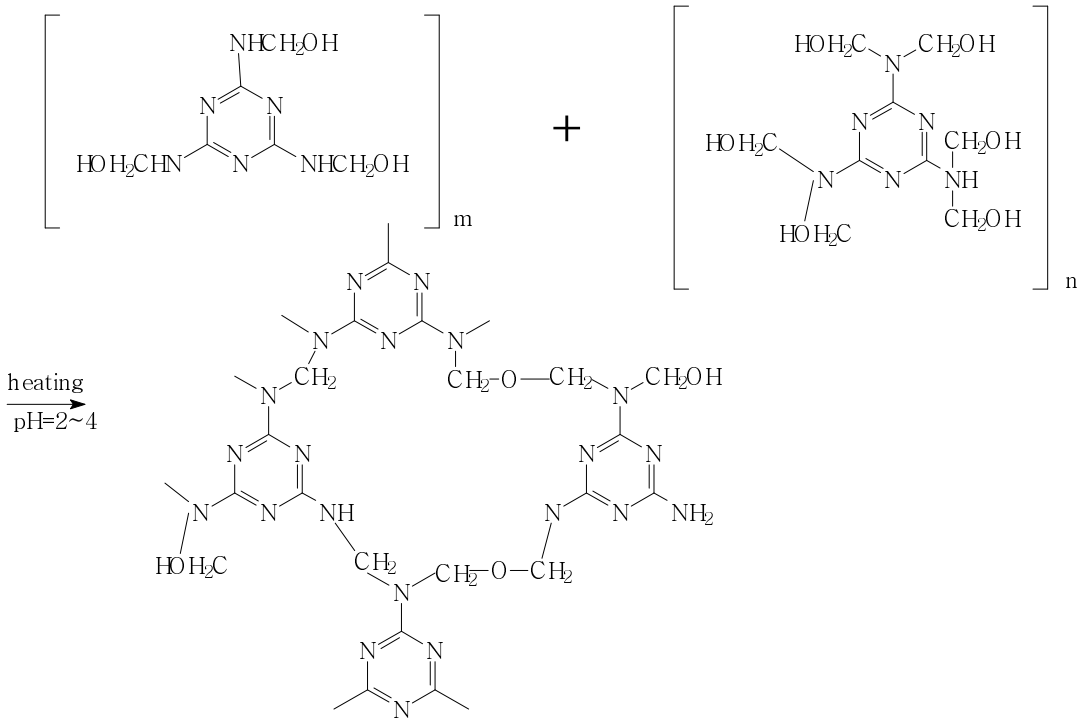

Figure 2-13 Mechanism of polymerization to form melamine formaldehyde resin in acid condition (Yuan *et al.*, 2007).

2.5.1.2 Applications of melamine-formaldehyde microcapsules

After over 70 years of commercial use (Bone *et al.*, 2011, Gindl *et al.*, 2003), MF resins have found a great number of applications as a shell material in products such as flame retardants (Luo *et al.*, 2007), phase change materials (Choi *et al.*, 2001, Li *et al.*, 2007b, Li *et al.*, 2007c), self-healing materials (Hu *et al.*, 2009, Yuan *et al.*, 2007, Yuan *et al.*, 2008b), pigments or dye (Seitz, 1990, Seitz, 1993) and also fragrances (Hong and Park, 1999a, Hwang *et al.*, 2006a, Hwang *et al.*, 2006b).

In 1971 MF microcapsules with a core organic oil were for the first time patented by Ciba company (Schibler, 1971); the same year, Fuji applied MF to encapsulate pigments (Masataka and Yasuhiro, 1976). Two years later NCR used MF resin to encapsulate ink (Foris *et al.*, 1978). A significant commercial success for MF microcapsules came when the companies Appleton and The Wiggins Teape Group Limited (WTG) developed pressure sensitive MF microcapsules to produce carbonless copy paper (Hayford, 1984, Sinclair, 1981). In addition, there are many patented work on MF microcapsules related to the encapsulation of fragrances, summarized in Table 2-1.

Table 2-1 Patented manufacturing processes on the microencapsulation of fragrances using MF for consumer product applications.

Year	Company	Description
1991 (Walley *et al.*)	Procter & Gamble (P&G) and Minnesota Mining & Manufacturing Innovative Properties Company (3M)	Fragrance microcapsules made with MF used in softeners.
1996 (Kukovič and Knez)	Aero, Kemicna, Graficna in Papir na Industrija, D.O.O.	Preparation of MF or urea–formaldehyde (UF) microcapsules to encapsulate scents (eg. essential oils) for the footwear industry.
2003 (Jahns *et al.*)	BASF	Preparation of MF microcapsules to encapsulate perfume oils for detergents or cleaning agents.
2003 (Ness), 2007 (Ness)	Quest International B.V.	Perfume encapsulated in aminoplast (MF or UF) with a copolymer, which may be use in aqueous environment.
2003 (Uchiyama *et al.,* Uchiyama *et al.*)	P&G	MF or UF microcapsules with odour control agents used in consumer products.

Year	Company	Description
2004 (Arellano and Vazquez)	3M	Abrasive particles and a "fresh" scent contained in urea-formaldehyde used in cosmeto-textiles.
2005 (Chevalier *et al.*)	L'Oreal	MF or UF microcapsules with cosmetic ingrediens.
2004-2005 (Bennett and Brain, Lee and Popplewell, Popplewell *et al.,* Popplewell *et al.*), 2006-2007 (Anastasiou *et al.,* Lee *et al.,* Popplewell *et al.*) (Colt *et al.,* Parekh *et al.*)	International Flavours & Fragrances Inc. (IFF)	MF or UF microcapsules used in personal care products to keep fragrances stable.
2005-2007 (Colt *et al.,* Parekh *et al.,* Pluyter and Anastasiou)	IFF	Pressure sensitive MF microcapsules containing fragrance used in freshening fabric.
2006 (Holzner and Verhovnik)	Firmenich S. A.	Fragranced aminoplast microcapsules for consumer products.

Year	Company	Description
2007 (Aussant *et al.*), 2008 (Aussant *et al.*), 2011 (Aussant *et al.*)	Takasago International Corporation	MF microcapsules with a core made of liquid oils or waxy solids for liquid consumer products.
2007 (St. Laurent *et al.*), 2008 (Bodet *et al.,* Bodet *et al.*), 2011(Aouad, Aouad, Denutte *et al.,* Smets *et al.,* Smets *et al.*), 2012 (Clare *et al.*)	P&G	Preparation of MF microcapsules with perfume oils for detergents and other laundry products.
2008 (Cavin *et al.*), 2009 (Quellet and Hotz)	Givaudan S. A.	Preparation of microcapsules comprising a core of fragrance and a shell of aminoplast polymer used in laundry and fabric care products
2012 (Ferguson and Jones)	Unilever	Preparation of MF microcapsules with perfume oil for detergents or fabric products.

2.5.1.3 Limitation of melamine formaldehyde

Although MF microcapsules have many commercial advantages, there are unavoidable health and safety concerns due to the use of formaldehyde. Formaldehyde is a well-known human carcinogen (Cole *et al.*, 2010, Hernandez *et al.*, 1994, Lazenby *et al.*, 2012, Yepes and Cremades, 2011). In addition, it also causes indoor air pollution (Kelly *et al.*, 1999, Li *et al.*, 2007b), which increases the chance for children to have allergy (Garrett *et al.*, 1999). Furthermore, there are safety concerns and many precautions have to be taken during manufacturing and processing (Nesic *et al.*, 2010), as well as to the potential release to the environment. In 1973 Japan was the first country that passed a law controlling harmful substances in household products (Sumiga *et al.*, 2011), including formaldehyde. At present, most European countries and some Asian countries allow very limited amounts of formaldehyde in consumer products (Sumiga *et al.*, 2011). The Oeko-tex standard 100 and EU eco label clearly define that the maximum amount of free formaldehyde in infant clothes is 20 ppm and 30 ppm for all other textile products (Sumiga *et al.*, 2011). For this reason, extensive research has been conducted on reducing the formaldehyde residue in MF microcapsules (Bone *et al.*, 2011, Frank *et al.*, 2001, Li *et al.*, 2007a, Su *et al.*, 2007, Su *et al.*, 2011, Zhang and Wang, 2009). For example, the companies WTG (Moira, 1986), P&G (Bodet *et al.*, 2008b), BASF (Frank *et al.*, 2001, Hoffman and Eisermann, 2003), IFF (Anastasiou *et al.*, 2007b), NAICOM (Karyakin *et al.*, 2012) and Givaudan (Quellet and Hotz, 2009) all have patents on

"formaldehyde-free" MF microcapsules. In the case of Givaudan, it has declared that the amount of formaldehyde in their final products must be much lower than 50 ppm after storage (Bone *et al.*, 2011).

Consumer and institutional pressures are nevertheless leading to the complete removal of cancer-inducing chemicals from consumer products, despite being present at lower concentrations than required by regulations. Although the amount of free formaldehyde in the final product is very small, there is a still the concern of a gradual slow release from the polymerized product during storage (Long *et al.*, 2009). Some companies have been addressing this issue of using formaldehyde in consumer product, such as Johnson & Johnson, by phasing out all carcinogens altogether from their products (Brian, 2012). From this point of view, it is clear that new shell materials are needed instead of MF to encapsulate perfume oils.

These new shell materials ought to be environmentally friendly and safe to use in consumer products. Like MF, they should also present good mechanical properties and chemical stability. There are many shell materials which have recently been used to encapsulate perfume oils for textile applications. Some natural materials, such as β-cyclodextrin (Wang and Chen, 2005), chitosan (Hu *et al.*, 2011) and bovine serum albumin protein (Tzhayik *et al.*, 2012) are environmental friendly but expensive. Polymeric materials have also been used to coat perfumes. Examples include polysulfones, with a good high mechanical strength but low stability (Pena *et al.*, 2012); polyurethanes-urea, chemical stable but toxic (Rodrigues *et al.*, 2009, Teixeira

et al., 2012b); polyamides, good mechanical properties but they absorb large amounts of water (Arshady, 1989, Ichiura *et al.*, 2012). Framed within the growing industrial need to find suitable materials to encapsulate perfume oils, the potential use of poly (methyl methacrylate) (PMMA) is analysed in the next section.

2.5.1.4 Poly (methyl methacrylate) (PMMA)

PMMA is a polymer with excellent properties, such as good mechanical strength and chemical resistance (Rasmussen, 2001). In addition, it is environmentally friendly and non toxic (Rasmussen, 2001). PMMA has already found diverse applications as a coating material, from the encapsulation of liquid crystals (Cho *et al.*, 2002, Ju *et al.*, 2002, Park *et al.*, 2002, Ryu *et al.*, 2004), to phase change materials (Alay *et al.*, 2011, Zhang and Rochefort, 2012, Zhang *et al.*, 2012), dyes (Zydowicz *et al.*, 2002), self-healing materials (Nordstierna *et al.*, 2010), active ingredients for pharmaceutical applications (Bakeine *et al.*, 2007, Kim *et al.*, 2004, Lee *et al.*, 2007a) as well as fragrances (Jafari *et al.*, 2007, Kantor *et al.*, 1997). Jafari (2007) described a phase separation method to coat perfume oils, resulting in microcapsules of around 400 nm that would subsequently aggregate forming 40 μm granules. Emisphere technology Inc. patented a method to coat perfume oil by PMMA polymerization (Kantor et al., 1997).

There are a variety of polymerization routes to synthesize PMMA. One of the most common synthesis is based on the free radical polymerization of methyl methacrylate (MMA) (Ramelow and Pingili, 2010, Rasmussen, 2001). Azobisisobutyronitrile (AIBN) is commonly used as catalyst to speed up the reactions in MMA polymerization. The polymerization steps to form PMMA from MMA using AIBN as a trigger and ethylene glycol dimethacrylate (EGDMA) as a cross-linker is illustrated in Figure 2-14 (Ramelow and Pingili, 2010, Rasmussen, 2001).

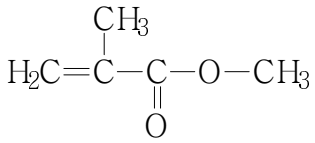

MMA

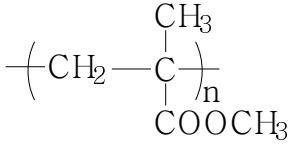

PMMA

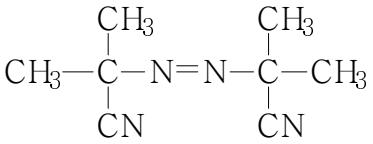

AIBN

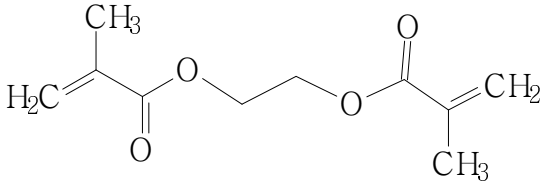

EGDMA

(a). Chemical structure of MMA, PMMA, AIBN and EGDMA.

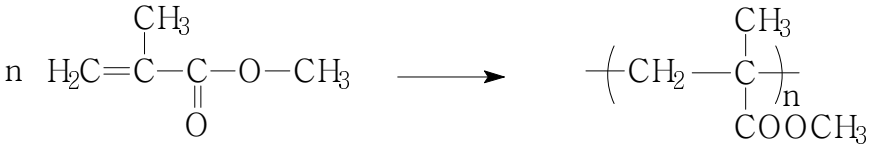

(b). polymerization of MMA monomer, which must be activated by a driving force

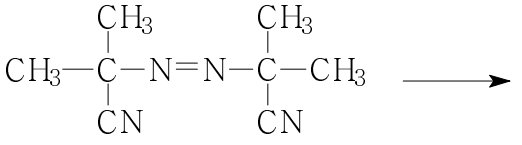

AIBN

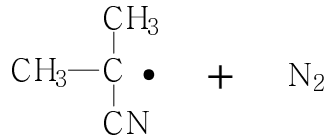

initiator radical

(c). formation of initiator radical

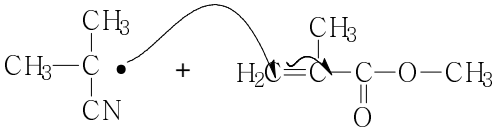

MMA

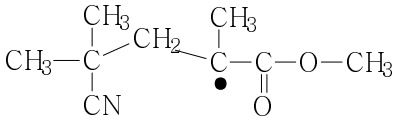

Growing MMA radical chain

(d). growth of MMA radical chain

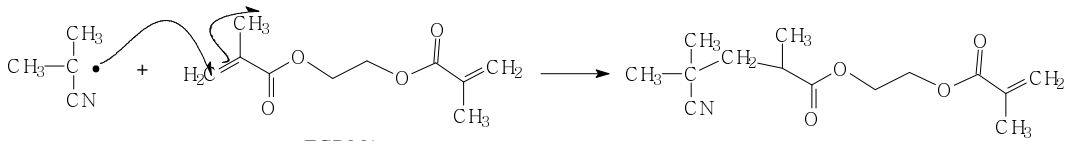

(e). growth of EGDMA radical chain

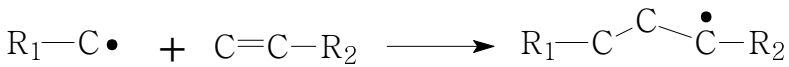

Radical growth of MMA and EGDMA

Figure 2-14 Mechanism of MMA free radical polymerization (Rasmussen, 2001).

PMMA is widely used to make microcapsules in industry. Several methods have been reported to prepare PMMA microcapsules, such as polymerization (emulsion polymerization) (Chang *et al.*, 2009, Kim *et al.*, 2003, Sari *et al.*, 2009), seeded suspension polymerization (Taguchi *et al.*, 2007) and surface-initiated photo polymerization (Chen *et al.*, 2011)), solvent evaporation (Lee *et al.*, 2007a, Loxley and Vincent, 1998, Xu *et al.*, 2008, Zydowicz *et al.*, 2002) and supercritical carbon dioxide processing (Hertz *et al.*, 2006). These methods produce microcapsules which have either wide size distributions (Chang *et al.*, 2009) or they involve complex reaction conditions, such as using seed particles (oil absorbable polymer particles (Taguchi *et al.*, 2007), $CaCO_3$ particles (Sato *et al.*, 2012), latex particles (Yuan *et al.*, 2010a)), supercritical carbon dioxide (Hertz *et al.*, 2006) or using nitrogen gas (Sari *et al.*, 2009), which can be expensive to scale up for industrial production.

2.6 Characterization of microcapsules

The detailed characterization of manufactured products is essential for successful formulation, and the same principle applies to perfume microcapsules. The performance of perfume microcapsules will depend on many parameters, from extrinsic parameters like their size, to intrinsic parameters like the shell permeability and mechanical strength. This section reviews common techniques previously used to

characterize microcapsules. However, it must be emphasized that due to the primarily commercial application of perfume microcapsules, there are not clear performance indicators that can be used by independent researchers to evaluate microcapsules. This kind of information, if it exists, is kept secret by the different companies involved in the trade, public information is scarce and ambiguous.

2.6.1 Determination of size and size distribution

The size and the size distribution of emulsion droplets and microcapsules are basic physical properties. Commercially available particle sizing methods used in research and industry are summarized in Table 2-2 (Webb, 2000). Among all these techniques, microscopy combined with image analysis (Aryanti *et al.*, 2009), laser diffraction (Zhang *et al.*, 2008, Zhou *et al.*, 2009) and sieving and screening (Ichikawa and Fukumori, 2000) are well established and widely reported in literature work for measuring size and size distribution of microcapsules.

Sieving is a simple well-established technique which has been used for particle separation as well as particle sizing. It is suitable to determine size and size distribution of dry or wet microcapsules with size ranges from microns to millimetres. However, it is more commonly used to measure solid particles than droplets and in most cases the resolution is poor (Malvern instruments limited, 2012). Laser

diffraction is a rapid and robust technique for quantifying the size and size distribution of droplets and microcapsules with a spherical shape. Most instruments measure tens of thousands of microcapsules within a couple of seconds. It covers a wide range of particle sizes, typically from 0.02 to 2000 μm, and the results have a high resolution and repeatability. It has been widely used in research as well as in industry to measure polymeric particles (Salgi and Rajagopalan, 1993, Zhou *et al.*, 2007), foams (Pugh, 2005), emulsion droplets (Zhang *et al.*, 2008) and biomaterials (Godderz *et al.*, 2005). The operating principle is described in Chapter 3.

Table 2-2 Techniques for characterizing particle sizes (Webb, 2000). The techniques mentioned in texts are framed in the table.

Microscopy Methods	
	Optical Microscopy and Imaging Analysis
	Transmission Electron Microscopy
	Scanning Electron Microscopy
	Atomic Force Microscopy
Light Interaction Methods	
	Laser Diffraction
	Photon Correlation Spectroscopy
	Single Particle Light Scattering
	Multi-Angle Light Scattering
	Single Particle light Obscuration
	Time of Flight
	Fiber Optic Doppler
	Anemometry (FODA)
Electrical Property Methods	
	Coulter (Electro zone) Principle
	Differential Mobility Analyzer (DMA)
	Zeta Potential
Sedimentation Methods	
	Photo sedimentation
	Centrifugal Sedimentation
	X-ray Sedimentation
Sorting and Classification Methods	
	Fluorescence Activated Cell Sorting
	Field Flow Fractionation (FFF)
	Sieving and Screening
	Air Classification

Microscopy or SEM combined image analysis (or automated image analysis) is another commonly used technique for the determination of microcapsules or droplets size. It is possible to determine the shape and morphology at the same time, and is particularly suitable for non-spherical particles. Furthermore, it can provide specific shape parameters that can be used, for example, to detect agglomeration. Compared with laser diffraction, most of microscopy or SEM combined image analysis are time consuming for investigating a large number of microcapsules (Malvern instruments limited, 2012, Malvern Instruments Ltd, 2007, Sympatec, 2012).

2.6.2 Measurement of the mechanical strength of single microcapsules

As mentioned in Section 2.4, the mechanical properties of microcapsules should be considered in many applications. For instance, the mechanical properties may also affect the adhesion properties of microcapsules (Fery and Weinkamer, 2007), as well as the shell permeability (Stenekes *et al.*, 2000). Knowing the mechanical properties of microcapsules can help formulators in selecting the right material for specific applications.

There are several techniques described in the literature to characterize the mechanical properties of microcapsules. Some techniques involve the characterization of whole populations of microcapsules, examples include compression of a layer of

microcapsules between two parallel plates (Ohtsubo *et al.*, 1991) or against a fixed balance (Taguchi and Tanaka, 2001, Taguchi *et al.*, 2007), determination of the breakage of microcapsules with a fixed shear force (Peirone *et al.*, 1998, Yin *et al.*, 2003), agitating microcapsules in a tube with glass beads (Leblond *et al.*, 1996) and by osmotic pressure shocks (Vinogradova, 2004, Zhang and Wang, 2009).

Other techniques are based on the determination of the mechanical properties for individual microcapsules. These techniques not only allow the determination of average population values, but can measure the variability of the mechanical properties, essential to analyse the performance perfume microcapsules.

The most common methodology to analyse individual microcapsules is by compressing them between two very small parallel plates. The technique was first developed in Japan to test rupture force of sea urchin eggs (Hiramoto, 1963). The compression force between the plates is measured with force transducers (Taguchi and Tanaka, 2001) or with a balance (Gaumann *et al.*, 2000).

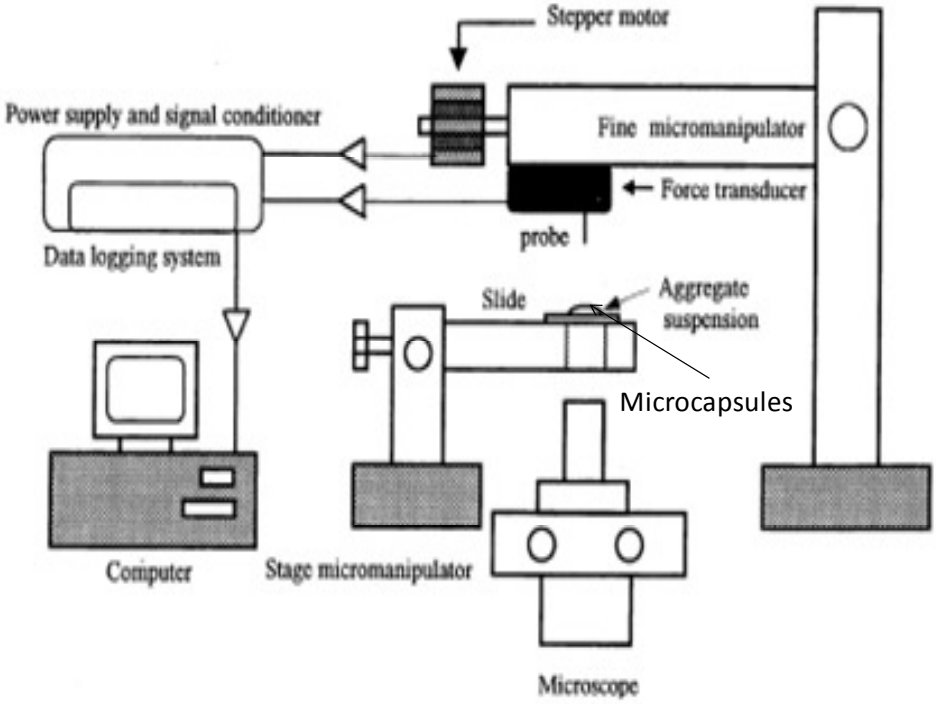

Figure 2-15 A typical schematic diagram of the mechanical measurement using micromanipulation rig (Sun and Zhang, 2001).

This technique has been extensively used by Zhang *et al.* (1991, 1999b, 2009a), termed compression testing by micromanipulation, has been used test individual cells (Zhang *et al.*, 1999a, Zhang *et al.*, 1992), microcapsules (Long *et al.*, 2009, Sun and Zhang, 2001, Sun and Zhang, 2002) or beads (Xue and Zhang, 2009, Yan *et al.*, 2009) (Figure 2-15). A thin glass probe attached to a force transducer is used to record the compression force at different times. Time is then converted to displacements and to actual deformation values using the compression speed and the transducer compliance (Liu, 2010). Nano-particles can also investigated by using a similar nano-manipulation technique but using Environmental Scanning Electron Microscopy

(ESEM) to monitor the testing (Liu *et al.*, 2005b, Ren *et al.*, 2007). The micromanipulation apparatus can perform different kind of experiments such as loading and unloading, compressions at different speeds, and compression until rupture (Hu et al., 2009, Sun and Zhang, 2001).

A critical and difficult part is to determine the mechanical properties from the experimental force-displacement data; this is valid for the micromanipulation as well as for other techniques. This is usually solved with a reverse engineering approach: analytical models or simulations are performed at different initial conditions, for example at different Young's modulus, obtaining force-deformation curves to which the experimental ones are compared.

Intrinsic mechanical properties of microcapsules, such as the Young's modulus and failure stress are fundamental properties of their materials. However, little has been done in past studies. Recently, the intrinsic mechanical properties have been determined for thin-shell microcapsules using a micromanipulation rig and finite element modelling (FEM) (Mercade-Prieto *et al.*, 2012a, Mercade-Prieto *et al.*, 2011a).

2.6.2.1 Control of microcapsule size and strength distribution

In many industrial applications microcapsules should have a specific size and mechanical strength for a consistent performance. In particular, microcapsules containing perfume oil should be strong enough to remain intact during manufacturing and further processing, such as pumping and mixing, to maintain long term stability. But at the same time, they should be weak enough in order to be ruptured when desired, particularly for triggered release applications by mechanical forces (Haefliger *et al.*, 2010). A narrow size distribution has been demonstrated to lead to a narrow rupture strength distribution, demonstrated recently for MF microcapsules (Hu et al., 2009, Pretzl et al., 2012), as there is a well known correlation between the size and the rupture force for MF microcapsules (Figure 2-16) (Hu *et al.*, 2009).

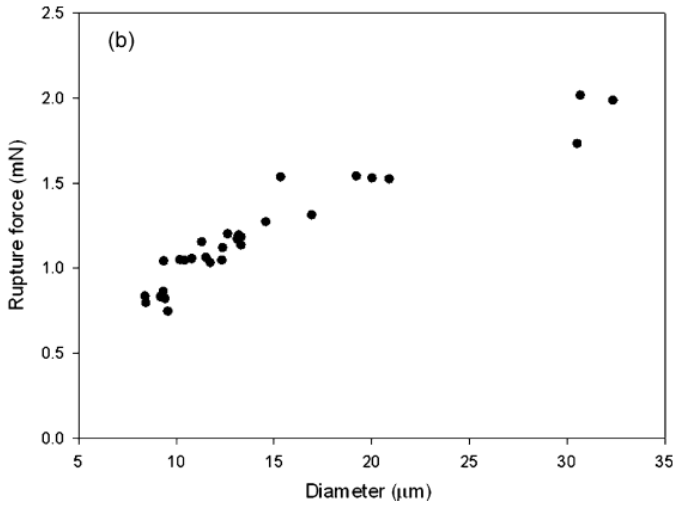

Figure 2-16. The relationship between the rupture force and diameter for MF microcapsules (Hu *et al.*, 2009).

Perfume microcapsules applied to detergents or softeners should survive in all processing steps from manufacturing to washing, after drying when deposited on fabric surface after washing, and until being ruptured by mechanical rubbing (Specos *et al.*, 2010). Another example are perfume microcapsules used in the paper industry for advertisement magazines, books or catalogues (Schaab and Tararuj, 1988). Figure 2-17(a) shows an example where perfume microcapsules are prepared and dried into powder, then printed inside a fold flap. The microcapsules need to be stable inside the flap, during the printing process, transportation and storage. When the flap is opened, the microcapsules rapture and the perfume is set free (Figure 2-17). Another highly successful application is typically known as "stretch-and-sniff ", used since the 1970's, whereby encapsulated scents printed in a paper are released by the active rubbing (Nelson, 2002). An example of this technology used in a commercial advertisement is given Figure 2-17(b).

A broad size distribution of microcapsules should be avoided, which is difficult for an industrial product. Homogenization or agitation are generally applied in consumer manufacturing production and provide relatively wide distributions compared with other emulsification methods, such as, membrane and micro-channel emulsification, as mentioned in Section 2.3.2 (Sgraja *et al.*, 2008, Wang *et al.*, 2009). Therefore, it is

seen as potentially advantageous to prepare microcapsules with a narrow size distribution, which may lead to narrow strength distributions.

(a) (b)

Figure 2-17 Examples of perfume microcapsules applied in papers. (a) Microcapsules rupture and release the fragrance after opening a folded flap. (b) Microcapsules rupture after scratching.

For many other applications, as in consumer care (Nazir *et al.*, 2011), chromatography (Zhou *et al.*, 2007), and pharmaceutics (Liu *et al.*, 2005a), a narrow size distribution of microcapsules is also desirable. For example, a pre-defined size and uniformity were demonstrated to be required in an innovative functional textile product with prolonged release properties (Hu *et al.*, 2012, Hu *et al.*, 2011). It was found that microcapsules with specific diameters could fix firmly within the pores of cotton fibres (Hu *et al.*, 2011) or yarns (Mercadé-Prieto *et al.*, 2012a). In microcapsules used for medical applications, a narrow size distribution can avoid side effects, such as blocking blood vessels (Salentinig *et al.*, 2008)), and have a better targeting ability

and control release behaviour (Freiberg and Zhu, 2004), since the rate of active release is proportional to the surface area of the microcapsules (Sawalha *et al.*, 2008). Moreover, from a characterization point of view, a narrow size distribution can help to determine their intrinsic properties and increase reproducibility (Liu *et al.*, 2005a, Wang *et al.*, 2006). For example, in release experiments to determine the shell permeability, microcapsules with a narrow size distribution are desirable to avoid poly-dispersity effects (Mercade-Prieto *et al.*, 2012b).

2.6.3 Release tests and shell permeability

The purpose of the microcapsule shell is to act as a barrier between the core and the capsule environment. For this reason, it is important to know the barrier properties of the shell as they will determine the release of the core. The release rate of a liquid active ingredient may be controlled by the diffusion inside the microcapsules, within the shell or by the mass transfer from the shell to environment; release can also be affected by the swelling or degradation of the shell (Zhang *et al.*, 2010). In order to predict the perfume release rate, the mass transfer mechanism of microcapsules containing perfume needs to be characterized. Laundering or rubbing tests (Erkan *et al.*, 2010, Monllor *et al.*, 2007) or weight loss test (Hwang *et al.*, 2006b) were applied in industrial trials for quantifying perfume release rate.

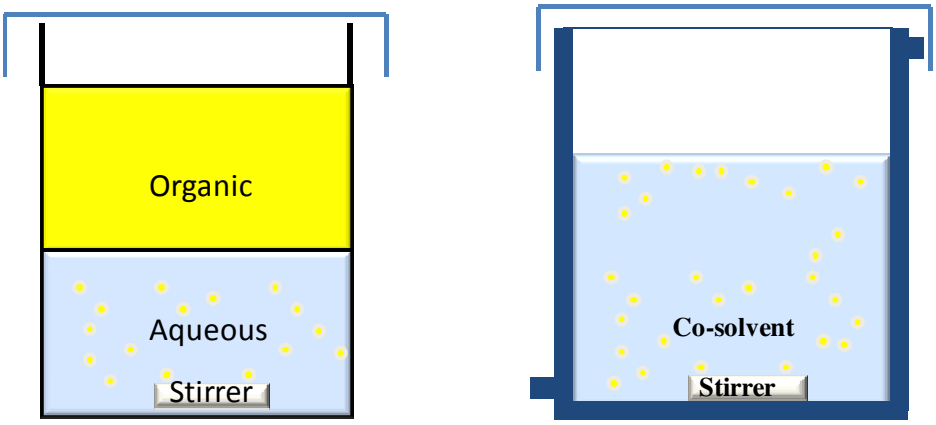

(a) (b)

Figure 2-18 Release experiments for perfume microcapsules. (a) Microcapsules are suspended in water; the perfume oil is quantified in the organic solvent above the aqueous solution. (b) A co-solvent is used in the aqueous phase with the microcapsules to avoid the mass transfer through a liquid-liquid interface as in (a).

One of the ways to test the release of perfume microcapsules is to add a slurry of microcapsules into a certain release solution, in most cases an aqueous solution with a fixed volume (Park *et al.*, 2005). Perfume oil is only partially dissolved in the solution typically due to poor solubility in water. Release is enhanced by adding an organic phase on top as shown in Figure 2-18(a), extracting the perfume oil from the aqueous phase. Hexane is commonly used as the organic phase because it is a good solvent to many chemicals found in perfumes. The oil concentration in the organic solvent is then evaluated, for example using gas chromatography (Long *et al.*, 2009), in order to calculate the oil release.

This methodology can be applied in some cases to compare the relative release of different microcapsules, but it cannot provide information of the intrinsic barrier properties of the shell. As mentioned above, many perfume ingredients are poorly soluble in water, resulting in a very slow solubilisation process that is not related to the barrier properties of the shell (Mercade-Prieto *et al.*, 2012b). In addition, the extraction step to the organic phase is controlled by the mass transfer in the inter-phase. Due to the limited agitation possible, and due to the small contact area, this step can be very slow. Therefore, the release rate measured in the organic phase includes many other mass transfer barriers than the microcapsules shells, which are rate-limiting for low solubility chemicals. For this reasons, release experiments performed with this methodology result in artificially very slow release profiles.

Another way to study release behaviour of microcapsules has been developed recently (Mercade-Prieto *et al.*, 2012b). In that study, thin-shell MF microcapsules (shell thickness to radius of microcapsules $h/r < 0.07$) with a single fragrance compound were studied as model systems. Instead of a two phase system with an aqueous solution and organic solvent, which presents many additional complications as discussed above, a single liquid phase was considered, thus greatly facilitating the mathematical analysis of the release (Figure 2-18(b)). The main problem when using a single phase is the low solubility of many of the perfume components as discussed

above. For the case of the model oil hexyl salicylate used by the previous study, the solubility in water was estimated to be of the order of $\sim 6 \times 10^{-6} \mathrm{g\,mL^{-1}}$. Considering that the test solution should be capable of solubilising more than five times the amount of core oil in the microcapsules tested, the solubility has to be increased substantially for reasonable experimental conditions. In the study of Mercadé-Prieto *et al.* (2012b) simple alcohols like ethanol and isopropanol were selected as co-solvents, resulting in increases by orders of magnitude of the solubility of hexyl salicylate, and moreover the aqueous co-solvent solutions were not found to damage the MF shells.

The release of the perfume oil is determined in this case directly in the aqueous phase with an appropriate analytical method, such as UV-Vis spectrophotometry that can be easily adapted for continuous measurements using a flow cell. The release of perfume oil from such kind of experiments has to be converted into a parameter that characterizes the barrier properties of the shell, such as the permeability. For this purpose analytical models should be developed that consider the morphology of the microcapsules. Mercadé-Prieto *et al.* (2012b) developed a simple model for thin-shell microcapsules based on the solution-diffusion model for transport through membranes (Wijmans and Baker, 1995). Figure 2-19 represents the schematic diagram of perfume oil release out of the thin shell, and Figure 2-20 shows the schematic diagram of a typical release curve (Antipov *et al.*, 2003).

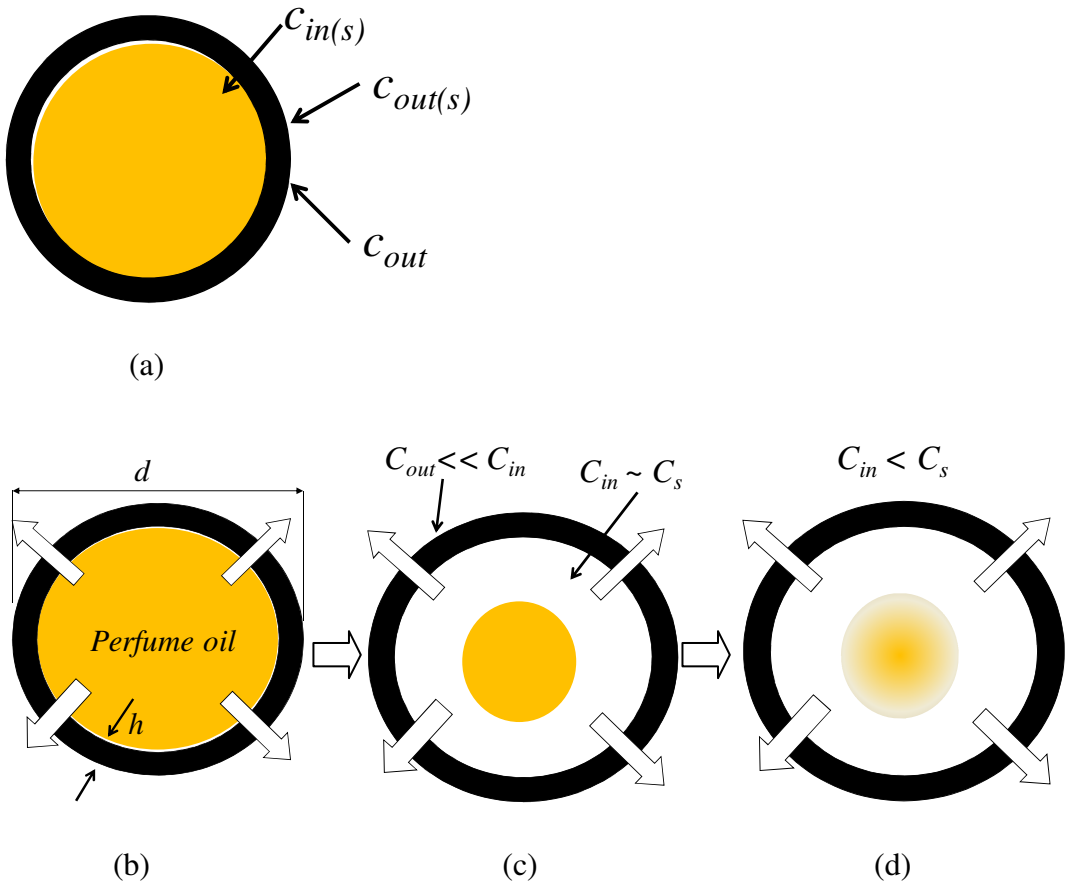

Figure 2-19 A schematic diagram of encapsulated perfume oil release through MF shell. (a) Thin-shell microcapsule full of perfume oil. (b) Perfume microcapsule with a shell thickness *h* beginning to release oil into solvent outside the shell. (c) Linear regime: there is a core of perfume oil inside the microcapsule in this release stage. The oil concentration in the solvent outside the shell is assumed much lower than the concentration inside the shell, and the concentration of oil in solvent inside the shell is assumed to be equal to the solubility value. (d) Exponential regime: Perfume oil core disappearing in this release stage. The concentration of oil in the solvent inside the shell is lower than the oil solubility (adapted from Mercadé-Prieto *et al.* (2012b)).

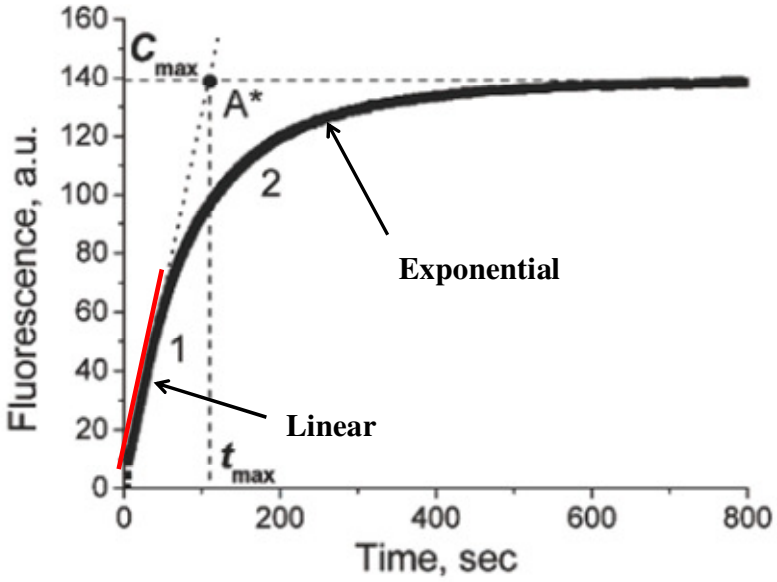

Figure 2-20 Typical release curve from thin-shell microcapsules. There are two stages on the release curve: the linear release regime and exponential release regime (Antipov *et al.*, 2003). The red line fits the slope of the linear release regime.

The perfume oil flux (J) passing through a single microcapsule shell, as shown in Figure 2-19(a), is defined using Fick's first law:

$$J = \frac{D}{h}\left(C_{in(s)} - C_{out(s)}\right) \quad \text{(Equation 2.23)}$$

where D is the diffusivity of the pure oil within the shell, $C_{in(s)}$ and $C_{out(s)}$ are the oil concentrations (w/v) at the inner and outer side of the shell-fluid interface.

Considering the partition coefficient in the shell

$$J = \frac{KD}{h}(C_{in} - C_{out}) = \frac{P}{h}(C_{in} - C_{out}) \quad \text{(Equation 2.24)}$$

where C_{in} and C_{out} are the oil concentrations in the solvent inside and outside the microcapsule, and $K = \frac{C_{in}}{C_{in(s)}} = \frac{C_{out}}{C_{out(s)}}$ is the partition coefficient, where it can be

assumed that $K \approx \frac{C_{s-shell}}{C_s}$ (Schwarb *et al.*, 1999). Here, $C_{s-shell}$ is the saturation solubility of core oil in the shell material, and $C_s$is saturation solubility of core oil in the co-solvent solution and h is the shell thickness of the microcapsules, P is the permeability of the oil in the shell.

The model considers the following assumptions:

I. Fast mass transfer inside the capsule, from the perfume oil core to the inner side of the shell, resulting in $C_{in} \approx C_s$ at all times. This assumption is reasonable if $\mathrm{P}/h \ll D_{water}/r$, where D_{water} is the diffusivity of core oil in water.

II. Experiments are designed in order that the oil concentration in the solution is much lower than the solubility concentration at all times, $C_{out} \ll C_s$, in order that Equation 2.22 can be simplified to $J \cong \frac{P}{h} C_s$;

III. The co-solvent solution is well-mixed at all times, resulting in that there is no concentration gradient in the co-solvent.

Considering these assumption, Equation 2.24 can be simplified to:

$$C_{out} \cong \frac{\pi d^2}{V_{cs}} \frac{P}{h} C_s t_r \qquad \text{(Equation 2.25)}$$

where, V_{cs} is the volume of the co-solvent, t_r is the diffusion time, C_s is the solubility of oil in the co-solvent, *d* is the diameter of the microcapsules.

Therefore, it is predicted for a single microcapsule that C_{out} increases linearly with the release time, as shown in Figure 2-19 (c), allowing to calculate *P/h* from the slope

of the release profile (red solid line in Figure in 2-20), called the linear regime (Antipov *et al.*, 2003).

After extensive release a point is reached when the concentration inside the microcapsule cannot be kept constant to that of the solubility. When this occurs at the late stage of release, $C_{in} < C_s$, as shown in Figure 2-19(d), the relative release is no longer linear with time, but follows an exponential decay (Antipov *et al.*, 2003), called exponential regime (Figure 2-20). The concentration of the released oil in the co-solvent in the exponential regime is given by :

$$C_{out} \sim (1 - e^{-\frac{\pi d^2 P}{V_{cs} h} t_r}) \qquad \text{(Equation 2.26)}$$

The relative oil release by weight $R(t_r)$ at a time t_r is defined as:

$$R(t_r) = \frac{V_{cs} C_{out}(t_r)}{1/6\pi(d-2h)^3 \rho_{oil}} \qquad \text{(Equation 2.27)}$$

where ρ_{oil} is the density of the core oil. For the linear regime, Equation 2.27 can be simplified for thin-shell capsules ($h \ll d$) as follows:

$$R(t_r) \cong \frac{6}{d\rho_{oil}} \frac{P}{h} c_s t_r \qquad \text{(Equation 2.28)}$$

This model predicts for a single capsule, or a mono-dispersed group of capsules, with a fairly insoluble core oils that most of the relative release with be linear. However, if the microcapsules are poly-dispersed, the model will predict an exponential-like release like in Figure 2-19, despite the fact that the individual release of all the microcapsules is mostly linear.

As discussed in a previous work (Mercade-Prieto *et al.*, 2012b), the desirable

experimental release time should be about 10^2 to 10^4 s. The final release time can be estimated from the expected end of the linear regime (termed t_{max} in Figure 2-20) as follows :

$$t_{end}(k) = \frac{\rho_{oil}\bar{d}}{6c_s P/h} \quad \text{(Equation 2.29)}$$

where $\bar{d}$ is the number mean diameter of the microcapsules.

2.6.4 Morphology, microstructure and shell thickness

There are many techniques to physically observe the existence of microcapsules, for example to verify the core-shell structure expected. Optical microscopy is a direct and simple technique commonly used for investigating the morphology, shape, structure as well as size of microcapsules (Bone et al., 2011, Pretzl et al., 2012), particularly when combined with image analysis software. In order to obtain high resolution images of microcapsules or even nano-capsules, scanning electron microscopy (SEM) or ESEM have been applied for the evaluation of their morphology and microstructure (Hong and Park, 1999a, Hwang *et al.*, 2006a, Ren *et al.*, 2007).

Transmission electron microscopy (TEM) has been extensively used to determine the shell thickness of microcapsules due to its excellent nano-scale resolution (Yang *et al.*, 2008). Before obtaining TEM images, microcapsules are pre-treated by embedding

then in an acrylic resin, which allows them to be cut very thin with a ultra-microtome (Long *et al.*, 2010).

Another technique frequently used to determine the shape and shell thicknesses of microcapsules is confocal laser scanning microscopy CLSM (Kim *et al.*, 2007, Lebedeva *et al.*, 2004, Tzhayik *et al.*, 2012). It benefits from being a non-destructive technique, does not need time consuming sample preparations and keeps the original structure of microcapsules without damaging the sample, see Figure 2-21. In addition, microcapsules can be observed in solution or dried. CLSM also allows us to select different height levels within one sample, providing three dimensional images (Ferrando and Spiess, 2000).

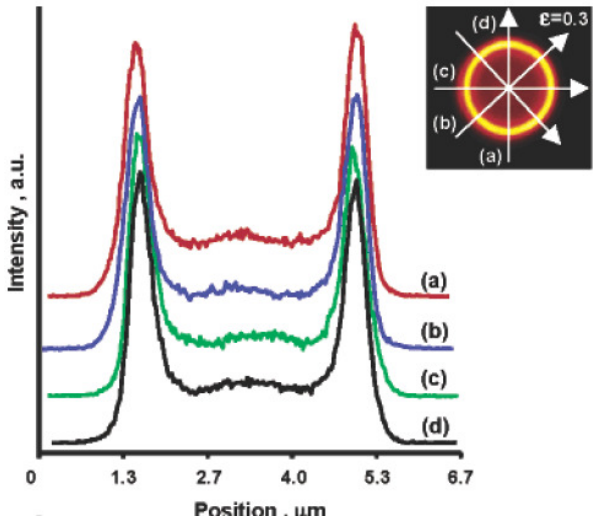

Figure 2-21. Example of the use of CLSM for the observation of the microcapsules shell cross section, from Lebedeva *et al.* (2004).

2.7 Conclusions

In this chapter the composition, manufacturing and applications of perfume microcapsules has been reviewed. This chapter covers basic aspects of emulsification and encapsulation methods, the importance to control the size and uniformity of microcapsules, the applications of MF and PMMA microcapsules and methods to characterize microcapsules reported in the literature.

The main use considered is that for microcapsules added to laundry detergents, increasing significantly the amount of perfume deposited on fabrics and thus reducing the amount of expensive material that is wasted. Microcapsules also allow a much prolonged perfume release compared when perfumes are added in free form, and particularly allow sudden “on demand” release when microcapsules are broken upon rubbing. The latter release mechanism is particularly interesting because it focuses the release of perfume mainly when the customer is handling the clothes, not when the clothes are idle in the wardrobe. Although the understanding on the performance of perfume microcapsules in real applications is still in its infancy, it is expected that microcapsules with well-defined properties are desirable to microcapsules with broad ones. A key property typically considered for perfume microcapsules, where burst upon rubbing is desired, is the mechanical strength under compression.

The initial step to manufacture perfume microcapsules is typically to form an aqueous emulsion of the perfume. This step is commonly followed by an *in situ* polymerization reaction to form a shell, as in the case of melamine-formaldehyde (MF) microcapsules that are extensively used in the industry. The mechanical strength distribution of previous MF microcapsules is quite variable, which is primarily due to the large size distributions in the batches made. Hence, one way to improve the performance of MF microcapsules would be to narrow the size distribution of the microcapsules, and therefore of the initial emulsions. Of the different emulsification techniques available, membrane emulsification is found to have great potential for this purpose and furthermore has the potential to be used in large scale operations.

A second improvement that the market requires for perfume microcapsules is to be able to formulate them from non-hazardous products or ones less than currently used for MF microcapsules. PMMA is considered to be a good candidate for perfume encapsulation, considering that it has already found many other encapsulation applications. In order to test the applicability of new kinds of microcapsules, and to compare them with the better-known MF ones, extensive characterization tests should be applied.

By taking the industrial needs and literature into consideration, this PhD project aims to encapsulate perfume oils in MF microcapsules with narrow size and strength distributions via membrane emulsification, and also to prepare user-friendly PMMA

microcapsules including characterisation of their physical, structural and mechanical properties.

Chapter 3 Materials and Experimental Techniques

3.1 Introduction

This chapter describes the materials used to prepare melamine-formaldehyde (MF) and poly (methyl methacrylate) (PMMA) microcapsules, as well as the techniques utilized for preparing and characterizing the microcapsules. A conventional homogenisation system and membrane emulsification systems were used to prepare the oil-water emulsions from which microcapsules were formed. The mean size and size distribution of the oil droplets produced in the stage of emulsification and the final microcapsules were determined using a laser diffraction technique. A well-established micromanipulation technique based on the parallel compression of single microcapsules was used to evaluate their mechanical properties (Sun and Zhang, 2001, Zhang *et al.*, 1999b). The microcapsules' morphology was analysed by optical microscopy, florescence microscopy, scanning electron microscope (SEM), environmental scanning electron microscopy (ESEM), transmission electron microscope (TEM). The wall thickness of microcapsules was determined using TEM and confocal laser scanning microscopy (CLSM). The physical properties of the encapsulating oils, like the viscosity and the interfacial tension, were determined using a rheometer and tensiometer, respectively. The rate of the oil release from

microcapsules was tested with a continuous release testing method using UV-Vis spectrophotometry. Details of these techniques are discussed in this chapter.

3.2 Materials

3.2.1 Materials used to prepare melamine formaldehyde (MF) microcapsules

The melamine formaldehyde (MF) precondensate used in this study (70 % (aq) w/w, formaldehyde to melamine molar ratio 0.20), Beetle resin PT336®, was supplied by British Industrial Plastics Ltd., Birmingham, UK. Formaldehyde (37 % (aq) w/w), acetic acid, sodium hydroxide (NaOH) and the fluorescent dye Rhodamine B (RB) were purchased from Sigma-Aldrich, UK, and polyacrylamide-co-acrylic acid-sodium salt was obtained from Polymersciences, Inc., US. Polyalkyleneoxide modified heptamethyltrisiloxane (as a membrane wetting agent) was supplied by Micropore Technologies Ltd., UK. The model core oils used were industrial precursor perfume oil A and perfume oil B, a key component of perfume oil is hexyl salicylate (oil HS), sunflower oil (oil S) and peppermint oil (oil P). Perfume oil A, perfume oil B and oil HS were supplied by Procter & Gamble (P&G), UK. Sunflower oil (oil S) and peppermint oil (oil P) were purchased from Sigma-Aldrich, UK. All the materials were used without further purification.

3.2.2 Materials used to prepare poly (methyl methacrylate) (PMMA) microcapsules

Methyl methacrylate (MMA), ethylene glycol dimethacrylate (EGDMA), 2,20-azobisisobutyronitril (AIBN), polyvinyl alcohol 18-88 (PVA), toluene, sodium chloride (NaCl), propenal-1 and glycerol were purchased from Sigma-Aldrich, UK. Partly hydrophobic fumed silica Aerosil® R816 was kindly provided by Evonik, Degussa A.G., Germany. The florescent dye pyrromethene 546 (PM 546) was supplied by Exciton, Ohio, US. The perfume oil used was an industrial precursor from Procter & Gamble (P&G), UK. All the materials were used without further purification.

3.3 Techniques to prepare microcapsules

3.3.1 Dispersion cell system

3.3.1.1 Cell system

The dispersion cell used to generate oil/water emulsions was purchased from Micropore Technologies Ltd., UK, shown in Figures 3-1 and 3-2. It is a batch membrane emulsification system with a mechanical stirrer on top of a flat membrane. The membrane with homogenous pores was placed on a PTFE base, connected with a

glass cylinder housing the continuous phase. The dispersed phase (oil) was pushed through the flat membrane into the continuous phase (aqueous solution of MF precondensate or PVA solution) with a peristaltic pump (Watson Marlow 101u, UK). In the continuous phase, there is a two-blade paddle stirrer controlled by a DC motor to ensure that enough shear is generated near the membrane surface. The agitation speed of the stirrer was adjusted with the motor. Details and more applications of this dispersion cell are described in Chapter 2 and reported in the papers produced by Professor Richard Holdich's group in the University of Loughborough, UK (2010, 2012, 2005, 2012a).

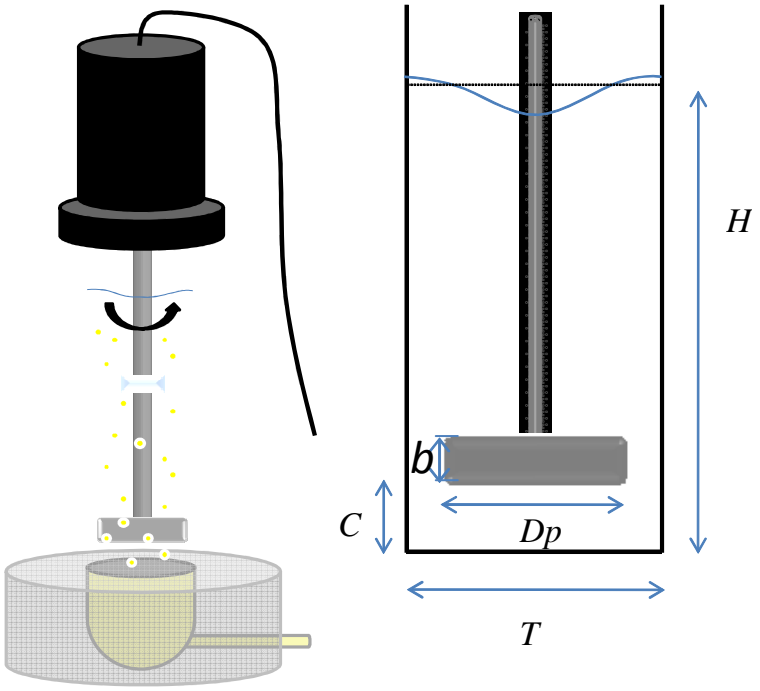

Figure 3-1 Illustration of the dispersion cell system: (a) during emulsification; (b) longitudinal section of the dispersion cell system ($H = 70\ mm,\ Dp = 35\ mm,\ T = 40\ mm,\ C=5\ mm$ and $b=12\ mm$.

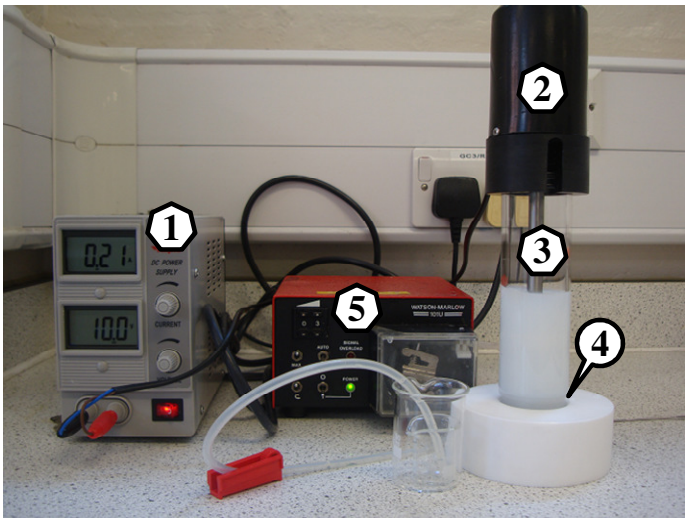

Figure 3-2 The set-up diagram of membrane emulsification process

(1) transformer (2) DC motor (3) Two-blade paddle stirrer

(4) One piece of flat thin metal membrane (5) Peristaltic Pump

A laser tachometer (from VWR Ltd, UK) was used to measure the agitation speed of the impeller in the dispersion cell. The agitation speeds at different voltages applied to the DC motor are shown in Figure 3-3.

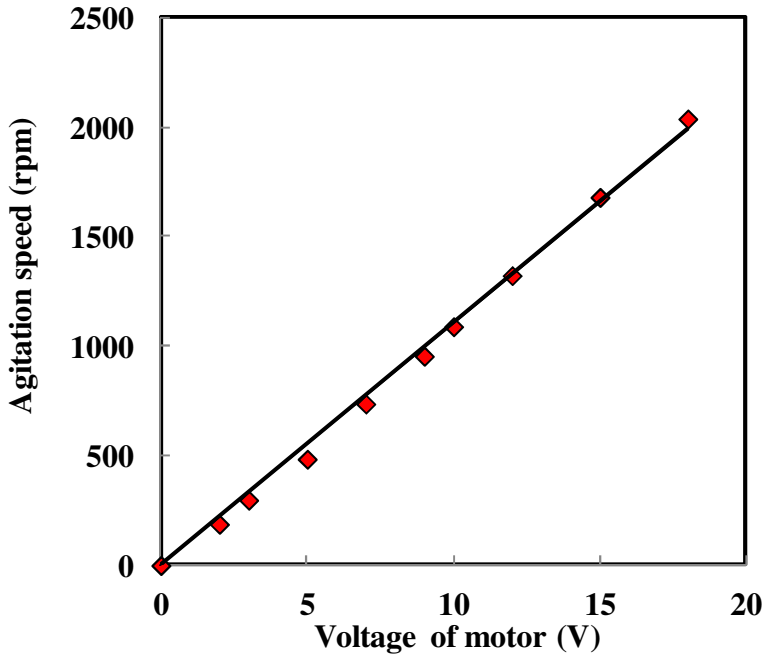

Figure 3-3 Agitation speed of the stirrer in continuous phase vs voltage of the DC motor driving the paddle stirrer. $\omega_m = 106(\pm 6)\, V_a$ where, ω_m is the agitation speed (rpm) and *Va* is the voltage of the DC motor (V). The solid line represents the best linear fit.

3.3.1.2 The membrane

The flat membranes utilised in this study are made of steel with a coating of polymer, polyalkyleneoxide modified heptamethyltrisiloxane, supplied by Micropore Technologies Ltd., UK., with about 20000 regular array pores. Each pore has a diameter of 2 to 15 µm and the distance between two adjacent pores is 200 µm, according to the specifications of the supplier. The membranes have a diameter of 40 mm, but the pores are evenly distributed only in the region of 4.75 mm < *r* < 13 mm

or 13 mm < *r* < 17.5 mm, where r is the distance from the centre of the membrane, as shown in Figure 3-4.

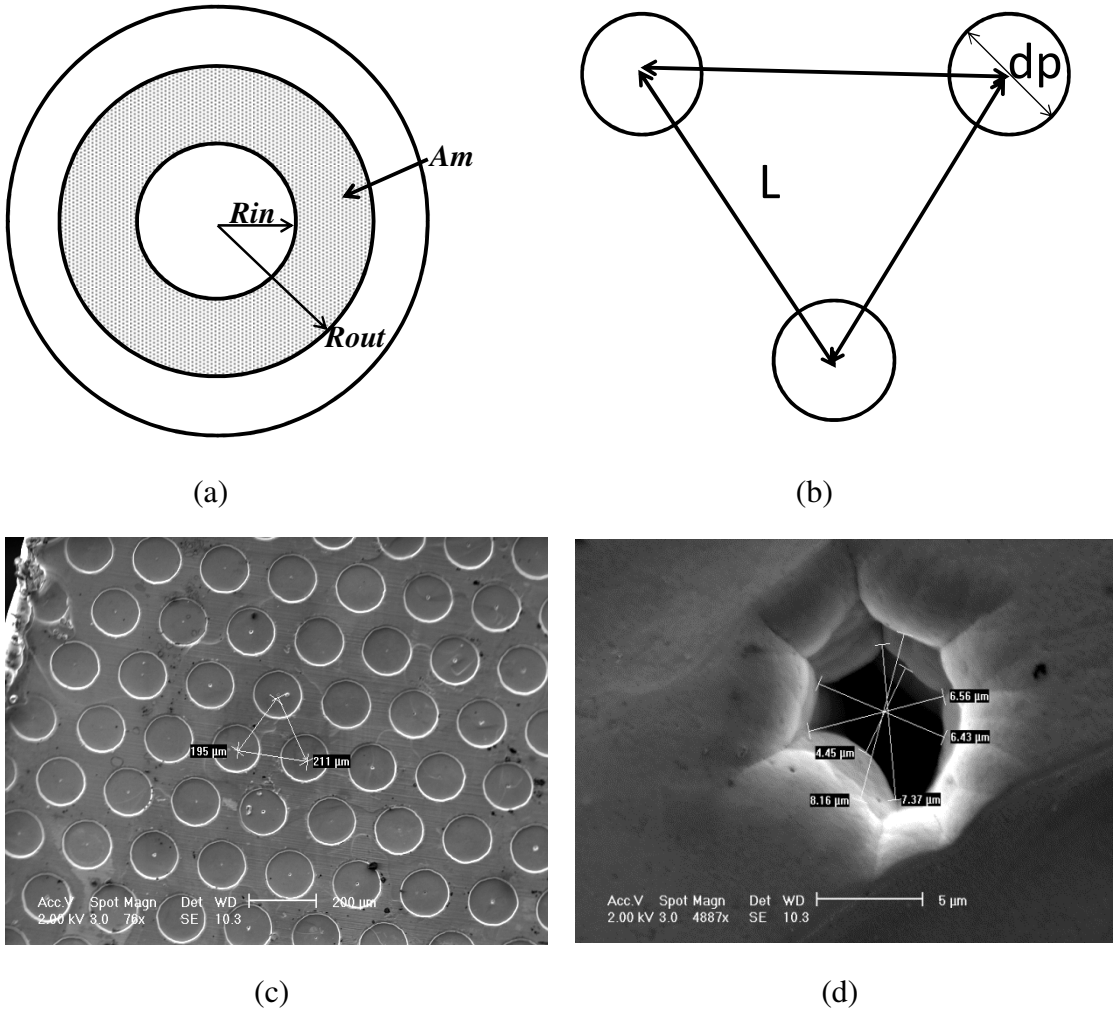

(a) (b)

(c) (d)

Figure 3-4 The schematic diagrams and the SEM micrographs of representative flat membrane used. (a) The annular radial ring membrane; (b) schematic diagram showing regular distribution of the pores in the membrane; (c) SEM micrograph of the pores; (d) SEM image of one pore in the membrane 15rcia. The pore diameter has been estimated from the narrower end.

The porosity of the membrane and the number of pores in a membrane were calculated using the following equations (Dragosavac *et al.*, 2008):

$$\varphi = \frac{\pi}{2\sqrt{3}}\left(\frac{d_p}{L}\right) \quad \text{(Equation 3.1)}$$

$$N = \frac{4\varphi A_m}{d_p^2 \pi} \quad \text{(Equation 3.2)}$$

where φ is the porosity of the membrane, d_p, L, N, and A_m are the pore diameter, distance between pores, the number of pores and the membrane area respectively . The details of the different membranes used are listed in Table 3-1.The ranges of pore diameter d_p were determined with the ESEM technique, shown in Figure 3-4 (d).

Table 3-1 Summary of membrane area (A_m), porosity φ, pore active membrane area ($Aac = Am \times \varphi$), the inner radium (*Rin*), the outer radium (*Rout*), pore distance *L*, pore diameter d_p, number of pores of the membranes *N* studied. The ranges of pore diameter d_p were determined with the ESEM technique, shown in Figure 3-4.

Type	Material	*L*	d_P	Φ	R_{in}	R_{out}	A_m	*Aac*	*N*
		µm	µm		m	m	m²	m²	
5cia	Metal	200	2-3	2.0E-04	0	0.0175	0.00096	2.0E-07	2.8E+04
10cia	Metal	200	4-5	4.6E-04	0	0.0175	0.00096	4.41E-07	2.8E+04
15cia	Metal	200	6-7	8.2E-04	0	0.0175	0.00096	7.84E-07	2.8E+04
20cia	Metal	200	8-9	1.8E-03	0	0.0175	0.00096	1.77E-06	2.8E+04
5rcia	Metal	200	2-3	2.0E-04	4.8E-03	0.013	0.00046	9.38E-08	1.3E+04
15rciaA	Metal	200	6-7	8.2E-04	4.8E-03	0.013	0.00046	3.75E-07	1.3E+04
15rciaB	Metal	200	6-7	8.2E-04	1.3E-02	0.0175	0.00043	3.52E-07	1.2E+04
15rciaC	Silica	200	6-7	8.2E-04	4.8E-03	0.013	0.00046	3.75E-07	1.3E+04
20rcia	Metal	200	9	1.8E-03	4.8E-03	0.013	0.00046	8.44E-07	1.3E+04

The membrane type “cia” mentioned in Table 3-1 stands for a membrane with pores equally distributed on the whole membrane area, whereas “rcia” is used for membranes where the pores are only present in an area of annular ring, as shown in Figure 3-4 (a). To change its surface hydrophilicity before emulsification, each membrane was exposed to the wetting agent at different concentrations for 30 min, then taken out and dried in ambient air.

3.3.2 Cross flow membrane system

3.3.2.1 Cross flow membrane system

A cross-flow membrane emulsification rig established in the University of Leeds was used in this research. As shown in Figures 3-5 and 3-6, the membrane rig has a specially fabricated tubular ceramic membrane, suited for the pilot plant-scale experiments to generate large amounts of oil-in-water emulsions.

The dispersed phase (perfume oil) was pushed through the membrane pores using compressed gas (number 2 in Figure 3-5) into the continuous phase (aqueous solution of MF precondensate). During emulsification, the compressed gas, which was supplied to the system from a nitrogen gas cylinder nearby, was used to control the oil pressure using a valve (Figure 3-7). It was circulating in the system through the inner channels of the membrane tube to generate the emulsion, as shown in Figure 3-8. The cross flow rate of the continuous phase was adjusted by the pump. At least 1 L of

emulsion was generated during each experiment (Yuan *et al.*, 2009a, Yuan *et al.*, 2008a).

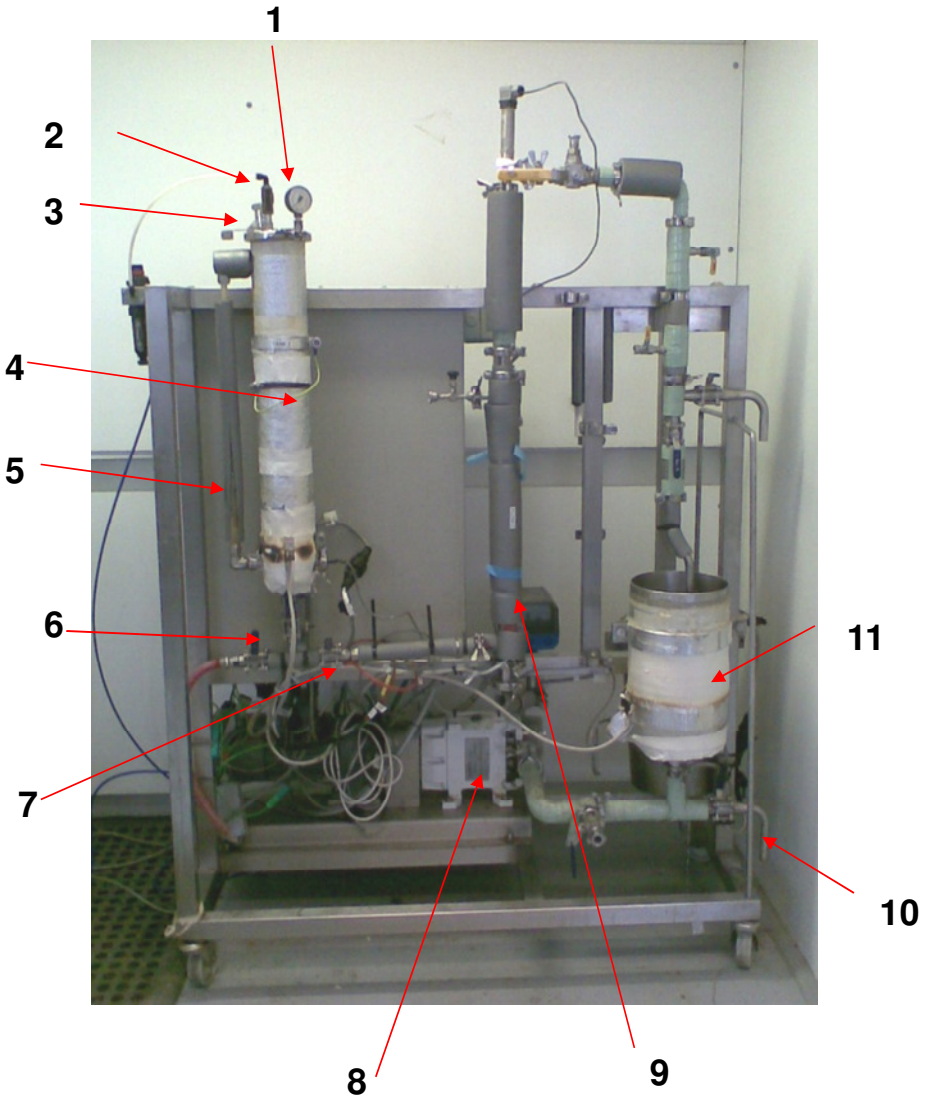

Figure 3-5 Pilot plant-scale cross-flow membrane apparatus (from the rear).

1 – Disperse phase tank lid (enlarged in Figure 3-6), 2 – Compressed gas line, 3 – Control valve for compressed gas (enlarged in Figure 3-7), 4 – Disperse phase tank, 5 – Control panel (Rear), 6 – Release valve (disperse phase tank), 7 – Disperse phase valve, 8 – Pump, 9 – Membrane housing, 10 – Continuous phase tank release tap, 11 – Continuous phase tank

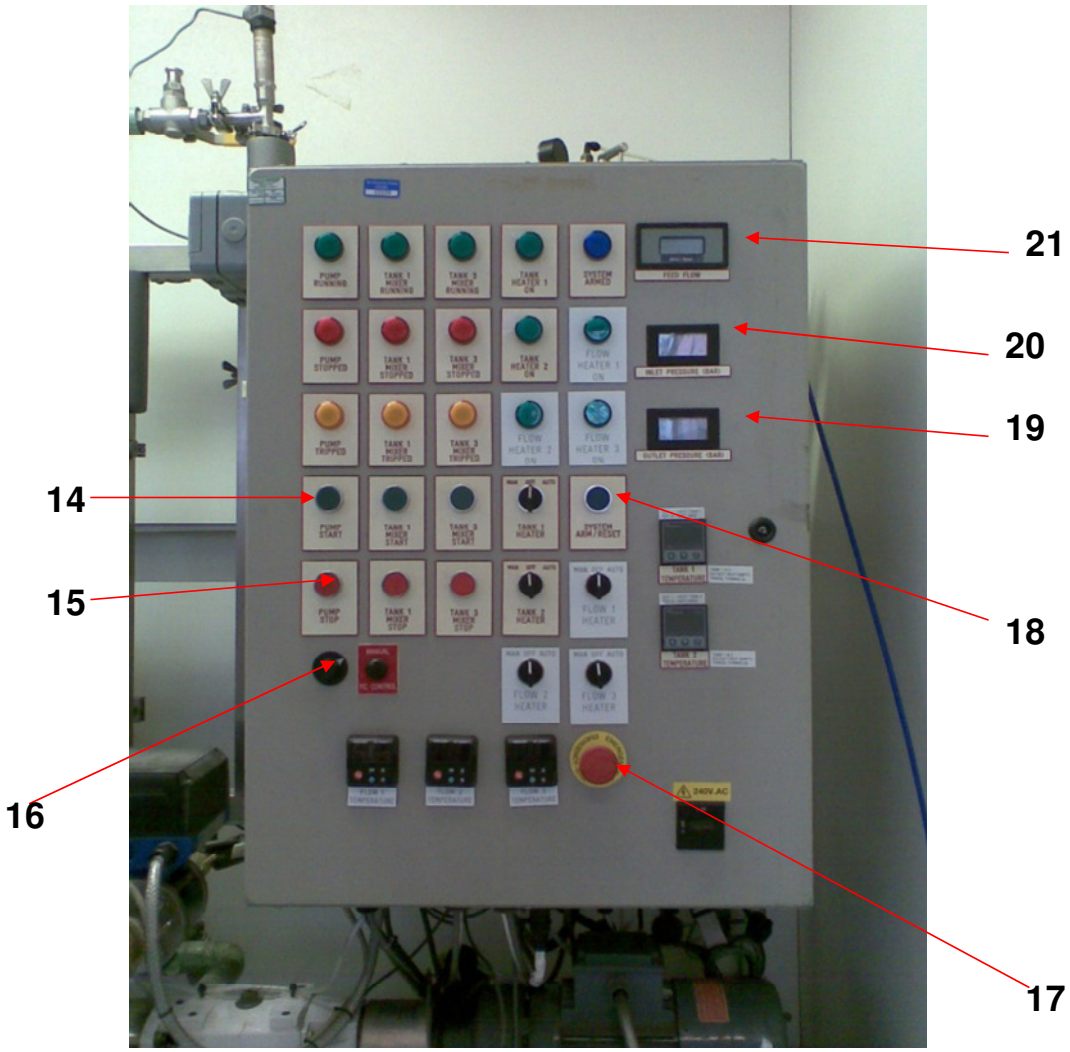

Figure 3-6 Front view of the control panel.

14 – Pump start button, 15 – Pump stop button, 16 – Flow speed control dial, 17 – Emergency stop button, 18 – System arm / Reset button, 19 – Outlet pressure meter, 20 – Inlet pressure meter, 21– Flow rate meter

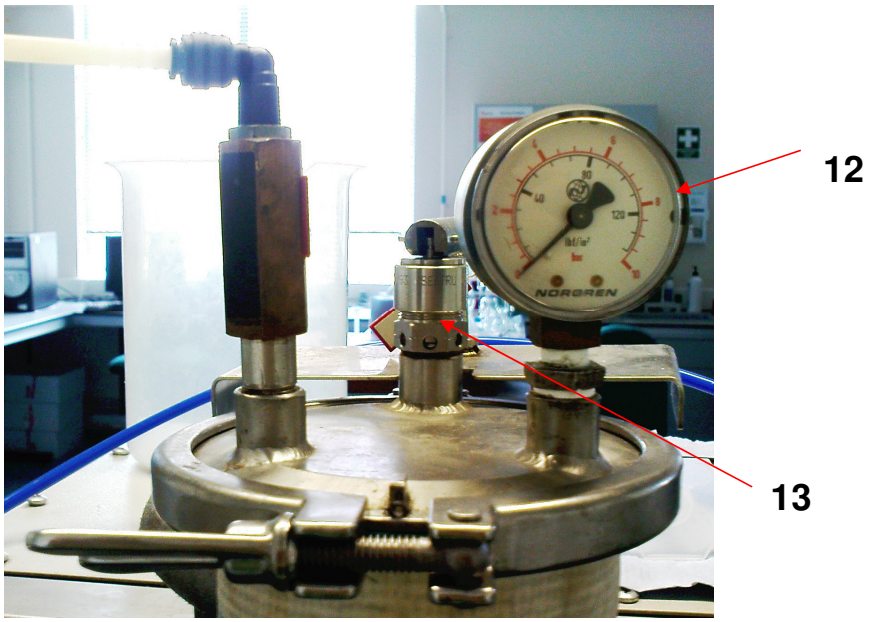

Figure 3-7 Disperse phase tank lid showing the gas pressure dial (12) and gas release valve (13), enlargement of (1) in Figure 3-5.

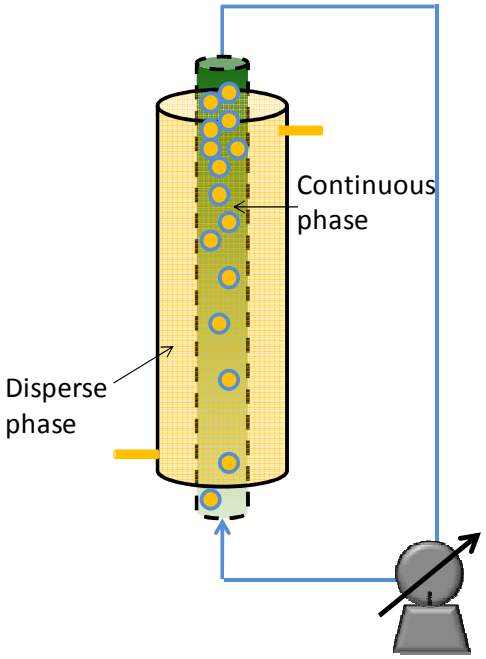

Figure 3-8 Schematic diagram showing emulsification of oil in water in the membrane system. The continuous phase was cross-flowed inside the membrane tube, while dispersed phase was passing through the membrane and forming droplets in continuous phase.

3.3.2.2 Membrane tube

Ceramic membrane tubes (code 021421) from Fairey Industrial Ceramics Limited, U.K. were used in this study. They were 600 mm in length and 20 mm in outer diameter, each having seven separate star-shaped channels with an inner diameter of around 4 mm, as shown in Figure 3-9. The ceramic membrane is porous (Figure 3-10), with random pores on the active inner surface, as shown in Figure 3-11. The average pore size is 0.2 μm, according to the specifications of the supplier.

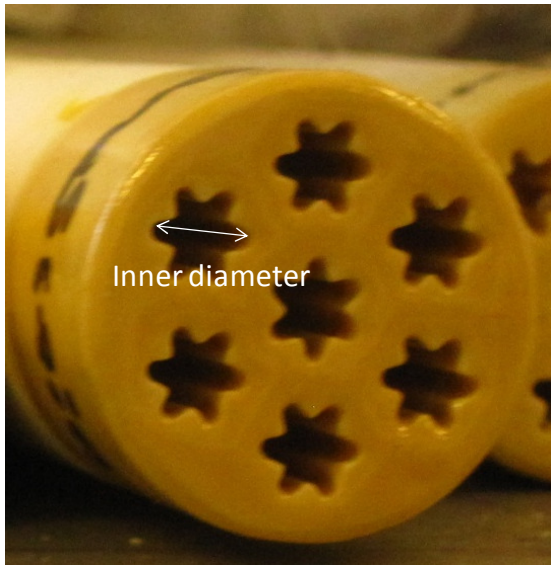

Figure 3-9 Photo showing the cross-section of the membrane tube with seven star-shaped channels. The smallest pores are located on the surface of the star-shaped channels. The double headed arrow represents the inner diameter of the star-shaped channel.

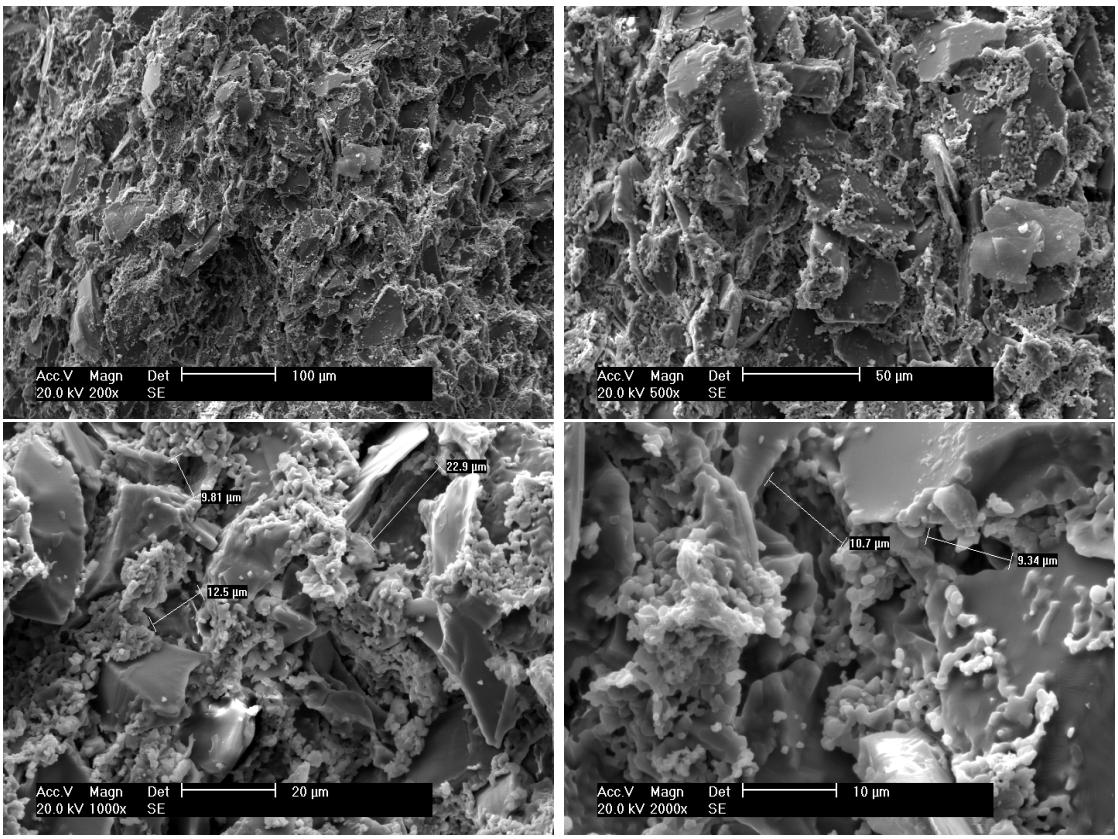

Fig 3-10 SEM images of the substrate material of 0.2 µm (pore size at the interface) cross-flow membrane tube. Broken portions of 0.2 µm cross-flow membrane tube (code 021421, 7 hole star shape) were mounted on a stub using Leit-c-plast (Agar) and then coated with gold for 4 (or 8) min, before being examined using SEM.

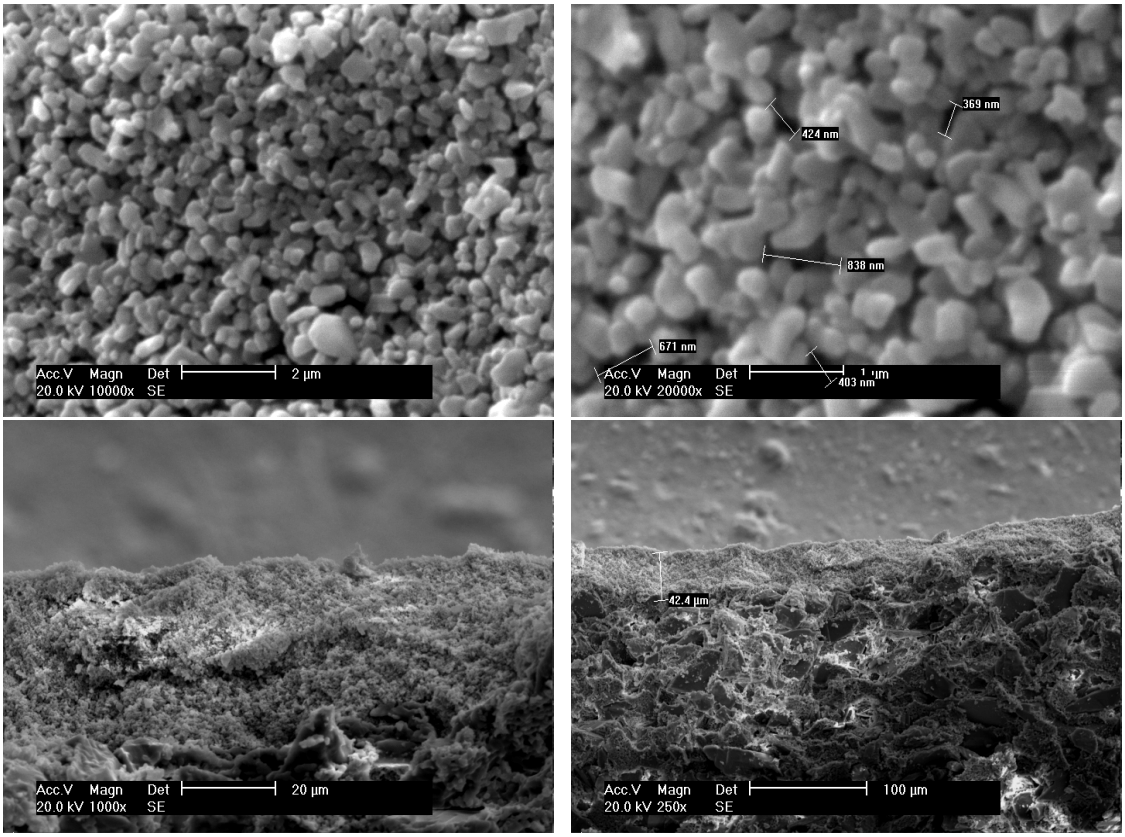

Fig 3-11 SEM images of the cross-flow membrane tube channel from inside. The rough porous inside surface of the channel, has pores with the nominal size of 0.2µm.

3.4 Techniques to characterise microcapsules

3.4.1 Particle size analyzer - laser diffraction

Laser diffraction or low angle laser light scattering (LALLS) is a technique which determines the size and size distribution of droplets or microcapsules in wet or dry samples (Webb, 2000). It is based on Mie theory, described by Equation 3.3 below, which predicts the angular intensity of light scattered by the interaction between the

laser light and particles (Webb, 2000). When a laser beam passes through a microcapsule, as shown in Figure 3-12, some part of the light beam passes without interaction, some reflects back, the other is refracted and diffracted. These result in light scattering patterns that are used to characterize the microcapsule size. In some cases, the microcapsule size is much bigger than the wavelength of the laser light, then the light scattering patterns will be caused by diffraction (Xu, 2000). The light scattering angle and the intensity are related to the size of the microcapsules. The observed scattering angle decreases with increasing of the microcapsule size, as shown in Figure 3-13. For the scatter of large microcapsules with a narrow angle, the light intensity is higher compared with that generated by small ones (Erik, 1999).

$$I_{sc} = I_{in}(\theta_{\mathrm{lsa}}, \lambda_{lsa}, d_{lsa}, n_{index}) \qquad \text{(Equation 3.3)}$$

Where, I_{sc} and I_{in} mean the intensity of scattered light and laser light (w m^{-2}), θ_{lsa} means the light scattering angle ($^{\circ}$), λ_{lsa} means the wavelength of the laser light (nm), d_{lsa} is the particle size (m) and n_{index} is the relative refraction index of the particle and the medium.

A Malvern Mastersizer 2000 (Malvern Instruments, UK) is based on this principle, which can measure the particles in the size range of 0.02 to 2000 μm, and its schematic is shown in Figure 3-14. Microcapsule samples were placed in a dispersion unit to make a homogeneous particle suspension, and then coherent and intense light beam

with a fixed wavelength which is provided by a light source passes through it. At the end, a large angle detector measures the scattered light in a wide range of angles.

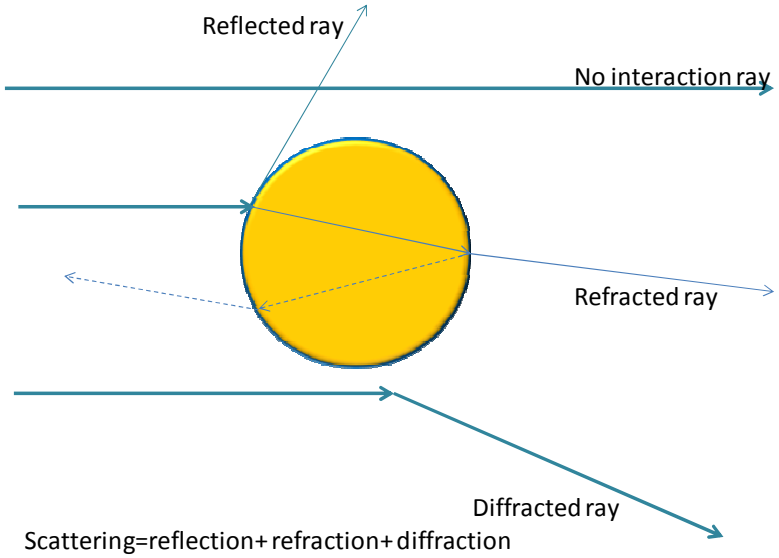

Figure 3-12 Schematic diagram of laser light rays interacting with a solid particle.

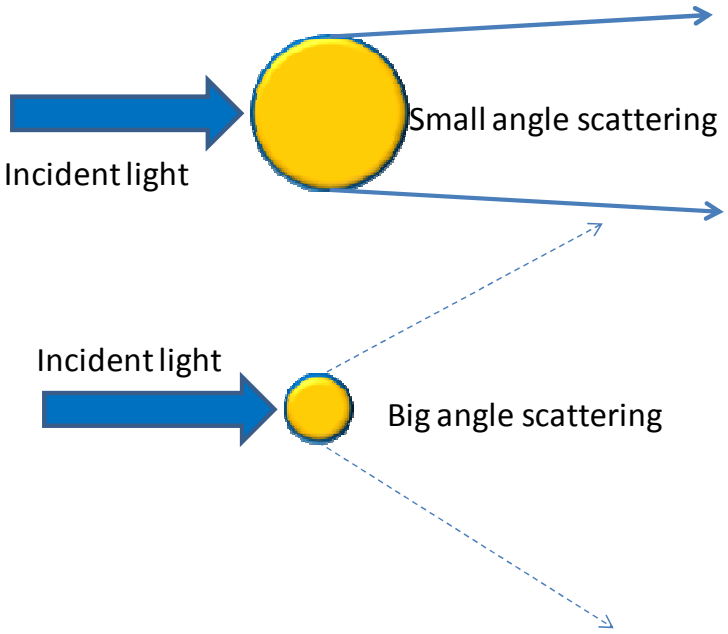

Figure 3-13 Schematic diagram of laser light rays interacting with particles of different sizes.

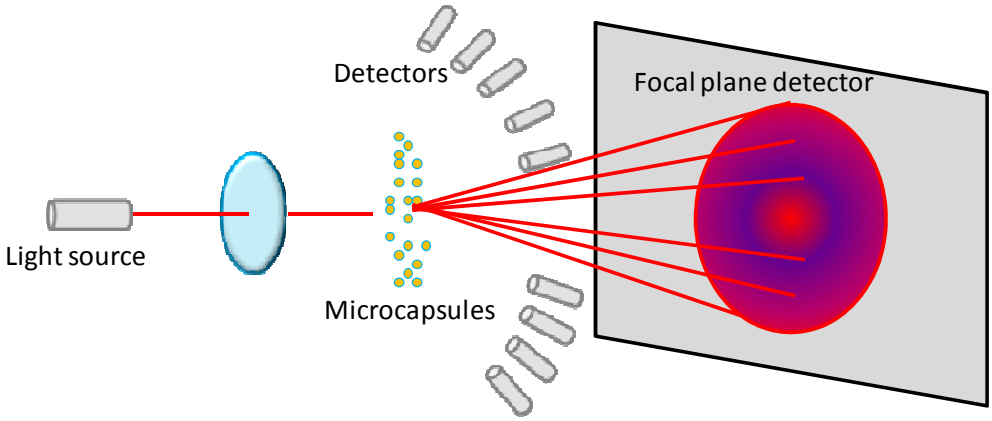

Figure 3-14 Schematic representation of laser diffraction instrument.

3.4.1.1 Typical data generated

A typical size distribution curve of microcapsules in aqueous dispersion is shown in Figure 3-15. The data of *SPAN* and coefficient of variation (*CV*) values, which represent the size distribution, the volume mean diameter $D_{4,3}$ and the Sauter mean diameter $D_{3,2}$ are recorded and are defined as follows.

$$SPAN = \frac{D_{90} - D_{10}}{D_{50}} \qquad \text{(Equation 3.4)}$$

$$CV = \frac{\sqrt{\frac{\sum_{i=1}^{i-n_i}(d_i - \bar{d})^2}{n_i - 1}}}{\bar{d}} \times 100\% \qquad \text{(Equation 3.5)}$$

$$D_{4,3} = \frac{\sum_{i=1}^{i=n_i} d_i^{\,4}}{\sum_{i=1}^{i=n_i} d_i^{\,3}} \qquad \text{(Equation 3.6)}$$

$$D_{3,2} = \frac{\sum_{i=1}^{i=n_i} d_i^{\,3}}{\sum_{i=1}^{i=n_i} d_i^{\,2}} \qquad \text{(Equation 3.7)}$$

Where D_{90}, D_{10} and D_{50} represent the diameter under which the cumulative volume of the droplets/microcapsules is 90%, 10% and 50% respectively; and d_i means the diameter of single droplets/microcapsules; $\bar{d}$ is the number- based mean diameter and n_i is the number of droplets/microcapsules measured.

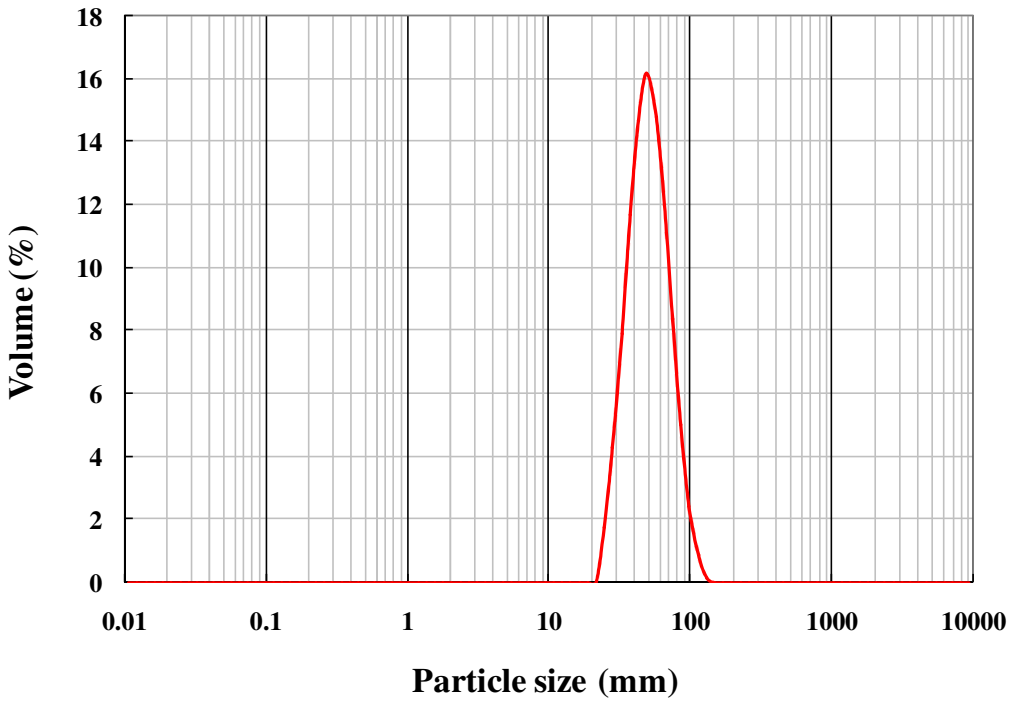

Figure 3-15 A typical size distribution curve of MF microcapsules obtained from laser diffraction measurement. The preparation details of the MF microcapsules are described in Section 4.2.1.

3.4.2 Micromanipulation technique

A well-established micromanipulation technique has been used to perform parallel compression of single microcapsules (Mashmoushy *et al.*, 1998, Mercade-Prieto and Zhang, 2012, Sun and Zhang, 2002). The experimental data of the compression force F versus displacement until rupture, diameter of single microcapsules were directly obtained by this technique. The intrinsic material properties of the microcapsule shells, such as failure stress σp, Young's modulus E, were calculated using finite element modelling (FEM, see Appendix A) based on the data generated by the micromanipulation rig (Section 6.2.4).

The schematic diagram of the micromanipulation rig (Micro Instruments Ltd., Oxon, UK) is shown in Figure 3-16. One drop of microcapsule suspension was placed on the top of a glass slide, subsequently placed on the sample stage to dry for 2-3 min. A single microcapsule was found through the microscope with both side and bottom view cameras and the image shown on the monitor, as seen in Figure 3-17(b). The size of the microcapsule was measured through the microscope and recorded, which can be verified later through the probe displacement data. A glass probe glued to a force transducer (Models 403A, 405A or 406A with different maximum operating

forces, up to 5 mN, 1mN, and 0.5mN, respectively; from Aurora Scientific Inc., Canada) held by a fine micromanipulator, shown in Figure 3-17(a), was programmed to travel towards the microcapsule at a speed of 2 μm/s to compress it on the glass slide (Figure 3-17(b)). The force transducer was connected to a data acquisition card where the voltage generated from the transducer due to compression of the microcapsule was collected. The system used can measure forces with a precision of ± 0.1 μN and probe displacement of ± 0.2 μm (Thomas *et al*., 2000). For each sample 20 to 50 microcapsules were randomly selected.

The glass probes in this study were made of borosilicate glass capillaries with an inner diameter of 0.58 mm and outer diameter of 1.0 mm. Each probe was first heated up in the middle by a glass puller (Micro Forge, MF-900 Narishige, Japan) and then pulled down to obtain two separate glass needles. One of them was placed on a grinding machine (EG-40, Narishige, Japan) for 24 hours, in order to flatten the contact surface. The probe was then attached to a force transducer using commercial superglue (01-30379 cyanoacrylate adhesive, Loctite, UK), as shown in Figure 3-17(a). To make sure microcapsules can be trapped between the two parallel surfaces (the flat surface of probe and sample glass slide), the diameter of the glass probe is required to be at least 2 times bigger than the microcapsule diameter, which in the case of the microcapsules tested in this work corresponds to about 160 to 200 μm.

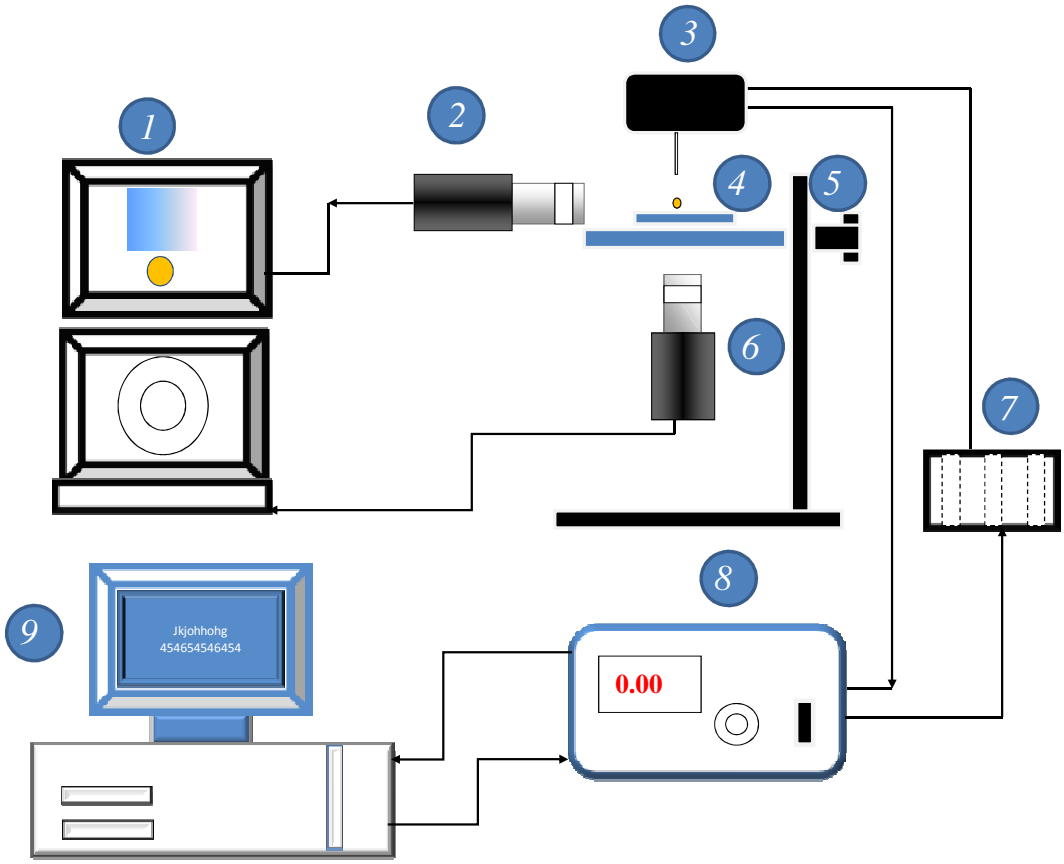

Figure 3-16 Schematic diagram of the micromanipulation rig. (1) TV Monitor, (2) side view camera, (3) force transducer connected to a probe, (4) microcapsule, (5) sample stage, (6) bottom view camera, (7) micromanipulator controlled by a servomotor, (8) power supply and motor control box, (9) computer with data acquisition board

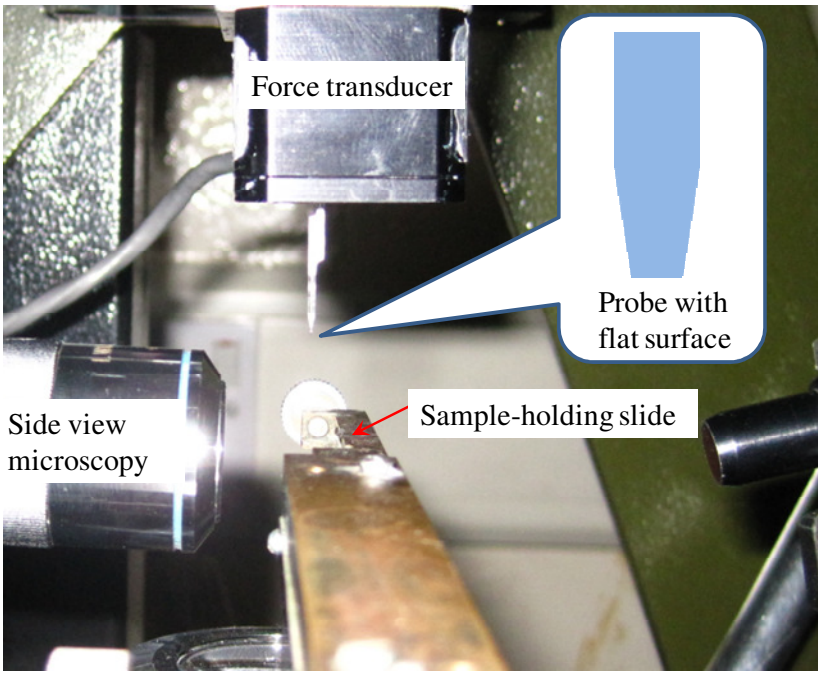

(a)

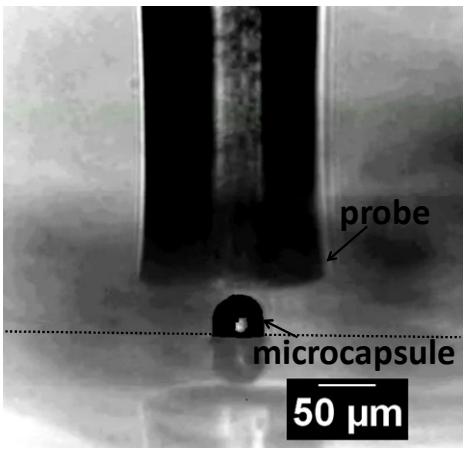

(b)

Figure 3-17 Photographs of a micromanipulation rig to compress single microcapsules. (a) Force transducer with an attached glass probe for the compression of single microcapsules. (b) The glass probe (top) with a microcapsule ready to be compressed.

3.4.2.1 Typical data generated

Figure 3-18 (a) shows a typical force versus displacement curve from compressing a single microcapsule to rupture using the micromanipulation rig. The force was calculated from the output voltage of the transducer signal multiplied by the transducer sensitivity, which defines the maximum force range of the transducer. Due to the material properties of an elastic beam inside the transducer, to which the glass probes are connected, there is deflection of the probe during compression of microcapsules. The compressive displacement here is defined as the result of the transducer probe moving distance minus the deflection of the probe. At Point A in Figure 3-18 (a), the probe made contact with the microcapsule. From A to B to C, the force increased as the microcapsule was compressed by the probe. B was defined as a pseudo-yield point in previous work (Sun and Zhang, 2001). At point C the microcapsule burst and the core oil was released.

A different situation occurred when the micromanipulation rig was used to compress a single microcapsule with thick shells. For this kind of microcapsule, the compression force increased constantly, without a clear bursting point (Figure 3-18 (b)), even if rupture was observed on the monitor. In such kind of capsules, the compression forces eventually soars to values larger than the maximum operational force of the transducer, which stops the test for safety. It is expected when this happens that the top and

bottom parts of the shell are touching each other, and therefore the rig is not compressing a solid material, no longer a core-shell structure.

The fractional deformation ε_m in the compression profile is defined as the displacement normalized by the capsule diameter. It is required to compare the compression profiles of capsules with different diameters, as well as to calculate intrinsic mechanical properties like the shells elastic modulus E and failure stress σ_p.

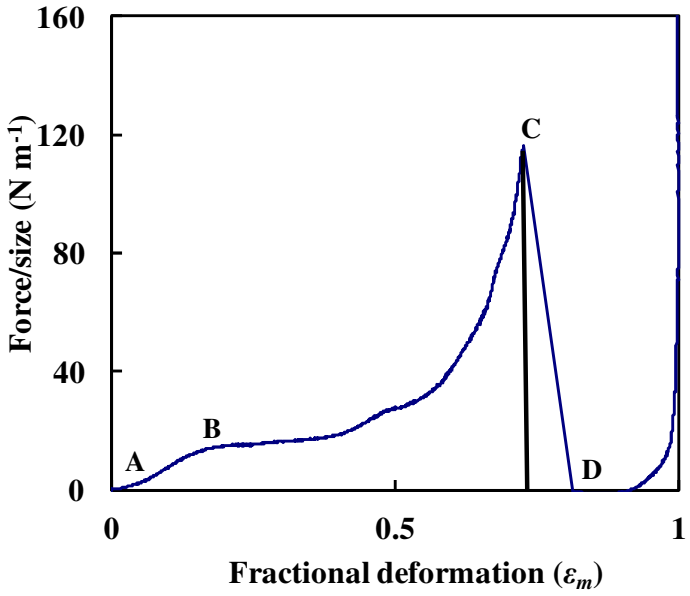

(a)

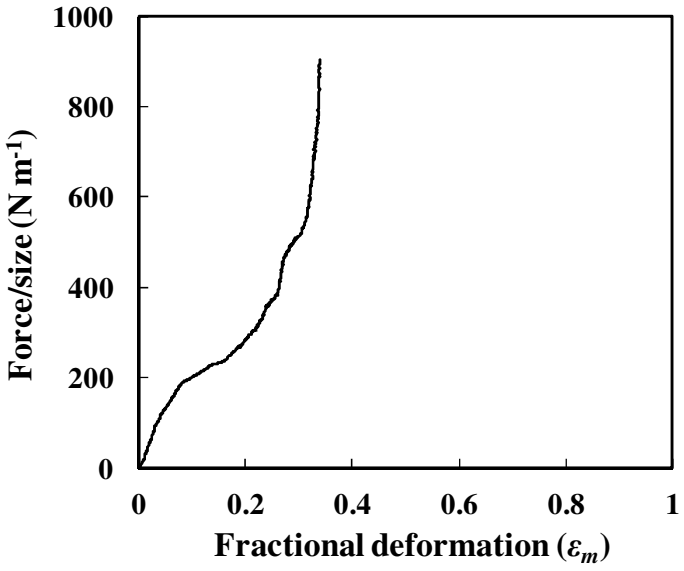

(b)

Figure 3-18 Typical curve of compressing a single microcapsule. **(a)** Force versus displacement curve for compressing a single MF microcapsule (the preparation method is described in Section 4.2.1.) to rupture. **(b)** Typical normalized compression force profile of PMMA microcapsules formed after a reaction time of 4h (the preparation method is described in Section 6.2.1.).

3.4.3 Ultraviolet-Visible spectrophotometry (UV-Vis)

Ultraviolet-visible (UV-Vis) spectrophotometry is a versatile technique to identify or quantify organic and inorganic compounds in solution. There are basic requirements for this instrument, such as: a radiation light with a suitable range of wavelengths, a monochromator and optical geometry, a sample holder and a detector. (Skoog *et al.*, 1999).

The principle of this technique is based on Beer-Lambert law, equation 3.8 (Skoog *et al.*, 1999, Weckhuysen, 2004).

$$A = log\frac{I_0}{I_t} = \varepsilon \times l \times c \qquad \text{(Equation 3.8)}$$

Where, A is the absorbance of sample, I_t is the intensity of the transmitted light, I_0 is the intensity of the incident light, l is optical path length (cm), in this study, which is 1 cm for the cuvette used here. c is the concentration of the sample (g mL^{-1}) and ε is the extinction coefficients (mL g^{-1} cm^{-1}), which is constant for a given material at a particular wavelength. The solution concentration can be obtained through the absorbance measurement and calculated by Equation 3.8, for a certain solute in a given solvent if the extinction coefficients ε is known.

A calibration of solution concentration versus absorbance is necessary to perform before using UV-Vis to detect solution concentration. The solution was first scanned over a range of wavelength to figure out the particular wavelength where absorbance is maximum λ_{max} (nm). The pure solvent was then scanned to use as a blank for

UV-Vis measurements. The absorbance of 10 to 12 samples with different given standard solution concentrations were measured at λ_{max} (nm). The absorbance values of these samples were then plotted versus their corresponding concentrations, the slope is proportional to the extinction ε (mL $g^{-1}cm^{-1}$), as shown in Figure 3-19.

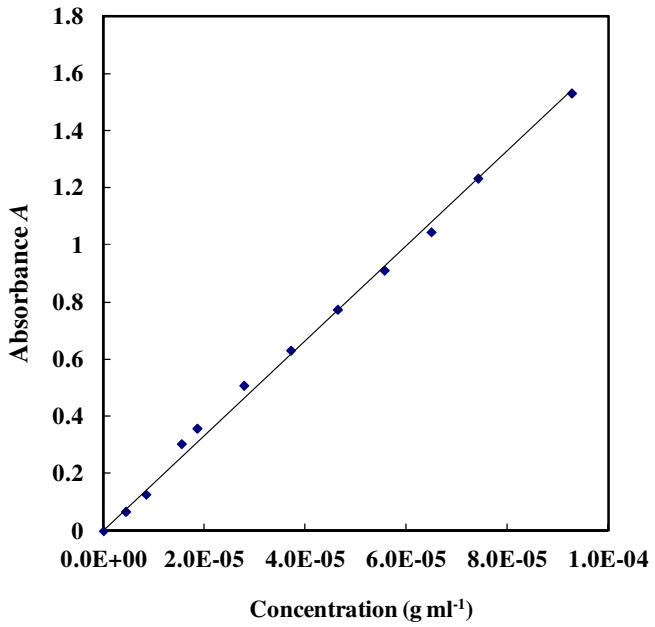

Figure 3-19 Example to calculate the extinction coefficients using calibration plats. The data points represent the absorbance of perfume oil A obtained by UV-Vis spectrophotometry versus the concentration (g mL^{-1}). The best linear slope represents the value of $\varepsilon = 16627 \pm 174$ mL $g^{-1}cm^{-1}$.The solute is perfume oil Ain 10% glucose aqueous solution.

In this study, a UV-Vis spectrophotometer (Cecil Instruments, Cambridge, UK) was used to measure the concentration of core oils released in solution. The solutions were pumped into the UV-Vis using a flow cuvette to test the absorbance continuously, providing the complete release profiles. The release behaviour was used in the determination of the shell permeability as reported in the literature (Mercade-Prieto *et al.*, 2012b); the details are described in Chapter 7.

3.4.3.1 Typical data generated

A typical oil release profile from microcapsules is presented in Figure 3-20, where the concentration measured is relative to in the solvent used The sample was an aliquot of MF microcapsules slurry tested in 60% v/v glycerol. The release data were collected continuously, and the absorbance values obtained through UV-Vis spectrophotometry were recorded by computer. The concentration was calculated using the absorbance and the previously determined ε.

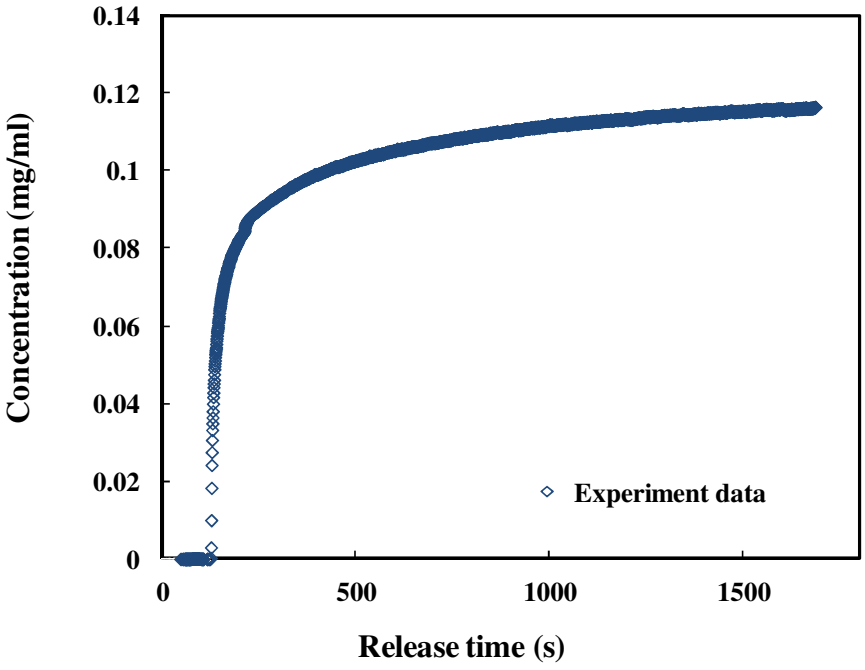

Figure 3-20 A typical curve showing perfume oil released from MF microcapsules in 60% v/v glycerol obtained using the UV-Vis spectrophotometry. The data points were calculated from experimental data of UV-Vis spectrophotometry.

3.4.4 Environmental scanning electron microscopy (ESEM)

Environmental scanning electron microscopy (ESEM) was employed to investigate the morphology of microcapsules in wet conditions, as well as the dry surface of the membranes used in the dispersion cell (Section 3.2.1). Unlike traditional electron microscopes, ESEM can be operated in dry or wet modes. Although sometimes spatial resolution of ESEM is lower in wet mode compared with dry one, the specimen does not need special prior preparation, and it is able to operate in a low vacuum (Clarke and Eberhardt, 2000, Danilatos, 1993).

As in conventional SEM, an electron gun in ESEM employs a scanned electron beam, and several electro-magnetic lenses are used to focus. The beam is direct on the surface of the specimen, which interacts with the specimen surface layer. Signals are then produced which are collected by the detectors, as shown in Figure 3-21 (Clarke and Eberhardt, 2000). The environmental secondary detector based on a gas ionization principle is specially designed in ESEM for using in low vacuum mode (Baumgarten, 1989). The unwanted gas ionization for the high vacuum SEM is used in a signal amplification process, as shown in Figure 3-22 (Danilatos, 1993).

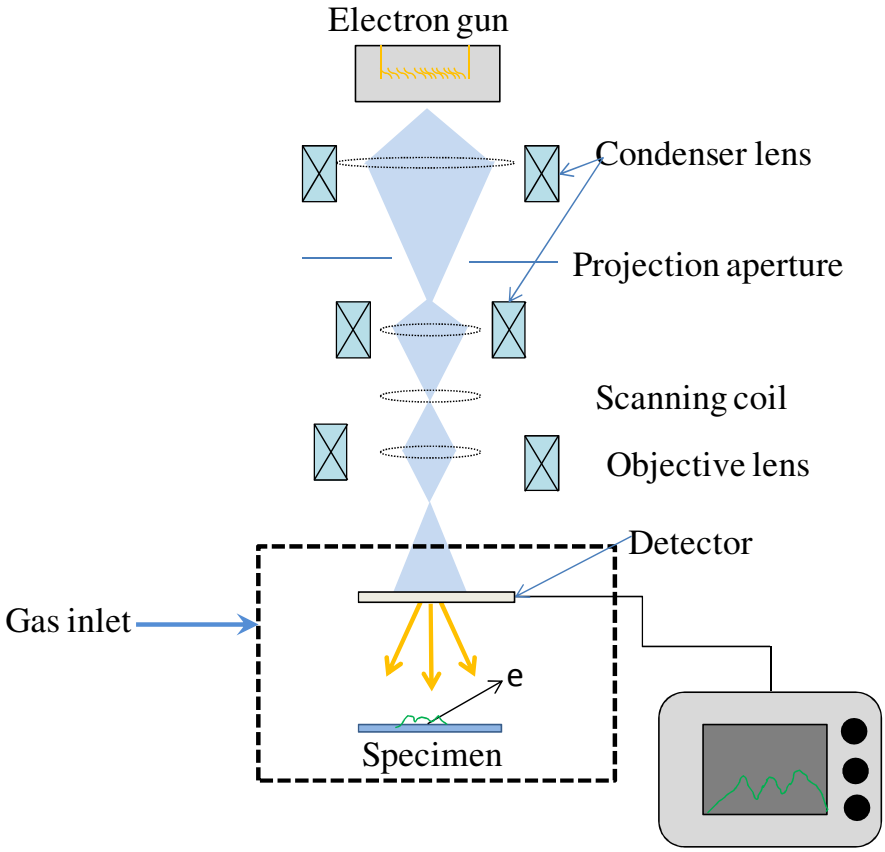

Figure 3-21 Schematic representation of environmental scanning electron microscopy (ESEM).

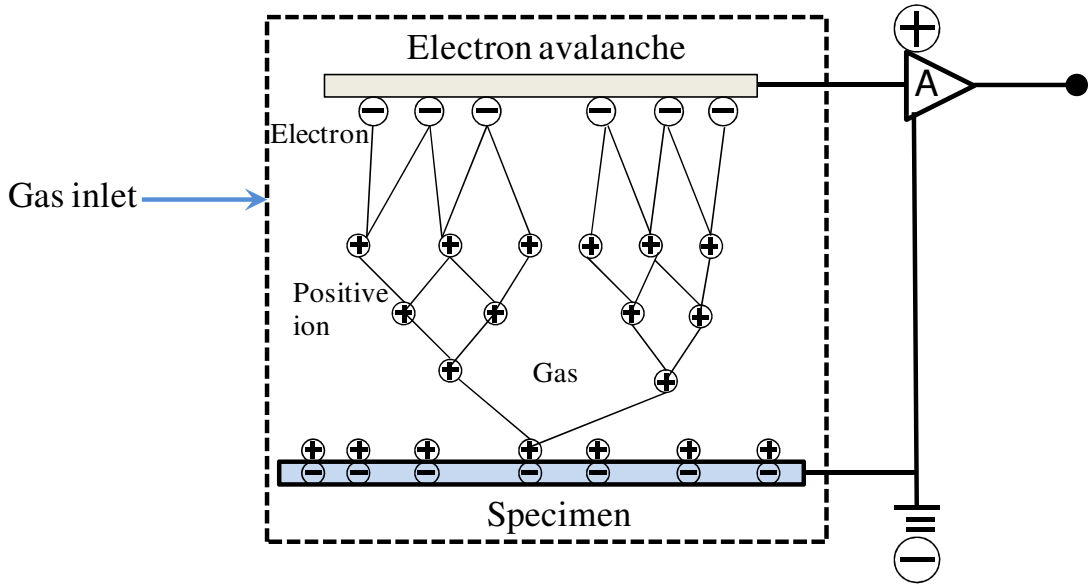

Figure 3-22 Schematic representation of the environmental secondary detector with gas.

3.4.4.1 Typical ESEM image

The ESEM system used in this study was a Philips XL30, Netherlands. The sample was directly loaded into the ESEM for characterisation when using the wet mode at an accelerating voltage from 10.0 to 15.0kV. Specimen preparation was needed when using the dry mode. In this case, the sample was first loaded in a sputter coater (Polaron S07640, Quorum Technologies Ltd, UK) to coat with a thin layer of gold (about 5-6 nm) for 3 min. After rendering the microcapsule surface conductive, the sample was loaded in ESEM and an accelerating voltage used varied from 15.0 to 20.0 kV.

A typical ESEM image of microcapsules is shown in Figure 3-23.

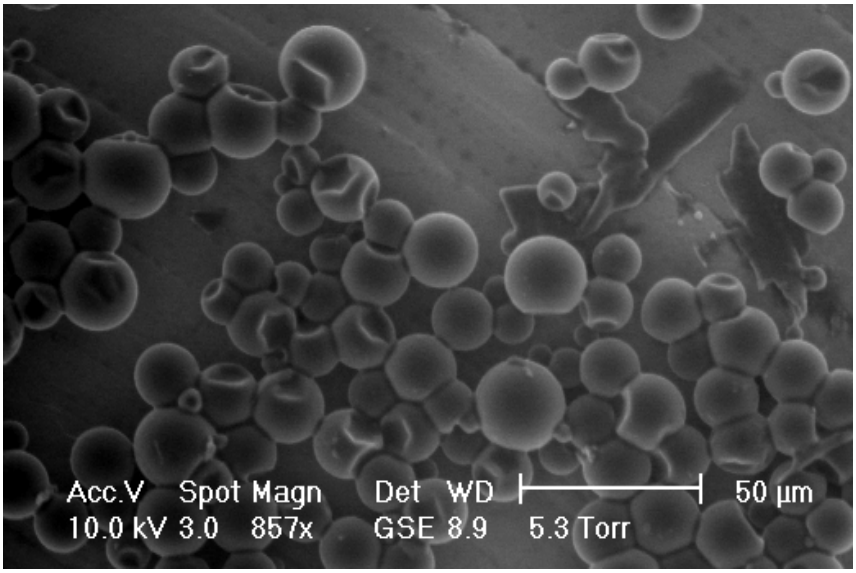

Figure 3-23 A typical image of MF microcapsules obtained by ESEM (Philips XL30) in wet mode at an accelerating voltage of 10.0 kV. The MF microcapsules were generated in a homogenizer, see Section 4.2.1 .

3.4.5 Transmission electron microscopy (TEM)

Transmission electron microscopy (TEM) has been used to determine the shell thickness of microcapsules (Yang *et al.*, 2008). Microcapsules were embedded in a LR acrylic resin, cut into thin slices, and are then made conductive by coating with gold. All TEM measurements are taken in vacuum conditions. A coherent beam, which is produced by an electron gun and condenser lenses, transmits through the thin specimen to generate an image. The image is then magnified by projector lenses in the TEM. The thicker or the denser part of the sample has less electrons transmitted

through, and it will be shown darker than the thinner or less dense part of the sample (Clarke and Eberhardt, 2000). In this study, the microcapsule samples were pre-processed at the Centre of Electron Microscopy of the University of Birmingham. The microcapsules were first centrifuged and then dehydrated. In order to support the shell structure of microcapsules, 50% of LR white acrylic resin and ethanol suspension was added into the dehydrated sample. The microcapsules were then embedded in pure resin by removing the supernatant. The sample after being polymerized by acrylic resin was cut by a diamond knife using a ultra-microtome (Ultracut E, Reichert-Jung, Austria) to ultrathin sections with a thickness about 80 nm. The ultra thin sections were imaged with a transmission electron microscope (Joel 1200EX, Joel UK Ltd, UK). The micro-images showing the cross-section of microcapsules were analysed by software Image J 1.46 (National Institute of Health, USA).

3.4.5.1 Typical TEM image

A typical TEM image for the cross-section of microcapsules is shown in Figure 3-24. MF microcapsules were embedded in LR acrylic resin, and sectioned using a ultra-microtome.

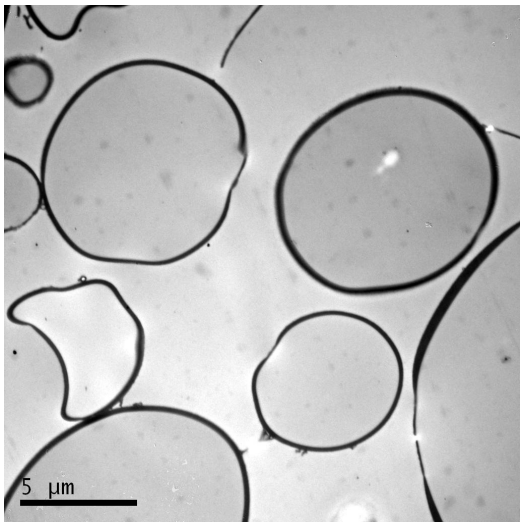

Figure 3-24 A TEM image of the cross section of MF microcapsules. The preparation details of the MF microcapsules are described in Section 4.2.1.

3.4.6 Confocal laser scanning microscopy (CLSM)

TEM is a costly and time consuming technique which is not suitable for many materials, such as PMMA. PMMA has similar physical properties as the acrylic resin used during the sample preparation, which means that the sample with PMMA was dissolved into the acrylic resin. This damages the sample and measurements cannot be performed. CLSM is a non-destructive technique that has been used to investigate the shell structure and thickness of microcapsules (Chen *et al.*, 2006, Corle and Kino, 1996, Lebedeva *et al.*, 2004, Paramita *et al.*, 2010, Tzhayik *et al.*, 2012).

CLSM permits observation of a selected layer within a relatively thick specimen, and allows 3D image reconstruction. A laser gives a focused light spot, which passes through an aperture and focuses within or on the surface of a specimen. In order to use CLSM under fluorescence condition, a fluorescence dye needs to be added into the sample before microencapsulation. Reflected light from the specimen is recollected and separated by dichroic mirror. The reflected emission fluorescence light then passes a pinhole, discarding all the light which does not come from the desired focal plane. Finally, the light intensity is quantified in a photomultiplier tube (PMT). The whole process is shown in Figure 3-25 (Chen *et al.*, 2006, Corle and Kino, 1996, Lebedeva *et al.*, 2004, Paramita *et al.*, 2010, Tzhayik *et al.*, 2012).

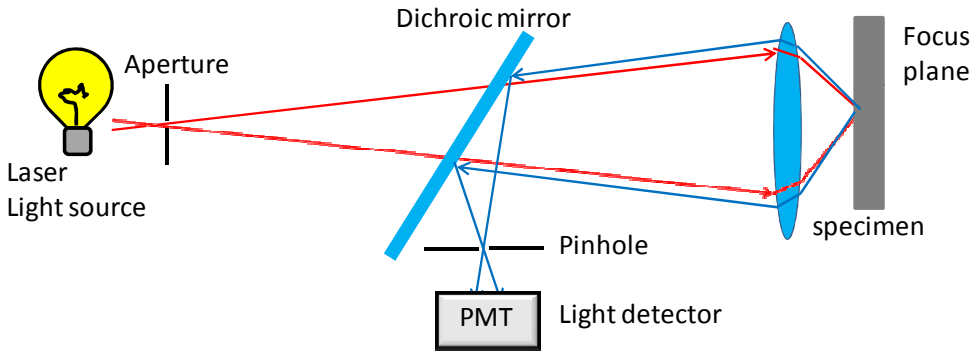

Figure 3-25 Schematic representation of confocal laser scanning microscopy (CLSM).

3.4.6.1 Typical CLSM image

A typical CLSM image of the cross section of the microcapsules is shown in Figure 3-26.

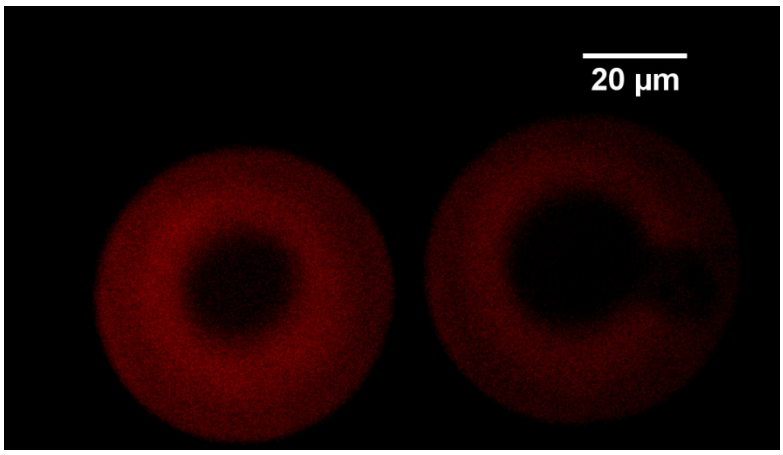

Figure 3-26 A CLSM micro-image of the cross-section of PMMA microcapsules.

3.4.7 Contact angle measurement device

A home-built apparatus with a side view microscope was used to determine the contact angle of water on the membrane, see Figure 3-27 (Pranzetti *et al.*, 2012). Contact angles were used to understand the hydrophilic or hydrophobic nature of the membrane surface used in the dispersion cell system (Micropore Technologies Ltd., UK.). Experiments were performed at a room temperature of 25ºC. A drop of Millipore water (approximately 0.01 mL, Millipore, UK) was carefully placed on the top of the membrane surface, particularly in a flat area between the pores. The image

of the liquid droplet was then taken and recorded by a CCD KP-M1E/K camera (Hitachi, UK). The contact angle between the water and the membrane surface was determined through the FTA image analysis software v1.96 (First Ten Angstroms). Fifty images of each droplet were taken and 5 droplets were measured under each condition.

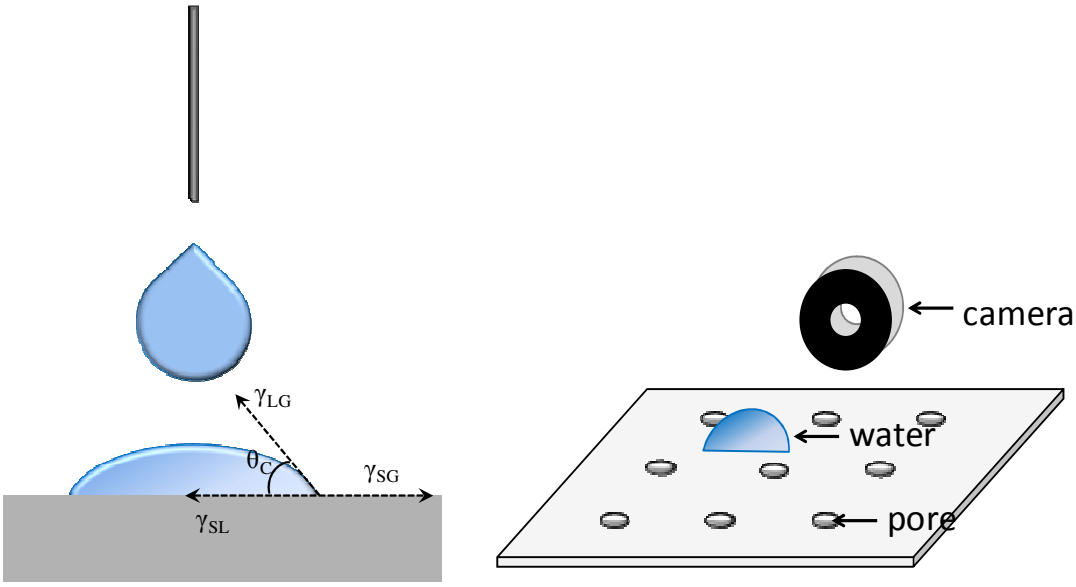

Figure 3-27 Schematic diagram of the device for measuring the contact angle.

3.4.8 Tensiometer

The interfacial tension between two immiscible phases in an emulsion was measured using a tensiometer (Processor Tensiometer K100, KRÜSS Advancing surface science, UK) shown in Figure 3-28. The experiment was carried out at 15±1°C, since the emulsification of the perfume oil with the MF precondensate and was performed at 15±1°C (Long *et al.*, 2009).

Figure 3-28 Photography of the tensiometer K100 used in this study

Interfacial tension measurements were performed using a Wilhelmy plate (Drelich *et al.*, 2002, Mulqueen and Huibers, 2002) (Processor Tensiometer K100, KRÜSS Advancing surface science, UK). The two tested liquid phases were placed in one vessel, with the heavy phase at the bottom and lighter phase added onto the top. The Wilhelmy plate is a thin platinum plate with an area of a few square centimetres, oriented perpendicularly to the interface of the two phases during the measurement. The plate was pushed up slowly and the force changes on the plate were measured by a force transducer inside the tensiometer, as shown in Figure 3-29. During the process, the force versus time data points were recorded through the tensiometer (Processor

Tensiometer K100, KRÜSS Advancing surface science, UK). The interfacial tension was calculated automatically using the Wilhelmy equation.

$$\gamma = \frac{F_{tension}}{l_w \cdot \cos\theta_p} \qquad \text{(Equation 3.9)}$$

where $F_{tension}$ is the force on the plate during the measurement, lw is length of the wetted area of the plate, and θp is the contact angle between the heavier phase and the Wilhelmy plate, as shown in Figure 3-29.

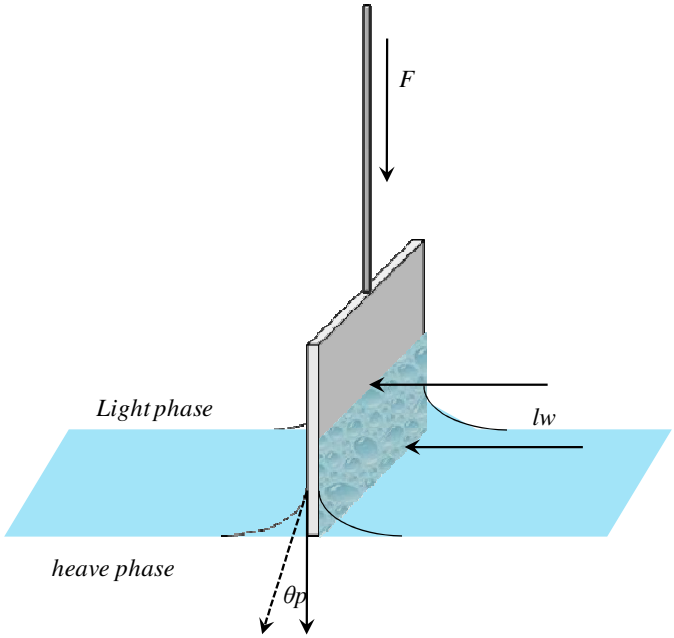

Figure 3-29 Schematic of the Wilhelmy plate method applied to an interface of two liquid phases.

3.4.8.1 Typical data generated

A typical output of the tensiometer is shown in Figure 3-30. Interfacial tension value of each data point was calculated by the tensiometer. Each experiment was repeated four times and interfacial tension value presented is the average of five measurements.

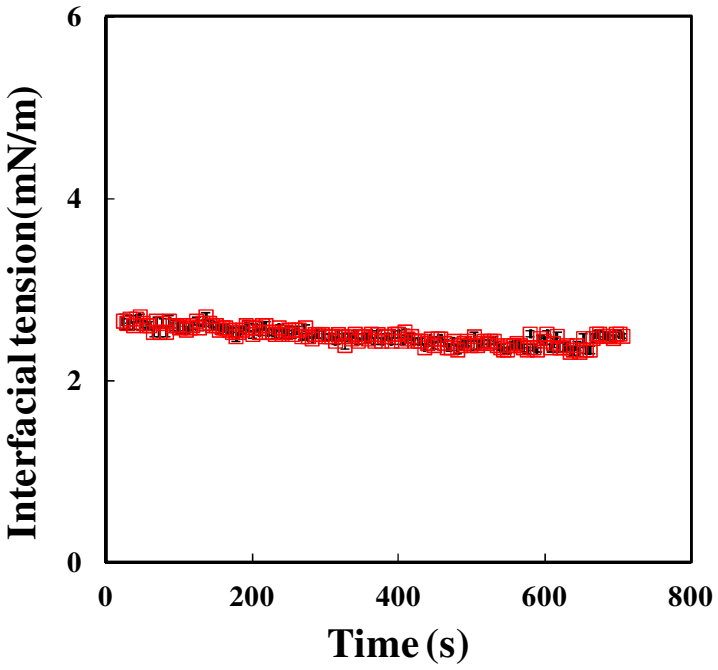

Figure 3-30 A interfacial tension versus time curve obtained through a Tensiometer. Perfume oil B was used as the light phase and MF precondensate as the heavy phase. The error bars in the figure represent the standard deviation, which are smaller than the symbols. The interfacial tension between the two phases considered is the mean value of all the data points.

3.4.9 Rheometry

The viscosities of the two phases were measured using a rotational rheometer (AR1000, TA instruments, UK) at 15±1°C according to the emulsification temperature of MF precondensate and perfume oil, shown in Figure 3-31. A methodology based on two plates or cone and plate was used to measure the samples viscosity. The sample was placed on one horizontal plate and another plate (or a shallow cone) placed on it. When the plate above was rotated and sheared the sample between the two plates, the force was measured. The temperature was controlled by a cooling pump during the whole experiment. The viscosity of the sample was calculated as the ratio of the shear stress to shear rate applied (Franck, 2010) automatically by the rheometer. Two different polymer-made parallel plates of 40 and 60 mm in diameter were used for oil phases and water phases, respectively.

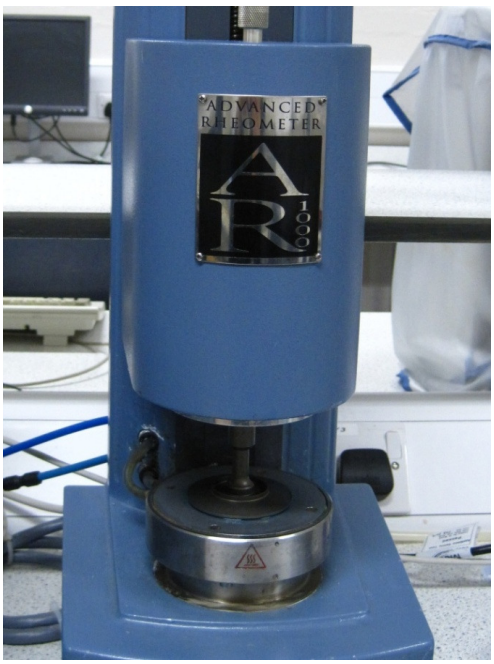

Figure 3-31 Photo of the rheometer AR1000 used in this study

3.4.9.1 Typical data obtained

A typical set of viscosity data is shown in Figure 3-32. Each experiment was repeated four times and viscosity value presented is the average of five measurements.

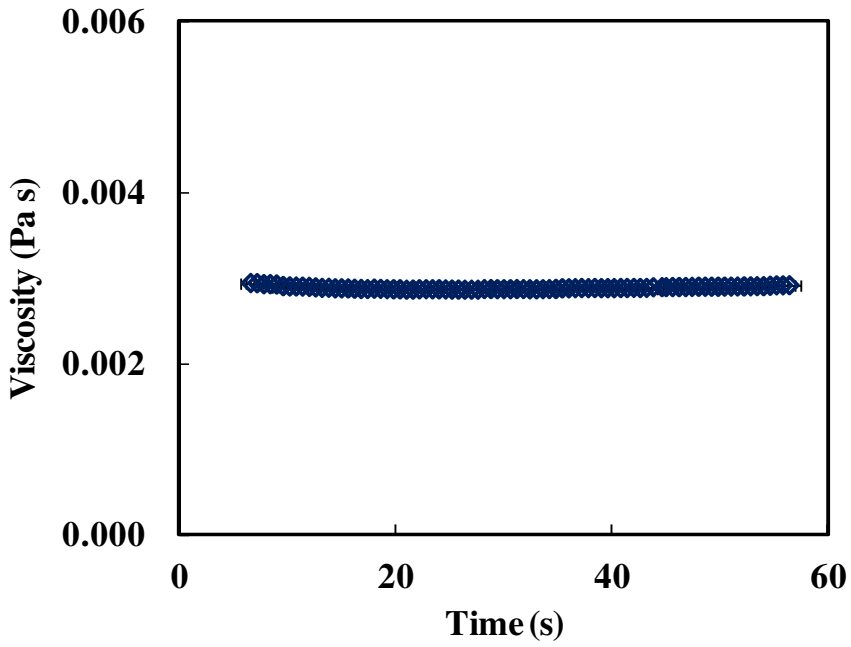

Figure 3-32 Viscosity of peppermint oil tested with the rheometer. The error bars in the figure represent the standard deviation and some are too small to be seen. The viscosity value considered in the study is the mean value of all the data obtained from the experiment.

Chapter 4 Size and Strength Distributions of Melamine-formaldehyde Microcapsules Prepared by Membrane Emulsification

4.1 Introduction

In this chapter, melamine formaldehyde (MF) microcapsules containing an oil-based active ingredient (oil A) were prepared using the dispersion cell system presented in Section 3.3. The generated emulsions were encapsulated by the *in situ* polymerization of melamine formaldehyde precondensate at the interface. The effect of the process conditions were investigated on the size and size distribution of the oil droplets produced in the stage of emulsification and the final microcapsule. The contact angle of the membrane surface was also studied in order to understand its impact on size and uniformity of droplets. A simple homogenization system was also used to prepare the microcapsules in order to compare with those produced by the membrane system. The effect of the homogenizer agitation speed on the formed droplets was studied. The microcapsules were characterized as described in the previous chapter.

4.2 Experimental

4.2.1 Preparation of microcapsules

4.2.1.1 Preparation of microcapsules using membrane emulsification

The formulation of MF microcapsules were produced based on the protocol developed by Long *et al.* (2009) for the encapsulation of perfume oils. However, the process and reaction conditions were modified in order to improve the size distribution of the microcapsules. An aqueous solution of MF precondensate (2.50 g), formaldehyde (0.30 g) and copolymer polyacrylamide-co-acrylic acid-sodium salt (0.58 g) in water (70 g) was stirred for 105 min with a Rushton turbine impeller (Φ32 mm) at 400 rpm in a 0.25 L vessel (Φ 65mm) with 4 baffles. The pH value was modified to 4.3 (adjusted with 20% (v/v) acetic acid), monitored by a pH meter (Seven easy, Mettle Toledo, UK) at room temperature (22 ±1°C).

The prepared precondensate solution was put into the glass chamber of the dispersion cell and the core oil A (9.33 g) was pumped through a "15 rcia A" metal membrane or "15 rcia C" silica membrane (see Section 3.3.1). The membranes were previously wetted with polyalkyleneoxide modified heptamethyltrisiloxane (Micropore technologies Ltd, UK) at a concentration of 0.25% - 2% (v/v) for 30 min. Emulsions were prepared using an agitation speed from 0 to 1210 rpm and a dispersed phase flux from 1.6×10^{-5} m s^{-1} to 3.9×10^{-5} m s^{-1}at 15 ± 1°C for about 30 min (the flux represents the oil velocity through pore area)

The resulting emulsion was transferred back to the stirred vessel, where it was agitated again with the Rushton turbine impeller at 125 rpm to make sure there was no oil droplet breakage at 15 ± 1°C for 30 min. Finally, the emulsion was placed into a water bath at room temperature (SUB SQUA5, Grant Instruments Cambridge Ltd., UK); which was then heated to 45 ± 1°C, 55 ± 1°C or 65 ± 1 °C., The high temperatures induced the polymerization of the MF precondensate, which were left for 6 h. The resulting microcapsules in suspension were cooled to 25 ± 1 °C, and the pH was raised to 10 (adjusted with 1 M NaOH) to terminate the polymerization reaction. The whole process is schematically shown in Figure 4-1.

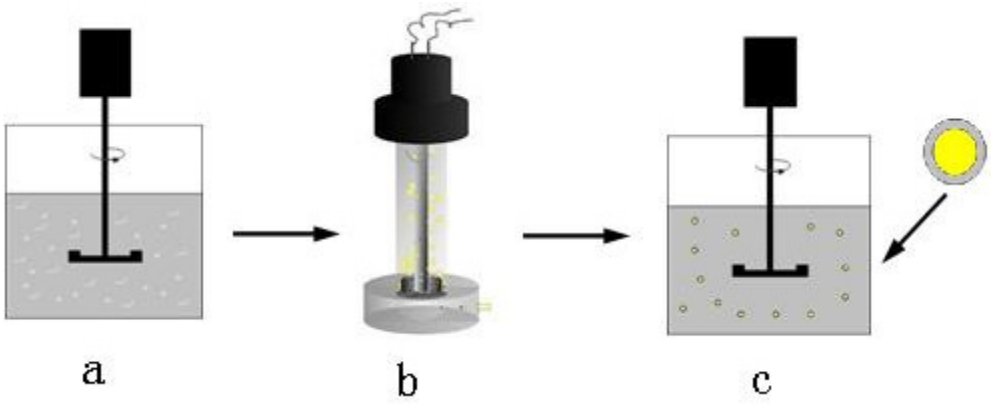

Figure 4-1 Schematic diagram of preparing MF microcapsules using a flat membrane combined with a stirred system.

(a) Pre-cross-linking (b) Emulsification (c) Polymerization

4.2.1.2 Preparation of microcapsules using conventional homogenization

Microcapsules were also prepared using a conventional homogenizer for comparison with a widely used technique. A homogenizer with 4 blades impeller (Φ 30mm) in the

middle coated with a membrane tube (Φ 35mm) with regular round pores (Model L4RT, Silverson Machines Ltd., UK) was applied to generate broad emulsions. Emulsions were generated at speeds from 400 rpm to 2500 rpm for 30 min at 15 ± 1 °C. The rest of the process conditions were the same as those for preparation of MF microcapsules by the membrane emulsification.

4.2.1.3 Preparation of microcapsules with fluorescent dye

Microcapsules with a fluorescent dye were prepared under the same conditions described above except that Rhodamine B with a concentration of 0.01% (w/w) was added to the core oil before the emulsification step.

4.2.2 Morphology and shell thickness of microcapsules

The surface morphology of the microcapsules was characterised by optical microscopy (Leica DMRBE, Leica, UK) and environmental scanning electron microscopy (ESEM) (FEI/Philips XL30 ESEM-FEG, Philips, UK).

The structure and thickness of the microcapsule shell were studied by transmission electron microscopy (TEM) (JEOL 1200EX, Jeol Ltd, UK). The ultrathin microcapsule sections of microcapsules were captured at an acceleration voltage of

10.0kV through TEM. For each batch, 50 microcapsules were randomly selected; 8-10 measurements along the circumference were made on each single microcapsule.

Confocal laser scanning microscopy (CLSM) (Leica TCS SPE, Germany) was also used to determine shell thicknesses of microcapsules with a fluorescent dye. The excitation wavelength (510 nm) was chosen according to the fluorescent dye Rhodamine B. For each batch, 20 microcapsules with the fluorescent dye RB were randomly selected and 4 measurements were performed on the cross-section at different directions. The micro-images obtained by both techniques: TEM and CLSM were then analysed by Image J 1.46 (National Institute of Health, USA).

4.2.3 Size analysis

The mean size and size distribution of the oil droplets produced in the stage of emulsification and the final microcapsules were determined using a laser diffraction technique (Mastersizer 2000, Malvern Instruments, UK). The data of *SPAN*, *CV*, Sauter mean diameters $D_{3,2}$ and volume mean diameter $D_{4,3}$ were recorded.

The experiments to measure oil droplet and microcapsule size distributions were performed at 25 ± 1 °C. The refractive index of the oil is 1.497 (given by the supplier P&G, UK) and that of the microcapsules is 1.65 (Long *et al.*, 2009). The values of the

mean diameter and size distribution data of droplets as well as microcapsules are the average of five measurements.

4.2.4 Measurement of the mechanical strength of single microcapsules

The rupture force, displacement at rupture, and diameter of single microcapsules were determined by a well-established micromanipulation technique (Sun and Zhang, 2001). One drop of suspension with microcapsules was diluted with double distilled water and placed on a glass slide and the microcapsules were left to dry in air for 2-3 min. Single microcapsules were observed with side-view and bottom-view microscopes (Micro Instruments Ltd., Oxon, UK). A glass probe of 160 μm in diameter which was connected to a force transducer (Model 405A, Aurora Scientific Inc., Canada) that was mounted on a fine micromanipulator (Micro Instruments Ltd., Oxon, UK), which was programmed to travel towards a single microcapsule at a speed of 2μm/s to compress the microcapsule to rupture. 50 microcapsules in each sample were randomly selected and tested at 25 ± 1°C. Details of this technique are described in Section 3.4.2.

4.3 Results and discussion

4.3.1 The effect of membrane surface hydrophilicity on the mean size and size distribution of oil droplets

The properties of the membrane can influence the performances of the emulsification process using the dispersion cell system (Peng and Williams, 1998b). The membrane surface hydrophilicity is one of the factors which may affect the size and size distribution of emulsion droplets produced by the membrane system. Contact angle between pure water and the membrane surface is one of the parameters used to determine the membrane surface hydrophilicity. Hydrophilic surface will have smaller contact angle using pure water than hydrophobic ones. This characterization is important because a hydrophilic membrane surface is one of the conditions to obtain uniform emulsion droplets (Wang *et al.*, 2005, Zhou *et al.*, 2007). One of the common ways to change the membrane surface hydrophilicity is by soaking the membrane into a wetting agent or in the solution used as the continuous phase (Boom, 2003). It is also mentioned in the literature that wetting the membrane with the dispersed phase must be avoided in order to generate mono-sized droplets (Nakashima *et al.*, 1991, Nakashima *et al.*, 2000). In this study, a special wetting agent was used to treat the membrane surface.

Figure 4-2 (a) shows the mean droplet diameter $D_{4,3,}$ *CV* and *SPAN* values for a given agitation speed of 1080 rpm and dispersed phase flux 1.6×10^{-5} m s^{-1}, using a membrane "15 rcia A", treated with different concentrations of wetting agent for 30 min. The mean diameter and *SPAN* values of the oil droplets are broadly in good agreement with those reported for sunflower oil droplets produced using a similar device (Kosvintsev *et al.*, 2005).

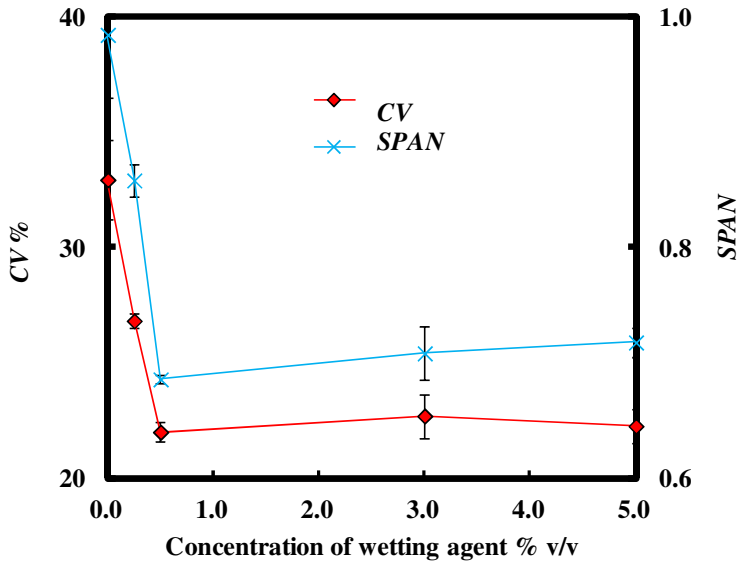

(a)

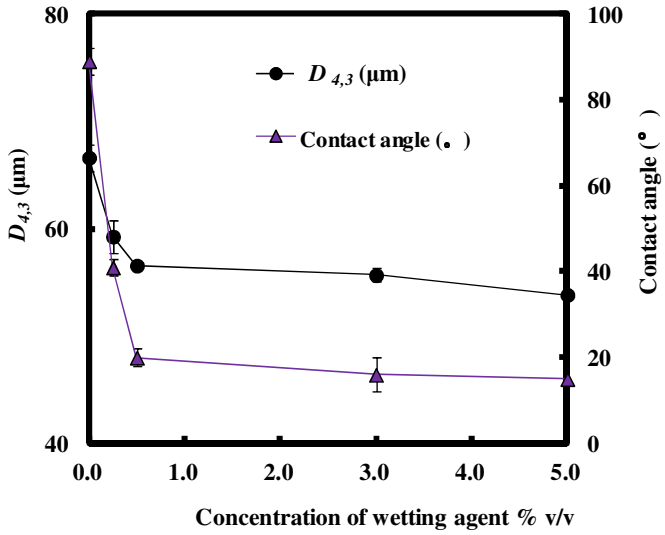

(b)

Figure 4-2. Effect of concentration of the wetting agent on (a) the size distribution of the droplets in the emulsion and (b) the size of the droplets in the emulsion and contact angle of water on membrane surface, prepared using an agitation speed of 1080 rpm, dispersed phase flux of 1.6×10^{-5} m s^{-1}, and a membrane "15 rcia A". The error bars represent the standard error of the mean (each experiment was conducted 11 times, and each sample was tested 5 time, number (N) =55.

When the wetting agent concentration is increased from 0 to 0.5% (v/v) there is a sharp decrease in the contact angle, but further addition of wetting agent does not result in a significant reduction in the contact angle (Figure 4-2(b)). This might be due to the membrane surface fully occupied by the molecules of the wetting agent with a concentration of 0.5% (v/v). Correspondingly, the mean diameter of the droplets, *CV* and *SPAN* value initially decrease with the contact angle and then level off.

At high concentrations of wetting agent the contact angle was much smaller (<20°), which implies a more hydrophilic membrane surface compared with when no wetting agent was used, the contact angle for pure water was 89 ± 3°. Wetting agent made the oil droplets more difficult to spread on the membrane surface during formation. This leads to the decrease of the mean droplet size and also causes shorter residue time, further reducing the coalescence of droplets residing on the membrane, narrowing the size distribution (smaller *SPAN* and *CV* values).

The size and size distribution using a hydrophilic silica membrane ("15 rcia C") with a contact angle of 25 ± 2°) very similar to the metal membrane "15 rcia A" with 0.5 wt% wetting agent (with a contact angle of 20 ± 2°), shown in Figure 4-3. This further indicates that the size and size distribution are determined by the contact angle rather than the type of membrane material.

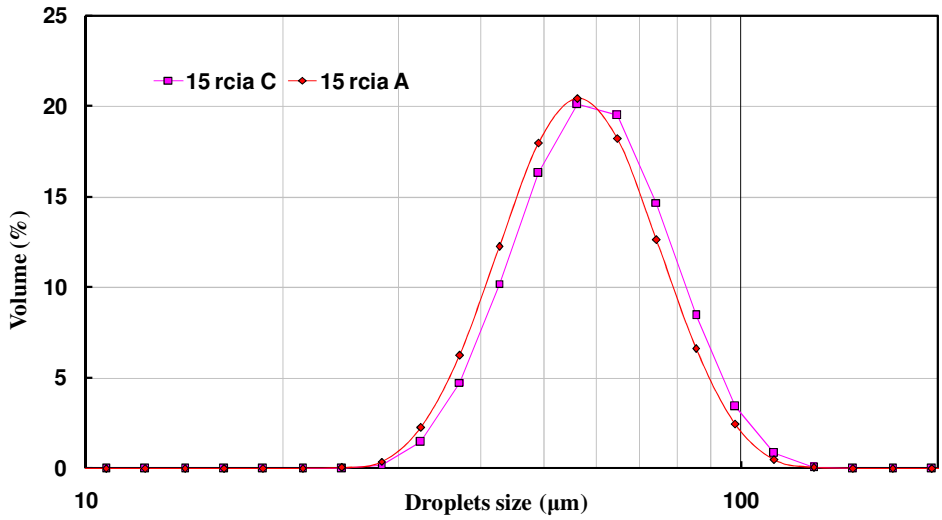

Figure 4-3. Size distribution of droplets in emulsions generated by different membrane materials. Squares: "15 rcia C" silica membrane; diamonds: "15 rcia A" metal membrane. The emulsions were prepared using an agitation speed of 1080 rpm and dispersed phase flux of 1.6×10^{-5} m s^{-1}. For "15 rcia A", a wetting agent concentration of 0.5% (v/v) was used.

Since the contact angle did not decrease significantly when the concentration of the wetting agent was greater than 0.5% (v/v) (Figure 4-2), this concentration was used in further experiments.

4.3.2 Stability of the oil/water emulsion

The size distribution of the droplets in the formed emulsion was measured after being stored up to 4 h to assess their storage stability. This was performed since it took a quite few minutes before microcapsules where formed from the emulsions. Figure 4-4 shows that there is no significant change of the values of mean diameter $D_{4,3}$, *CV* and *SPAN* of the droplets within 4 h. Therefore, the emulsions were considered stable during this period.

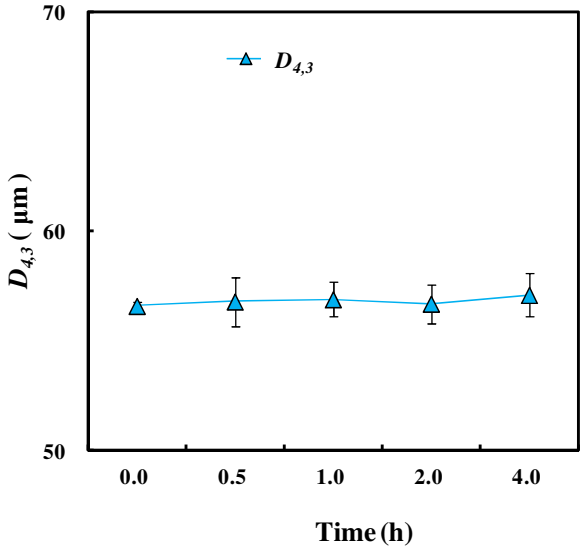

(a)

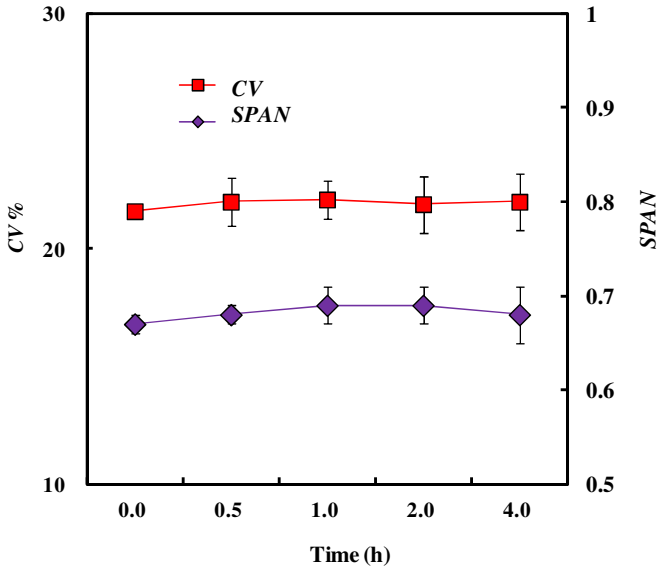

(b)

Figure 4-4. The (a) mean diameter ($D_{4,3}$) and (b) *CV and SPAN* values of the oil emulsions measured at different times after their formation at 25°C. Emulsions were prepared using an agitation speed of 1080 rpm, dispersed phase flux of 1.6×10^{-5} m s^{-1} and a "15rcia A" membrane. The error bars represent the standard error of the mean (N=100).

4.3.3 Effects of process conditions on the mean size and size distribution of oil droplets

Figure 4-5 presents the effect of the agitation speed in the dispersion cell on the droplet size and size distribution at a fixed dispersed phase flux. The *SPAN/CV* values first decrease and then increase with increasing agitation speed, reaching a minimum at an agitation speed of ~1080 rpm. In contrast, the mean diameter $D_{4,3}$ decreases continuously with increasing agitation speed. When droplets are formed on the membrane surface, they can stay there for a period of time, and their size can grow (Christov *et al.*, 2002). To a certain point, the adjacent droplets may meet each other and coalesce, which can result in an increase in the size distribution, i.e. increase in *SPAN/CV* values. As the stirred speed increases, the shear force generated on the membrane surface also increases, which reduces the residence time of the formed droplets on the surface, leading to smaller mean droplet diameter and less coalescence (reducing *SPAN/CV* values), as observed in Figure 4-5. However, a too high agitation speed (> 1080rpm) might cause breakage of the droplets, resulting in further reduction in the mean size but also a wider size distribution. It is difficult to predict the optimum agitation speed theoretically, but the speed can be determined from experiments.

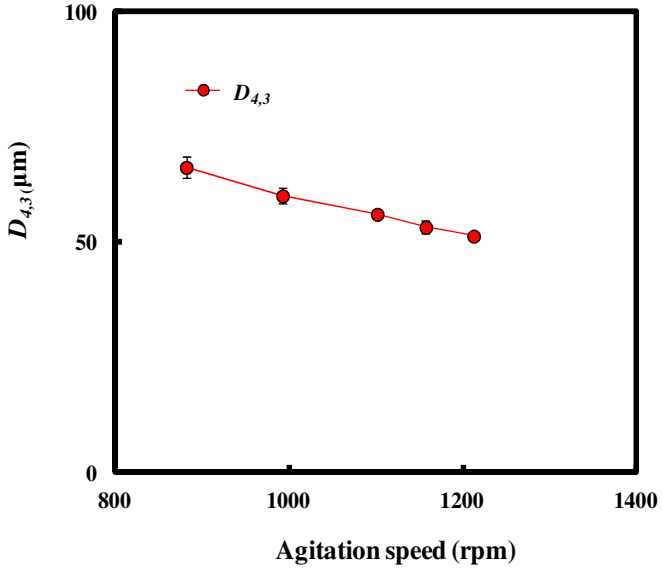

(a)

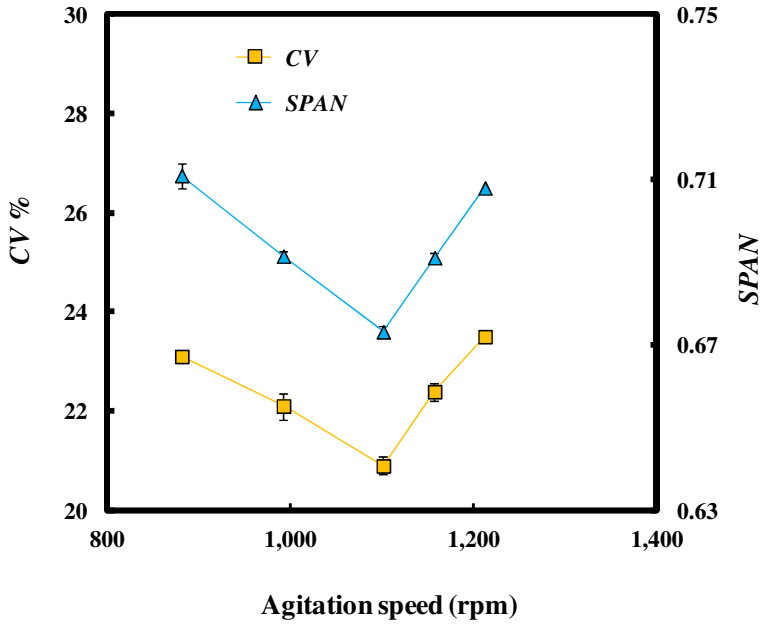

(b)

Figure 4-5. The effect of agitation speed in the dispersion cell on the (a) size and (b) size distribution of the droplets in emulsion, prepared with a dispersed phase flux of 1.6×10^{-5} m s^{-1}, and "15 rcia A" membrane. Some of the error bars are smaller than the symbols used. The error bars represent the standard error of the mean (N=100).

Figure 4-6 shows that at a fixed agitation speed of 1080 rpm, when the dispersed phase flux varies from 1.6×10^{-5} m s^{-1} to 3.9×10^{-5} m s^{-1}, both the mean droplet diameter $D_{4,3}$ and *SPAN/CV* values increase with the flux. This might be due to that a higher flux can cause the droplet volume to increase prior to detachment and generate droplets with a higher frequency that promote their coalescence before the droplets are detached, leading to a wider size distribution (Abrahamse *et al.*, 2002, Xu *et al.*, 2005).

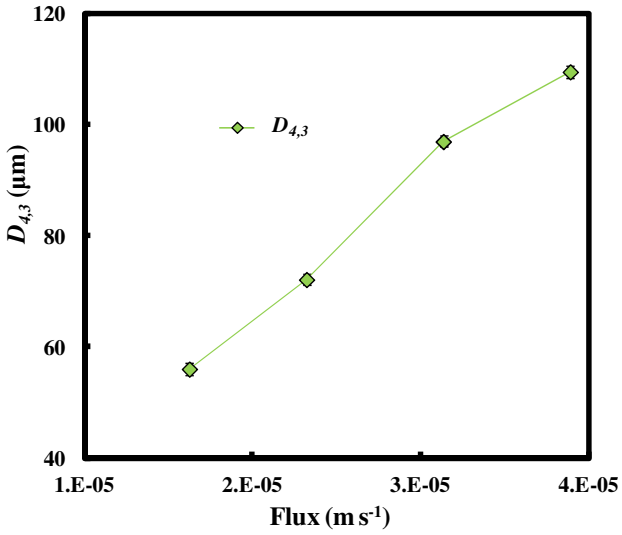

(a)

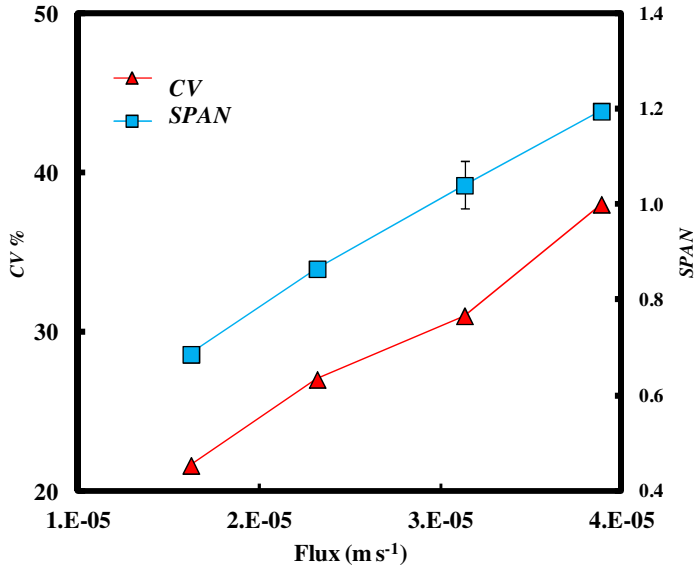

(b)

Figure 4-6. The influence of the flux of the dispersed phase pumped through the membrane on (a) the size and (b) size distribution of the droplets in emulsion prepared using an agitation speed of 1080 rpm and a membrane "15 rcia A". The error bars represent the standard error of the mean (N=100).

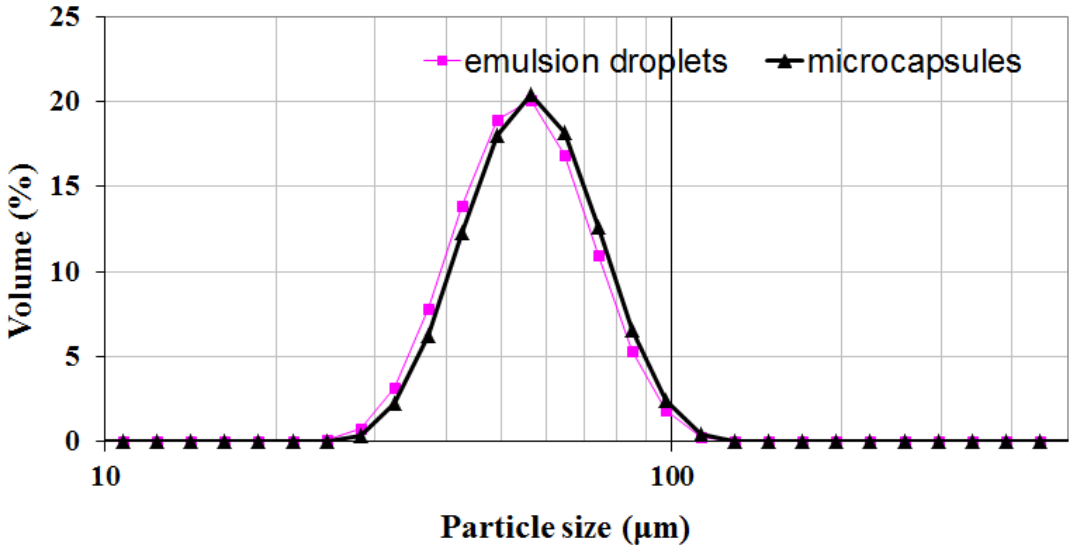

Figure 4-7. Size distributions of the emulsion droplets and the formed microcapsules, prepared by membrane emulsification using an agitation speed of 1080 rpm, dispersed phase flux of 1.6×10^{-5} m s^{-1} and a membrane "15 rcia A".

The size distributions of the oil droplets in the emulsion and the formed microcapsules are shown in Figure 4-7, corresponding to an agitation speed of 1080 rpm and dispersed phase flux of 1.6×10^{-5} m s^{-1}. The $D_{4,3}$ of the droplets is 56.0 ± 1.2 µm. Their corresponding *CV* and *SPAN* values are 21.0 ± 0.5 % and 0.67 ± 0.02 respectively. The $D_{4,3}$ of the microcapsules is 57.4 ± 1.2 µm, and their *CV* and *SPAN* values are 21.0 ± 0.5%, and 0.68 ± 0.02 respectively. There is no significant difference in the size distribution between the oil droplets and microcapsules.

4.3.4 Effects of reaction temperature on the mean size and size distribution of microcapsules

The effect of the reaction temperature on the formation of microcapsules was also investigated. As shown in Figure 4-8, when the reaction temperature is set at 45°C the size distribution of the microcapsules is very broad, the *CV* value is 64.2 ± 1.1 % and $D_{4,3}$ of the microcapsules is 56.7 ± 1.2 μm. This might be due to the slow reaction rate at 45°C in forming a solid MF shell. The droplets were susceptible to agitation, allowing them to break and coalesce, before a solid shell was formed. When the reaction temperature is increased to 55°C, the *CV* value drops to 22.4 ± 0.3 %, and the volume mean diameter increases slightly to 64.7 ± 1.1 μm. The size distribution only changes marginally when the reaction temperature is increased from 55°C to 65°C.

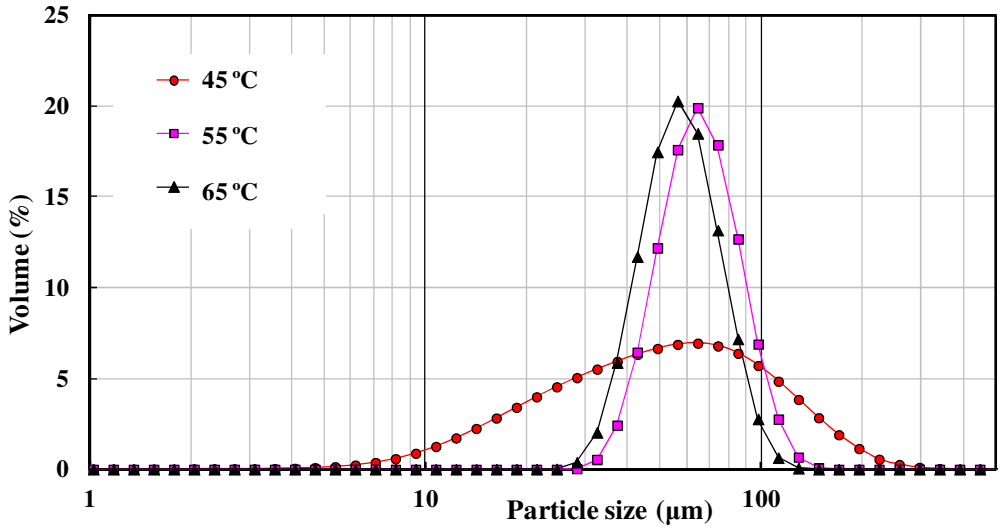

Figure 4-8. Size distribution of the microcapsules prepared at different temperature by membrane emulsification (with an agitation speed of 1080 rpm, dispersed phase flux of 1.6×10^{-5} m s^{-1} and a "15rcia A" membrane).

4.3.5 Morphology

Figure 4-9 gives typical optical and ESEM images of the microcapsules prepared by the membrane emulsification method. Microcapsules were found to be spherical with smooth surfaces and of roughly similar size. Figure 4-9 (a) shows that there is a small bubble inside each microcapsule, which is considered to result from different extents of contraction between the shell material and liquid core from the reaction temperature of 65 ± 1°C to room temperature.

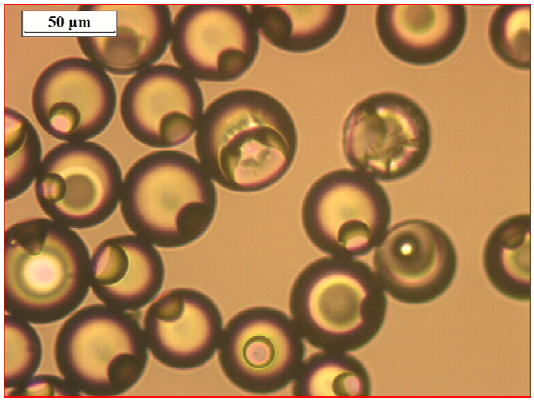

(a)

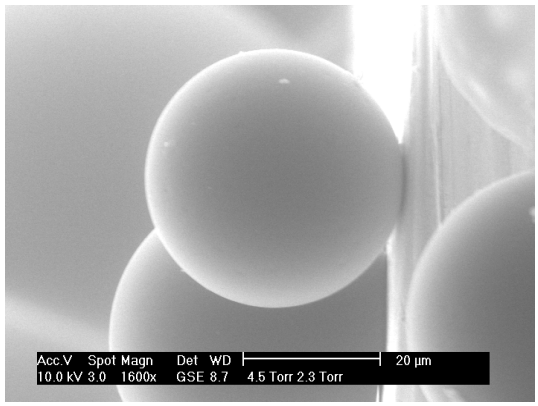

(b)

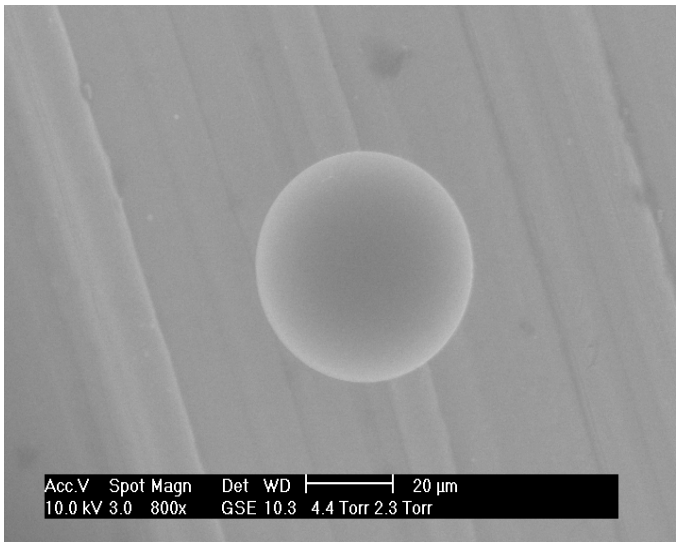

(c)

Figure 4-9. Micrographs of the microcapsules obtained using (a) optical microscopy, (b) and (c) ESEM. (b) Microcapsules were prepared using the dispersion cell with a stirring speed of 1080 rpm, dispersed phase flux of 1.6×10^{-5} m s^{-1} and a membrane "15 rcia A". (c) Microcapsules were prepared using homogenization with an agitation speed of 600 rpm.

4.3.6 Shell thickness

The typical TEM and CLSM micrographs of microcapsules prepared using the membrane emulsification and homogenization methods are presented in Figures 4-10 and 4-11, respectively. The shell thickness is reasonably homogeneous within a given cross-section. TEM measurements for the MF sample made using membrane emulsification resulted in a mean diameter of 57.3 ± 1.4 μm (Standard error, number of microcapsules analyzed n = 50) and a mean shell thickness of 408 ± 3 nm (n = 50); for the sample using homogenization a mean diameter of 63.8 ± 2.3 μm (n = 50) and mean shell thickness of 395 ± 10 nm (n = 50) were obtained. The results of microcapsules with a Rhodamine B florescence dye measured under CLSM are shown in Figure 4-11. The sample prepared by membrane emulsification had a mean diameter of 56.1 ± 9.0 μm (SE, n = 20) and mean shell thickness of 450 ± 36 nm (n = 20), whereas the sample by homogenization had a mean diameter of 64.5 ± 4.0 μm (n = 20) and mean shell thickness of 435 ± 44 nm (n = 20). The diameter of MF microcapsules determined by two different methods (TEM and CLSM) gave slightly different values, which may be due to different resolutions of these two techniques. The results obtained through TEM had higher accuracy compared with CLSM, which is consistent with the reports in literature (Ferrando and Spiess, 2000, Poux and Meier, 2005) .

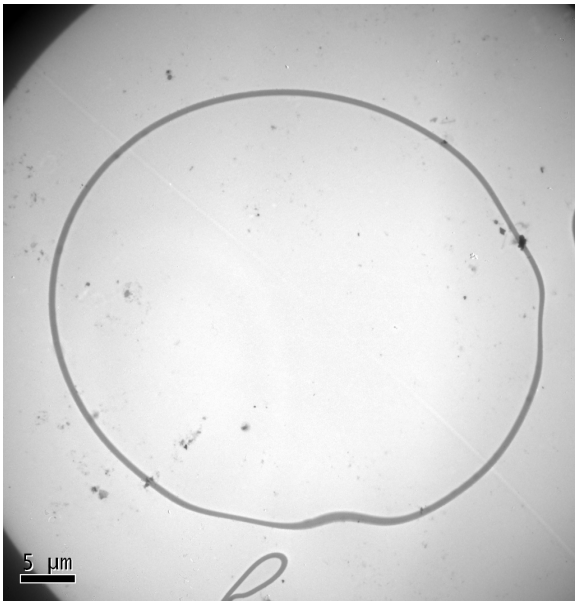

(a)

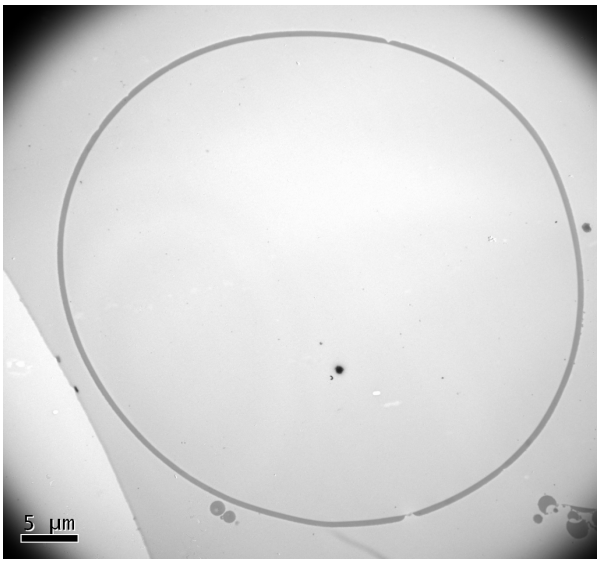

(b)

Figure 4-10. TEM micrographs of microcapsules prepared using the membrane emulsification and homogenization methods. (a) Prepared using the dispersion cell with a stirring speed of 1080 rpm, dispersed phase flux of 1.6×10^{-5} m s^{-1} and a "15 rcia A" membrane. (b) Prepared by homogenization with an agitation speed of 600 rpm.

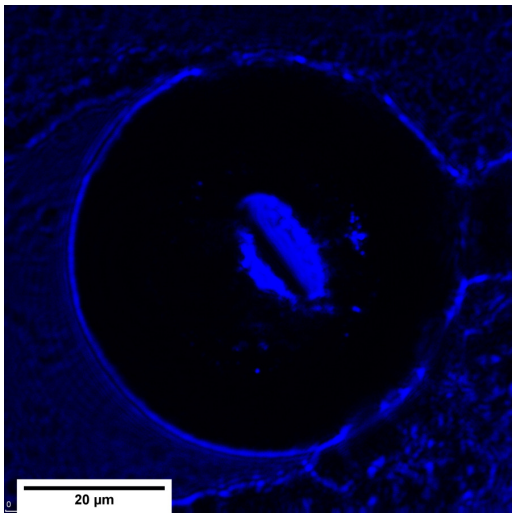

(a)

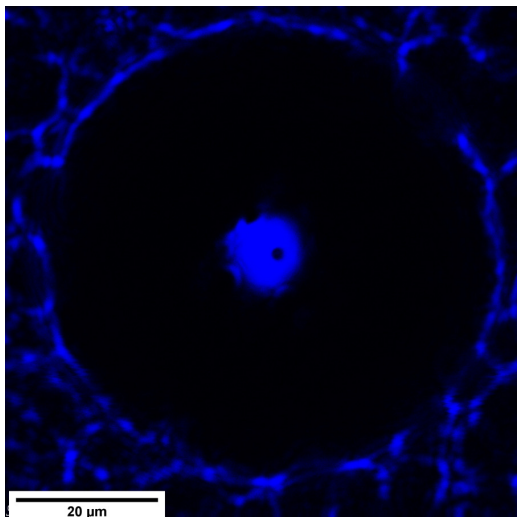

(b)

Figure 4-11. CLSM micrographs of microcapsules prepared using the membrane emulsification and homogenization methods. The pictures from CLSM is black and white,; the colour was added only for observation. (a) Prepared using the dispersion cell with a stirring speed of 1080 rpm, dispersed phase flux of 1.6×10^{-5} m s^{-1} and a "15 rcia A" membrane. (b) Prepared by homogenization with an agitation speed of 600 rpm.

4.3.7 Size analysis of microcapsules

Figure 4-12 presents the size distributions of the microcapsules prepared by two different methods. There is a clear difference in the mean diameter of the microcapsules prepared by the two methods, 57.4 ± 1.2 μm for membrane emulsification and 64.5 ± 2.4 μm for homogenization. The *CV* and *SPAN* values of the microcapsules for the membrane emulsification are 21.0 ± 0.5 % and 0.68 ± 0.02 respectively; the values for homogenization are 37.6 ± 1.4 % and 1.18 ± 0.05. Clearly, the microcapsules prepared by the membrane emulsification had a narrower size distribution than those made by homogenization.

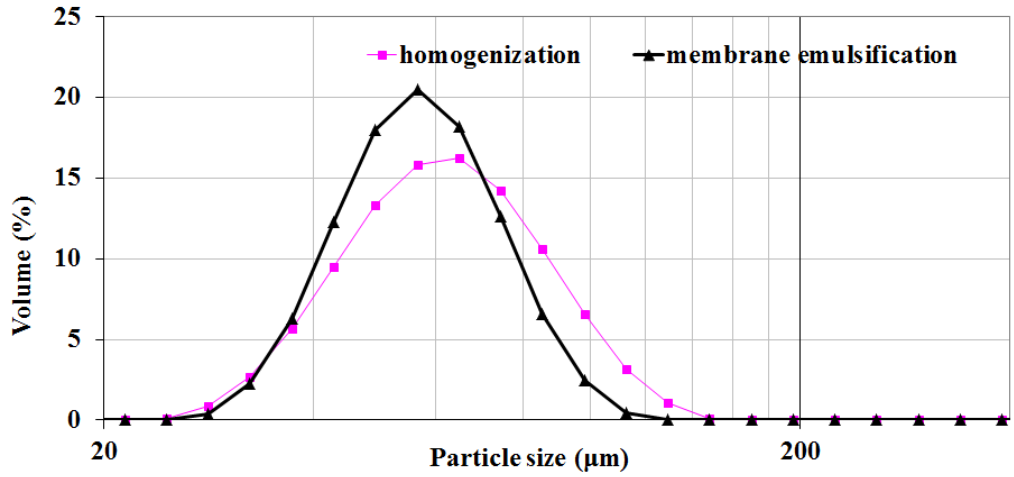

Figure 4-12. Size distribution of the microcapsules prepared by two different methods: homogenization (at 600 rpm) and membrane emulsification (with an agitation speed of 1080 rpm, dispersed phase flux of 1.6×10^{-5} m s^{-1} , a "15 rcia A" membrane wetted with an agent concentration of 0.5% (v/v)).

In previous work (Calabrese *et al.*, 1986a, Hu *et al.*, 2009), Equation 2.1 has been proposed to describe the relationship between the Sauter mean diameter of droplets in an emulsion and the agitation speed in a stirred vessel (Figure 4-12). The value of A_h was found to be equal to 10,299 ± 89 and B was −1.2 which is consistent with the relationship between Sauter mean diameter of droplets and agitation speed in the previous work (Calabrese *et al.*, 1986a), where breakage of droplets is the dominant mechanism. It was also proposed in the previous work that in a system where physical properties of the two phases and their interfacial tension were fixed, the value of A_h mainly depends on the kind of agitation used in the system (Calabrese *et al.*, 1986a).

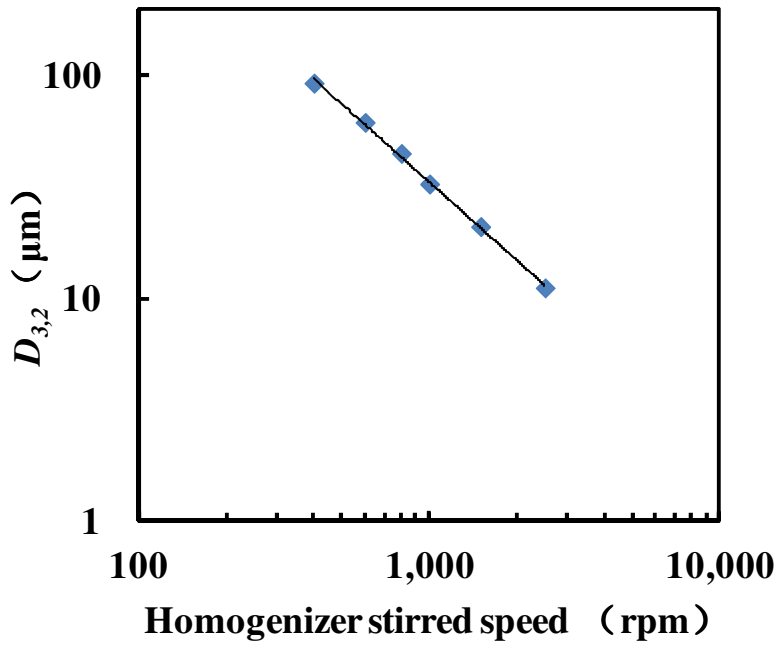

Figure 4-13. Double logarithmic representation of the effect of the agitation speed on $D_{3,2}$ for MF microcapsules prepared using homogenization. The points are the experimental data; the line is the best fit using Equation 2.1.

4.3.8 Mechanical properties of microcapsules

Figure 4-14 shows typical profiles of force divided by diameter of microcapsules versus fractional deformation at rupture ε_B obtained when single MF microcapsules were compressed to rupture. The fractional deformation at rupture ε_B is defined as the displacement at rupture normalized by the capsule diameter (Mercade-Prieto *et al.*, 2011b).

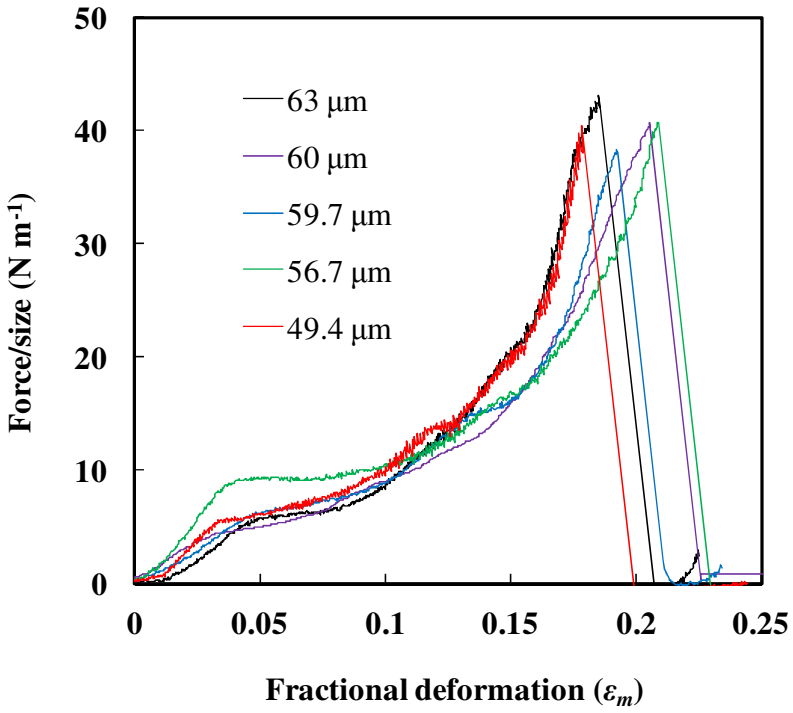

Figure 4-14. Typical profiles of force divided by diameter of microcapsules versus fractional deformation at rupture ε_B. The microcapsules were prepared by membrane emulsification with a mean diameter of 57.4 ± 1.2 µm.

A few mechanical property parameters of microcapsules were obtained in this study: the nominal rupture stress δ_B, defined by the ratio of the rupture force to the initial cross sectional area of the microcapsule (Xue and Zhang, 2009); the fractional deformation at rupture ε_B; and the nominal wall tension T_B, defined as the rupture force normalized by the circumference of the uncompressed microcapsule (Liu, 2010). The mechanical properties of microcapsules prepared by membrane emulsification and by homogenization are shown in Figure 4-15 and the mean values are summarised in Table 4-1.

The rupture force increases with displacement at rupture; the nominal rupture stress decreases with the diameter; and the fractional deformation at rupture and nominal wall tension have no discernible change. These trends are in agreement with previous work reported in the literature (Sun and Zhang, 2001). Figure 4-15 also shows that for a given size there is variation in the nominal rupture stress but there is no significant difference in the variation between the microcapsules prepared by the two methods. It should be pointed out that the mean nominal rupture stress of the microcapsules prepared by each method (see Table 4-1) is smaller than that reported before (Long *et al.*, 2009) for the same weight ratio of formaldehyde to melamine. This is because the microcapsules made by Long *et al.* (2009) were significantly smaller. Consequently the ratio of their wall thickness to diameter (*h/r*) is much greater than that in this work since it was found that the wall thickness did not vary with microcapsule diameter (Mercade-Prieto *et al.*, 2011).

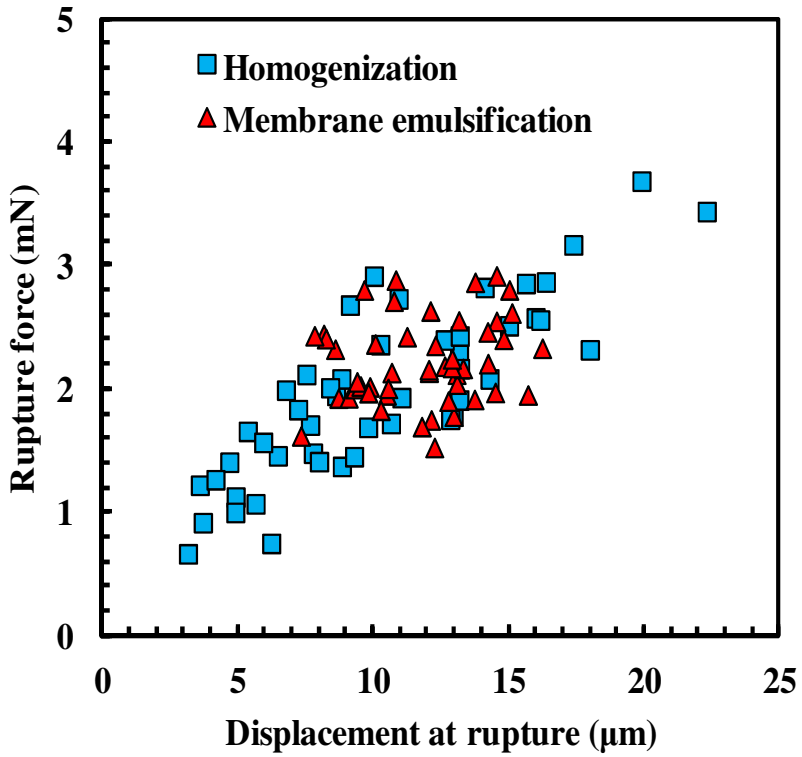

(a) Rupture force versus fractional deformation;

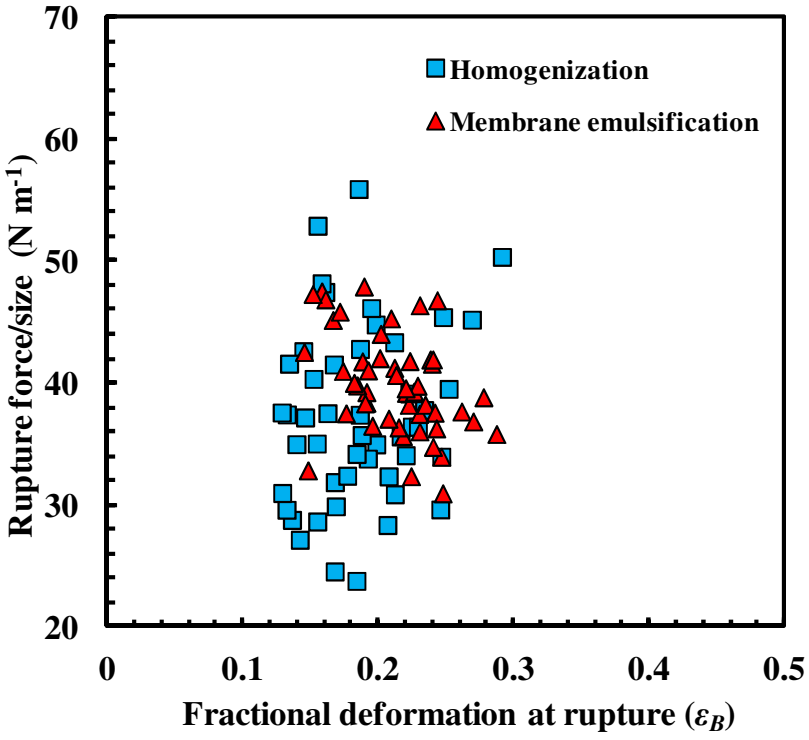

(b) Rupture force divided by size versus fractional deformation;

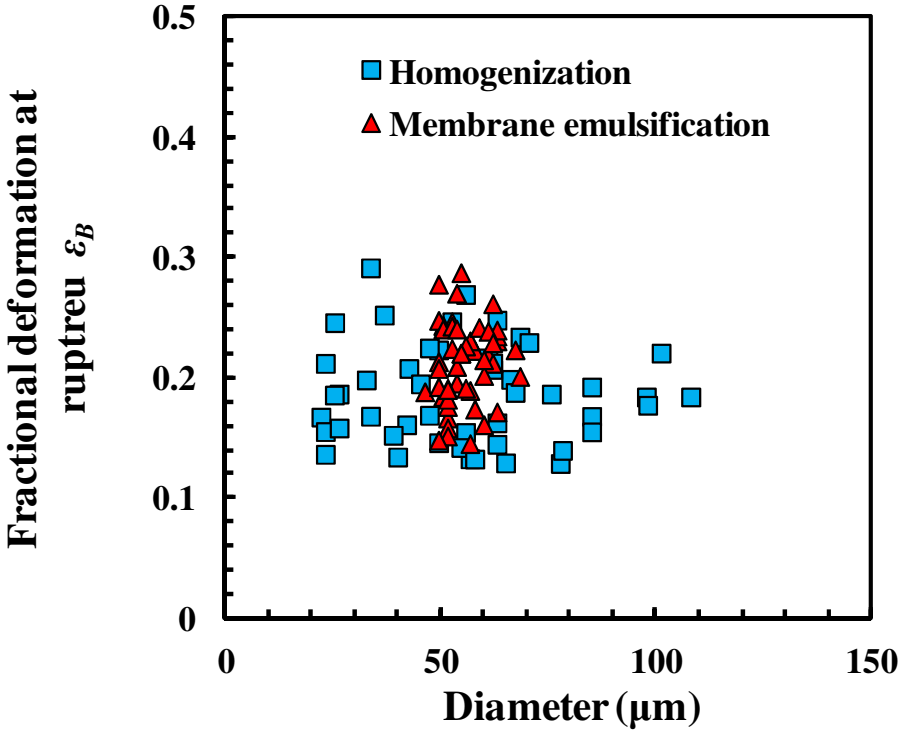

(c) Fractional deformation versus diameter;

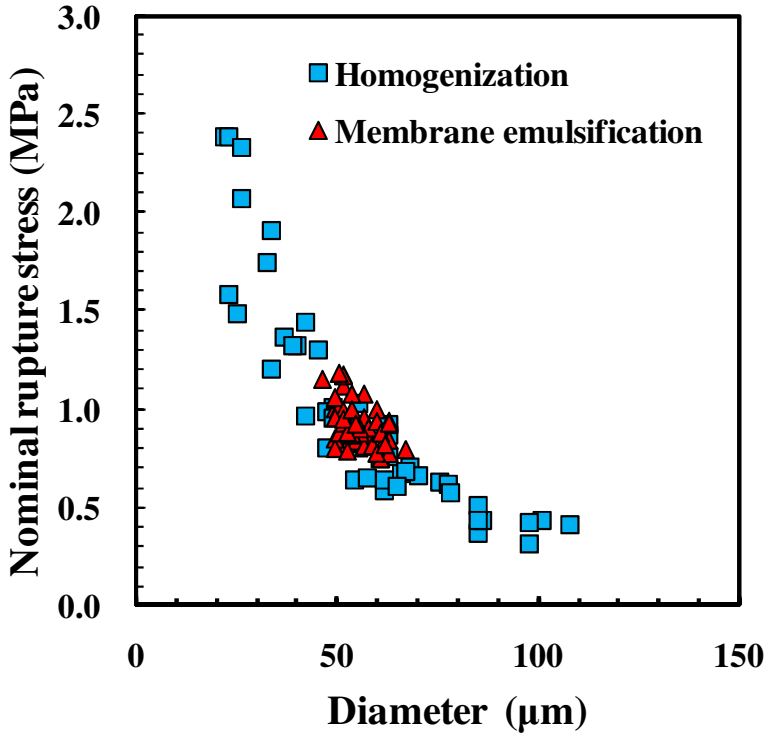

(d) Nominal rupture stress versus diameter;

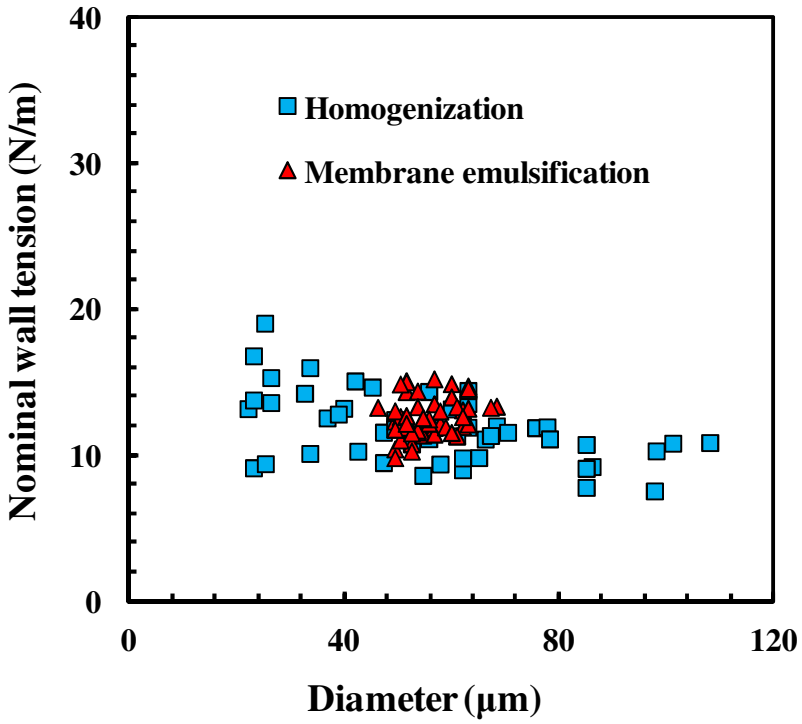

(e) Nominal wall tension versus diameter.

Figure 4-15. Strength parameter distributions of the microcapsules prepared by two different methods.

Table 4-1. Summary of the mechanical property data of the microcapsules prepared by membrane emulsification and homogenization.

Confidence intervals represent the standard error of the mean, with 50 microcapsules for each group.

Methodology		Diameter （μm）	Rupture force （mN）	Fractional deformation at rupture ε_B	Nominal rupture stress （Mpa）	Wall tension (mN/μm)
Membrane emulsification	**Average**	**57.4±1.2**	**2.2±0.1**	**0.21±0.01**	**1.03±0.02**	**0.04±0.01**
	CV %	**21.0±0.5**	**18.6±0.5**	**15.9±0.4**	**12.9±0.2**	**12.4±0.2**
Homogenization	**Average**	**64.3±2.4**	**1.9±0.1**	**0.19±0.01**	**1.06±0.10**	**0.04±0.01**
	CV %	**34.1±0.3**	**34.4±1.7**	**21.8±0.7**	**63.1±5.7**	**20.1±0.6**

Table 4-1 shows the *CV* values of the diameter, rupture force; displacement at rupture, nominal rupture stress and nominal wall tension of the microcapsules prepared by membrane emulsification are significantly smaller than the corresponding values of the microcapsules prepared by homogenization. The reduced variation in the rupture force, displacement at rupture, nominal rupture stress or nominal wall tension resulted from the narrower size distribution. Membrane emulsification system produced narrower distributions of the size and mechanical strength of microcapsules, in comparison with those made by conventional homogenization. This is significant, which demonstrates the benefit offered by membrane emulsification in making microcapsules with narrower size/strength distributions.

4.4 Conclusions

A membrane emulsification method was employed to prepare microcapsules with MF as a shell material and an oil-based industrial precursor as core with narrow size and strength distributions. The mean diameter and size distribution of the microcapsules depended on not only the process conditions of the dispersion cell (agitation speed and dispersed phase flux through the membrane in the emulsification stage), but also on the membrane surface hydrophilicity (contact angle). The best condition to minimise the size distribution has been found to be an agitation speed of 1080 rpm and dispersed phase flux of 1.6×10^{-5} m s^{-1} with a concentration of the wetting agent of 0.5% (v/v) for the conditions investigated. Correspondingly, the distributions of the size and mechanical strength of microcapsules prepared by the membrane emulsification had been significantly narrowed, in comparison with those made by conventional homogenization. In Chapter 5, the results on how the mean size and size distribution of microcapsules may be affected by the physical properties of different core material and a different membrane system will be presented.

Chapter 5 Scale-up of Membrane Emulsification to Prepare Melamine-formaldehyde Microcapsules and Microencapsulation of Different Oils

5.1 Introduction

Microcapsules with narrow size distribution have shown unique advantages in consumer industrial productions, especially, for perfume oil microcapsules used in detergents, as mentioned Chapter 4. Current industrial manufacturing practices to generate microcapsules include homogenization or simple agitation, which despite their simple operation they produce emulsions with broad size distributions. Hence, in order for narrow size microcapsules to become industrially feasible in the future, it is required to test the scale up capability of membrane emulsification systems.

The focus of this chapter is to formulate Melamine-formaldehyde (MF) microcapsules with a narrow size distribution using a pilot plant-scale cross flow membrane emulsification system. The size and size distribution of the droplets in the emulsions, as well as the MF microcapsules formed in the later stage of the operation, were

compared with those obtained from the lab-scale dispersion cell described in Chapter 4.

The effect of different processing parameters on the droplets formed were studied in order to improve our understanding of what determines the size and size distribution of the oil droplets produced in the emulsification stage. For instance, MF microcapsules were made with emulsions made with different core oils. Other parameters studied included the membrane properties (*e.g.* membranes with different pore locations), the physical properties of the two phases (*e.g.* viscosities, interfacial tension), and the processing conditions (*e.g.* agitation speed in the continuous phase and dispersed phase flux). The obtained experimental data were compared with predictions of theoretical models developed in the literature. The morphology, the shell thickness and microstructure of the microcapsules were investigated by optical microscopy, environmental-scanning electron microscopy (ESEM) and transmission electron microscopy (TEM) respectively.

5.2 Experimental methods

5.2.1 Scale up experiment with cross-flow membrane emulsification

The scale up experiment was carried out on a cross-flow membrane rig which had been established in the University of Leeds, the details of which was described in Section 3.3.2.

Firstly, aqueous solution of MF precondensate (34.3 g), formaldehyde (2.9 g) and polyacrylamide-co-acrylic acid-sodium salt (8.3 g) in water (1000.0 g) was stirred (200 rpm) for 105 min in a 2 L standard stirred vessel and its pH value was kept at 4.3 (adjusted using 20% (v/v) acetic acid) at room temperature (23 ± 2 °C), following the method described in Section 4.2.1.

Secondly, the prepared aqueous phase was cooled down to 15 ± 1 °C , then put into an open tank reservoir (Figure 3-5 (11) in Section 3.3.2), i.e. continuous phase tank. The core oil A (133.0 g) was added into the disperse phase tank (see Figure 3-7). The dispersed phase was then pushed through the membrane pores into the continuous phase, which passed through the inner channels of the membrane with a flow rate of 1.1×10^{-4} m^3 s^{-1}, under an oil phase pressure from 0.3×10^5Pa to 1×10^5Pa for about 20 min (Figure 3-8).

Thirdly, the resulting emulsion was transferred back to the standard vessel, and stirred at a speed of 200 rpm at room temperature 23 ± 2 °C for 30 min.

Finally, the emulsion was placed into a water bath (Clifton, Nickel-electro Ltd., UK) at 65 ± 1 °C, allowing the MF polymerization reaction for 4 h. The suspension was

cooled to room temperature, and its pH increased to 10 (adjusted with 1M NaOH) to terminate the polymerization reaction.

5.2.2 Preparation of microcapsules with different core oils using a dispersion cell

Microcapsules with different core oils were also prepared using a dispersion cell illustrated in Section 3.3.1. The model core oils used were perfume oil B, sunflower oil, a key component of perfume oil hexyl salicylate and peppermint oil. Membranes "15 rcia A" and "15 cia" were used to generate emulsions; the details of membranes are provided in Section 3.3.1. The rest of the process conditions were the same as those for preparation of MF microcapsules with core oil A, which are described in Section of 4.2.1.

5.2.3 Characterization of MF microcapsules

The surface morphology and micro-structure of the microcapsules were characterised by optical microscopy (Leica DMRBE, Leica, UK), environmental-scanning electron microscopy (ESEM) (FEI/Philips XL30 ESEM-FEG, Philips, UK) respectively. Samples were imaged at high vacuum mode, and the operating voltage is shown on the images (Figure 5-17).

Shell thickness of the microcapsules was measured by transmission electron microscopy (TEM) (JEOL 1200EX, Jeol Ltd, UK). Samples were embedded in the LR white hard grade acrylic resin, and the ultra thin sections were obtained using a ultra-cut microtome apparatus (Reichert-Jung). The operating voltage was 10.0 kV.

The mean size and size distribution of the oil droplets produced in the stage of emulsification and the final microcapsules were determined using a laser fraction technique (Malvern Instruments Mastersizer 2000). The data of *SPAN, CV* value, $D_{4,3}$ and $D_{3,2}$ were recorded. All the oils used for the work presented in this chapter can be considered insoluble in water (solubility are less than 0.01g/g). The refractive indexes of the materials used are listed in Table 5-1.

Table 5-1. Refractive indexes of the materials used in the study on encapsulation of different core oils by MF.

oil A	oil B	Sunflower oil (oil S)	Hexyl salicylate oil (oil HS)	Peppermint oil (oil P)	MF
1.497*	1.496*	1.475 (Fereidoon, 2005)	1.505**	1.46***	1.65 (Long *et al.*, 2009)

*given by the supplier P&G, UK

**given by the supplier SAFC, USA

***given by the supplier Sigma-Aldrich, UK

The details of encapsulation experiments are described in Section 4.2.1.

The densities of the oils were measured with a pycnometer. The interfacial tension between the two phases was measured by a Tensiometer (Processor Tensiometer K100, KRUSS) at 15 ± 1°C. Details are described in Section 3.4.8. The viscosities of the two phases were measured with a rheometer (AR1000, TA Instrument), at 15 ± 1°C. The Wilhelmy plate method was used to measure the interfacial tension and a method based on using the two plates (or a cone and plate) was used to measure the viscosity. Details are described in Section 3.4.9.

5.3 Results and discussion

5.3.1 Cross-flow membrane system

5.3.1.1 Stability of the oil/water emulsion

The storage stability of the emulsion was investigated for 72 h since a few hours are required to form microcapsules from the emulsion. Figure 5-1 shows that there is no significant change of the values of mean diameter $D_{4,3,}$ coefficient of variance (*CV*) and *SPAN* of the droplets in the emulsion. Therefore, the emulsion is considered to be stable during this period.

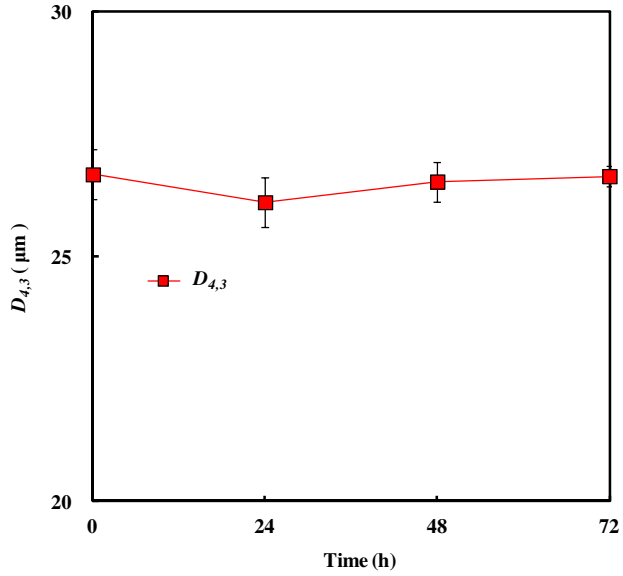

(a)

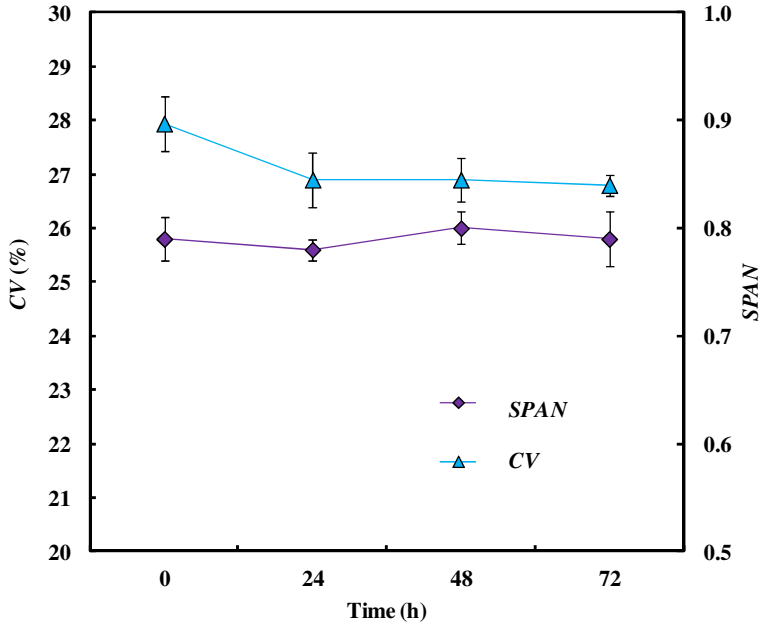

(b)

Figure 5-1 The (a) mean diameter ($D_{4,3}$) and (b) size distribution (*CV* and *SPAN* values) of the oil droplets measured at different storage times without agitation at room temperature. The emulsion was prepared using a circulation flow rate of 1.1×10^{-4} m^3 s^{-1} and an oil pressure of 0.3×10^5Pa. The error bars represent the standard error of the mean (N=10).

5.3.1.2 Effect of the processing conditions on the mean size and size distribution of oil droplets

Figure 5-2 presents that for a fixed circulation flow rate of 1.1×10^{-4} m^3 s^{-1}, increasing the oil pressure from 0.3×10^5Pa to 1×10^5Pa, both the mean droplet diameter $D_{4,3}$ and the *SPAN/CV* values first increase slightly then increase sharply. One explanation of this could be that a higher oil pressure can generate bigger droplets before detachment. It could generate droplets with high frequencies and promote their coalescence before the droplets were fully detached, leading to a broader size distribution.

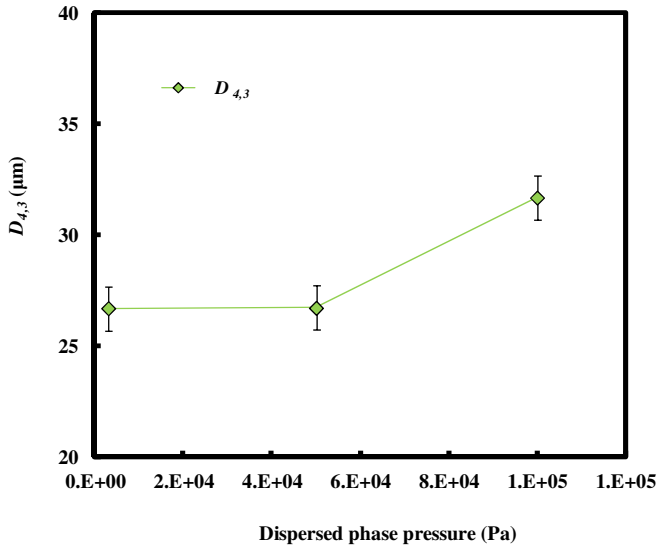

(a)

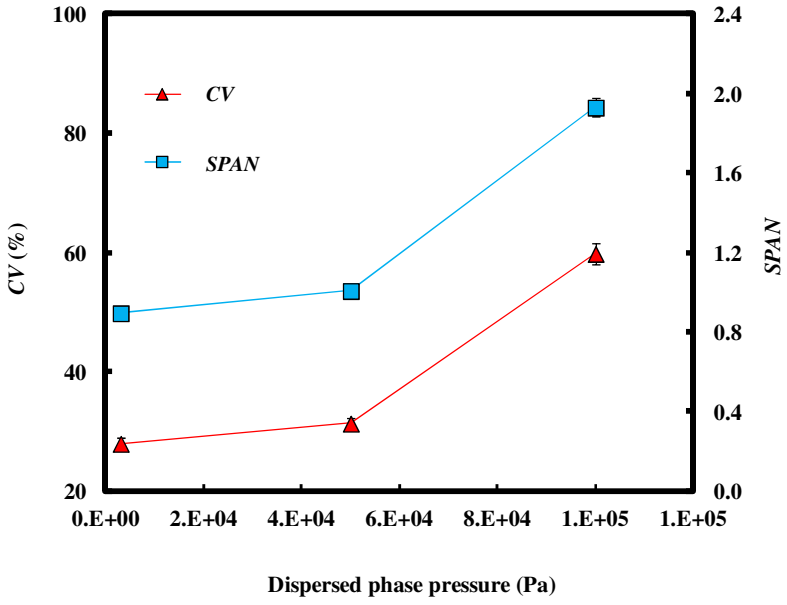

(b)

Figure 5-2 The effect of oil pressure on the (a) size and (b) size distribution of the emulsions droplets, prepared with a circulation flow rate of 1.1×10^{-4} $m^3\cdot s^{-1}$ and a dispersed phase pressure of 0.3×10^5Pa. Error bars represent the standard error of the mean (N=10).

An example of the size distributions of the oil droplets and the formed microcapsules are shown in Figure 5-3. The $D_{4,3}$ of the droplets is 26.7 ± 0.7 μm. Their corresponding *CV* and *SPAN* values are 27.9 ± 0.8% and 0.81 ± 0.02 respectively. The $D_{4,3}$ of the microcapsules is 26.5 ± 0.7 μm, and their *CV* and *SPAN* values are 30.5 ± 0.9%, and 0.88 ± 0.02 respectively. Statistical analysis shows that both the size distributions can be fitted with Gaussian, with 95% confidence, and there is no significant difference in the size distribution between the oil droplets and microcapsules.

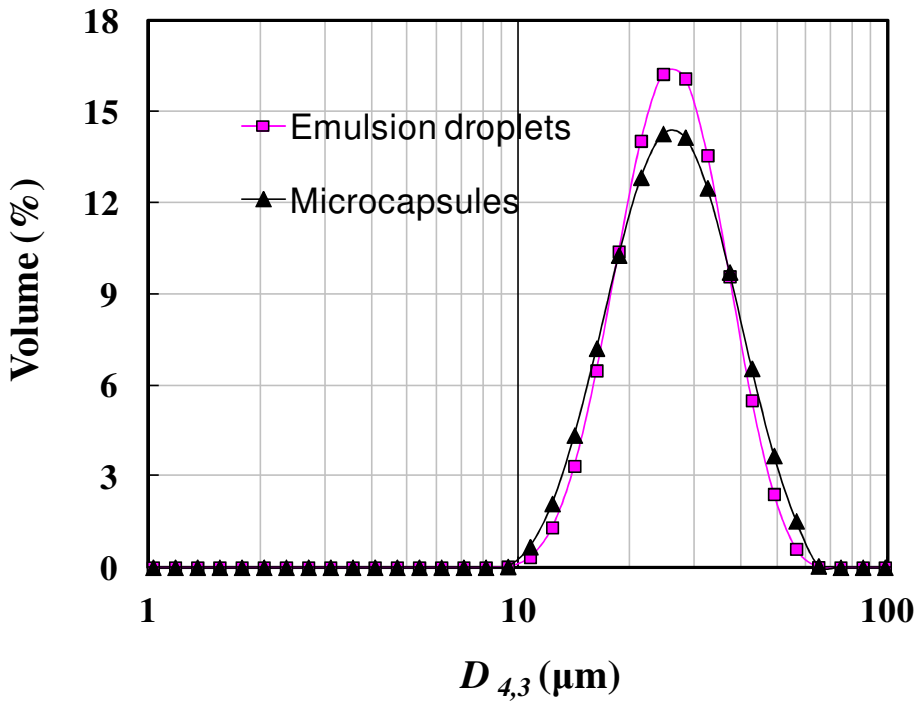

Figure 5-3 Size distribution of the emulsion droplets and the formed MF microcapsules, prepared using a circulation flow rate of 1.1×10^{-4} m^3 s^{-1} and an oil pressure of 0.3×10^5Pa.

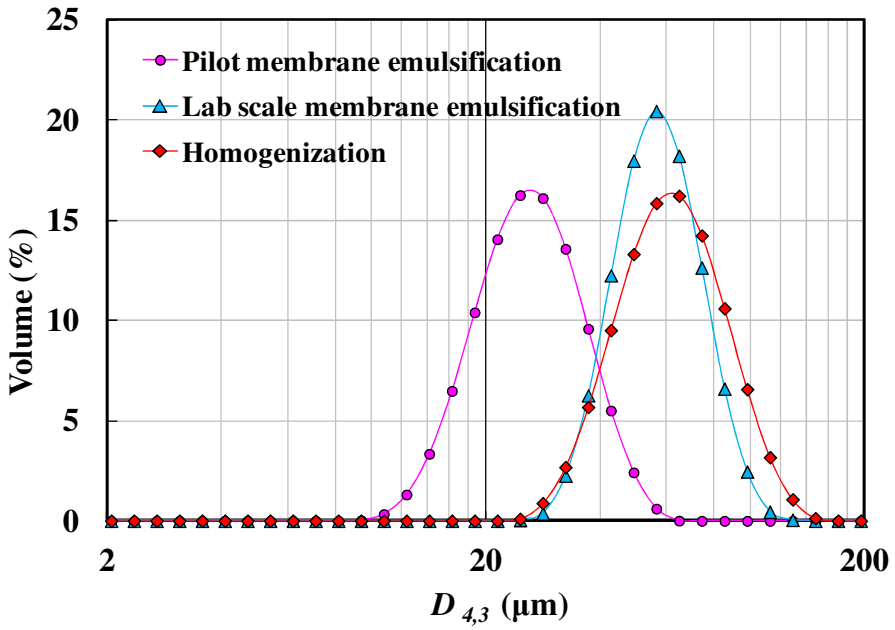

Figure 5-4. Size distributions of microcapsules prepared by three different methods: lab- scale membrane emulsification (with an agitation speed of 1080 rpm and dispersed phase flux of 1.6×10^{-5} m s^{-1}), pilot plant-scale membrane emulsification (using a flow rate of 1.1×10^{-4} m^3 s^{-1} and oil pressure of 0.3×10^5Pa) and lab-scale homogenization (600 rpm).

Figure 5-4 displays the size distributions of the microcapsules made with three manufacturing methods. The mean diameter of the microcapsules was 57.4 ± 1.2 µm for lab scale membrane emulsification, 26.5 ± 0.7 µm for the pilot plant-scale membrane emulsification and 64.5 ± 2.4 µm for lab-scale homogenization. The *CV* and *SPAN* values of microcapsules made using the lab scale membrane emulsification system were 21.0 ± 0.5 % and 0.68 ± 0.02 respectively; 30.5 ± 0.9 %, and 0.88 ± 0.02 for pilot plant-scale membrane emulsification; 37.6 ± 1.4 % and 1.18 ± 0.05 for

lab-scale homogenization. The microcapsules prepared by the lab-scale membrane emulsification were more uniform than using the other two methods. Note that the pilot plant-scale experiment used a cross-flow membrane system, which is different from the lab-scale dispersion cell membrane system. Different systems or even different membranes may deliver various results (Vladisavljevic and Williams, 2005). For example, SPG membrane may produce the microcapsules with typical *CV* values of 11 % - 23 %, and polyamide hollow fibres may generate the emulsion with a *CV* value of 33 % (Vladisavljevic and Williams, 2005). The cross-flow system used in this study could produce the mono-dispersed droplets with *CV* value around 30 % (Yuan *et al.*, 2009a, Yuan *et al.*, 2009c) which is slightly bigger than the common *CV* value of dispersion cell, around 20 % (Egidi *et al.*, 2008, Stillwell *et al.*, 2007). The difference in the *CV* and *SPAN* values resulting from the dispersion cell and the cross flow membrane system might not be due to the effect of scale up, rather than due to different membrane systems. It may become one of the future developments in membrane emulsification systems.

5.3.2 Preparation of MF microcapsules with different core oils using a dispersion cell

In Section 4.3.3, it is demonstrated that the size distribution of microcapsules mainly depended on the operation conditions during the membrane emulsification. In this

section the effects of different membrane configurations, the physical properties of the two liquid phases and processing conditions on the size distribution of oil droplets produced using a dispersion cell are presented.

5.3.2.1 The effect of membrane configurations on the size distribution of droplets in emulsion

Two membranes "15 cia" and "15 rcia A" were used subsequently, having the same pore size but different pore locations. Membrane "15 cia" has the pores fully located on the membrane surface, whilst membrane "15 rcia A" presents pores only in a ring between $48\ \text{mm} \leq r \leq 130\ \text{mm}$ as shown in Figure 3-4 (Section 3.3.1). The size distributions of the oil droplets generated with the two membranes are presented in Figure 5-5. $D_{4,3}$ using membrane "15 cia" was 57.6 ± 1.5μm, similar to that using membrane "15 rcia A", 56.0 ± 1.2 μm. However, the *CV* and *SPAN* values with membrane "15 cia" are 26.3 ± 0.5 % and 0.72 ± 0.02, larger than those prepared by membrane "15 rcia A", 21.0 ± 0.5% and 0.67 ± 0.02, respectively. The membrane which had the pores located in a ring area under r_{trans}, as shown in Figure 2-7, resulted in a narrower size distribution. This may be due to the existence of a more homogeneous shear stress distribution in the ring area on membrane surface, generated by the impeller than the whole membrane area in the latter case (Horie *et al.*, 2011). For this reason, membrane "15 rcia A" was selected for subsequent experiments.

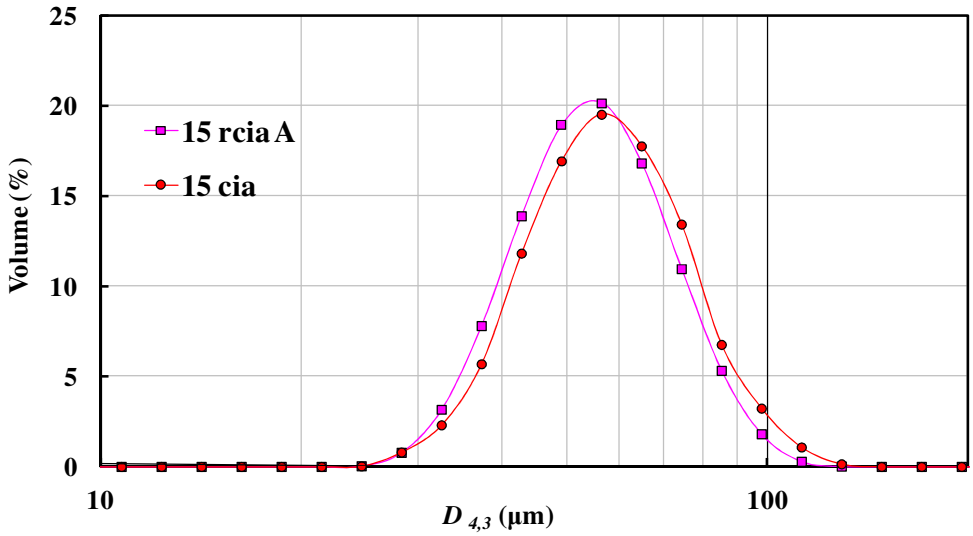

Figure 5-5. Size distributions of droplets in the emulsions generated using membranes with different pore locations. "15 rcia A" (square) and "15 cia" (circle). The microcapsules were prepared using an agitation speed of 1080 rpm and a dispersed phase flux of 1.6×10^{-5} m s^{-1}.

5.3.2.2 Effect of the phase physical properties on the size distribution of droplets of different oils.

Interfacial tension between the two liquid phases, their viscosities and densities may affect the size distribution of the formed oil droplets. The physical properties of different oils used in this study are listed in Table 5-2. Since the densities of the oils used in this study varied in a small range, only the effects of the interfacial tension and viscosities were investigated; the results are presented in the following section.

Table 5-2. Physical properties of the dispersed and continuous phases: viscosity, density and interfacial tension between the two phases.

Error represents the standard error of the mean.

T=15°C	Viscosity (mPa s)	Density (g cm^{-3})	T=15°C	Interfacial Tension (mN m^{-1})
MF solution	2.5±0.02	ND	MF/oil A	1.26±0.04
Water	1.29	1	MF/oil B	2.20±0.18
oil A	3.52±0.03	0.94	MF/Hexyl salicylate	3.25±0.18
oil B	3.47±0.03	0.94	MF/Sunflower oil	8.95±0.21
Hexyl salicylate	10.62±0.01	1.04	MF/Peppermint oil	5.05±0.21
Sunflower oil	50.83±0.01	0.92		
Peppermint oil	2.85±0.03	0.9		

At 15 ± 1°C, the viscosity of the pre-cross linked MF aqueous solution was 2.5 ± 0.02 mPa s (Table 5-2). The interfacial tension between the MF precondensate solution and the oil to be encapsulated varied in the range of 1.26 ± 0.04 to 8.95 ± 0.21 mN/m (Table 5-2) with all the oils considered.

Figure 5-6 shows the experimental data of droplet size versus interfacial tension. It increases with the interfacial tension, as expected. The model D, which was described in Section 2.3.3, has been used to predict the droplet size; the results are also presented in Figure 5-6. k_{wl} represents viscosity modification factors. For oils with different viscosities, two dispersion phase viscosity modification factors k_{wl} =2.8 ($\mu_d < 10\mu_c$, model D-1) and k_{wl} =3.5 ($\mu_d \geq 10\mu_c$, model D-2) were used. The model D developed previously (Holdich *et al.*, 2010) underestimates the predicted droplet size, which may be due to that the model does not consider the affect of dispersion phase flux on the size. Nevertheless, the experimental trend whereby the droplet size increases with the interfacial tension is also observed in the model.

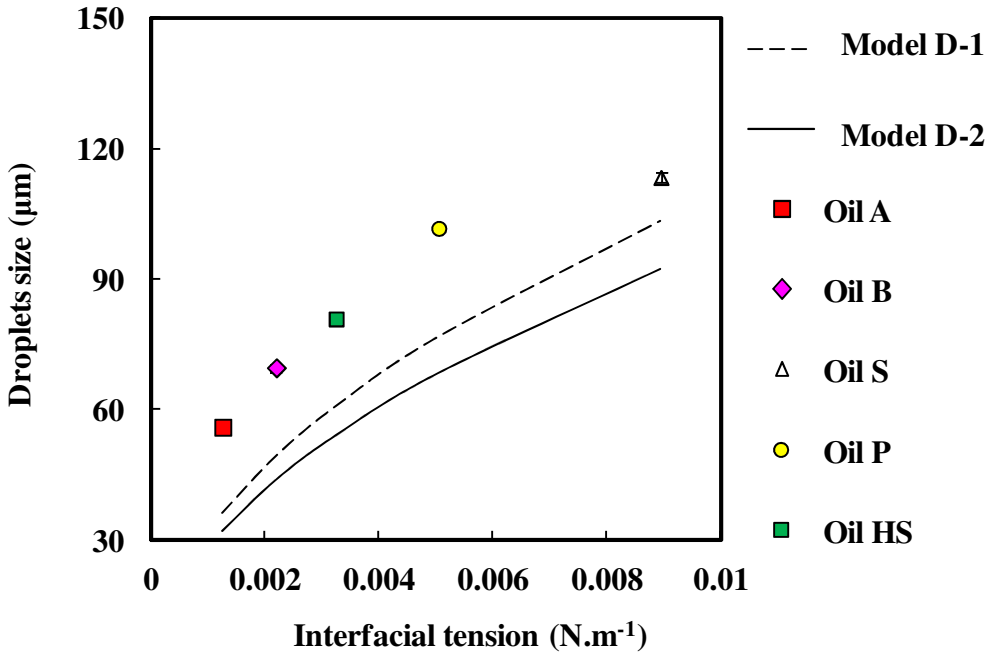

Figure 5-6. Experimental measurements and theoretical predictions of droplet sizes in the emulsions with varying physical properties. For model D, the dashed line represents the value calculated using k_{wl}= 2.8 ($\mu_d \approx 10\mu_c$) ; the solid line using k_{wl} =3.5 ($\mu_d \geq 10\mu_c$). The droplets were prepared using an agitation speed of 1080 rpm and a dispersed phase flux of 1.6×10^{-5} m s^{-1}, by a membrane "15 rcia A". The droplet size here represents number mean size of droplets in emulsion. The error bars represent the standard error of the mean (N=15).

5.3.2.3 The effects of processing conditions on size distribution of droplets with different oils.

In a dispersion cell system, there are at least two factors which affect the mean size and the uniformity of emulsion droplets: the agitation speed in the continuous phase, which provides shear stress on the surface of the membrane, and dispersed phase flux, which is related to the pressure difference across the membrane (Holdich *et al.*, 2010, Kosvintsev *et al.*, 2005, Stillwell *et al.*, 2007). In this section, the size and size distribution of emulsion droplets with various core oils were determined at different operation conditions. The experimental data were also compared with predictions by theoretical models mentioned in literature work, described in Section 2.3.3.

5.3.2.3.1 Impeller agitation speed

The *CV* and $D_{4,3}$ values of the oil droplets in the emulsions prepared at different agitation speeds of the impeller in the dispersion cell are shown in Figure 5-7 and Figure 5-8. At a fixed dispersed phase flux 1.6×10^{-5} m s^{-1}, as expected, all the oil droplet diameters decreased with increasing agitation speed, which were in good agreement with the trend of predicted values (Figure 5-7). The theoretical value was calculated according to the well-established model D (Holdich *et al.*, 2010, Xu *et al.*, 2005), which are reviewed in Section 2.3.3. Higher agitation speed should generate

greater shear stress on the membrane surface, resulting in bigger drag force, and detachment torque, which can shorten the residence time of the droplets formed at the membrane surface and prevent their growth and coalescence into bigger ones (Hao *et al.*, 2008, Kosaraju *et al.*, 2006). The predicted diameters should be smaller than the experimental values (Figure 5-7 (b)), since the models does not consider the influence of dispersed phase flux, which will be discussed in next section.

Given a lower agitation speed, at a fixed dispersed phase flux, there would be a longer time for the drag force F_D to act to detach droplets apart from membrane surface. So the droplets might easily grow bigger before they depart the surface, compared to a higher agitation speed. This explains that $D_{4,3}$ reduced monotonically as agitation speed increased.

At a fixed dispersed phase flux 1.6×10^{-5} m s^{-1}, although different core oils were used, the uniformities of all the microcapsules ameliorated, shown by *CV* reaching the smallest value at an agitation speed around 1080 rpm, then deteriorated as agitation speed continuously increased from 880 rpm to 1210 rpm as expected (Figure 5-8). Different oils did not show significant effects on the size distribution of emulsion droplets. The change of the droplet size distribution with agitation speed was explained in Chapter 4. With increasing agitation speed, there was a dominant mechanism of droplet breakage until the agitation speed was too high, causing breakage of the formed droplets in the emulsion.

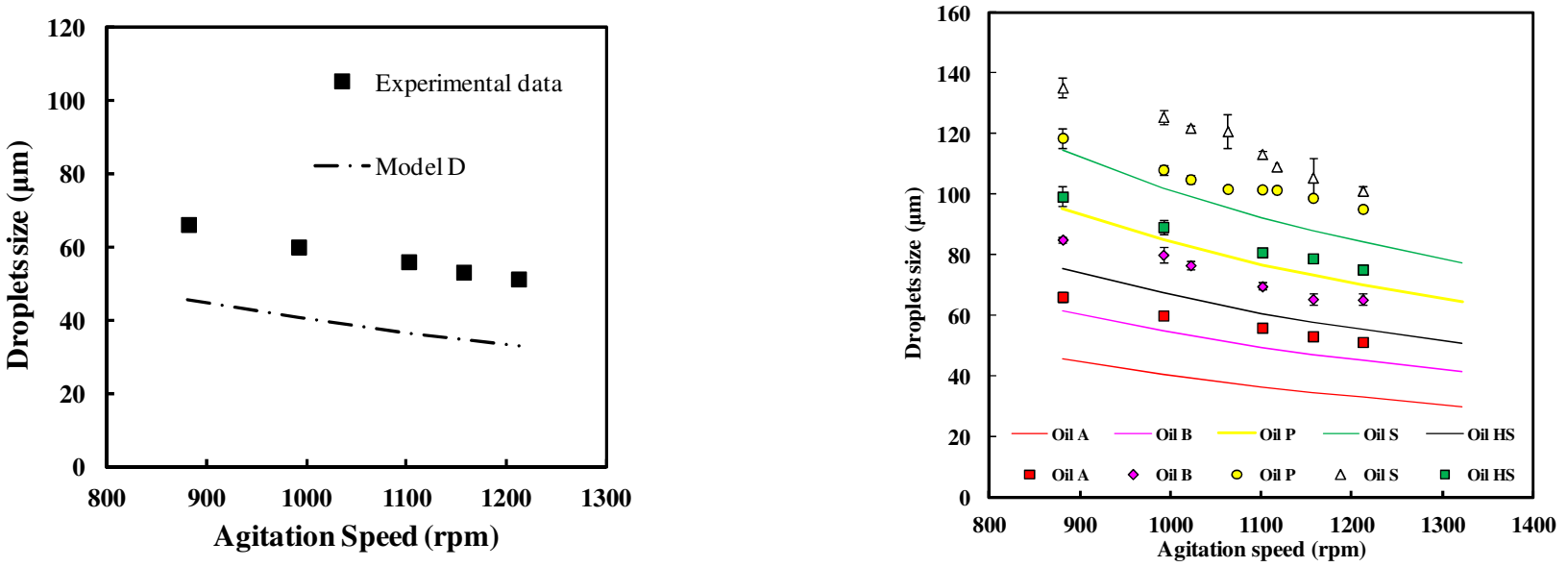

(a) (b)

Figure 5-7. The model predictions and experimental measurements of droplet size in the emulsions versus agitation speed in the dispersion cell. The lines represent model predictions and symbols the experimental data. (a) Experimental data of oil A droplet sizes and theoretical values according to Model D. (b) Experimental data of different oil droplet sizes with their predicted values, which were calculated using Model D. The droplets were prepared using a dispersed phase flux of 1.6×10^{-5} m s^{-1}. The droplet size here represents number mean size of droplets in emulsion. The error bars represent the standard error of the mean (five batches, every batch measured five times).

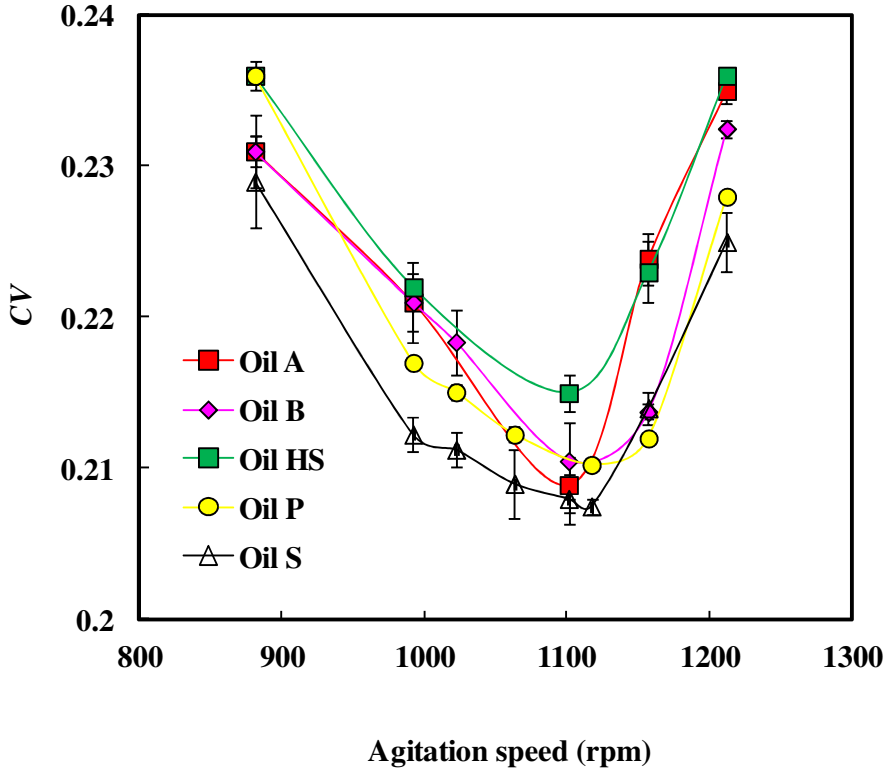

Figure 5-8 The effect of agitation speed in the dispersion cell on size distribution of droplets of different oils in emulsions. The error bars represent the standard error of the mean (N=15). The droplets were prepared using a dispersed phase flux of 1.6×10^{-5} m s^{-1}.

5.3.2.3.2 Dispersed phase flux

Figure 5-9 shows that at a fixed agitation speed of 1080 rpm increasing the dispersed phase flux increases both the size and the size distribution parameters of the droplets. Size of emulsion droplets was changing with three variables: the interfacial tension of the two phases γ (N/m), the viscosity of dispersed phase μ_d (Pa s), the flux of

dispersed phase J_d (m s^{-1}) (from 1.6×10^{-5} m s^{-1} to 3.9×10^{-5} m s^{-1}). In Figure 5-9 (a), the experimental data and best linear fitting of droplets sizes varying with these variables are plotted. The calculations were done with commercial software Sigma-plot®, Systat Software Inc. via multiple linear regression function. The equation is shown as follows:

$$d_d = 24.05 + 8575.85\gamma - 0.55\mu_d + 2206924.22\,J_d$$

Standard error of estimate = 6.953 (Equation 5.1)

where d_d is the diameter of droplet during detachment, γ is the interfacial tension of the two phases (N m^{-1}), μ_d is the viscosity of dispersed phase (Pa s), J_d is the flux of dispersed phase (m s^{-1}). In general, for all the oils investigated both the mean droplet diameter and *CV* values increased with the flux, as shown in Figure 5-9.

There is no significant difference for the *CV* values of different oils, shown in Figure 5-9 (b). This might be explained according to Equation 5.2, as shown below. The volume of a droplet generated from a pore on a membrane changes with the forming time (Peng and Williams, 1998):

$$V_f = V_g + Q \times t_d \quad \text{(Equation 5.2)}$$

where V_f is the final volume of a droplet (m^3); V_g is the initial volume of the droplet (m^3); Q is the actual flow rate of the dispersed phase through the pore (m^3 s^{-1}) and t_d is the duration of detachment period (s). According to this equation, the final droplet

diameter will increase linearly with the flux of the dispersed phase if t_d remained as a constant. The higher flux may cause generation of droplets with a higher frequency, and lead to bigger droplets prior to detachment. In addition, droplets produced at a higher frequency tend to coalesce more given a stirring speed, leading to a wider size distribution (Abrahamse *et al.*, 2002, Xu *et al.*, 2005), as observed here (Figure 2-9(b)).

Despite considerable difference in physical properties of the two liquid phases and operating conditions utilized, MF droplets with a *CV* value as small as 21.0 ± 0.5% were readily produced from the dispersion cell. This demonstrates that membrane emulsification based on using the dispersion cell is a fairly reliable technique to prepare different emulsion droplets and microcapsules of narrow size distributions.

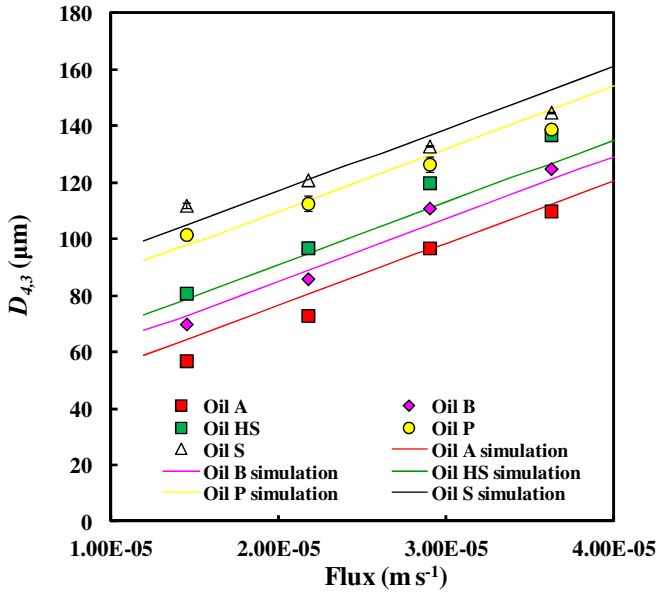

(a)

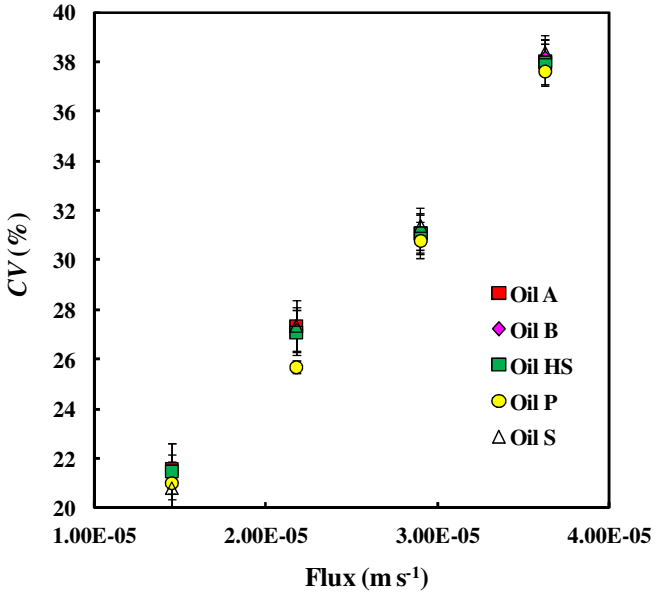

(b)

Figure 5-9 The influence of the flux of the dispersed phase pumped through the membrane on the (a) size and (b) size distribution of the droplets in emulsion. (a) The experimental measurements and mathematical calculations of droplet size in the emulsions of core oil with viscosity of dispersed phase and interfacial tension versus dispersed phase flux in the dispersion cell. The symbols represent experimental data and lines are the best fitting through Sigma-plot® multiple linear regression calculation. The droplets were prepared using a agitation speed of 1080 rpm. The error bars represent the standard error of the mean (N=15).

5.3.3 Morphology of emulsion droplets and microcapsules

The prepared emulsion droplets and corresponding microcapsules were observed using optical microscopy and ESEM (Figures 5-10 and 5-11). The emulsion droplets were produced at an agitation speed of 1080 rpm and a dispersed phase flux of 1.6×10^{-5} m s^{-1}. Both the oil droplets and microcapsules were spherical with smooth surfaces. The small dimples inside the microcapsules shown in Figure 5-11 were considered to result from different extents of contraction between the shell material and liquid core from the reaction temperature of 65 ± 1°C to room temperature, described in Section 4.3.5.

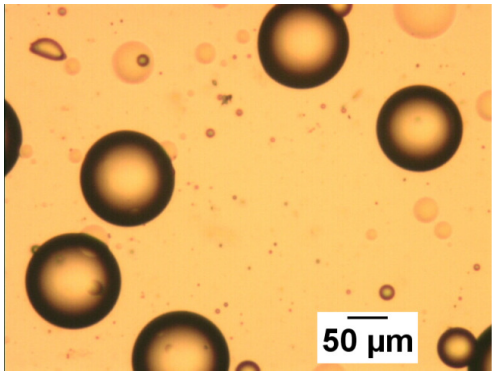

(a) sunflower oil droplets

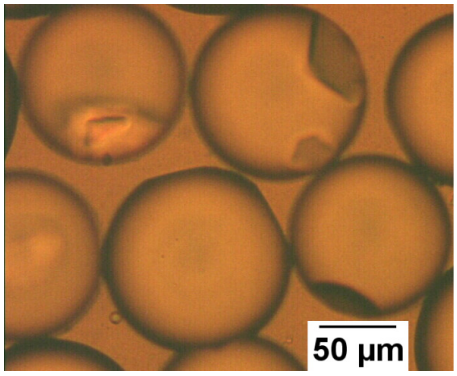

(b) MF-sunflower microcapsules

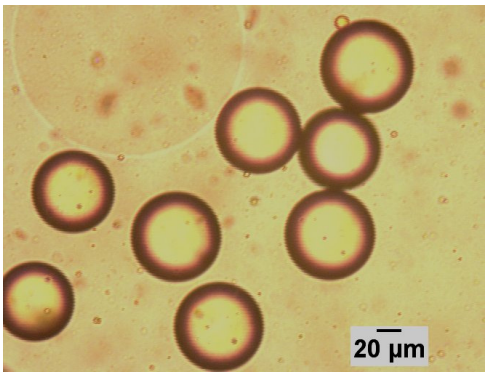

(c) oil B droplets

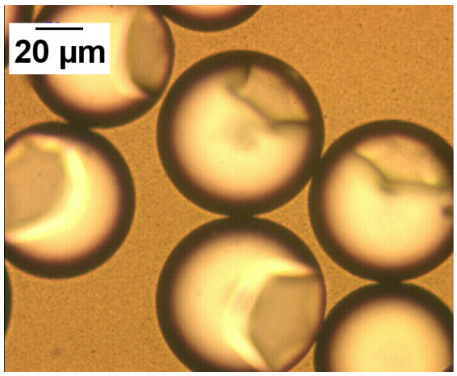

(d) MF-oil B microcapsules

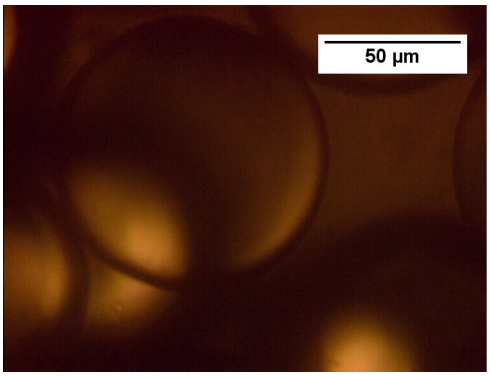

(e) peppermint oil droplets

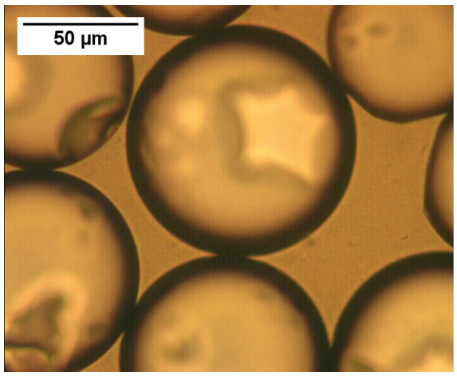

(f) MF- oil P microcapsules

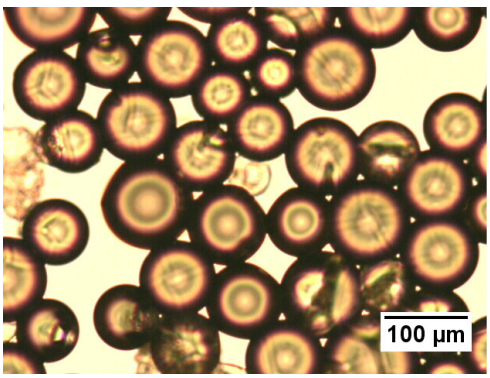

(g) oil HS droplets

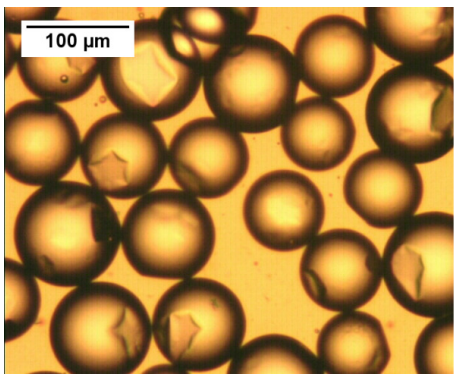

(h) MF-oil HS microcapsules

Figure 5-10. Images of the oil droplets in emulsion and microcapsules obtained by optical microscopy. All the emulsions were generated with an agitation speed of 1080 rpm and dispersed phase flux of 1.6×10^{-5} m s^{-1}.

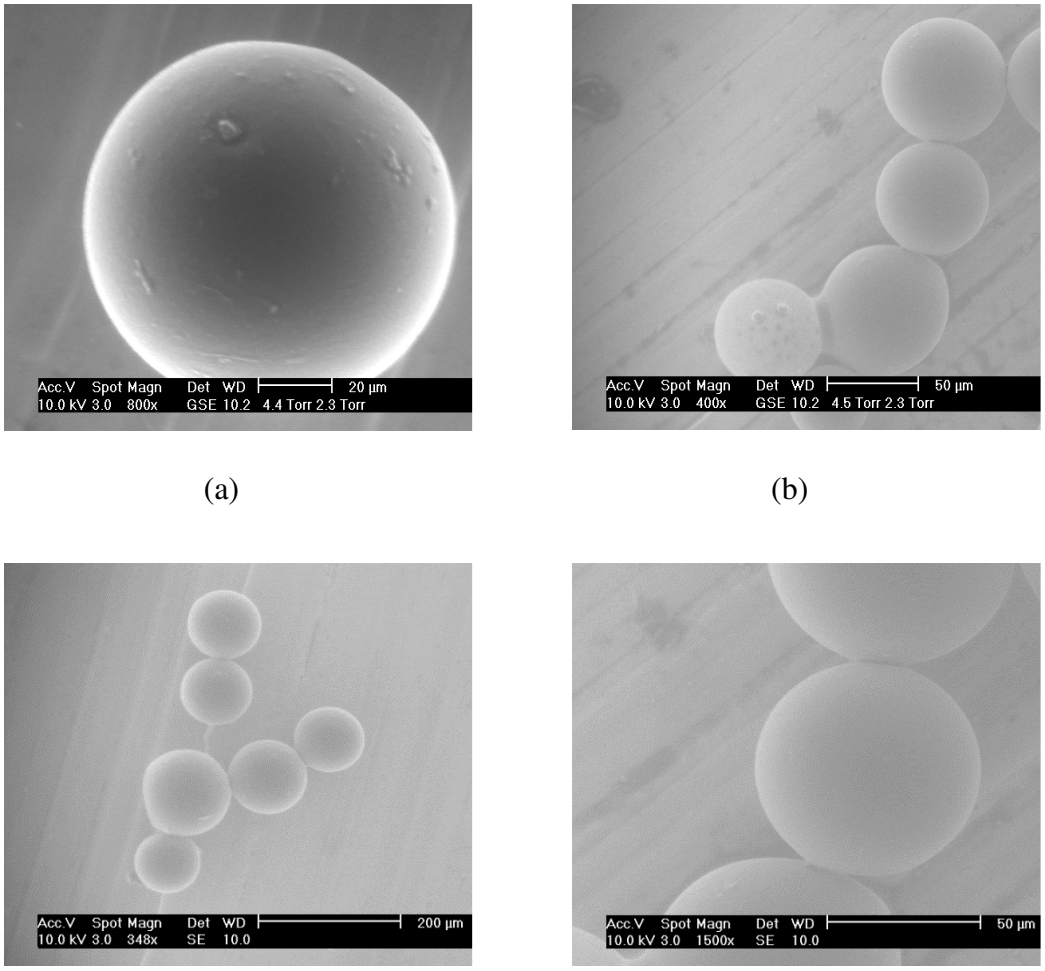

Figure. 5-11. Micrographs of MF microcapsules with different core oils obtained by ESEM. (a) sunflower oil as core; (b) oil B; (c) peppermint oil; (d) oil HS. All the emulsions were generated with an agitation speed of 1080 rpm and dispersed phase flux of 1.6×10^{-5} m s^{-1}.

5.3.4 Shell thickness of MF microcapsules

The shell thicknesses of microcapsules was determined using TEM. The typical micrographs of MF microcapsules prepared with different core oils are presented in Figure 5-12. The sample with sunflower oil had a mean diameter of 113.9 ± 2.4 (SE, n = 50) μm and mean shell thickness of 385 ± 12 nm (SE, n = 50); the sample with peppermint oil had a mean diameter of 100.5 ± 2.2 μm and mean shell thickness of 420 ± 11 nm; with oil B had a mean diameter of 69.3 ± 1.5 μm and mean shell thickness of 410 ± 10 nm; and with oil HS had a mean diameter of 79.6 ± 1.7 μm and mean shell thickness of 396 ± 12 nm. The mean size of the microcapsules in each sample obtained from TEM has no significant difference compared with the one measured using laser diffraction, see Table 5-3. The core oils had no noticeable effect on the shell thickness of microcapsules, based on the TEM measurements.

Table 5-3 Summary of sizes of the droplets and microcapsules as well as shell thickness obtained through laser diffraction and TEM. The mean size is based on number and the error means standard error (50 microcapsules were measured).

	Mean size of droplets	**Mean size of microcapsules**		**Shell**
	laser diffraction	**TEM**	**laser diffraction**	**thickness**
	(μm)	**(μm)**	**(μm)**	**(nm)**
oil A	55.9 ± 1.1	57.3 ±1.4	57.3 ± 1.1	408 ± 3
oil B	67.8 ± 1.2	69.3 ± 1.5	69.8 ± 1.3	410 ± 10
oil P	101.7 ±2.0	100.5 ±2.2	101.5 ± 2.0	420 ± 11
oil HS	80.9 ± 1.6	79.6 ± 1.7	81.0 ± 1.5	396 ± 12
oil S	113.3 ±2.3	113.9 ±2.4	113.4 ±2.3	385 ± 12

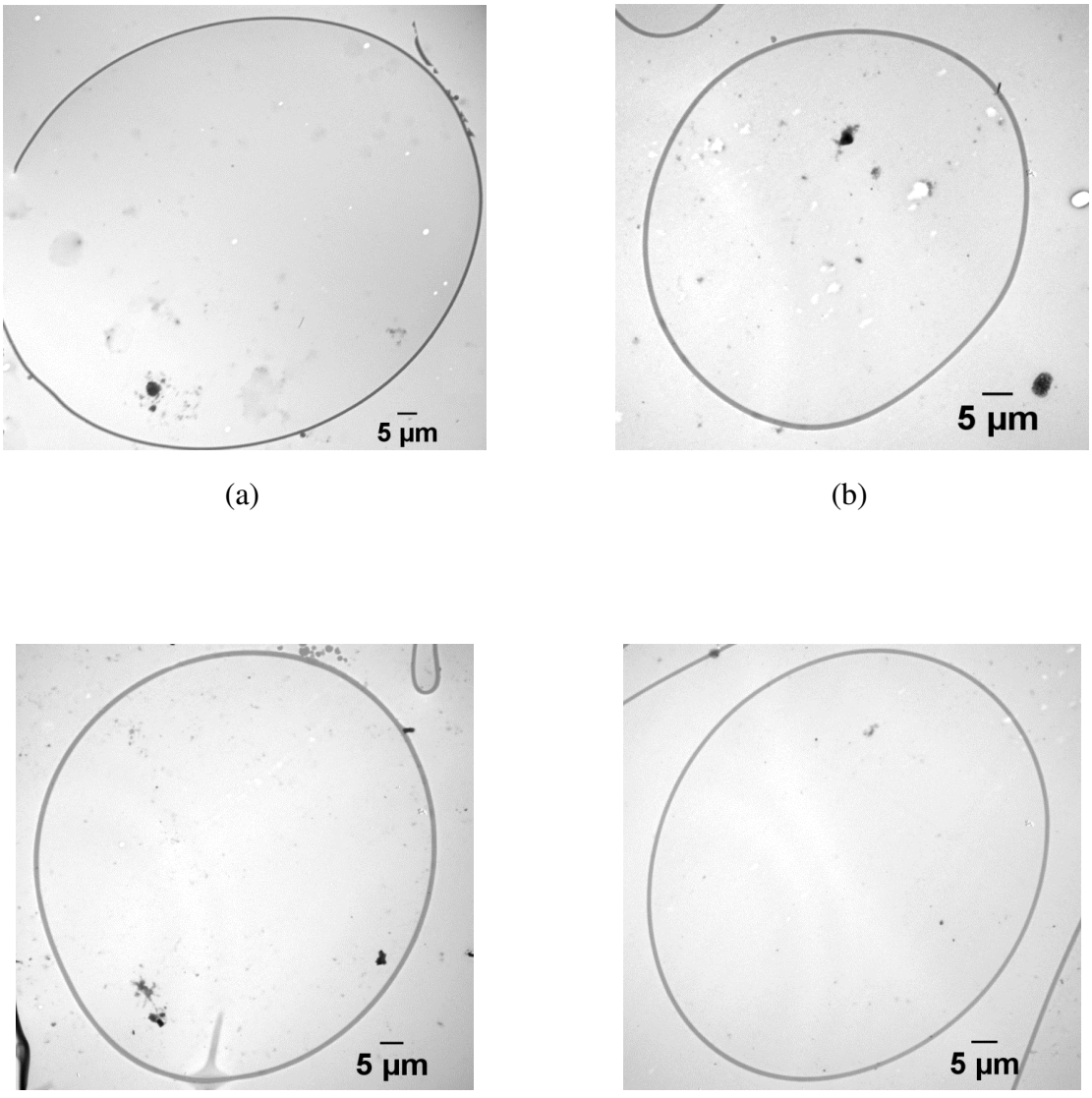

(a) (b)

(c) (d)

Figure. 5-12. Typical TEM micro-images of MF microcapsules with different core oils prepared using the dispersion cell. (a) a microcapsule with sunflower oil; (b) oil B; (c) peppermint oil; (d) oil HS. All the emulsions were generated with an agitation speed of 1080 rpm and dispersed phase flux of 1.6×10^{-5} m s^{-1}.

5.4 Conclusions

MF microcapsules containing an oil-based industrial precursor were prepared using a pilot plant-scale cross-flow membrane system. Compared with the results obtained from the dispersion cell, the cross flow membrane system produced MF microcapsules with a slightly wider the size distribution. This difference likely resulted from different membranes used, rather than the effect of scale up since the oil-MF precondensate emulsion was stable for at least 4 h. Different core oils were encapsulated with a MF shell through membrane emulsification and then in situ polymerization. The size and size distribution of the droplets were affected by membrane configurations, physical properties of the two liquid phases and operation conditions. The experimental data were compared with the predictions of a model reported in the literature. The model overall underestimates the mean droplet size since it does not consider the effect of the dispersed phase flux. Therefore, a new correlation to account for the dispersed phase flux has been proposed. Moreover, the morphology and shell thickness of the microcapsules were determined through microscopy, ESEM and TEM, respectively.

Though MF microcapsules have found industrial applications, there is a safety concern about using formaldehyde in consumer products, Therefore, there is a demand for new coating materials. In this study, environmental friendly PMMA microcapsules were prepared and characterized, and the details will be described in Chapter 6.

Chapter 6 Structure and Mechanical Properties of Consumer-friendly PMMA Microcapsules

The modelling part was performed in collaboration with Dr. R. Mercadé-Prieto at the University of Birmingham, shown in Appendix A.

6.1 Introduction

Preparation and characterization of MF microcapsules containing perfume oil with narrow size and strength distributions have been extensively described in Chapters 4 and 5. Although MF microcapsules are currently used in industry, there are potential health and safety concerns of formaldehyde usage in consumer product, as mentioned in Section 2.5.1. Therefore, it would be desirable to make perfume microcapsules using formaldehyde-free shell material.

In this chapter, the research work presented is to focus on preparation and characterization of environmentally and consumer-friendly poly (methyl methacrylate) (PMMA) microcapsules containing perfume oils, with the aim to be delivered to fabric surfaces via liquid detergents. Microcapsules were produced using a membrane

emulsification system; the results are compared with those obtained using a standard homogenization procedure.

Proper characterization and understanding of novel microcapsules is necessary to evaluate their potential applications, especially to compare with the better known MF microcapsules. Transmission electron microscopy (TEM) is commonly used to determine the wall thickness of microcapsules, though sample preparation is expensive. However, acrylic resin used during the sample preparation for TEM is not suitable for many materials, for example, PMMA. In the work presented in this chapter, a non-destructive technique confocal laser scanning microscopy (CLSM) was used to measure the wall thickness of microcapsules.

A micromanipulation was commonly used to test the mechanical properties of single microcapsules. The data of diameter, rupture force and displacement at rupture of single microcapsules can be obtained. However, in order to determine intrinsic mechanical property parameters of the shell materials, such as elastic modulus, theoretical or numerical models combined with the experimental data are required. Previous modelling work was based on thin-shell microcapsules, such as MF microcapsules mentioned in Chapter 4. There has been no report on modelling of microcapsules with various thick shell. Compression testing by micromanipulation together with finite element modelling (FEM) has been applied to PMMA microcapsules with different shell thickness in order to determine their mechanical properties.

6.2 Experimental section

6.2.1 Preparation of microcapsules

6.2.1.1 Preparation of PMMA precondensate

The protocol developed by Chang *et al.* (2009) for encapsulation of phase transfer materials was adopted to encapsulate perfume oil A, but the formulation and reaction conditions were modified in order to improve the size distribution of the microcapsules. A PMMA precondensate was obtained by mixing toluene (10 g), MMA (9 g), a cross-linker EGDMA (1 g), and a trigger AIBN (0.5 g). The mixture was stirred at 300 rpm with a two-paddle impeller (Φ 75 mm) in a 250 mL 3-necked flask with round bottom, connected to an Allihn condenser. The precondensate was allowed to react for 60 min at 60 ± 1°C.

6.2.1.2 Preparation of emulsion using conventional homogenization

A stock of fluorescent dye was first prepared by dissolving 0.1 wt% of PM546 in acetone. Primary oil in water emulsion was made by homogenizing (Model L4RT, Silverson Machines Ltd., UK) perfume oil A (10 g) with 0.3 wt% of dye-acetone solution and 150 g of an aqueous solution of 0.1 wt% PVA with 5 wt% NaCl for 30 min at 800 rpm. AIBN (0.5g) was added into the precondensate, followed by mixing

with the primary emulsion in the homogenizer for 5 min at 400 to 800 rpm at 25 ± 1 °C.

6.2.1.3 Preparation of double emulsions using the dispersion cell

Emulsion droplets with narrow size distributions were generated by pushing 75 g of an emulsion generated by homogenization at 400 rpm through the membrane system into 75 g of 0.1 wt% PVA and 5 wt% NaCl aqueous solution, using an agitation speed from 880 to 1210 rpm and a dispersed phase flux from 1.6×10^{-5} m s^{-1} to 3.1×10^{-5} m s^{-1} at 25 ± 1 °C.

6.2.1.4 Preparation of PMMA microcapsules

The emulsion formed using a homogenizer or the dispersion cell was transferred back to the round bottom flask, where it was agitated with the double paddle impeller at 150 rpm. The flask was placed into a water bath and its temperature increased to 65 ± 1 °C, allowing the in situ-polymerization reaction of the PMMA to take place for 1 to 24 h. The resulting microcapsules in suspension were cooled to 25 ± 1°C, filtered and washed with distilled water.

6.2.2 Morphology and shell thickness of microcapsules

6.2.2.1 Morphology

Optical microscopy (Leica DMRBE, Leica, Germany) and environmental scanning electron microscopy (ESEM) (FEI/Philips XL30 ESEM-FEG, Philips, UK) were used

to characterise the surface morphology and the core/shell structure of the microcapsules.

6.2.2.2 Determination of shell thickness of microcapsules

The shape of the oil droplets produced during emulsification and the shell thickness (*h*) of the microcapsules at different stages of the polymerization reaction were also studied with confocal laser scanning microscopy (CLSM) (Leica TCS SPE). The excitation wavelength (540 nm) was chosen according to the fluorescent dye PM546 added into the core oil. In order to prove that the dye can diffuse and is soluble in PMMA in the presence of perfume oil A, PMMA micro-particles of ~100 μm were prepared with the methodology described above but without adding perfume oil A. The PMMA micro-particles were then soaked into labelled perfume oil A for one to two weeks, in order to let the oil and dye diffuse into the polymer. Afterwards, the particles were filtered out, and observed under CLSM, which showed strong fluorescence.

The shell thickness and diameter of microcapsules were determined from the cross section of CLSM micrographs using Image J 1.46 (Pretzl *et al.*, 2012). The thicknesses and diameters were determined from the intensity midpoints of the cross-section profiles. A correction factor was applied following that the cross-section

image was not necessarily taken at the equator (Mercade-Prieto *et al.*, 2011b) (see Figure. 6-1 and 6-2). For each batch, 20 microcapsules were randomly selected and 4 measurements were performed on the cross-section at different directions.

6.2.2.3 Shell thickness and radius corrections from CSLM measurements

When measuring radius and shell thicknesses of microcapsules from cross sectional images, as in previous work using TEM or in the present work using CSLM, it is required to correct the measured values considering that the measurement plane is likely to be different from the equator of the capsules (Figure. 6-1), the only plane where the measured shell thickness (h_m) and radius (r_m) are equal to the real shell thickness (h) and radius (r). Smith *et al.* (2000) developed the trigonometric equations for a given plane, and Mercade-Prieto *et al.* (2011b) estimated the typical shell thickness correction for MF microcapsules. Here, what is desired is a correction factor of the shell thickness ratio *h/r* for capsules with a wide range of *h/r* values. The correction factor has been calculated using the equations described by Smith *et al.* (2000) in a Matlab program that simulates 106 random measurement cuts, in microcapsules with a random size between 40 to 70 μm. The measurement plane is randomly distributed within a distance α_{ri} from the equatorial plane. When the maximum $\alpha = 1$, all the planes possible where a core-shell structure is still observed are considered, but not when only shell is measured. As discussed by Mercadé-Prieto *et al.* (2011b), measurements planes very close to the shell ($\alpha \approx 1$) are unlikely to occur in practice, meanwhile they heavily influence the mean correction factor. For

this reason, α values of 0.9 and 0.8 have also been considered; the effect of α on correction factor is plotted in Figure 6-2. A maximum α value of 0.9 is considered here to correct the CSLM measurements. Note that more correction is required for thin shells, like PMMA 1 h, than for thicker shells, such as the PMMA 4 h.

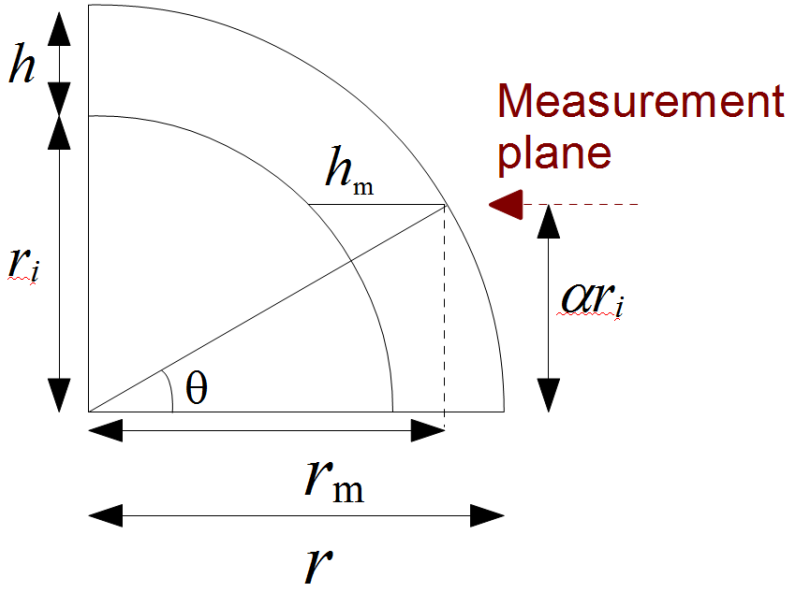

Figure 6-1. Schematic diagram of a cross section measurement plane at a distance αr from the equatorial plane.

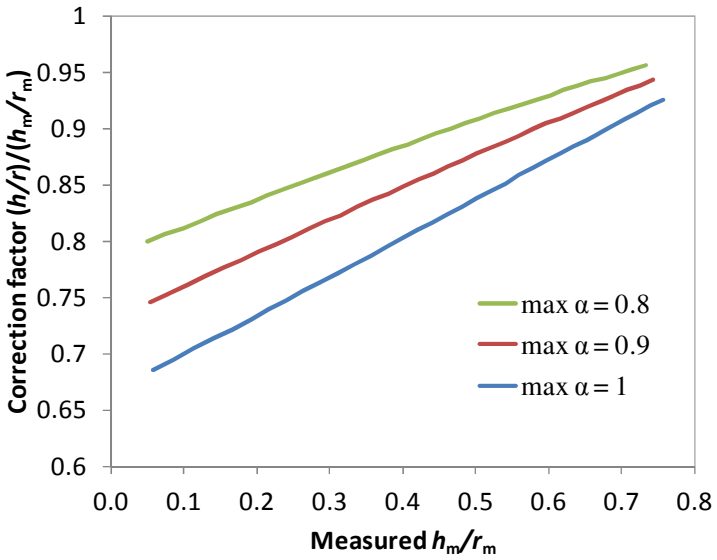

Figure 6-2. Correction factor of the measured shell thickness ratio from simulations with different maximum measurement planes away from the equator, parameter α as described in Figure 6-1.

6.2.3 Size analysis

The mean size and size distribution of the oil droplets produced in the emulsification step and the final microcapsules were determined using laser diffraction (Mastersizer 2000, Malvern Instruments, UK). The values of *SPAN*, coefficient of variance (*CV)*, and the volume-based mean diameter $D_{4,3}$ were recorded. The refractive index of the perfume oil A was 1.497 (given by the supplier P&G) and that of the microcapsules was 1.49 (Huisman *et al.*, 2012). The size values given are the average of five measurements.

6.2.4 Determination of the mechanical properties of PMMA microcapsules

The parallel compression of single microcapsules was performed by a well-established micromanipulation technique (Sun and Zhang, 2001), and more details are described in Chapter 3, Section 3.3.

One drop of suspension with microcapsules was placed on a glass slide and left to dry for 2-3 min. Single microcapsules were observed from a side-view video camera (Micro Instruments Ltd., Oxon, UK). A glass probe of 160 μm in diameter connected to a force transducer (Maximum scale 5mN, Model 403A, Aurora Scientific Inc., Canada) held by a fine micromanipulator was programmed to travel towards a single microcapsule at a speed of 2 μm s^{-1}. The system used can measure forces with a precision of ± 0.1 μN and probe displacement of ± 0.2 μm (Thomas *et al.*, 2000). For each sample 20 to 30 microcapsules were randomly selected.

Theoretically, the capsule shell can be elastic, viscoelastic and elastic-plastic. Full characterisation of these properties requires a series of carefully designed experiments, including compression to different deformations and holding, loading and unloading, and compression at different speeds, as carried out on melamine formaldehyde microcapsules with difference cores (Hu *et al.*, 2009, Sun and Zhang, 2001) and

polymer pharmaceutical excipients (Yap *et al.*, 2008). It has been found the capsule shell and these polymeric particles were mainly elastic-plastic, and the viscous effect was negligible. Moreover, previous work on the viscoelasticity of a macroscopic PMMA material (Capodagli and Lakes, 2008) showed that it was mainly elastic and its apparent Young's modulus varied only by approximately ± 10%, measured by a broadband viscoelasticity spectrometer when the applied frequency was changed by several orders of magnitude. Therefore single microcapsules were only compressed at a given speed to large deformations or rupture. The parallel compression of microcapsules with thick shells was studied using finite element modelling (FEM) to determine their elastic-plastic properties; the details are given in Appendix A.

6.3 Results and Discussion

6.3.1 Stability of the oil/water emulsion

The size distribution of the emulsion droplets during storage was measured since it took a few hours to form microcapsules from the emulsion. The mean diameter $D_{4,3}$ varied from 55.1 ± 1.2 μm when the emulsification was finished to 55.8 ± 1.3 μm after 72 h, while the corresponding *CV* value varied from 22.1 ± 0.5 % to 23.5 ± 0.6%. Therefore, the emulsion droplets were considered to be stable during this period (Figure 6-3).

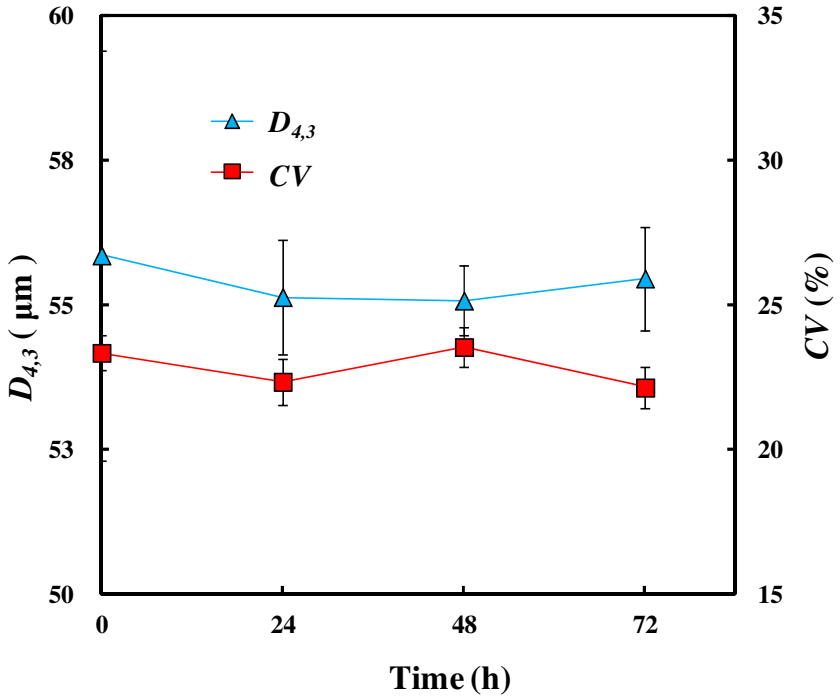

Figure 6-3 The mean diameter ($D_{4,3}$) and *CV* values of the oil droplets measured at different times after their formation, which were prepared by membrane emulsification using an agitation speed of 1080 rpm and dispersed phase flux of 1.6×10^{-5} m s^{-1}.

6.3.2 Size and size distribution of oil droplets and microcapsules

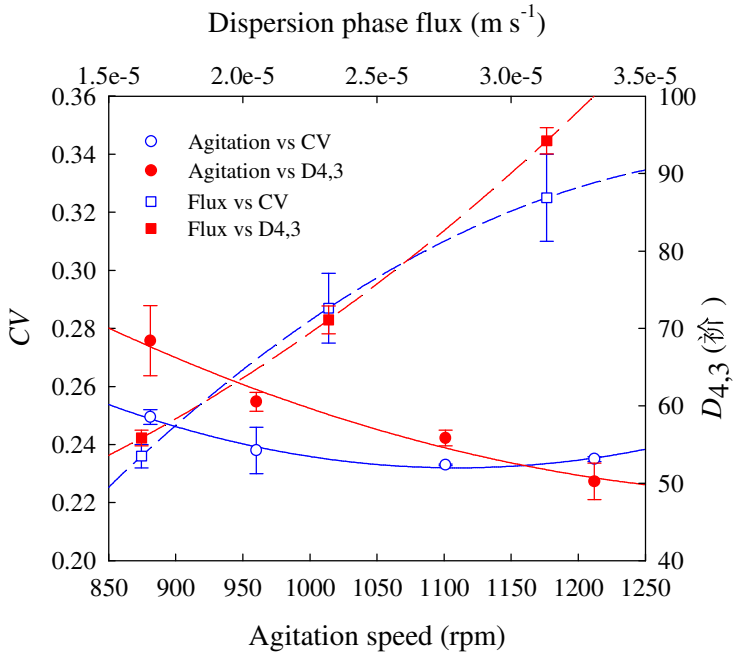

Figure 6-4. Effect of the process parameters: agitation speed (circles) and dispersed phase flux (squares) on the mean size and the size distribution of the resultant emulsion droplets. Empty points refer to the *CV* value, and filled points to $D_{4,3}$. Lines only indicate the trends.

Processing conditions during the membrane emulsification step were investigated to obtain droplets with narrow size distributions. As reported in Chapter 4, Section 4.3.3, the *CV* value of the droplets presents a minimum with an agitation speed of the dispersion cell at ~1080 rpm, shown in Figure 6-4. In contrast, the mean diameter $D_{4,3}$ decreases monotonically with the agitation speed. For a fixed agitation speed of 1080 rpm, higher dispersed phase fluxes increase both the mean droplet diameter $D_{4,3}$ and *CV*

(Figure 6-4).

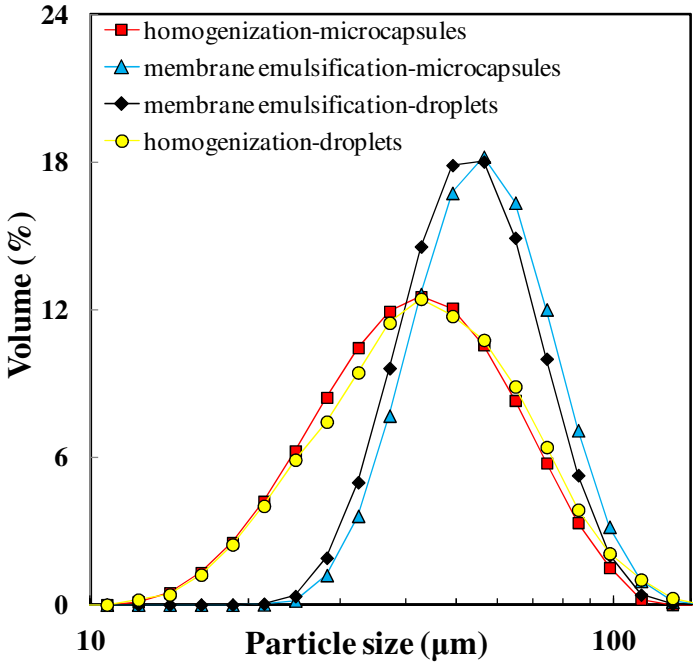

Figure 6-5. Size distributions of the emulsion droplets and microcapsules with reaction time 4 h, prepared by two different methods: membrane emulsification (with an agitation speed of 1080 rpm and dispersed phase flux of 1.6×10^{-5} m s^{-1}) and homogenization (800 rpm).

The size distributions of the emulsion droplets and the formed microcapsules with reaction time 4 h, produced by two different methods are shown in Figure 6-5. Statistical analysis of the size distributions shows that they can be fitted with Gaussian, and that there is no significant difference between the oil droplets and microcapsules. Microcapsules made with membrane emulsification and homogenization differed slightly in size, with $D_{4,3}$ of 56.1 ± 1.3 and 44.8 ± 1.5 μm

respectively, which could be modified if desired (Hu *et al.*, 2009, Pretzl *et al.*, 2012). In order to produce droplets/microcapsules of the exact same size by these two methods, extensive optimization of operating conditions would be required. Crucially, the *CV* and *SPAN* values of the microcapsules made using homogenization were significantly larger, 34.4 ± 1.2 % and 1.12 ± 0.03, compared to membrane emulsification, 23.8 ± 0.6 %, and 0.72 ± 0.01, respectively. Similar results have been reported previously in Chapter 4, Section 4.3.3 for MF microcapsules.

Figure 6-6 shows typical optical and ESEM images of microcapsules prepared by membrane emulsification. These microcapsules were spherical and had smooth surfaces. Figure 6 (c) shows a PMMA microcapsule which was cut with a microtome under a microscope before an ESEM analysis. The microcapsule shows a clear core-shell structure.

6.3.3 Morphology

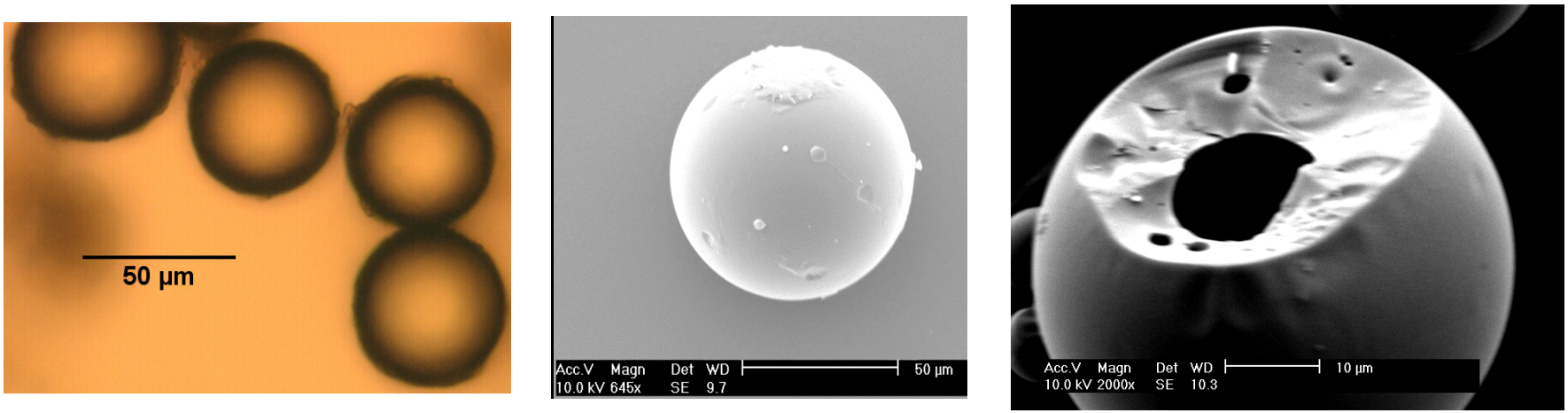

(a) **(b)** **(c)**

Figure 6-6. Micrographs of PMMA microcapsules with reaction time 4 h, obtained using (a) optical microscopy and (b-c) ESEM. In (c) the microcapsule was cut with a microtome under a microscope. Microcapsules were prepared using the dispersion cell with an agitation speed of 1080 rpm and dispersed phase flux of 1.6×10^{-5} m s^{-1}.

6.3.4 Determination of the shell thickness using CLSM

Transmission electron microscopy (TEM) is commonly used to determine the wall thickness of microcapsules due to its excellent resolution, particularly for MF microcapsules (Long *et al.*, 2009). Microcapsules investigated by TEM were embedded in an acrylic resin before ultra-cutting (Long *et al.*, 2010). This sample preparation method is costly and time consuming, which is not suitable for many materials that have similar physical properties to the acrylic resin, such as PMMA, as their shells dissolve in the resin. On the other hand, CLSM is a non-destructive technique that has recently been used to investigate the shell structure and thickness of microcapsules (Chen *et al.*, 2006, Lebedeva *et al.*, 2004, Paramita *et al.*, 2010, Tavera *et al.*, 2009, Tzhayik *et al.*, 2012), but it requires a clear contrast between the shell and core of microcapsules.

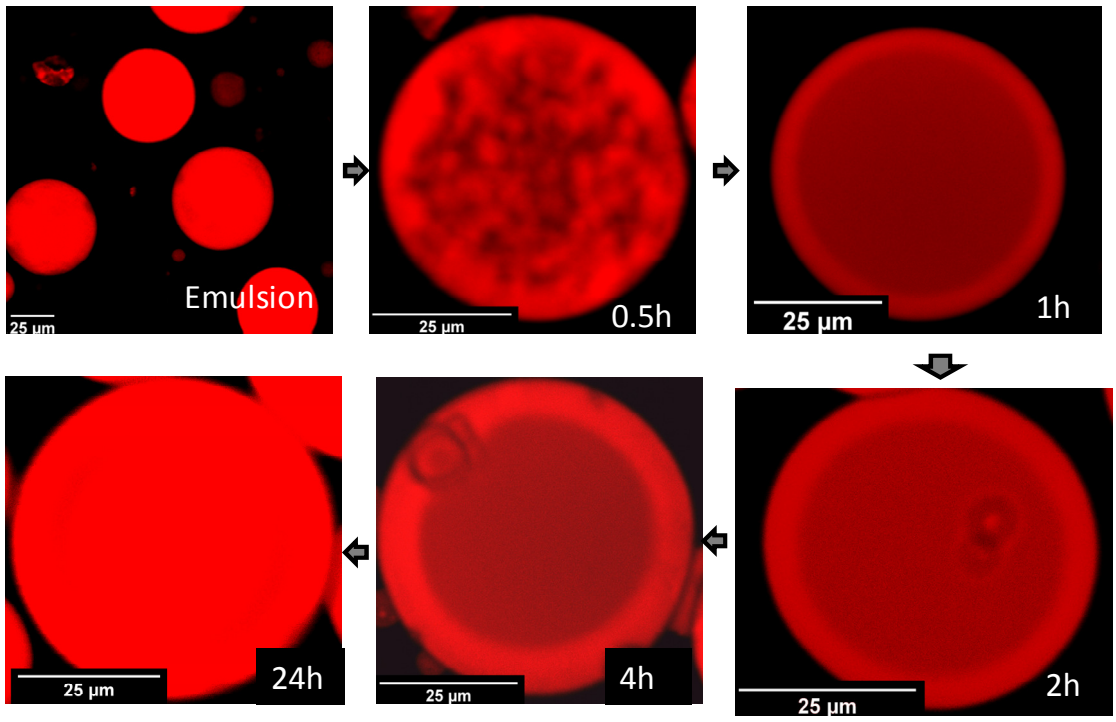

Figure 6-7. CLSM micrographs of oil droplets and PMMA microcapsules at different stages of polymerization. The scale bar is 25 µm for all 6 images. Microcapsules were prepared using the dispersion cell with an agitation speed of 1080 rpm and dispersed phase flux of 1.6×10^{-5} m s^{-1}.

The morphology of oil droplets and of PMMA microcapsules at different stages of polymerization was visualized with CLSM; typical micrographs are shown in Figure 6-7. Before polymerization, when only an emulsion was present, the fluorescent dye was uniformly distributed inside the oil droplets. After reaction for 0.5 h, the dye had a punctuated distribution inside the droplets, which could be caused by an incipient shell formation. After 1 h, an outer shell is clearly discernible in the micrograph, with an average thickness $h = 2.4 \pm 0.2$ µm. After a shell was formed, h increased with the

polymerization time, from 10.2 ± 0.8 µm after 2 h to 14.2 ± 1.6 µm after 4 h. After 24 h, the PMMA microcapsules became homogeneous particles without core. From the images, it seems the perfume oil A was dissolved in the shell of microcapsules, particularly for a polymerization time of 24 h.

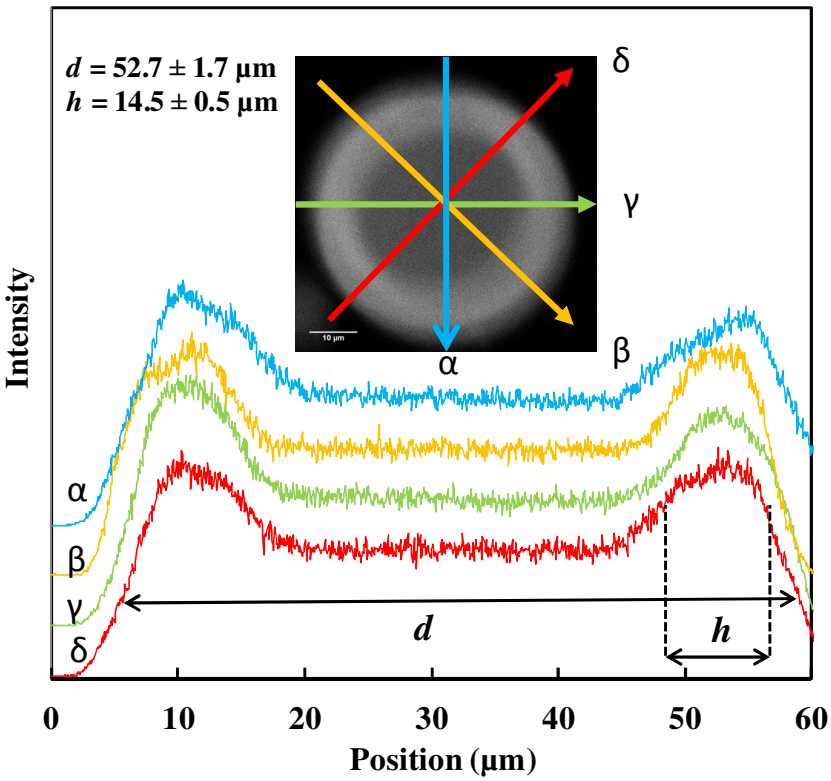

Figure 6-8. CLSM micrograph (inset) and fluorescence intensity profiles of a microcapsule (52 µm) measured at four different directions. The diameter (*d*) and shell thickness (*h*) determined are indicated by black arrows. The microcapsule is PMMA with 4h reaction prepared by membrane emulsification.

Figure 6-8 shows a CLSM micrograph of a PMMA microcapsule formed after reaction for 4 h (denoted by 4 h PMMA microcapsules later), together with the fluorescence intensity profiles at four different directions. The diameter *d* and the shell thickness *h* were determined from the intensity profiles as the mid points of the convex sigmoidal-like curves. Figure 6-9 summarizes the shell thickness *h* of PMMA microcapsules formed after a reaction for 1 h (denoted by 1 h PMMA microcapsules later), and 4 h using the two methods considered. As expected, the emulsification method has no effect on the posterior shell thickness formed. The shell thickness is found to increase with the capsule diameter *d*, unlike previously reported for MF microcapsules where *h* was found independent of size (Hu *et al.*, 2009). Formation of the PMMA shell resulted from migration of PMMA from the inside of oil phase to its surface, which is different from the mechanism to form melamine formaldehyde microcapsules. In the latter case, the precondensate of melamine formaldehyde was soluble in aqueous phase surrounding oil droplets and then moved to oil surface (Sun and Zhang, 2001). Loxley and Vincent (Loxley and Vincent, 1998) also observed that the shell thickness was proportional to the diameter of PMMA microcapsules although they were produced by solvent evaporation.

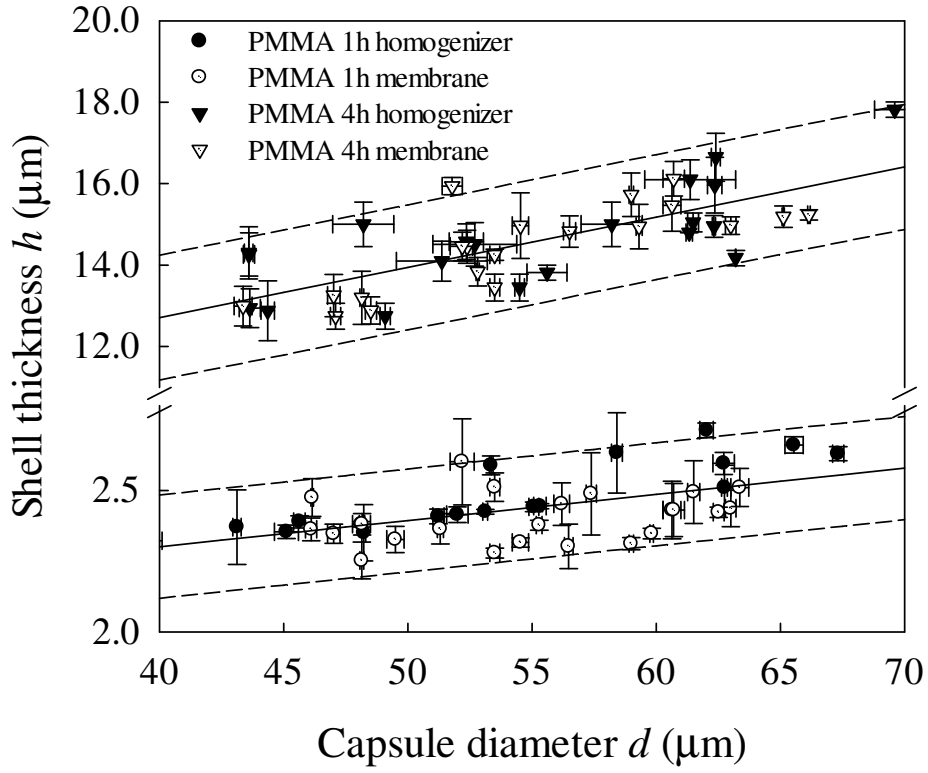

Figure 6-9. Shell thickness h measured with CSLM for microcapsules larger than 40 µm prepared by membrane emulsification (empty points) and homogenization (filled points), after a reaction time of 1 h (circles) and 4 h (triangles). The error bars represent the standard deviation of the mean. Continuous lines are the best linear fits, for 1 h PMMA microcapsules: $h = 0.009d + 1.9$; and 4 h PMMA microcapsules: $h = 0.12d + 7.8$. Dashed lines represent the 95% confidence intervals of the linear fits.

6.3.5 Experimental determination of the mechanical properties of PMMA microcapsules

The mechanical characterization of single microcapsules is commonly performed using a parallel plate compression apparatus (Zhang *et al.*, 2009b). The compression

force profiles with the fractional deformation ε_m, defined as the displacement normalized by the capsule diameter, are used to calculate the mechanical properties of the shell, such as the elastic modulus. Theoretical or numerical models are required to perform this analysis, and the right model to use depends on the characteristics of the shell, particularly the shell thickness to radius ratio (*h/r*). Most of the previous characterization studies have been carried out on MF or similar microcapsules, which have thinner shells compared to the PMMA microcapsules of the present study. The wide range of *h/r* values for PMMA microcapsules formed at different reaction times, see the micrographs of Figure 6-7, results in very different compression force profiles, shown in Figure 6-10, which are summarized as follows:

(a) Compression profiles of thin-shell microcapsules with a bursting point

A bursting point is observed when there is a sudden decrease of the force. The force can decrease to zero after bursting, as commonly observed from MF microcapsules (point A in Figure 6-10) (Hu *et al.*, 2009, Long *et al.*, 2009, Mercade-Prieto *et al.*, 2011b, Pretzl *et al.*, 2012), or a residual strength can still be present in the shell that maintains a significant resistance force after bursting, as observed for urea-formaldehyde (UF) (Brown *et al.*, 2003) and silica-based microcapsules (Mercade-Prieto *et al.*, 2012a, O'Sullivan *et al.*, 2009). Bursting is observed from microcapsules with thin shells, typically $h/r < 0.07$ for MF and UF microcapsules, and $h/r < 0.25$ for silica-based microcapsules (Mercade-Prieto *et al.*, 2012a, O'Sullivan *et*

al., 2009). The 1 h PMMA microcapsules, where $0.08 < h/r < 0.11$, also show a bursting point as shown by point B in Figure 6-10.

(b) Compression profiles of thick-shell microcapsules without a bursting point

PMMA microcapsules produced after a polymerization time of 4 h or longer had much thicker shells (for capsules larger than 40 μm $0.47 < h/r < 0.62$) than any other microcapsules reported in the literature where the mechanical properties have been investigated. For 4 h PMMA microcapsules, the compression force increases continuously with deformation, up to a point where the both shells touch each other in the compressed capsule (point C in Figure 6-10), which can be confirmed using the expected *h/r* ratio of the capsule from Figure 6-9. Although 4 h PMMA microcapsules without a doubt break during compression, as observed from the debris left after the compression experiment, there is not a clear force drop that can uniquely indentify at which deformation the capsules break.

(c) Compression profiles of full spheres

After polymerizing for 24 h, PMMA microcapsules became full homogenous spheres as inferred from CLSM micrographs (Figure 6-7). Similar to 4 h PMMA microcapsules, a bursting point is not observed either, with the compression force soared at small fractional deformations (point D in Figure 6-10). The force versus displacement corresponding to small deformations for 24 h PMMA microcapsules may be fitted using Hertz model to estimate the Young's modulus, see (Equation A2) in Appendix A and Figure 6-11. There is a single case in the literature whereby type

(a) and (b) compression profiles have been observed from a same batch of alginate microcapsules (Rehor *et al.*, 2001). Due to the large variability in the shell thickness, 1.9% < *h/r* < 47.1%, only 55% of the measurements showed a clear bursting point. The presence of a bursting point is important because it has been used in the past as a simple strength parameter (Long *et al.*, 2009). However, under this approach it is impossible to analyze samples that do not burst, like 4 h and 24 h PMMA microcapsules.

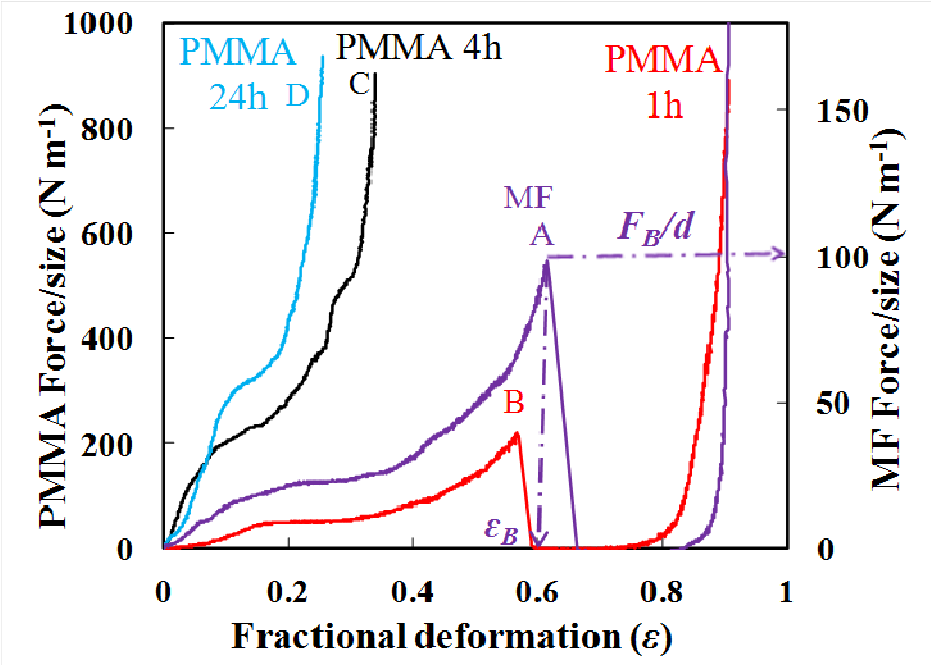

Figure 6-10. Typical normalized compression force profiles of 1 h, 4 h and 24 h PMMA microcapsules, together with that of a MF microcapsule described elsewhere (Mercade-Prieto *et al.*, 2011a). Points A and B are the bursting points of MF and 1 h PMMA microcapsules, respectively.

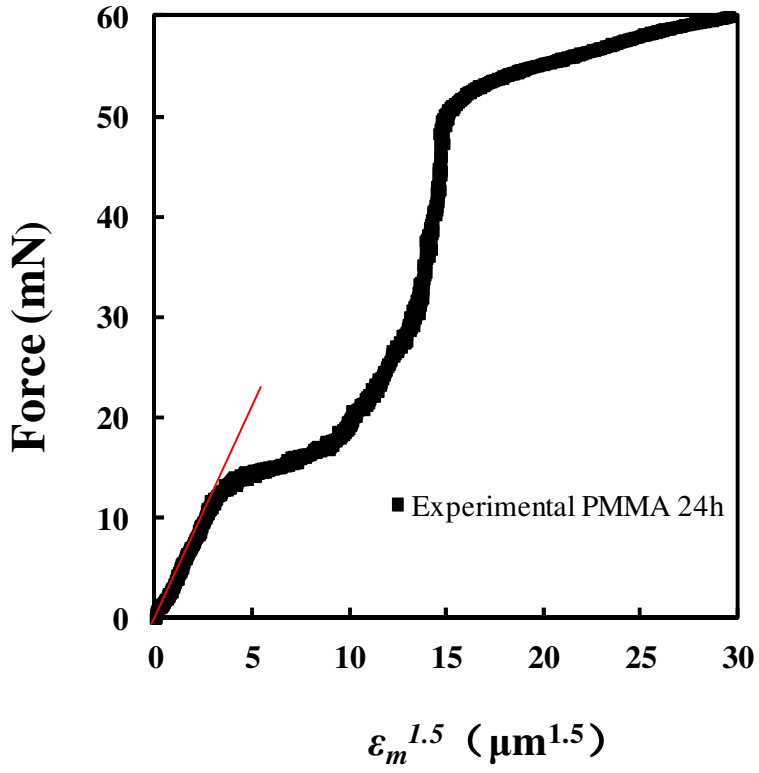

Figure 6-11. Force versus $\varepsilon_m^{1.5}$ data for compression of a PMMA capsule (47 μm in diameter) formed after a reaction time of 24 h. The straight line in red represents the fitting by Hertz model. The Young's modulus value estimated by Hertz model is 423 MPa.

A new methodology has been developed from the work of Mercadé-Prieto *et al.* (2012a) which considers that irreversible damage occurs in the shell during compression, which can lead or not to bursting after additional deformation. For the case of silica-based microcapsules studied by Mercadé-Prieto *et al.* (2012a), where a busting point was indeed observed at a fractional deformation ε_B of ~0.16, it was argued that a better parameter to characterize the onset of fracture within the shell was the elastic limit ε_{LE}. ε_{LE} is defined as the fractional deformation above which there is

a continuously increasing difference between the experimental force profile and the theoretical elastic profile (Mercade-Prieto *et al.*, 2011a). As has been discussed elsewhere (Mercade-Prieto *et al.*, 2012a), it at present is not possible to determine if the non elastic behaviour above ε_{LE} is caused by the onset of fracture within the shell or due to yielding of the material, leading to plastic deformation. Pure PMMA is known to be brittle at room temperatures (Vincent, 1972), and it has been described as a semi-brittle glassy polymer between 20-40°C (Shen *et al.*, 1985), but the crystalline state of the PMMA in the microcapsules is not known, and amorphous PMMA presents extensive plastic deformation before rupture (Stachurski, 2003).

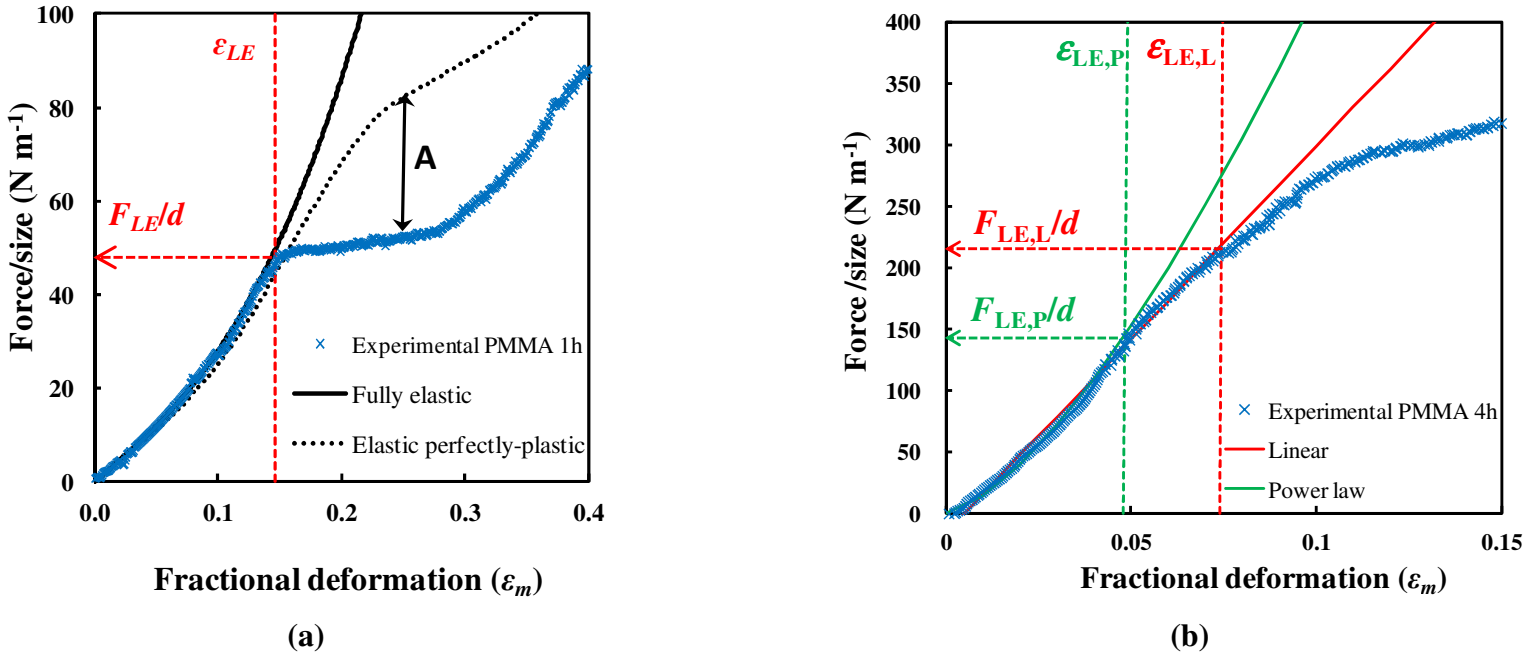

Figure 6-12. Experimental compression results of single PMMA microcapsules made at different reaction time and simulation profiles of the initial elastic regime. (a) 1 h PMMA microcapsule (47 µm) with the best fit of elastic (continuous line) and elastic perfectly-plastic scenario from Mercade-Prieto *et al.* (2011a). Arrow *A* highlights the force gap between experimental data and the elastic perfectly-plastic profile. Vertical dashed lines represent the elastic limit $\boldsymbol{\varepsilon_{LE}}$. (b) 4 h PMMA microcapsule (54 µm) at small fractional deformations. Continuous lines represent the best fit using a linear approach (red line) with *E* ~840 MPa, and using a power law methodology (green line) with *E* ~747 MPa. Vertical dashed lines represent the elastic limit using both methodologies, $\boldsymbol{\varepsilon_{LE,L}}$ and $\boldsymbol{\varepsilon_{LE,P}}$, respectively.

6.3.5.1 Fractional deformation at the elastic limit ε_{LE}

The elastic limit ε_{LE} has two key functions: (*i*) to provide the maximum fractional deformation value whereupon the elastic regime exists, and wherein the elastic modulus can be calculated; and (*ii*) allows determining a lower threshold value of the shell rupture stress (σ_B) (Mercade-Prieto *et al.*, 2012a). Further discussion on the nature of this rupture stress is provided later. How ε_{LE} is determined depends on the *h/r* value of the microcapsules measured. For the 1 h thin-shell PMMA microcapsules (type (a)), ε_{LE} was determined following the model developed by Mercadé-Prieto *et al.* (Mercade-Prieto *et al.*, 2011a, 2011b) for MF microcapsules with $0.04 < h/r < 0.12$. Figure 6-12 (a) shows an example of how ε_{LE} is determined from the point where the predicted elastic behaviour deviates from the experimental data. Note that ε_{LE} is determined by fitting the force profile, hence it primarily determines large deviations from a linear elastic behaviour. Therefore, if a plastic hardening regime exists with a modulus similar to *E,* it could not be differentiated, as discussed in details elsewhere (Mercade-Prieto *et al.*, 2012a). Unique characterization of elastic behaviour at fractional deformation smaller than ε_{LE} would require loading-unloading and loading-holding experiments (Hu *et al.*, 2009, Sun and Zhang, 2001), but due to the small value of ε_{LE} this was not performed.

In order to analyze the 4 h PMMA microcapsules with thicker shells (type (b)), a new methodology has been developed to estimate the elastic regime, described in Appendix A. Two approaches are proposed, one considering a linear increase of the

force at small fractional deformations, and a second approach considering a power law increase. In general, both methods provide reasonably good fits for all the microcapsules tested, however the ε_{LE} estimated with each method can be different, being that determined with the power law model ($\varepsilon_{LE,P}$) lower than with the linear model ($\varepsilon_{LE,L}$) (Figure 6-12 (b)). For the analysis of full spheres (type (c) profiles), such as 24 h PMMA microcapsules, only the power law model was used to determine ε_{LE} by plotting the force versus fractional deformation on a log-log scale (graphs not shown).

Figure 6-13 shows the individual results for microcapsules larger than 40 µm prepared using membrane emulsification and homogenization methods. Note that despite the significant scatter, no trend is observed between ε_{LE} and the capsules size, as reported previously (Mercade-Prieto *et al.*, 2012a). The mean population ε_{LE} values determined for 4 h PMMA microcapsules made by membrane emulsification were $\varepsilon_{LE,P}$= 0.031 ± 0.012 (SD, number of compressions *n*=30) and $\varepsilon_{LE,L}$= 0.053 ± 0.018, and using homogenization $\varepsilon_{LE,P}$= 0.036 ± 0.013 (*n*=30) and $\varepsilon_{LE,L}$= 0.053 ± 0.017, resulting in a total average of ε_{LE}= 0.043 ± 0.014. Similar values were obtained for 24 h PMMA microcapsules, $\varepsilon_{LE,P}$= 0.036 ± 0.018 (*n*=20), whereas much higher values were determined for 1 h PMMA microcapsules ε_{LE}= 0.11 ± 0.04 (*n*=24) using membrane emulsification and ε_{LE}= 0.12 ± 0.05 (*n*=29) using homogenization (Figure 6-14). No statistical difference in ε_{LE} is found between the capsules made by membrane emulsification and homogenization (Figure 6-15 (a)).

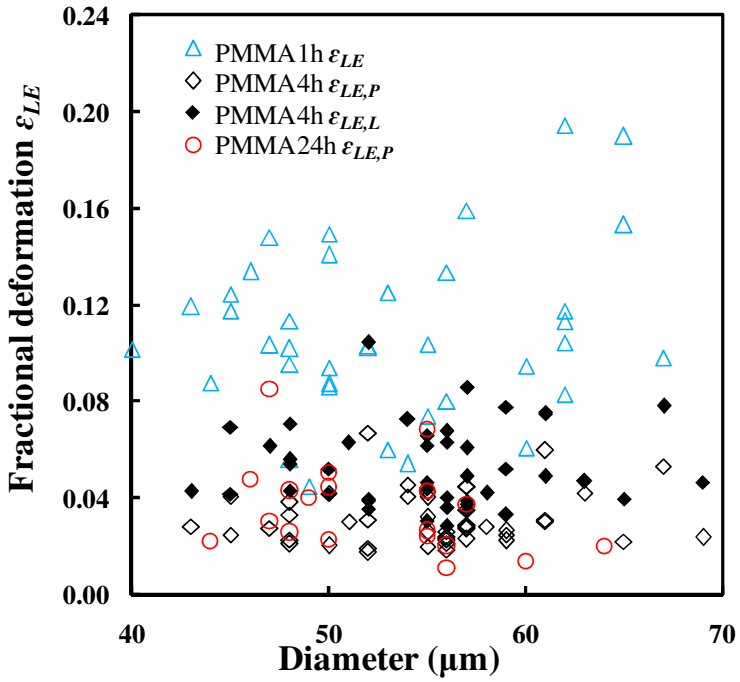

Figure 6-13. Fractional deformation at the elastic limit ε_{LE} of individual microcapsules larger than 40 μm prepared by both emulsification methods, which were determined using two different models: 1 h (thin-shell model : triangles), 4 h (linear model: filled diamonds and power law model: empty diamonds) and 24 h (power law model: circles) PMMA microcapsules.

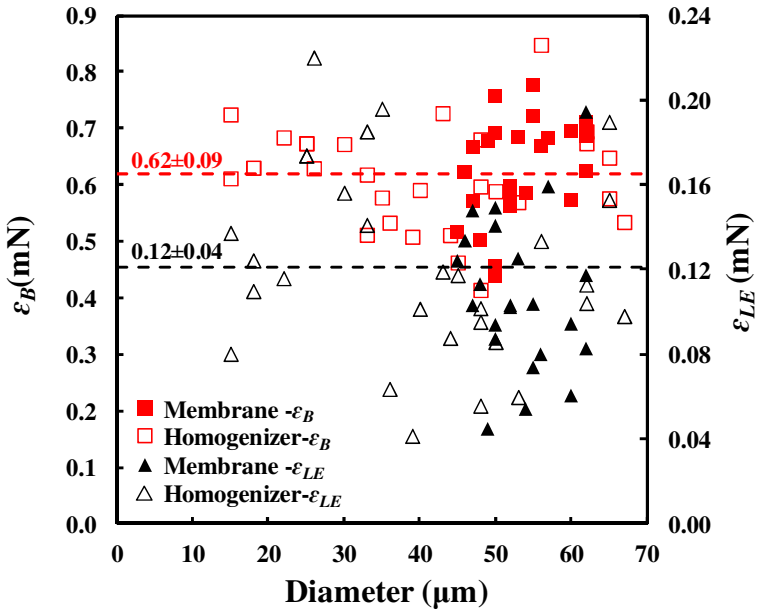

Figure 6-14. Fractional deformation at bursting point ε_B (squares) and fractional deformation at the elastic limit ε_{LE} (triangles) versus diameter for 1 h PMMA microcapsules prepared by membrane emulsification (filled points) and homogenization (empty points). The horizontal dash line represents the mean value of the fractional deformation at the bursting point (red) and at the elastic limit (black).

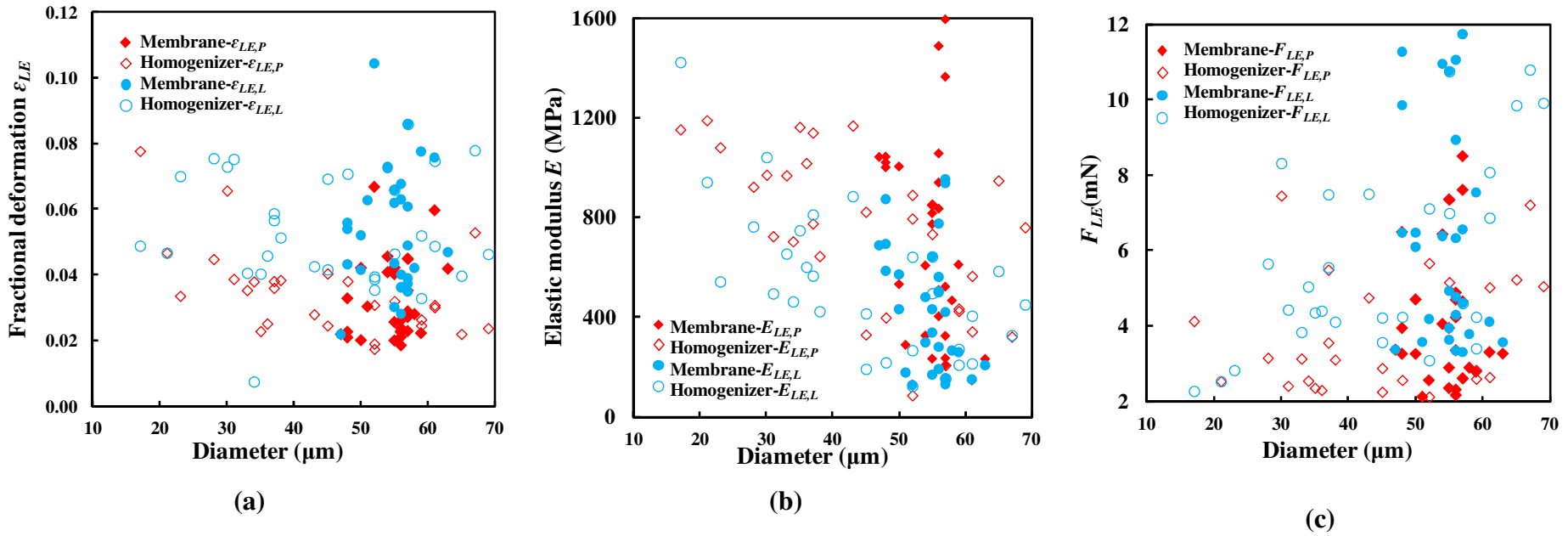

Figure 6-15. (a) Elastic limit, (b) elastic modulus and (c) force at the elastic limit of individual 4 h PMMA microcapsules prepared by membrane emulsification (filled points) and homogenization (empty points) determined using different methodologies: power law model (diamonds) and linear model (circles).

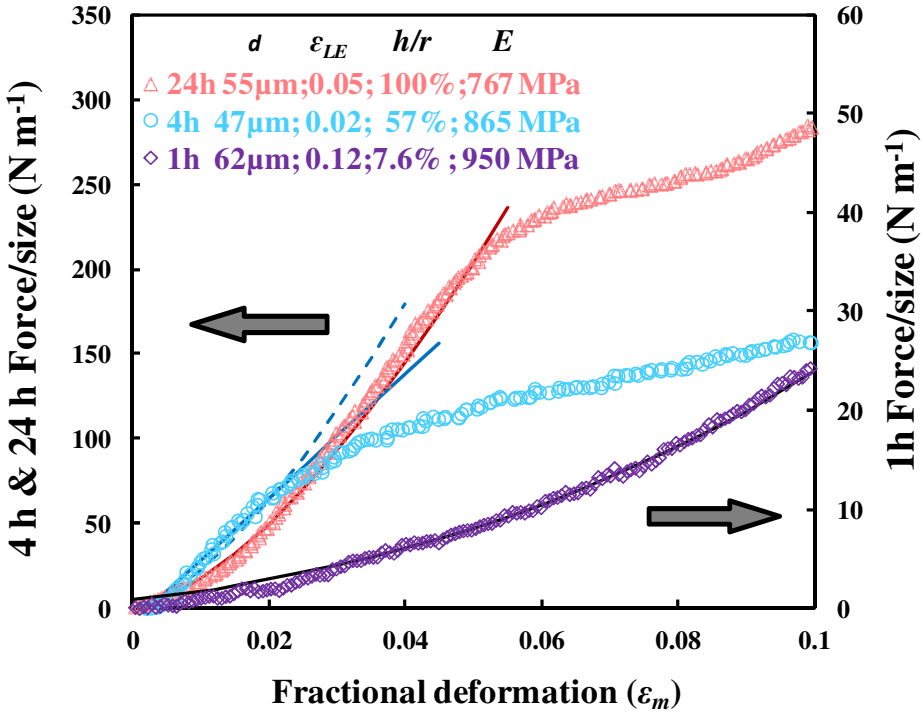

Figure 6-16. Comparison between experimental compression data (points) and the best fit profiles of elastic regime from FEM simulations (lines) of individual PMMA microcapsules produced with different reaction times: 1 h (thin-shell model (Mercade-Prieto *et al.*, 2011a, Mercade-Prieto *et al.*, 2011b)), 4 h (continuous line - linear model; dashed line - power law model), and 24 h (power law model) PMMA microcapsules. The *E* and ε_{LE} values determined from the best fitting curves are shown in the legend (for 4 h PMMA microcapsules, average of the two models is given).

6.3.5.2 Elastic modulus E

After the determination of the fractional deformation whereupon the elastic regime exists, the elastic modulus E of the shell material at fractional deformation smaller than ε_{LE} was determined. The methodologies used to determine E are the same as that to determine ε_{LE}. For core-shell microcapsules, such as types (a) and (b), it is also necessary to know the h/r value of the microcapsules. This has been estimated from the capsule size, experimentally determined using the micromanipulation rig, and the h correlations given in Figure 6-9. Figure 6-16 shows typical fitting curves of the elastic regime for PMMA microcapsules of different reaction times.

The mean E determined for 1 h PMMA microcapsules is 806 ± 549 (SD, n = 24) MPa for membrane emulsification and 591 ± 459 (n = 29) MPa for homogenization, resulting in a total average of 680 ± 506 (n = 53) MPa. The average E values of 4 h PMMA microcapsules made with the membrane system are 687 ± 402 (n = 30) MPa and 432 ± 251 MPa, and with the homogenizer are 751 ± 320 MPa and 533 ± 300 MPa, using the power law and linear methodologies, respectively. The slightly higher E values of microcapsules produced in the homogenizer were caused by the compression of small microcapsules (Figure 6-15 (b)). Considering only microcapsules larger than 40 µm, the total E average is 534 ± 300 MPa. 24 h PMMA microcapsules, the full spheres, have an average E of 793 ± 424 (n = 20) MPa, similar to 4 h PMMA microcapsules smaller than 30 µm (957 ± 241 (n = 18) MPa), which also have very high h/r (>80%) (Figure 6-17). Moreover, the values of E

by FEA are consistent with that estimated by Hertz model, see Figure 6-11. Nevertheless, due to the large scatter of the *E* values, it was not found that the reaction time has a significant effect on the elastic modulus (Figure 6-18 (a)). The *E* values determined for PMMA microcapsules are l at the lower end of those reported for pure macroscopic PMMA (Ishiyama and Higo, 2002, Kusy *et al.*, 2001, Shen *et al.*, 1985, Yap *et al.*, 2008), at 0.8-3.5 GPa, although it is known that *E* decreases in the presence of water (Ishiyama and Higo, 2002, Stachurski, 2003, Vincent, 1972) (oil and water were expected inside the PMMA shells).

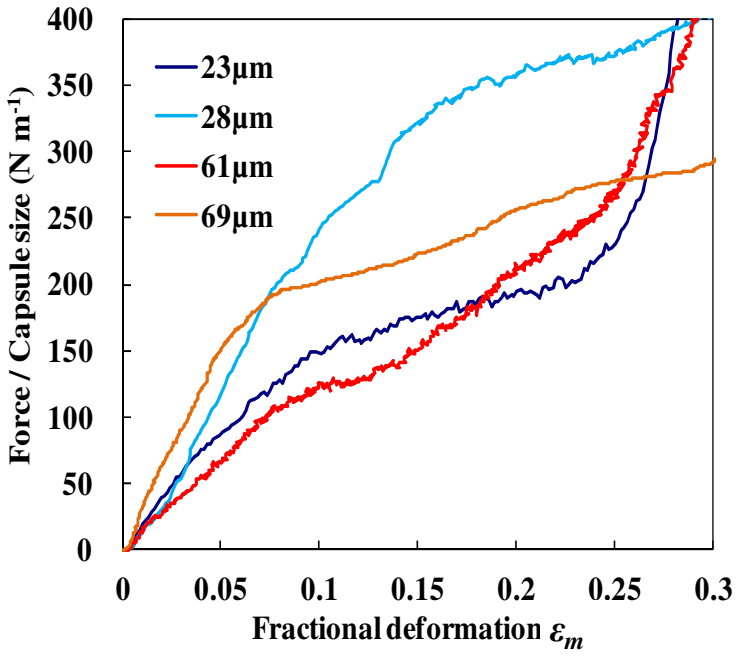

Figure 6-17. Compression profiles of four different PMMA microcapsules 4 h with two different sizes, < 30 µm and > 60 µm. Note that no salient difference is observed between both groups at fractional deformation bigger than $\boldsymbol{\varepsilon_{LE}}$ ~0.05, despite both groups of microcapsules having very different estimated $\boldsymbol{h/r}$ values, 80-90% and ~48% respectively.

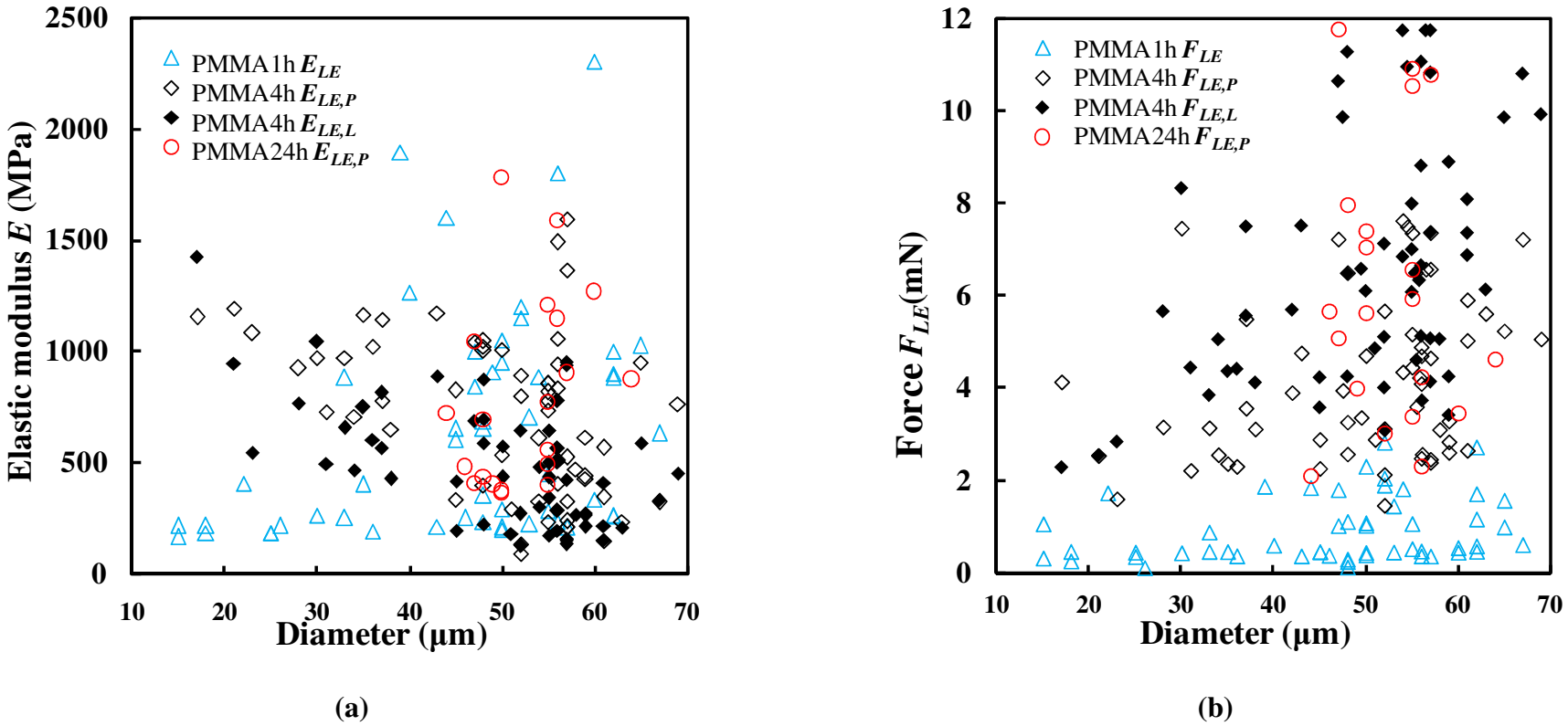

Figure 6-18. (a) Elastic modulus and (b) force at the elastic limit determined for individual PMMA microcapsules prepared at different reaction times: PMMA 1 h (thin-shell model : triangles), 4 h (linear model: filled diamonds and power law model: empty diamonds) and 24 h (power law model: circles).

6.3.5.3 Failure force F_{LE}

The data of force at the bursting point (F_B) are useful to compare melamine-formaldehyde microcapsules made under different formulation and processing conditions. A similar approach can also be applied to non-bursting microcapsules. For this purpose, the force at ε_{LE} termed F_{LE} (Figure 6-12) was chosen. Above F_{LE} the compression force deviates from the elastic fit. Like ε_{LE} and E, F_{LE} was calculated by different models: the thin-shell model for 1 h PMMA microcapsules, the linear ($F_{LE,L}$) and power law ($F_{LE,P}$) models for 4 h PMMA microcapsules, and the power law model for 24 h PMMA microcapsules.

For the 4 h PMMA microcapsules, F_{LE} was found to increase with the capsule diameter, but there was no clear linear trend between them (Figure 6-15 (c)). In addition, there is no significant difference in F_{LE} between the two preparation methods: $F_{LE,L} = 7.6 \pm 2.6$ (SD, $n = 30$) mN and $F_{LE,P} = 4.8 \pm 1.8$ mN for membrane emulsification, and $F_{LE,L} = 5.6 \pm 2.3$ ($n = 30$) mN and $F_{LE,P} = 3.6 \pm 1.6$ mN for homogenization. Note the large variability of F_{LE} for a given capsule size, which is quantified for the whole sample using *CV* values (as in Equation 2). The *CV* value of F_{LE} using membrane emulsification is 32 ± 11% (SD), and that using

homogenization is 41 ± 17%, which are not statistically different, unlike when membrane emulsification was used for the formation of MF microcapsules (see Section 4.3.8). Similar behaviour, where the rupture force was heavily scattered and no trend was observed with the capsule size, was reported for the silica-based microcapsules discussed previously (Mercade-Prieto *et al.*, 2012a), which despite having a thinner shell also failed at small deformations ($\varepsilon_{LE,L}$ ~0.09). The force results for the full spheres of 24 h PMMA, $F_{LE,P}$ =6.1 ± 2.3 mN, are similar to those for 4 h PMMA.

For the 1 h thin-shell PMMA microcapsules, it is possible to determine the bursting force F_B as well as F_{LE}. For the batch of microcapsules made using homogenization, which had a wide size distribution, it was found that F_B increases with the capsule size (Figure 6-19), despite ε_B being constant with size at 0.62 ± 0.09 (Figure 6-14). The *CV* value of F_{LE} is 47 ± 22%. Less scattered F_B values were found for the microcapsules made using membrane emulsification, with a *CV* of 26 ± 7% mainly due to the narrower size distribution. However, the F_B scatter is so large in a narrow size range, such as 45-60 μm for the microcapsules using membrane emulsification. Consequently, the benefit of having a narrower size distribution is limited (Figure 6-18 (b)). Similar results were obtained from the analysis of F_{LE}, with a mean value of 0.9 ± 0.6 mN.

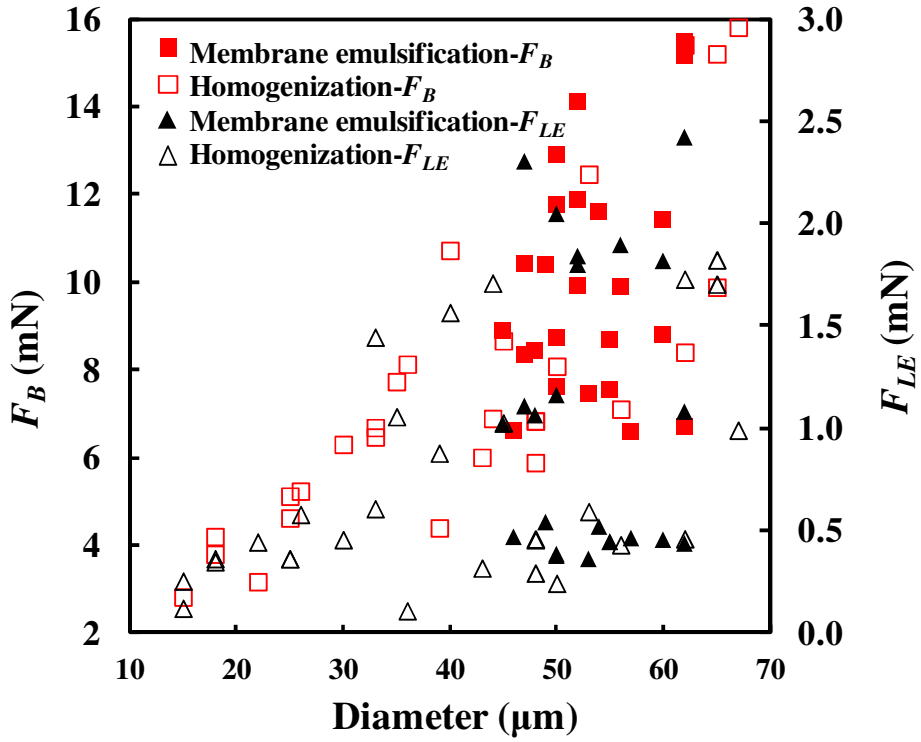

Figure 6-19. Bursting force F_B (squares) and force at elastic limited F_{LE} (triangles) versus diameter for 1 h PMMA microcapsules prepared by membrane emulsification (filled points) and homogenization (empty points).

6.3.5.4 Failure stresses σ_p

Despite being useful to characterize bursting or the onset of rupture of microcapsules, the force value at this point is not an intrinsic mechanical property of the shell material. An example is the dependence of F_B on the capsule size discussed in the previous section. Recently, the use of stresses to characterize the rupture of microcapsules has been proposed (Mercade-Prieto *et al.*, 2012a, Mercade-Prieto *et al.*,

2011a, Mercade-Prieto and Zhang, 2012), in the same way that they are used for any other materials. In the absence of the full stress-strain relationship of the shell material, the elastic limit ε_{LE} represents the largest deformation whereupon the shell is largely expected to be undamaged. At higher ε_m the force deviation from a fully elastic behaviour can either be due to incipient cracking of the shell, or due to yielding of the shell material (Mercade-Prieto *et al.*, 2012a). At present, it is not possible to analyze the nature of rupture due to the small size of the microcapsules, and therefore both mechanisms ought to be considered in the absence of further evidence.

Analysis of the compression profiles of 1 h PMMA microcapsules suggests, however, that a brittle rupture mechanism is the most likely scenario. Firstly, a severe discontinuity around ε_{LE} was commonly observed, as shown in Figure 6-12 (a). Secondly, if the force deviation above ε_{LE} was due to yielding, an elastic perfectly-plastic fit of the force profile should provide at least force values lower than the experimental ones. However, Figure 6-12 (a) shows clearly that the experimental force above ε_{LE} is significantly lower than what would be obtained due to yielding, strongly suggesting a brittle failure for 1 h PMMA microcapsules. The force profiles of the 4 h and 24 h PMMA microcapsules do not provide equal hints of a brittle rupture, but it is considered unlikely that they would behave differently.

Considering a brittle failure for all PMMA microcapsules, rupture will start to occur at fractional deformation bigger than ε_{LE} when the largest principal stress σ_p in the shell equals the material rupture stress (von Mises stresses should be used if yielding was a plausible hypothesis as discussed elsewhere (Mercade-Prieto *et al.*, 2012a)). There are two likely places in the shell where failure can start to occur. As discussed in Figure A6, if failure occurs in the inner side of the shell it will be due to tensile stresses $\sigma_{P,T}$, whereas if it occurs in the external side of the shell it will be due to compressive stresses $\sigma_{P,C}$.

The largest principal stresses σ_p were estimated using the mean ε_{LE}, E and h/r for each microcapsule, as described in Appendix A. The population mean values for 4 h PMMA microcapsules larger than 40 μm were $\sigma_{P,C} = 87 \pm 44$ (SD, n = 47) MPa, and $\sigma_{P,T} = 11 \pm 5$ MPa; whereas for those smaller than 30 μm, where h/r >0.8, $\sigma_{P,C} = 147 \pm 93$ (n = 5) MPa and $\sigma_{P,T} = 9 \pm 3$ MPa. For the 24 PMMA spheres $\sigma_{P,C} = 117 \pm 43$ (n = 20) MPa, and $\sigma_{P,T} = 3.9 \pm 1.3$ MPa; whereas for the 1 h thin-shell PMMA microcapsules $\sigma_{P,C} = 122 \pm 76$ (n = 52) MPa, and $\sigma_{P,T} = 51 \pm 44$ MPa. It was thus found that the compressive principal stress did not change significantly with the reaction time. The most likely mode of failure, under tension or compression, is discussed subsequently.

These failure stresses are of the same order as those reported for macroscopic PMMA, with a tensile strength of ~60 MPa and a compressive strength of ~85 MPa, at a strain rate ~0.1 s^{-1} (Chen *et al.*, 2002). Yet both the compressive and tensile strengths can decrease significantly when absorbing water, about 16-24 MPa lower when PMMA is saturated with water (Shen *et al.*, 1985, Soderholm and Calvert, 1983) (note that the PMMA shell is saturated with the core perfume oil A). In 24 h PMMA full spheres and in the small microcapsules of 4 h PMMA (d < 30 μm) compressive stresses are highly dominant, see Figure A6, and failure is certainly due to compression, not tension. When comparing the force profiles of these very thick shell capsules with those of thinner-shell capsules, no salient difference is observed (Figure 6-12 and 6-20). This, together with the fact that the estimated compressive $\sigma_{P,C}$ is higher than the typical macroscopic PMMA compressive strength, while the tensile $\sigma_{P,T}$ is lower than the macroscopic tensile strength, suggests a failure due to compression for all microcapsules.

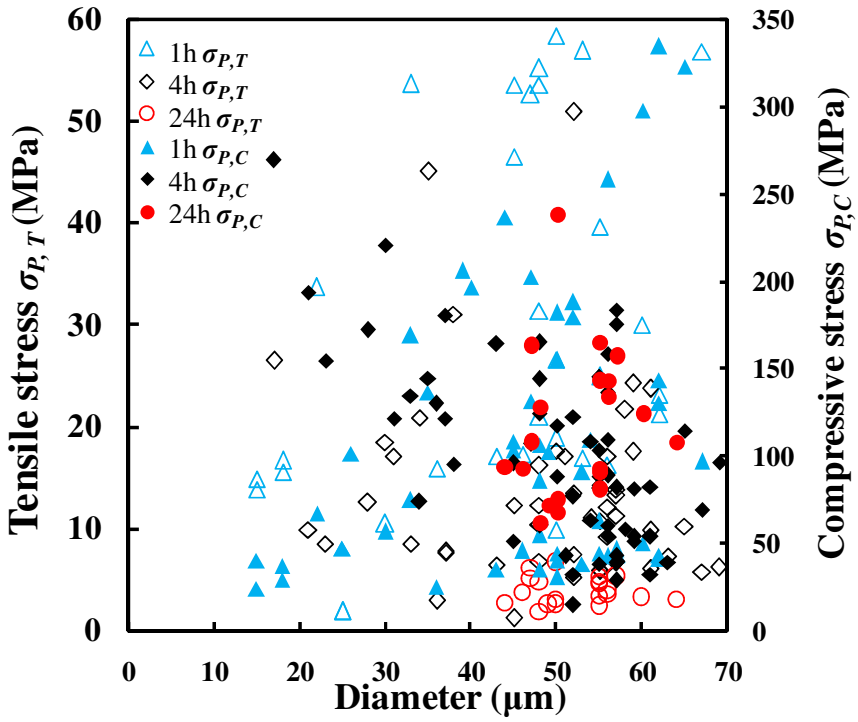

Figure 6-20. Largest tensile (empty points) and compressive (filled points) principal stress determined for individual PMMA microcapsules at ε_{LE} prepared at different reaction times: PMMA 1 h (triangles), 4 h (diamonds) and 24 h (circles).

6.3.5.5 Weibull distribution analysis for failure stress

In the present study, the principle stress is presented in Figure 6-20, which was not enough to characterize the whole population. The Weibull distribution was shown to be a useful model for describing material mechanical properties in previous studies (Curtis and Juszczyk, 1998, Mercade-Prieto *et al.*, 2012a). A three- parameter Weibull

distribution was adopted here in Equation 6.4, and the details are reported in Mercadé-prieto *et al.*'s work (2012a).

$$CDF(x) = 1 - exp\left[-\left(\frac{x-x_0}{x_c}\right)^{\beta}\right] \quad \text{(Equation 6.4)}$$

Where, *CDF(x)* is the cumulative distribution function and *x* is the compressive stress of microcapsules, x_0 is the location parameter,(x_c+x_0) is about the median value, and β is the shape parameter.

Figure 6-21 shows the fit of Equation 6.4 using a method of median ranks. The compressive failure stresses of 1 h, 4 h (d > 40μm) and 24 h PMMA microcapsules were calculated using both individual *E* and mean *E* value. Figure 6-22 shows the cumulative failure probability using a compressive stress failure criterion of PMMA microcapsules. Seen from Figure 6-22, from 1 h to 24 h, the curve has no significant difference. The stress data calculated using individual *E* value, have a shape parameter $\beta \approx 1$ and the data calculated using population average *E* value $\beta \approx 3$.

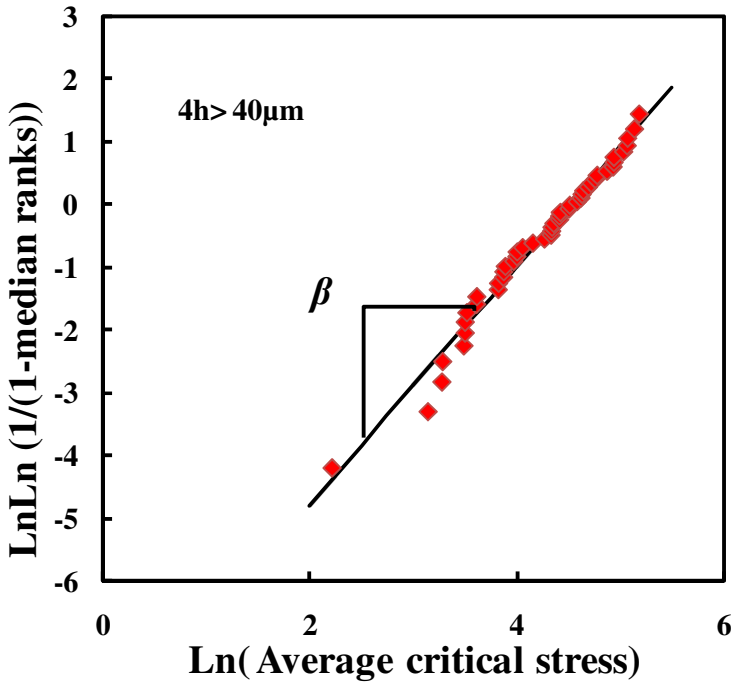

Figure 6-21. Three- parameter Weibull distribution using the median ranks method fitting with experimental compressive stress data of 4 h (d > 40µm) PMMA microcapsules.

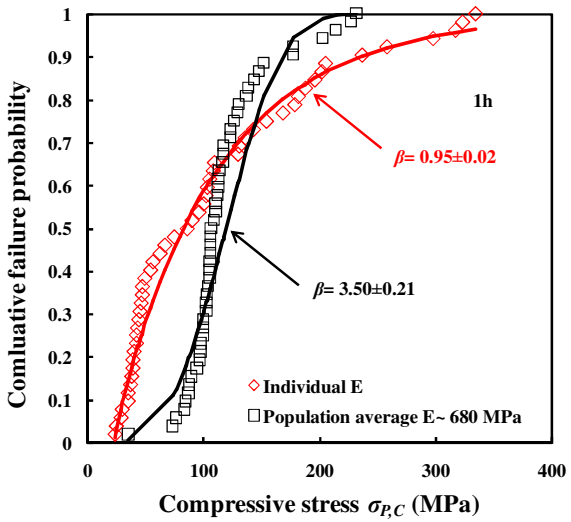

(a) 1 h PMMA microcapsules

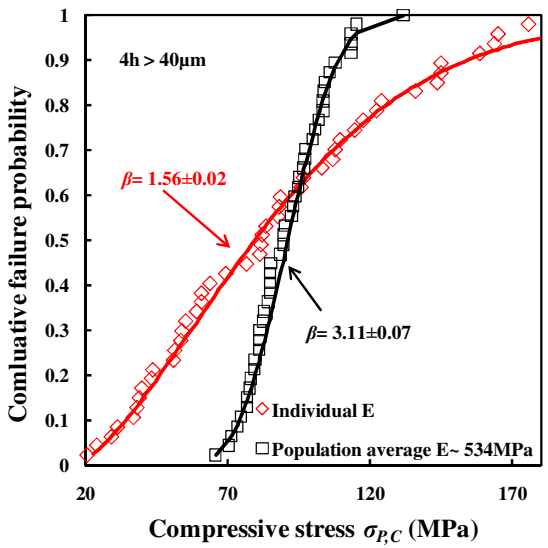

(b) 4 h (d > 40µm) microcapsules

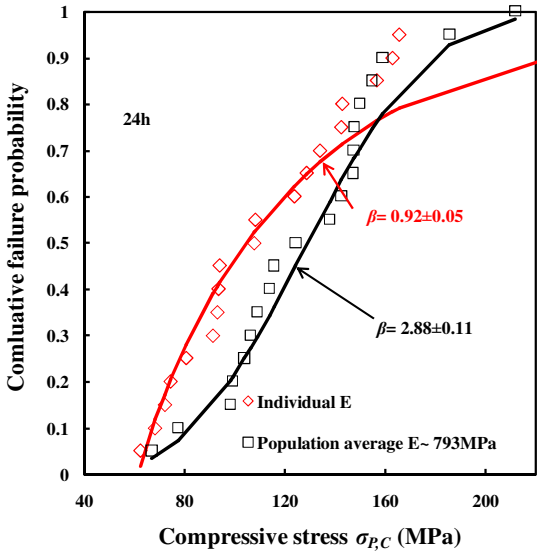

(c) 24 h microcapsules

Figure 6-22. Cumulative failure probability using a compressive stress failure criterion of PMMA microcapsules. Red diamond symbols represent the compressive stress calculated using individual E value and the black square ones using population average E value.

Despite the huge effect of the reaction time on the shell thickness, it is remarkable that the mechanical properties of the shell remain unchanged by taking into account the large variability of mean population values. As discussed above, both the elastic modulus E and the rupture stress $\sigma_{P,C}$ are found to be independent of shell thickness (polymerisation time) based on the experimental data measured when factional deformation is smaller than 0.15. Because the shell grows inwards with the reaction time, this could simply imply that the external section of the shell remains unchanged, but may not affect the later formed inner part of the shell. This may also indicate the formed shell of microcapsules was porous, which allowed MMA molecules to penetrate through it from the outside and to polymerise inside. If the microcapsules are required to be incorporated in liquid detergents, they should possess not only optimum mechanical properties, but also no or very low shell permeability, which requires further study.

PMMA microcapsules are the second system that has been characterized, and they likely fail at small deformations due to brittle failure (Mercade-Prieto *et al.*, 2012a). These microcapsules seem to be characterized by a huge variation of the mechanical properties, probably caused by the random presence of micro-cracks or flaws in the shell. In comparison, microcapsules fail after extensive plastic deformation, such as MF ones, present more homogeneous mechanical properties (Mercade-Prieto *et al.*, 2011a). Hence, systems that can produce microcapsules with a narrow size

distribution, such as the dispersion cell used here, can do little to improve the variability of the mechanical properties.

6.4 Conclusions

In this chapter, preparation of microcapsules with PMMA as a shell material and an oil-based industrial precursor as core with narrow size distributions has been demonstrated through membrane emulsification. The *CV* and *SPAN* values of the microcapsules generated by membrane emulsification are significantly smaller compared with the ones made by homogenization. CLSM has been used to determine the shell thickness *h* of the PMMA microcapsules labelled with a lipophilic fluorescence dye, showing that *h* increased with the reaction time until the core-shell capsules became homogeneous spheres. Experiments based on compression of single microcapsules showed different force-displacement profiles depending on the *h/r* value: thin-shell microcapsules showed a clear bursting point, whereas for thicker shells no bursting was observed. Intrinsic mechanical properties were obtained from the analysis of FEM simulations and micromanipulation experiments. The elastic modulus and the rupture stress, determined with different models according to *h/r*, were found constant with the polymerization reaction time despite large variations in *h*.

The major difference between the present PMMA microcapsules and any other microcapsule used for encapsulation of perfumes is the much thicker shells of the former. The polymerization reaction time had a major effect on the capsules' shell thickness. Novel methodologies were required to characterize these thick shells, which are described here at length for the benefit of future researchers. At short reaction times, thin-shell microcapsules were formed that burst under compression, similar to MF microcapsules. The capability of microcapsules to burst is an essential property to achieve sudden perfume release when clothes are being worn, as described in Chapter 4. However, bursting may not be desirable for long lasting applications if microcapsules cannot survive mechanically challenging environments. PMMA capsules reacted for more than 1 h did not show bursting points under compression, hence even if the capsules were completely broken the perfume oil would not release instantaneously. Future work includes investigation of the permeability of PMMA microcapsules, and how it can be controlled by changing formulation and processing conditions will be described in Chapter 7.

Chapter 7 Determination of Perfume Release Rate and the Shell Permeability of Microcapsules

7.1 Introduction

In Chapters 4 and 6, the preparation and characterization details of MF and PMMA microcapsules were described. In this chapter, the release behaviour of perfume microcapsules was studied to understand the properties of microcapsules better.

In previous work (Long et al., 2009), perfume microcapsule slurry was added into aqueous solution in contact with but phase separated from an organic solvent. The perfume oil concentration resulting from the release was evaluated in the organic phase (Long et al., 2009). Following this methodology, the mass transfer of perfume between aqueous and the organic phases likely limits the release rate, especially when the solubilities of the perfume oil components are low in water. Therefore, the release profiles from these previous experiments cannot be used to characterize the intrinsic properties of the shell, such as the permeability, as it depends on many other parameters, the most important of all being the mass transfer coefficient between the aqueous and organic phases.

This limitation was solved in a recent study by using instead a single miscible release liquid (Mercade-Prieto *et al.*, 2012b). Instead of an aqueous solution and an organic solvent, a "co-solvent" was added to the aqueous phase for the release of perfume from microcapsules. In this way, the total mass transfer problem is simplified enormously by eliminating the mass transfer coefficient between two phases, which depends on many parameters such as the stirring conditions. This study proved this methodology with a single component model oil (hexyl salicylate – oil HS), whereas real perfume oils used in industrial applications are complex mixtures of many chemicals with various functionalities. In this chapter this methodology will be used with oil A, an industrial precursor containing a mixture of several perfume components, as well as oil HS as a single component of perfume oil for comparison purposes.

The mathematical modelling detailed in Section 2.7.3 to analyse release data was developed for thin shells with $h \ll r$, where h is the shell thickness, and r is the radius of microcapsules, as in the case of MF microcapsules. On the other hand, the PMMA microcapsules discussed in Section 6.3 present a wide range of shell thicknesses that cannot be analyzed with thin-shell models. For this reason, in addition to the release model discussed by Mercade-Prieto *et al.* (Mercade-Prieto *et al.*, 2012b) for thin shell, two new models will be developed for thick shell ($0.47 < h/r < 0.62$) and full spheres ($h/r \sim 1$). The shell permeability and diffusivity values will be calculated compared with the different methodologies.

7.2 Experimental methods

7.2.1 Formation of MF and PMMA microcapsules

Section 4.2.1 describes the preparation processes of MF microcapsules containing oil A and oil HS, and Section 6.2.1 describes the preparation of PMMA microcapsules containing oil A using a dispersion cell and homogenizer. The different formulations and operation conditions used are shown in Table 7-1. Membrane "15 rcia A" was used to generate an oil-aqueous emulsion; the details of the membrane are given in Section 3.3.1.

Table 7-1 Formulations and operation conditions used for preparation of microcapsules in this study. ME represents membrane emulsification, HG represents homogenization in this chapter.

No.	Shell material	Oil	Operation method	Reaction time (h)	*h/r*
1	MF	A	Membrane emulsification (ME)	6	< 0.07
2	MF	A	Homogenization (HG)	6	< 0.07
3	MF	HS	ME	6	< 0.07
4	MF	HS	HG	6	< 0.07
5	PMMA	A	ME	1	0.08< h/r<0.11
6	PMMA	A	ME	4	0.47< h/r<0.62
7	PMMA	A	ME	24	= 1

7.2.2 Perfume oil calibration using UV-Vis spectrophotometry

The concentration of the perfume oils in the aqueous solutions was measured with a UV-Vis spectrophotometer (Cecil Instruments, Cambridge, UK).

Standard calibrations were performed for each different solvent considered. Each perfume oil was dissolved into a solvent to make 10-12 standard solutions concentrations lower than 10^{-4} g mL^{-1}. The solutions were first scanned between 250-300 nm at 5 nm s^{-1} in order to determine the wavelength where absorbance was maximum, termed λ_{max}, using pure solvent as a blank. The absorbance A of 10-12 standard solutions with concentrations C (g mL^{-1}) was measured at λ_{max} (nm) to obtain a calibration plot, an example is shown in Figure 3-19. The extinction coefficients ε (mL g^{-1} cm^{-1}) are calculated using Equation 3.8 with least squares fitting of the linear slope.

7.2.3 Solubility measurements

The solubility of the perfume oil in a solvent was determined as follows. About 0.5 g of perfume oil was initially mixed in 10 mL of solution, kept at 25 ± 1°C. The perfume oil concentration in the aqueous phase, measured with the UV-Vis spectrometer as described above, was monitored until a constant value was obtained, typically in less than 24 h. This final constant concentration is considered the perfume oil solubility in the solvent, termed (Cs g mL^{-1}). Reported solubility values are the mean of triplicate experiments.

7.2.4 Encapsulation efficiency measurement

Microcapsules were filtered out from a known amount of slurry, termed m_{slurry} (g), which were then dispersed into pure propan-1-ol. Glass beads about 30 to 35g with a diameter of 3 mm were added into a fixed amount V_{sus} (mL) suspension of microcapsules in propanol. The suspension was then agitated with a magnetic stirrer at 150 rpm for several hours until microcapsules were completely broken, as confirmed by observation under an optical microscope. The suspension with broken microcapsules was centrifuged to separate the solution from the debris. The clear layer of the solution was stabilized at 25 ± 1°C and perfume oil concentration C_{sus} (g mL^{-1}) was analysed with a UV-Vis spectrometer. The encapsulation efficiency (EE (% w/w)) was calculated using Equation 7.1. Each experiment was repeated twice.

$$EE = \frac{C_{sus} \times V_{sus}}{\Phi_{oil0} \times m_{slurry}} \times 100\% \qquad \text{(Equation 7.1)}$$

where Φ_{oil0} (g g^{-1}) is the initial concentration of perfume oil used in slurry.

The total amount Φ_{slurry} (% w/w) of perfume oil in the slurry after the polymerization reaction was determined, in order to verify that all the oil was released completely during the release experiment described in the next section. Instead of filtering out the microcapsules, a known amount of slurry m_{slurry} (g) was added

directly into propanl-1-ol to prepare the suspension. The other steps involved are the same as described above.

$$\phi_{slurry}\ (\%\,\mathrm{w/w}) = \frac{C_{sus} \times V_{sus}}{m_{slurry}} \times 100\% \qquad \text{(Equation 7.2)}$$

Non-encapsulated oil in slurry may be due to oil solubilised in water phase, oil sticking on the surface of the microcapsules or floating in the slurry. It is also possible that microcapsules are damaged by the agitation during polymerization. Whatever the reason, the percentage of oil that will not be released through the shell membrane, called waste oil, is calculated using:.

$$W_{oil} = \phi_{slurry}/\phi_{oil0} - EE \qquad \text{(Equation 7.3)}$$

7.2.5 Continuous release experiments

Continuous release experiments are essential to investigate the fast oil release of microcapsules when a co-solvent is used. A good co-solvent is that considered to be capable of solubilising at least more than ~5 times (v/v) the oil present in the microcapsules tested (Mercade-Prieto *et al.*, 2012b).

A 250 mL jacket vessel (Lenz, Germany) and a UV Vis spectrophotometer were used for the release experiment, as shown in Figure 7-1, the experimental set up schematic.

Chosen co-solvent aqueous solution *V* (mL) were added into the vessel. A continuous agitation was provided by a magnetic stirrer at ~300 rpm. A small amount of the solution inside the vessel was pumped continuously through a small tube (ϕ 1.6 mm, Viton L/S 14, Masterflex, UK) at a flow rate of 18-21 mL min^{-1}. There was a quartz cuvette (Quartz glass, #634-9097, VWR, UK) inside the UV-Vis, and the solution was pumped into the cuvette and continuously measured at the selected λ_{max} (nm) by UV Vis. A piece of tea bag (t-sac GmbH, Hannover, Germany) with selected pore sizes was fixed at the suction part of the tube to stop the recirculation of microcapsules through the cuvette. The blank absorbance measurements were taken for the first 120 s, ensuring that the set up was working properly (i.e. no bubbles were stuck inside the cuvette). Thereafter, a known amount of microcapsule slurry, typically 100 mg was added to the vessel. The data were collected continuously and recorded by a computer connected to the UV-Vis spectrophotometer until at least more than 80% of the perfume oil was released (according to ϕ_{slurry}). The oil concentration *C* (g mL^{-1}) was normalized using oil relative release (%) (which was calculated according to Equation 7.4). Each experiment was repeated at least 2 times.

$$\text{Relative oil release} = \frac{C \times V}{m_{slurry} \times \phi_{slurry}} \times 100\% \qquad \text{(Equation 7.4)}$$

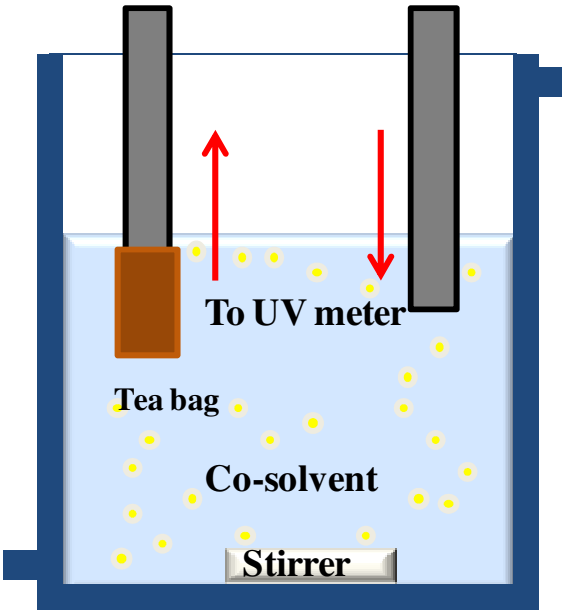

Figure 7-1 Schematic diagram of the device used to conduct continuous release experiments. The folded tea bag sheet, which had pores big enough to release the solution but small enough to stop the microcapsules, was glued on one end of the small tube by sellotape. This kept the cuvette clean. The top part of jacket reactor vessel was covered with plastic wrap film to reduce the evaporation of the co-solvent.

7.2.6 Perfume oil solubility in PMMA microspheres

It was discussed in Chapter 6 that 4 h PMMA microcapsules had really thick shells ($0.47 < h/r < 0.62$), and PMMA microspheres were obtained after a reaction time of 24 h. In these scenarios, the volume of polymer shell is so large that is possible the most of the perfume oil is solubilised in the shells, and not present in free form in the

core, as in MF microcapsules. For this reason, knowing the solubility of the perfume oil in PMMA polymer is of great relevance. The release mechanisms for a microcapsule with an oil core and with oil solubilised in the shell are quite different.

Another reason for determination of oil solubility in the PMMA polymer is to obtain partition coefficients K, which would allow the calculation of the diffusivity D (Equation 7.5).

$$P = KD \qquad \text{(Equation 7.5)}$$

where D is the diffusion coefficient of the pure oil within the shell, P is the permeability of the oil in the shell, $K = \frac{C_{in}}{C_{in(s)}} = \frac{C_{out}}{C_{out(s)}}$ is the partition coefficient, where it can be assumed that $K \approx \frac{C_{s-shell}}{C_s}$ (Schwarb *et al.*, 1999). Here, $C_{s-shell}$ is the saturation solubility of the core oil in the shell material, and C_s is saturation solubility of core oil in the co-solvent solution.

The PMMA micro-particles described in Section 6.2.1 were selected to test the oil solubility in polymerized PMMA, since they had similar sizes and microstructures to PMMA microcapsules used in this study. The PMMA microspheres were soaked into perfume oil labelled with a fluorescence dye PM546. The micro-particles were soaked for two to four weeks, in order to allow ample time for the oil to diffuse into the polymer until saturation. Afterwards, the particles were filtered out, and observed under CLSM, showing strong fluorescence. The solubility of perfume oil in PMMA microspheres $C_{s-shell}$ (g mL^{-1}) was also determined using the same procedures as described in this chapter, Section 7.2.4.

7.3 Release models for spherical microcapsules

7.3.1 Oil release from a thin-shell microcapsule

The permeability of perfume oil in microcapsules with a thin shell ($h \ll r$, as shown in Figure 7-2(a)), was determined using a model from the literature (Antipov *et al.*, 2003, Mercade-Prieto *et al.*, 2012b). This model was developed for a single pure core component only, later its use for a multi-component perfume oil will be discussed. This model only applies to thin shells, such as MF microcapsules ($h/r < 0.07$) and PMMA microcapsules formed after 1 h reaction ($0.08 < h/r < 0.11$) described in previous chapters. Data analysis was implemented using commercial software Excel®, by Microsoft.

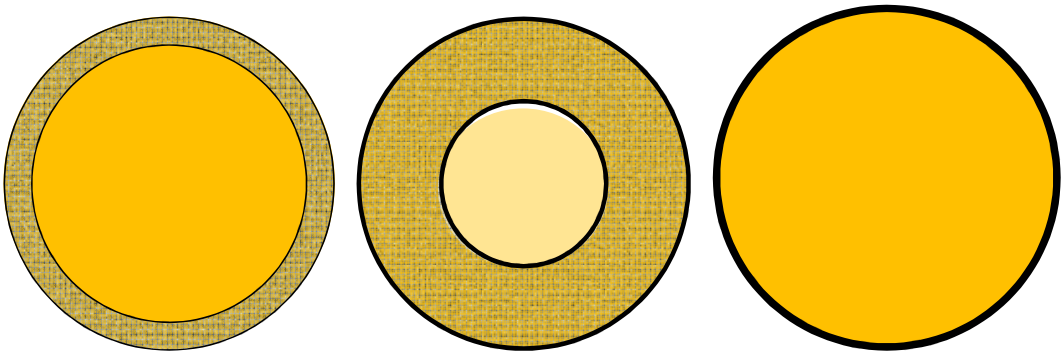

(a) (b) (c)

Figure 7-2 Schematic diagram of PMMA perfume microcapsules with different shell thicknesses. (a) PMMA microcapsule with a thin shell (reacted for 1 h, $0.08 < h/r < 0.11$) (b) PMMA microcapsule with a thick shell (reacted for 4 h, $0.47 < h/r < 0.62$) (c) PMMA microsphere (reacted for 24 h).

The release equation developed from Fick's first law was described in Section 2.6.3. The relative release at a given time in the linear regime is given by Equation 2.27. In this study, the density of core oil $\rho_d \approx 1\,\mathrm{g\,mL^{-1}}$ and $C_s < 0.01\mathrm{g\,mL^{-1}}$ for all the oils used (as shown later in Table 7-2). Therefore in the exponential regime release curve discussed for Figure 2-15, there is less than the one percent of the total oil released. For this reason, the exponential regime is not considered in the model. The whole release profile will be analysed based on the linear regime for thin-shell microcapsules ($h<<r$) (Equation 2.28).

The above model was developed for a single microcapsule. For a population of microcapsules with the same size, the same Equation 2.28 is obtained. For the real case scenario of poly-dispersed microcapsules, it has been shown that the relative release R is fairly linear with time at least up to R ~0.6. It is in this early stage of release where the permeability will be determined.

7.3.2 Oil release from a homogeneous microsphere

The previous methodology valid for core-shell spheres cannot be applied when the microcapsule no longer has a liquid core, as in the case of PMMA microcapsules formed after a reaction time of 24 h (shown in Figure 7-2(c)). The release of oil from

a solid spherical matrix has been considered before in the literature (Crank, 1975, Polakovic *et al.*, 1999). The model describes the diffusion within in a sphere placed in a well-stirred solution of limited volume. The diffusion equation within a spheres is given by the second Fick law:

$$\frac{\partial C_{in}}{\partial t_r} = D\left(\frac{\partial^2 C_{in}}{\partial {r_r}^2} + 2\frac{\partial C_{in}}{\partial r_r}\right) \qquad \text{(Equation 7.6)}$$

where r_r is the distance from the centre of the spherical particle to the location where the concentration of the oil is calculated (g mL^{-1}), t_r is the microcapsules release time (s). The oil balance at the boundary surface is:

$$V\frac{\partial C_{out}}{\partial t_r} = -\frac{V}{K_p}\left(\frac{\partial C_{in}}{\partial t_r}\right)_{r_r=r} = \frac{3V_S}{R}D\left(\frac{\partial C_{in}}{\partial r_r}\right)_{r_r=r} \qquad \text{(Equation 7.7)}$$

where V_s is the volume of the sphere, r is the radius of microcapsule. $K_p = \frac{c_{in\,\infty}}{c_{out\,\infty}}$ is the partition coefficient, the ratio of the concentration inside ($C_{in\,\infty}$) and outside ($C_{out\,\infty}$) the particle at the end of release, which are calculated using Equation 7.8:

$$V_S C_{in0} = VC_{out\,\infty} + V_S C_{out\,\infty} K_p \qquad \text{(Equation 7.8)}$$

where C_{in0} is the initial concentration inside the particle. The analytical solutions of Equations 7.6, 7.7 and 7.8 can be found somewhere else (Crank, 1975):

$$\frac{C_{out}}{C_{out\,\infty}} = 1 - \sum_{n=1}^{\infty} \frac{6\,\alpha_r(1+\alpha_r)}{9+9\,\alpha_r+(\alpha_r q_n)^2} \exp\left(-\frac{D q_n^2 t_r}{r^2}\right) \quad \text{(Equation 7.9)}$$

where $\alpha_r = V/V_S\,K_p$ represents the ratio of oil released to that remaining in the particle at equilibrium, and q_n are the non-zero positive roots of the transcendent equation $q_n = \frac{3q_n}{3+\alpha_r q_n{}^2}$.

Based on this model, calculations were implemented using commercial software Matlab®, Mathworks. The function *fminsearch* based on the Simplex search method was used to optimize the fitting parameters by comparing the experimental data and calculated result.

7.3.3 Oil release from a thick shell microcapsule

The solubility of perfume oil A in PMMA microspheres $C_{s\text{-}shell}$ is 7.98 ± 0.18 ×10^{-1} g mL^{-1}, the determination method was described in Section 7.2.6. This high solubility value may mean that most of the oil in the microcapsules is absorbed by PMMA shell, particularly if the shell is thick. PMMA microcapsules formed after a reaction time of 4 h had a shell thickness in the range $0.47 < h/r < 0.62$ for those larger than 40 µm, as shown in Figure 7-3(b). In this case, microcapsules can be assumed as a hollow sphere. In the present scenario, most of the oil is considered to have solubilised the shell, while in the core there is an aqueous solution saturated with oil. The diffusion of

a solute for of this particular case, usually referred as 'hollow sphere', has been analysed by Crank (1975). The solution of this diffusion problem is:

$$\frac{C_{out}}{C_{out\infty}} = 1 - \frac{6}{\pi^2(r_{inner}^2 + r_{inner}r + r^2)} \sum_{n=1}^{\infty} \left(\frac{r\cos n\pi - r_{inner}}{n}\right)^2 \exp\left(-\frac{Dn^2\pi^2 t_r}{(r-r_{inner})^2}\right)$$

(Equation 7.10)

where r_{inner} is the radius of hollow space in the microcapsule, r is radius of microcapsule and *n* is the total root number of Equation 7.10.

Commercial software Matlab®, Mathworks was used to calculate the shell permeability through the model. The function *fminsearch* based on the Simplex search method was used to optimize the fitting parameters by comparing experimental data and simulation results.

7.4 Results and discussion

7.4.1 Co-solvent selection and solubility measurements

It was highlighted in Section 2.6.3 that in order to perform good release experiments

under continuous conditions, the desirable time for a complete release should range between 10^2 to 10^4 s (Mercade-Prieto *et al.*, 2012b). MF microcapsules in the present study had a mean $D_{4,3}$ around 57 μm, similar to 1 h PMMA microcapsules at ~56 μm; whereas oil A and oil HS have similar densities to water. Assuming a value $\overline{P/h} = 2.5 \times 10^{-5}\text{m s}^{-1}$ from a previous study (Mercade-Prieto *et al.*, 2012b), C_s of the oil in the co-solvent should be around $4 \times 10^{-5} \sim 4 \times 10^{-3}\text{g mL}^{-1}$ using Equation 2.29. For microcapsules containing HS oil, the oil solubility in water is increased substantially. This was achieved using propan-1-ol as a co-solvent as suggested previously (Mercade-Prieto *et al.*, 2012b). The concentration range of propan-1-ol to perform release experiments in a reasonable time frame is 26-36% v/v, which resulted in solubility values between 0.6-5×10^{-3} g mL^{-1}.

However, oil A is much more soluble than oil HS, with solubility value in water already being 4.53×10^{-3} g mL^{-1}, which would result to a very short release time of 90 s according to Equation 2.29.

The shell permeability for thin-shell microcapsules is calculated from the slope of relative release versus time plot, as discussed for Equation 2.28. If the release experiments are very fast, as in high solubility conditions, it is difficult to obtain experimentally good linear release rates, which could affect the accuracy of permeability data obtained later. Hence, for the case of oil A the solubility in pure

water is considered already quite high, and therefore different kind of co-solvents had to be found in order to increase the total release time, not decrease as in the case of using oil HS.

Several limitations have to be observed in the selection of a new co-solvent for release tests. The co-solvent has to be fully miscible with water, avoiding multiple phases, and it should not interfere with the perfume oil detection method (here UV-Vis spectroscopy). Following Equation 2.29, the only parameter that can be easily modified to increase significantly t_{end} is the permeability P. The shell permeability P, as defined in Equation 7.5, incorporates the oil diffusion coefficient in the shell D. D can be externally modified by changing the viscosity of the solution, following the well-known Stokes-Einstein equation (Equation 7.11) for small solutes. Mercadé-Prieto *et, al.* (2012b) already showed that the measured P will be reduced when using highly viscous co-solvents. A similar approach was performed here by selecting glucose and glycerol as co-solvents. They were found to successfully increase the viscosity of aqueous solutions, thus resulting in slower release profiles, while fulfilling the other co-solvent requirements for release tests. Note that glucose slightly decreased the oil solubility but is increased with glycerol (Table 7-2).

$$D = \frac{k_B T_{\mathrm{ab}}}{6\pi \mu_{\mathrm{cs}} r_{solute}} \qquad \text{(Equation 7.11)}$$

where k_B is Boltzmann's constant, T_{ab} is the absolute temperature, μ_{cs} represents viscosity of co-solvent, and r_{solute} is the radius of the solute. For larger diffusing solutes it is found instead a lower viscosity effect (Harris, 2009), such as

$$D \propto {\mu_{\mathrm{cs}}}^{-\tau} \qquad \text{(Equation 7.12)}$$

where τ is between $2/3 < \tau < 1$.

Table 7-2 lists the results of the average value of wavelength where absorbance is maximum (λ_{max}), extinction coefficients (ε), and the saturation concentration (C_s) of different core oils in water, for several co-solvents at various concentrations.

Table 7-2. The wavelength where absorbance is maximum (λ_{max}), extinction coefficients (ε) as well as the saturation concentration (C_s) of oil A and oil HS in water and in aqueous co-solvent solutions. The viscosities (μ_{cs}) of the pure compounds (Kestin *et al.*, 1978, Wohlfarth, 2009) and aqueous solutions (Dorsey, 1940, Soliman and Marschall, 1990) at room temperature 25 ± 1 ºC are taken from the literature. The error values represents the standard deviation of the mean.

Oil	**Co-solvent**	**ε (mL g^{-1} cm^{-1})**	**λ_{max} (nm)**	***Cs* (g mL^{-1})**	**μ_{cs} (mPa s)**
HS	pure propan-1-ol	23230±65	305.5±0.5	ND	ND
HS	36% v/v propan-1-ol	18000±104	305.5±0.3	$5.2 \pm 0.4\times10^{-3}$	2.3
HS	26% v/v propan-1-ol	16450±49	305.5±0.3	$6.1\pm 0.2\times10^{-4}$	1.9
A	pure propan-1-ol	20681±88	281.5±0.5	ND	1.9
A	water	15229±33	280.5±0.4	$4.5 \pm 0.1\times10^{-3}$	0.89
A	10% v/v glucose	16227±174	282.0±0.5	$4.2 \pm 0.5\times10^{-3}$	1.2
A	40% v/v glucose	17363±54	283.5±0.3	$3.7 \pm 0.5\times10^{-3}$	5.2
A	50% v/v glucose	17581±83	283.5±0.3	$3.7 \pm 0.3\times10^{-3}$	8.8
A	50% v/v glycerol	18659±61	285.0±0.3	$7.6 \pm 0.2\times10^{-3}$	5.8
A	60% v/v glycerol	20972±107	285.5±0.3	$8.0 \pm 0.3\times10^{-3}$	8.8

7.4.2 Encapsulation efficiency

The encapsulation efficiency *EE*, the total amount of perfume oil in the slurry ϕ_{slurry} % and waste oil in slurry W_{oil} % of MF and PMMA microcapsules prepared with different formulations and using different preparation methods are listed in Table 7-3. The encapsulation efficiency for all MF microcapsules was about 73.7%. *EE* was found independent of the core oil and the method used to generate the emulsions. The encapsulation efficiency for PMMA microcapsules was slightly lower, about 70.1%, but did not vary with the reaction time and the preparation methods either. Most probably, the core oil loss was due to high solubility of oil A in water, as well as the waste oil in slurry, and the evaporation caused by using elevated temperature (65 °C to 70 °C).

Table 7-3. The list of encapsulation efficiency s *EE* %, the total amount of perfume oil in the slurry ϕ_{slurry} % and waste oil in slurry *Woil* % of MF and PMMA microcapsules. The figures after +/- represent the standard deviation of the mean. ME represents membrane emulsification, HG represents homogenization in this chapter.

No.	Shell material	Operation method	Reaction time (h)	Oil	*EE* (%)	ϕ_{slurry} (%)	W_{oil} (%)
1	MF	ME	6	A	74.1 ± 1.2	12.0± 0.5	32.1 ± 1.3
2	MF	HG	6	A	73.3± 0.9	11.9± 0.2	32.0± 1.3
3	MF	ME	6	HS	73.5± 1.1	12.0± 0.3	12.0± 1.3
4	MF	HG	6	HS	73.2± 0.7	11.9± 0.5	11.9± 1.3
5	PMMA	ME	1	A	70.1± 1.5	5.1± 0.2	28.0 ± 1.1
6	PMMA	ME	4	A	69.8± 0.8	5.0± 0.1	26.4± 0.5
7	PMMA	ME	24	A	70.3± 1.3	5.1± 0.1	27.8± 0.4

7.4.3 Determination of permeability of thin-shell microcapsules from release data

The continuous release method was used in this section to study MF and PMMA microcapsules with a thin shell (PMMA microcapsules prepared after a reaction time of 1 h, sample No.5 in Table 7-1) .

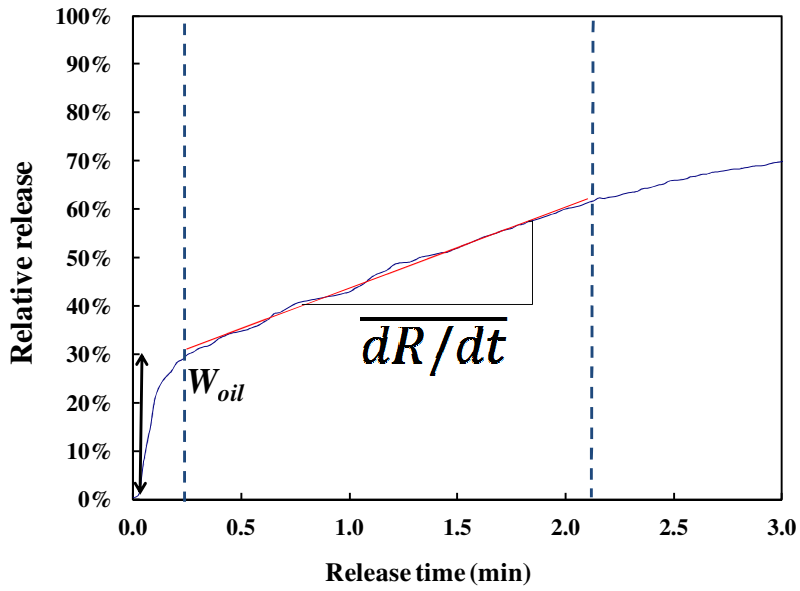

Figure 7-3 Determination of *P* using the thin-shell method. The red line is the best fitting of the linear regime for R <0.6 and $R > W_{oil}$. The dashed lines highlight the range used for calculating $\overline{dR/dt}$. Conditions: oil A MF microcapsules generated through the membrane system at 65 °C for 6 h, 60% v/v glycerol was used as solvent.

The release profile of MF microcapsules in a 60% v/v glycerol solution is shown in Figure 7-3. A large concentration "jump" is observed in a matter of seconds after the slurry was added to the solution. This perfume oil corresponds mostly to that which

had not been encapsulated: good agreement is found between the parameter W_{oil} (%) from the release profile and the data from Table 7-3.

The average permeability was determined from the linear regime of release profile between $W_{oil} < R(t) < 60\%$, as shown in Figure 7-3. Figure 7-4 shows the release profiles of microcapsules with the same shell material but prepared by different processes: membrane emulsification (Sample No.1, $D_{4,3}$ = 57.4 ± 1.0 (SE) μm) and homogenization (Sample No.2, $D_{4,3}$ = 64.3 ± 1.4 μm). The *CV* values of these two samples are 21.0 ± 0.5% and 37.6 ± 1.4%, respectively. The two release profiles did not show any significant difference. This is consistent with the prediction of the model described in Section 7.3.1 that the different size distributions, but with the same mean diameter, do not affect significantly the release between $W_{oil} < R(t) <$ 60%. The mean permeability $\bar{P} = 1.6 \pm 0.2 \times 10^{-12}\text{m}^2\ \text{s}^{-1}$ was calculated using the mean slope $\overline{dR/dt}$ (Mercade-Prieto *et al.*, 2012b), according to Equation 7.13.

$$\bar{P} \cong \frac{\overline{dR/dt}\ d_{4,3}\rho_{oil}h}{6(1-W_{oil})C_s} \qquad \text{(Equation 7.13)}$$

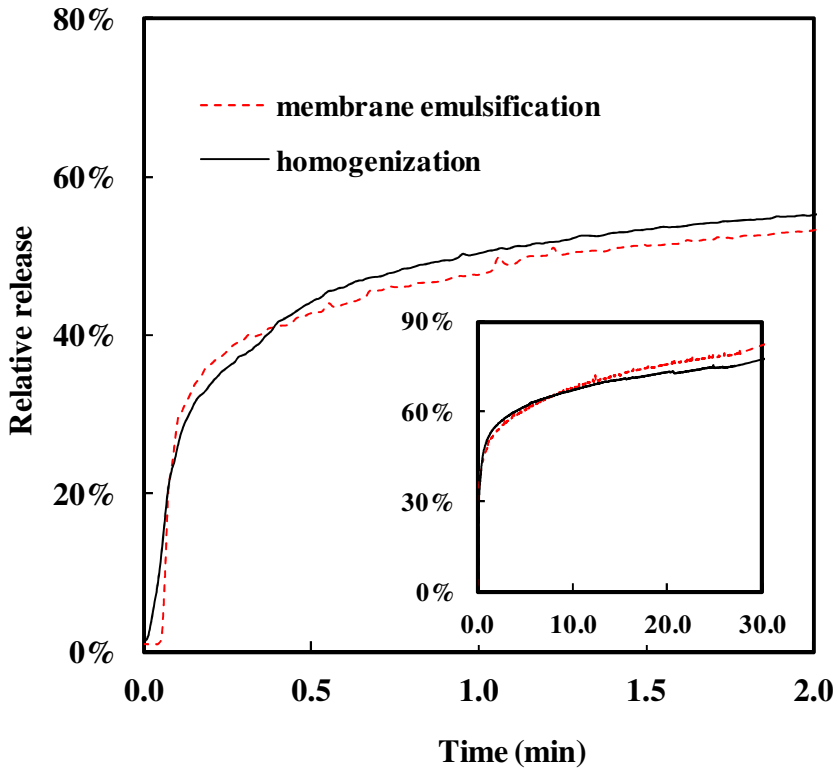

Figure 7-4 Comparison of the release profiles of MF microcapsules prepared with different methods in 60% v/v glycerol aqueous solution: membrane (Sample No.1 in Table 7-1) and homogenization (Sample No.2). The insert shows the same profiles with longer release time.

MF microcapsules containing oil A were tested in 50 v/v %, 60 v/v % of glycerol and 40 v/v %, 50 v/v % of glucose. The mean permeability divided by shell thickness $\overline{P/h}$ of MF microcapsules containing oil A in different release co-solvents is $\overline{P/h} = 5.1 \pm 0.5\, m\, s^{-1}$, the release profiles are shows in Figure 7-5. The different types of co-solvents and the co-solvent concentrations do not affect the oil release profiles considerably, which suggests that the co-solvent did not damage the shell of

microcapsules. The slight differences among the release profiles due to the viscosity divergences and the different solubilities of the oil in co-solvents. Due to the effect of the viscosity of co-solvent (μ_{cs}) on diffusion coefficient (D), as shown in Equation 7.12, for non-ideal systems, (Harris, 2009, Hiss and Cussler, 1973), Equation 7.13 was correspondingly modified to :

$$\overline{P_{ma}} = \bar{P} \times \mu_{cs}^{\frac{2}{3}} \cong \frac{\overline{dR/dt}\, d_{4,3}\rho_{oil}h}{6(1-W_{oil})C_s} \times \mu^{\frac{2}{3}} \quad \text{for } \tau = 2/3 \qquad \text{(Equation 7.14)}$$

$$\text{Or } \overline{P_{mb}} = \bar{P} \times \mu_{cs} \cong \frac{\overline{dR/dt}\, d_{4,3}\rho_{oil}h}{6(1-W_{oil})C_s} \times \mu \quad \text{for } \tau = 1 \qquad \text{(Equation 7.15)}$$

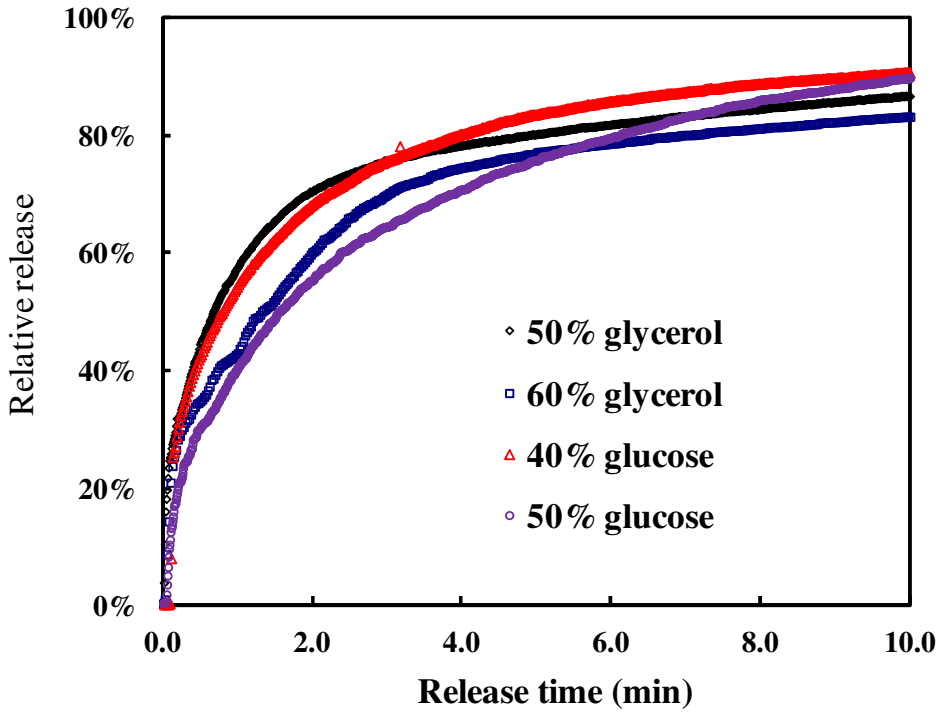

Figure 7-5 Comparison of release profiles of MF microcapsules containing same core oil A exposed to different co-solvents. The black diamonds are for 50 v/v% glycerol, blue squares for 60% glycerol, red triangles for 40% glucose and purple circles for 50% glucose. The MF microcapsules were generated with the dispersion cell after a reaction time of 6 h at 65 °C.

Figure 7-6 (a) and (b) compare the modified permeability results of MF microcapsules prepared with same process conditions but with two different kinds of core oil released in different co-solvents. For the same batch of microcapsules, shown in Figure 7-6, the type of co-solvent and its concentrations did not influence the shell permeability, taking solubility of oil in the co-solvent and its viscosity into consideration, which is consistent with previous work (Mercade-Prieto *et al.*, 2012b). The total average shell permeability of MF capsules after modification $\overline{P_{ma}}$ was $7.3 \pm 1.2 \times 10^{-12}(\text{mPa s})^{0.85}\ \text{m}^2\ \text{s}^{-1}$ and $\overline{P_{mb}}$ was $1.2 \pm 0.1 \times 10^{-11}\ \text{mPa m}^2$, respectively. The mean modified $\bar{P}_m$ of MF microcapsules containing oil A released in glycerol solution $\overline{P_{ma}}$ was $6.0 \pm 0.2 \times 10^{-12}(\text{mPa s})^{0.85}\ \text{m}^2\ \text{s}^{-1}$ and $\overline{P_{mb}}$ was $1.1 \pm 0.1 \times 10^{-11}\ \text{mPa m}^2$; while the one released in glucose solution had a similar result, $\overline{P_{ma}}$ was $7.5 \pm 0.3 \times 10^{-12}(\text{mPa s})^{0.85}\ \text{m}^2\ \text{s}^{-1}$ and $\overline{P_{mb}}$ was $1.3 \pm 0.1 \times 10^{-11}\ \text{mPa m}^2$.

There is no statistical difference with the results shown before for oil A, despite the oils are very different: one is a single component oil, while the other is a complex mixture. Hence, the core oils were found not to change the permeability values determined in spite of the large solubility differences. This suggests that the core oils do not affect the shell properties of MF microcapsules. The $\bar{P}_m$ values for MF microcapsules containing oil HS $\overline{P_{ma}}$ is $8.4 \pm 0.7 \times 10^{-12}\text{cP}^{0.85}\ \text{m}^2\ \text{s}^{-1}$ for τ = 2/3 and $\overline{P_{mb}}$ is $1.1 \pm 0.1 \times 10^{-11}\ \text{mPa m}^2$ for τ = 1, respectively, also shown in Figure 7-7 as blue filled points.

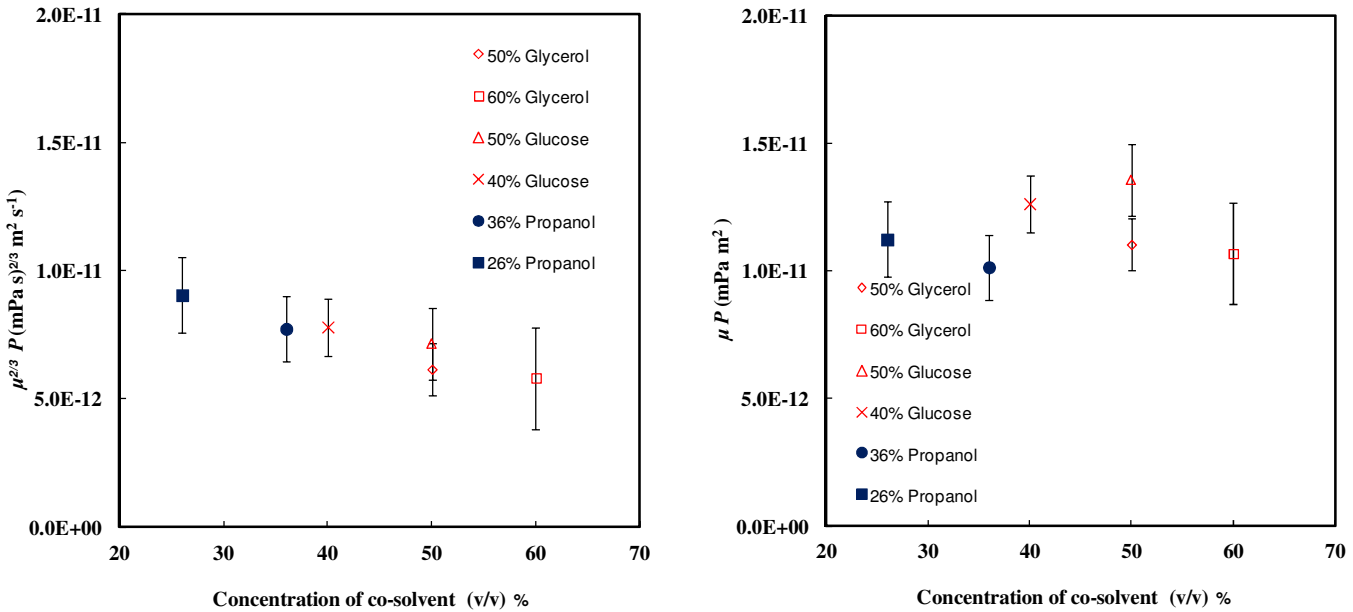

(a) D $\propto {\mu_{cs}}^{-\tau}$, when $\tau = 2/3$ (b) D $\propto {\mu_{cs}}^{-\tau}$, when $\tau = 1$

Figure 7-6 Modified permeability results of MF microcapsules prepared with same process conditions but with two different kinds of core oil; the microcapsules were tested using different co-solvents, given in the legend. (a) $\overline{P_{ma}} = P \times {\mu_{cs}}^{\frac{2}{3}}$ (b) $\overline{P_{mb}} = P \times \mu_{cs}$. The red emptied points represent MF microcapsules containing oil A (Sample No.1) and blue filled points show the ones containing oil HS (Sample No.3). MF microcapsules were generated with the dispersion cell after a reaction time of 6 h at 65 °C. Each experiment was repeated 4 times, and the error bars represent the standard deviation of the mean.

The thin-shell PMMA microcapsules ($0.08 < h/r < 0.11$) containing oil A, made through membrane emulsification after a reaction time of 1 h, were tested using the same method described above. The release profile of MF and PMMA microcapsules tested in an aqueous solution with 60% v/v glycerol is shown in Figure 7-7. The two samples have a comparable amount of waste oil W_{oil}, consistent with the results of Table 7-3. The release profile of PMMA microcapsules is much steeper than for MF. The figure also shows that in PMMA microcapsules most of the perfume oil (around 80%) is released within two minutes.

The permeability of microcapsule shell is related to the shell material, the solute and the solvent used, as discussed in the literature (Mercade-Prieto *et al.*, 2012b, Shen *et al.*, 2011). In this case where the solute and the solvent are the same, the permeability difference is related to the properties of the shell material. A higher permeability could be due to a more porous structure, or due to the presence of larger pores, which could imply that a reaction time of 1 h was not enough to form a dense shell for PMMA, but it could also be due to a higher solubility of the oil in the shell. The permeability values adjusted with the solvent viscosity for 1 h PMMA microcapsules are $P \times \mu_{cs}^{\frac{2}{3}} = 1.3 \pm 0.2 \times 10^{-10}(\text{mPa s})^{0.85}\ \text{m}^2\ \text{s}^{-1}$ for $\tau = 2/3$ and $P \times \mu_{cs} = 2.7 \pm 0.3 \times 10^{-10}\text{mPa m}^2$ for $\tau = 1$, respectively. These values are higher than those found for MF microcapsules generated by the same equipment.

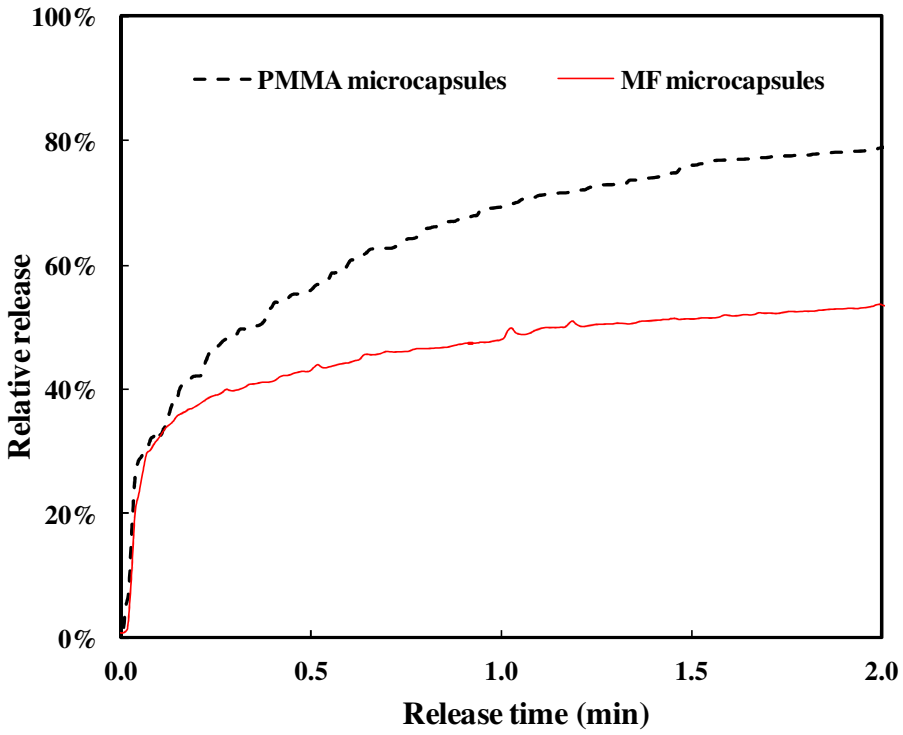

Figure 7-7 Comparison of the release profiles of MF microcapsules (Sample No.1) and 1 h PMMA microcapsules (Sample No.5). The red solid line represents the release profile of MF microcapsules and black dash line PMMA ones. The two samples were both generated with the dispersion cell.

7.4.4 Oil release from full microspheres

In this section it is analysed the release profile of full PMMA microspheres lacking an inner core, obtained after a long reaction time of 24 h (Section 6.2.1). Figure 7-8 shows a typical release profile of microspheres containing oil A prepared through the membrane emulsification method released in a 60% (v/v) glycerol aqueous solution. The analysis of the release profiles was performed considering the diffusion process of an initially homogeneously loaded sphere, described in Section 7.3.2.

Equation 7.9 was used to calculate the diffusivity, the Matlab code was described in Appendix B, Section B.1, and the parameters used in the analysis with Matlab are listed as follows: α_r, which is ratio of the oil released to that remaining in the particle at equilibrium, was equal to 1.5 ± 0.3; n the number of root for equation $q_n = \frac{3q_n}{3+\alpha {q_n}^2}$, was 1000; t_{end} represents the end of release time, 3600 s; and radius of microsphere $r = 28 \times 10^{-6}$m. The maximum fractional release ratio below which the diffusion coefficient was optimized was 0.8. More details of the modelling calculations are provided in Section B.1. The calculated release profile with the best fit diffusion coefficient is found to represent the experimental data fairly well (Figure 7-8). The release experiments were repeated for four times for each sample.

The mean diffusion coefficient of the oil A for PMMA microspheres was $D = 2.6 \pm 0.7 \times 10^{-13}$ m^2 s^{-1}, with $K \approx \frac{C_{s-shell}}{C_s} = 100.3$, in Equation 2.24. The modified permeability values for the PMMA shell were calculated according to Equation 7.5, which was $P \times {\mu_{cs}}^{\frac{2}{3}} = 1.1 \pm 0.3 \times 10^{-10}$(mPa s)$^{0.85}$ m^2 s^{-1} and $P \times \mu_{cs} = 2.1 \pm 0.6 \times 10^{-10}$mPa m^2 . The permeability values for PMMA microspheres were slightly lower than those obtained from the 1 h PMMA microcapsules (No.5, *h/r* <0.11).

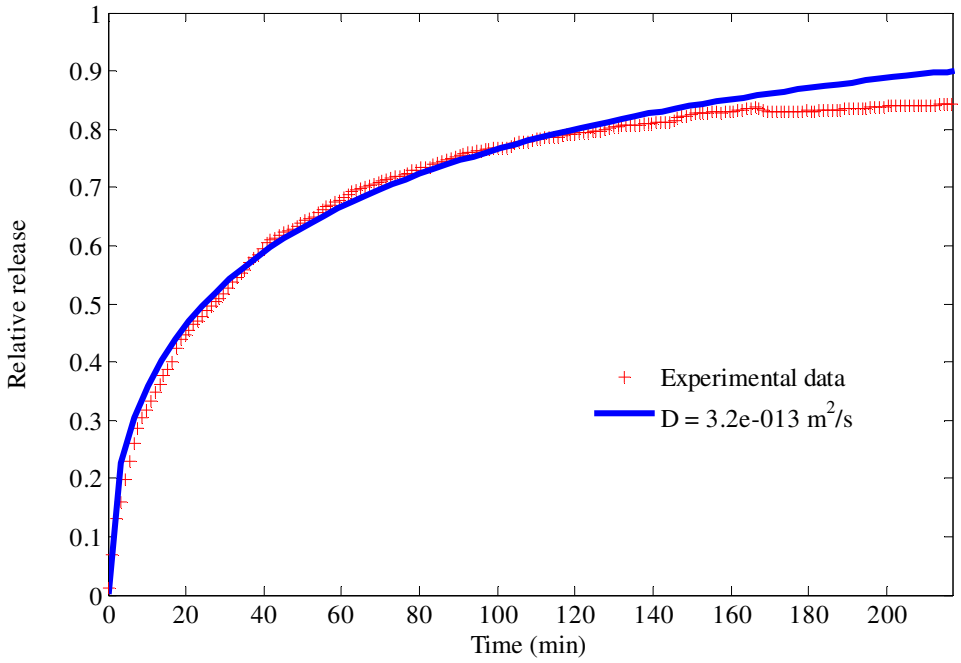

Figure 7-8 Experimental and best-fitted release profile for 24 h PMMA microspheres (Sample No. 7) tested in 60% (v/v) glycerol aqueous solution. The best fitted diffusion coefficient value is $D = 3.2 \times 10^{-13} \mathrm{m}^2\ \mathrm{s}^{-1}$ using the homogenous sphere model for $R(t)<0.8$ (Section 7.3.2), the continuous line shows all the predicted release.

7.4.5 Oil release from a thick shell microcapsules

The intermediate scenario of the previous two sections, with very thin shells or a full sphere, is considered here for the 4 h PMMA microcapsules. As shown in Section 7.3.3, these microcapsules had shell thickness ratios $0.47 < h/r < 0.62$, resulting in that most of the encapsulated oil was solubilised in the thick shell, as shown in Figure

7-3, and the liquid core was not made of pure oil as in the case of MF microcapsules.

Figure 7-8 shows an example of the release profile of such samples (Sample No. 6, $0.47 < h/r < 0.62$) in 60% (v/v) glycerol aqueous solution. In addition, the best fits of the hollow sphere as well as full sphere models are shown for comparison. The model parameters used in Equation 7.9 and Equation 7.10 are: $r_{inner} = 1.7 \pm 0.2$, n =1000, $t_{end} = 3600$ s, $r = 28 \times 10^{-6}$m, and the inner radius of microcapsules $r_{inner} = 11.8 \times 10^{-6}$m. The maximum fractional release considered to optimize the diffusivity of the permeability was 0.8. The experiments were repeated four times for each sample. More details of the modelling calculations are described in Appendix B, Section B.2.

The hollow sphere model was found to be able to reproduce satisfactorily the release profile for the whole release, unlike the full sphere model that can only fit part of the release data. The mean diffusion coefficient value for PMMA microspheres using the hollow sphere model is $D = 3.0 \pm 0.1 \times 10^{-13}$ m^2 s^{-1}, and the one for the sphere model is $D = 3.8 \pm 0.3 \times 10^{-13}$ m^2 s^{-1}. For $K \approx \frac{C_{s-shell}}{C_s} = 100.3$, according to Equation 7.5, the modified permeability values for the PMMA shell using the hollow sphere model were $P \times \mu_{cs}{}^{\frac{2}{3}} = 1.3 \pm 0.4 \times 10^{-10}$(mPa s)$^{0.85}$ m^2 s^{-1} and $P \times \mu_{cs} = 2.7 \pm 0.9 \times 10^{-10}$mPa m^2, which was slightly higher than those obtained from the 24 h PMMA microcapsules (No.7), which are not significantly different compared with 1 h PMMA microcapsules (No. 5) and MF microcapsules with the

same core oil, prepared using the same method.

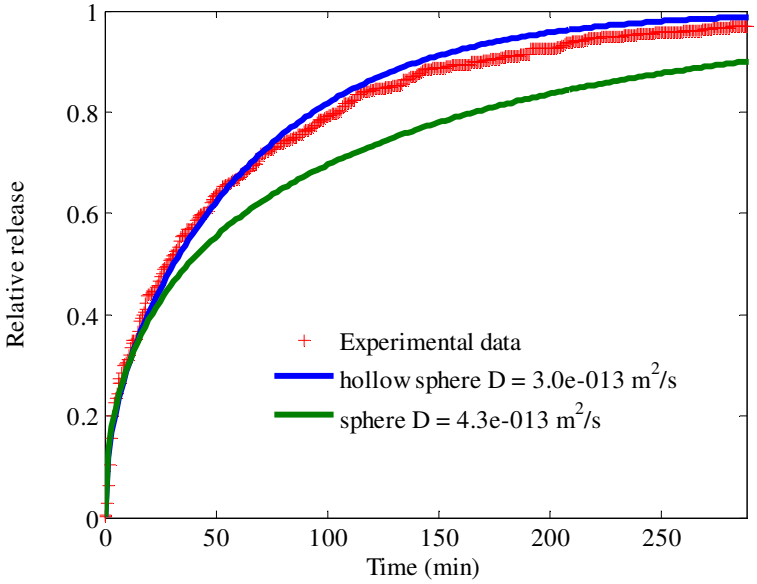

Figure 7-9 Release profiles of 4 h PMMA microcapsules analysed using the sphere and hollow sphere models. The best-fitted diffusion coefficient values are $D = 3.0 \times 10^{-13}\mathrm{m}^2\ \mathrm{s}^{-1}$ from the hollow sphere model, and $D = 4.3 \times 10^{-13}\mathrm{m}^2\ \mathrm{s}^{-1}$ from the sphere model. The blue line shows the best fits using the hollow sphere model. The green line represents the best fits using the sphere model. It can be seen that the hollow sphere model for PMMA microcapsules with a thick shell fits the experimental data reasonably well.

For comparison, the hollow sphere model was also used to calculate the diffusivity of thin-shell PMMA microcapsules. Figure 7-10 shows the results of using the hollow sphere model to fit the release profile of 1 h PMMA microcapsules (Sample No. 5, $0.08 < h/r < 0.11$). The microcapsules were prepared through membrane emulsification and exposed to 60% (v/v) glycerol aqueous solution to release the oil. The model parameters used are: n =1000, $t_{end} = 3600\mathrm{s}$, $r = 28 \times 10^{-6}\mathrm{m}$, and the

inner radius of microcapsules $r_{inner} = 21.6 \times 10^{-6}\text{m}$. The maximum fractional release ratio is 0.7. The simulation profile using the hollow sphere model is inconsistent with the experimental data, but the thin-shell model provides better fitting for the linear regime at *R(t)* <0.6, as presented in Figure 7-10. For the PMMA microcapsules with 0.08 < *h/r* < 0.11, the thin-shell model is more desirable rather than the hollow sphere model.

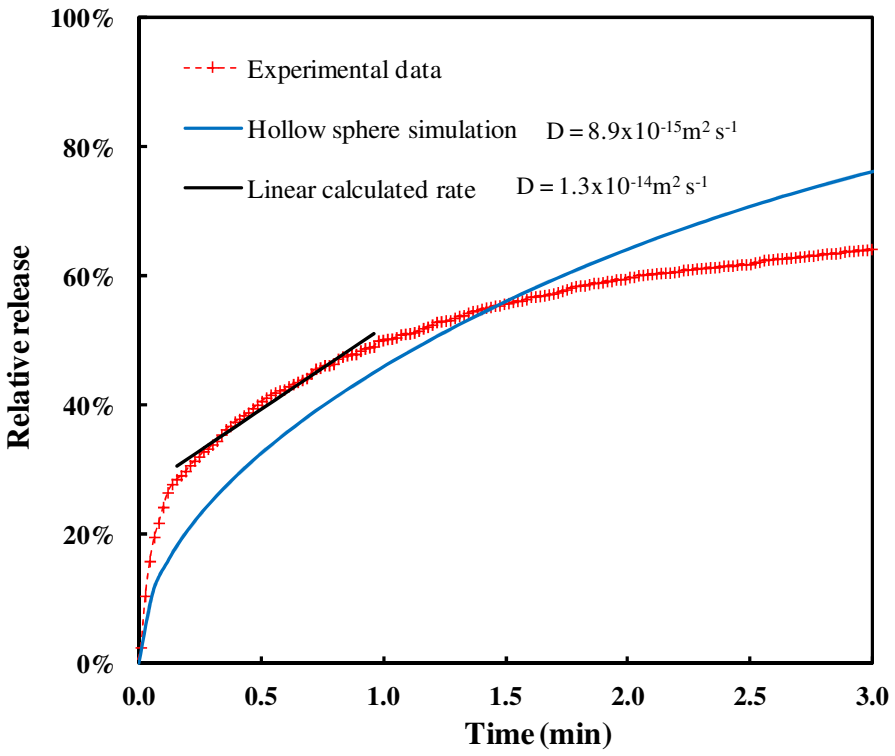

Figure 7-10 Experimental release profile of 1 h PMMA microcapsules (Sample No.5) tested in 60% (v/v) glycerol aqueous solution. The blue line shows the best fits using the hollow sphere model. The black solid line represents calculated relative release using the thin-shell model in the linear regime at *R(t)* <0.6. The diffusion coefficient value $D = 1.3 \times 10^{-14}\text{m}^2\ \text{s}^{-1}$ from the thin-shell model; and $D = 8.9 \times 10^{-15}\text{m}^2\ \text{s}^{-1}$ from the hollow sphere model.

7.5 Conclusions

MF and PMMA microcapsules with different types of core oil and prepared using different conditions were tested in different co-solvents to release the encapsulated oils usually close to completion. The oil release was analyzed using three mathematical models to calculate the shell permeability and diffusion coefficient, corresponding to the three different kinds of microcapsules formed here: microcapsules with a thin shell ($h/r < 0.11$), thick shell ($0.47 < h/r < 0.62$) and full spheres.

For MF or PMMA microcapsules, the shell permeability mainly depends on the structure properties of the shell material and solute. It was found out that for a fixed size, the same shell material and reaction conditions, neither the size distribution of microcapsules nor core oil or co-solvent which were selected in this study, would be able to have a manifest impact on the shell permeability. The thin-shell model reported by Mercadé-Prieto *et al.* (2012b) is more suitable for the thin-shell microcapsules within the linear regime, such as the MF microcapsules or the 1 h PMMA microcapsules in this study. The hollow sphere model reported by Crank (1975) was used for the release data of 4 h PMMA microcapsules. The sphere model reported by Crank (1975) is the best to describe the release profiles the 24 h PMMA

microspheres. Using these approaches, the intrinsic mass transfer parameters for the shell, such as permeability and diffusion coefficient of the oil, have been obtained. This allows a comparison based on physical shell properties between very different microcapsules prepared using different formulations, processing conditions and core perfume oils.

Chapter 8 Overall Conclusions and Recommendations for Future Work

8.1 Overall conclusions

This PhD project aimed to produce various perfume microcapsules with narrow size and strength distributions using membrane emulsification. The endeavour was to advance the understanding of encapsulation process of complex functional oils and to characterize the microcapsules, in order to improve the quality of the microcapsules in industrial products and to control release of the functional ingredients to solid surface.

Perfume oils were selected with multifaceted compositions, added into liquid detergents and expected to be delivered to the fabric surface. A membrane emulsification method was used to generate uniform sized oil droplets in order to provide microcapsules with narrow mechanical strength distribution, which may provide better release performance. A number of factors which impact on size and size distribution of microcapsules were investigated, including operation conditions, phase properties and membrane properties. Melamine formaldehyde (MF) was used as a shell material and microcapsules were produced from an *in-situ* polymerization

method. Subsequently, membrane emulsification was employed on a larger scale; the encapsulation method with MF shell material was later applied to various core oils.

An environmentally friendly shell material poly-methyl-methacrylate (PMMA) was employed to produce perfume oil microcapsules instead of MF, in order to remove completely formaldehyde from the formulation. Various properties of the microcapsules were investigated, such as the morphology, shell thickness, size and size distribution and mechanical properties. Innovative methodologies were applied to the new microcapsules to understand their intrinsic mechanical properties and shell permeability. Table 8-1 summarizes the encapsulation efficiency, size and size distribution, mechanical properties and shell permeability of all the microcapsules made in this study.

Table 8-1. Overview summary of shell materials, reaction conditions, encapsulation efficiency, size and size distribution, mechanical properties and permeability data of microcapsules. Errors given correspond to the standard error (SE) or standard deviation (SD) of the mean.

Chapters	Shell material	Core oil	Emulsification method	System/Membrane	Reaction time (h)	*EE* (%)	$D_{4,3}$ (SE) (μm)	*CV* (SE) (%)	*Span* (SE)	Shell thickness (SE) (nm or μm)
4	MF	A	Membrane emulsification	Dispersed cell/ 15rcia	6	73.1 ± 1.2	57.4 ±1.0	21.0 ± 0.5	0.68 ± 0.06	400 ± 3 nm
5	MF	A	Membrane emulsification	Cross-flow	6	71.4 ± 1.1	26.7 ± 0.7	27.9 ± 1.0	0.79 ± 0.04	378 ± 16 nm
4	MF	A	Homogenization (600rpm)	–	6	73.3 ± 0.9	64.3 ± 1.4	34.1 ± 0.3	0.80 ± 0.02	395 ± 10 nm
5	MF	HS	Membrane emulsification	Dispersed cell/ 15rcia	6	73.5 ± 1.1	81.1 ± 1.1	21.5 ± 0.3	0.69 ± 0.08	396 ± 12 nm
7	MF	HS	Homogenization (600rpm)	–	6	73.2 ± 0.7	58.9 ± 1.5	31.6 ± 0.7	0.94 ± 0.04	389 ± 19 nm
5	MF	S	Membrane emulsification	Dispersed cell/ 15rcia	6	74.1 ± 1.3	113.4 ±1.1	21.1 ± 0.2	0.66 ± 0.03	385 ± 12 nm
5	MF	P	Membrane emulsification	Dispersed cell/ 15rcia	6	72.8 ± 0.9	101.5 ± 0.6	21.2 ± 0.1	0.68 ± 0.06	420 ± 11nm

Chapters	Shell material	Core oil	Emulsification method	System/Membrane	Reaction time (h)	*EE* (%)	$D_{4,3}$ (SE) (μm)	*CV* (SE) (%)	*Span* (SE)	Shell thickness (SE) (nm or μm)
6	PMMA	A	Membrane emulsification	Dispersed cell/ 15rcia	1	70.1 ± 1.5	55.8 ± 1.3	23.4 ± 0.5	0.69 ± 0.08	2.4 ± 0.2 μm
6	PMMA	A	Homogenization (800rpm)	–	1	68.2 ± 1.7	44.5 ± 0.8	34.1 ± 0.7	1.12 ± 0.06	2.4 ± 0.2 μm
6	PMMA	A	Membrane emulsification	Dispersed cell/ 15rcia	2	69.9 ± 1.2	55.8 ± 1.2	23.4 ± 0.6	0.71 ± 0.05	10.2 ± 0.8 μm
6	PMMA	A	Membrane emulsification	Dispersed cell/ 15rcia	4	69.8 ± 0.8	56.1 ± 1.1	23.8 ± 0.2	0.72 ± 0.04	14.2 ± 1.6 μm
6	PMMA	A	Homogenization (800rpm)	–	4	69.5 ± 1.3	44.8 ± 0.7	34.4 ± 0.2	1.12 ± 0.06	13.2 ± 1.9 μm
6	PMMA	A	Membrane emulsification	Dispersed cell/ 15rcia	24	70.3 ± 1.3	56.4 ± 1.8	24.5 ± 0.4	0.74 ± 0.08	–

Chapters	Shell material	Reaction time (h)	Core oil	Emulsification method	Rupture force mN	CV (SD) (%)	Deformation at rupture (%)	Failure force $F_{L,E}$ (SD) mN	Fractional deformation $\varepsilon_{L,E}$ (SD)	Elastic modulus E MPa	Failure stresses σp MPa	Permeability m^2/s
4	MF	6	A	Membrane emulsification	2.2 ± 0.2	18.6 ± 0.1	21.3 ± 0.2	–	–	–	–	$7.3 \pm 1.2\times10^{-12}$ ~$1.2 \pm 0.1\times10^{-11}$
4	MF	6	A	Homogenization (600rpm)	2.0 ± 0.3	34.4 ± 0.2	18.6 ± 0.2	–	–	–	–	$7.3 \pm 1.2\times10^{-12}$ ~$1.2 \pm 0.1\times10^{-11}$
5	MF	6	HS	Membrane emulsification	–	–	–	–	–	–	–	$7.3 \pm 1.2\times10^{-12}$ ~$1.2 \pm 0.1\times10^{-11}$
6	PMMA	1	A	Membrane emulsification	10.0 ± 2.6	26 ± 7	62.7 ± 8.7	1.1 ± 0.7	0.11 ± 0.04	806 ± 549	125 ± 87	1.3 ± 0.2 ~2.7 ± 0.3×10^{-10}
6	PMMA	1	A	Homogenization (800rpm)	7.4 ± 3.6	47 ± 22	60.0 ± 10.6	0.7 ± 0.5	0.12 ± 0.05	591 ± 459	118 ± 50	–
6	PMMA	4	A	Membrane emulsification	–	–	–	5.1 ± 2.4	0.042 ± 0.015	644 ± 292	90 ± 47	1.3 ± 0.4 ~2.7 ± 0.9×10^{-10}
6	PMMA	4	A	Homogenization (800rpm)	–	–	–	4.6 ± 2.1	0.044 ± 0.013	559 ± 326	114 ± 58	–
6	PMMA	24	A	Membrane emulsification	–	–	–	6.1 ± 2.3	0.036 ± 0.018	793 ± 424	117 ± 43	1.1 ± 0.3 ~2.1 ± 0.6×10^{-10}

8.1.1 Membrane emulsification process

The size and size distribution of droplets were studied with a membrane emulsification process based on using a dispersion cell. They were impacted by operation conditions, such as dispersed phase flux and impeller agitation speed, membrane properties, including membrane surface hydrophilicity and membrane configurations as well as physical properties of the two liquid phases, such as viscosity and interfacial tension. Among these factors, operation conditions provided the biggest influence on the sizes of droplets and their uniformity. The best condition to minimise the size distribution has been found to be an agitation speed of 1080 rpm and dispersed phase flux of 1.6×10^{-5} m s^{-1} for the conditions investigated. The experimental data were compared with the predictions of a model reported in the literature, which show the same trend as the existing model.

A pilot plant-scale cross-flow membrane system was used for scale up of the process of membrane emulsification and a homogenizer was also used for comparison as a common manufacturing device. Compared with the cross-flow membrane system, the dispersion cell system produced MF microcapsules with a narrower size distribution. This is attributed to the different membrane systems used. Nevertheless, the oil-aqueous MF precondensate produced in the pilot plant-scale membrane system was found stable for 72 h, which demonstrates that it is possible to scale up the process of membrane emulsification to produce MF microcapsules.

8.1.2 Preparation of PMMA microcapsules

The environmental friendly shell material PMMA was used for the first time to generate perfume microcapsules with a narrow size distribution in this study. Oil/water/MMA emulsions were produced through both a homogenizer and dispersion cell membrane system. The *CV* values of PMMA microcapsules generated through the membrane system with different reaction times are all below 25%, significantly smaller than those produced by the homogenizer, which are around 35%.

8.1.3 Novel methodology development

8.1.3.1 Determination of shell thickness using CLSM

In this study, the shell thickness of PMMA microcapsules was determined using CLSM and fluorescent dyes. It is a fast and low-cost method compared with the traditional TEM approach extensively used for MF microcapsules. This methodology was developed to solve the problem with PMMA microcapsules that could not be analyzed with TEM, since PMMA has similar properties to the poly acrylic resin used for TEM sample preparation. The shell thickness of PMMA microcapsules increased with the reaction time until 24 h when the core-shell capsules became homogeneous spheres.

8.1.3.2 Investigation of intrinsic mechanical properties of microcapsules with different shell thickness

PMMA microcapsules with different *h/r* values were prepared with different reaction times: thin-shell microcapsules ($h/r < 0.11$) with 1 h reaction time, thick-shell ($0.47 < h/r < 0.62$) with 4 h and full spheres with 24 h. These microcapsules had different force-displacement profiles obtained from experiments based on compression of single microcapsules by micromanipulation. The intrinsic mechanical properties of PMMA microcapsules with different shell thickness was obtained for the first time from the analysis of FEM simulations and micromanipulation data. The elastic modulus and the rupture stress, determined with different models according to *h/r*: the thin-shell model for thin-shell ($h/r < 0.11$) microcapsules, the linear and power law models for thick-shell ($0.47 < h/r < 0.62$) microcapsules, and the power law model for full spheres. The intrinsic mechanical properties of PMMA microcapsules were found constant with the polymerization reaction time despite large variations in *h*. This novel approach could also be used in the future to determine the intrinsic mechanical properties of other microcapsules with a thick shell.

8.1.3.3 Investigation of intrinsic mass transfer parameters for microcapsules with different shell material and thickness

The encapsulated oil release from microcapsules with different shell materials, different types of core oil and prepared through different processes was studied using a novel methodology. An aqueous solution in which the core oil has a high solubility was selected as a "co-solvent" for the release the perfume oils, Experiments were performed under continuous operation, allowing observation of the whole release profiles in its completeness, and furthermore allowing the determination of the intrinsic mass transfer parameters. Three mathematical models were used to calculate the shell permeability and diffusion coefficient, corresponding to the three different kinds of microcapsules formed here: the thin-shell model for thin-shell ($h/r < 0.11$) microcapsules within the linear regime, the hollow sphere model for thick-shell ($0.47 < h/r < 0.62$) microcapsules and the sphere model for full spheres. This allows a comparison based on intrinsic mass transfer parameters, which are mainly determined by the shell structure and the core oil, between very different microcapsules prepared using different formulations, processing conditions and core perfume oils.

8.2 Future work

In the work presented in Chapters 4 and 6, MF as well as PMMA microcapsules with narrow size and strength distributions were prepared with a dispersion cell membrane system. The best *CV* value among all the samples was ~20%. To produce microcapsules with even narrower size distribution, micro-channel (Vladisavljevic *et al.*, 2008) or flow-focusing (Takeuchi *et al.*, 2005) techniques could be applied in the future.

In the study presented in Chapter 5, a cross-flow membrane system was used for scaling up to pilot plant-scale. Further studies could include scale up of other membrane systems, including the dispersion cell membrane system and recently developed membrane systems, the oscillating system and the pulsed (oscillatory) flow membrane system (Holdich *et al.*, 2010, Piacentini *et al.*, 2013), which may have a great potential for using in industrial manufacture of microcapsules.

Different models to describe droplet formation at the membrane surface were reviewed in Chapter 2, with " Model D" used to analyse the experimental data in this study. However, this model does not consider the effect of dispersed phase flux on size and size distribution of emulsion droplets. A technique to observe and determine the single droplet formation on the membrane surface was mentioned in literature,

which was used in a cross-flow membrane system (Peng and Williams, 1998b). This technique may determine the whole process of droplet formation on the membrane surface online. Also, the percentage of active pores during the membrane emulsification stage could be determined. It can be extremely helpful for determining the duration of the detachment period, which can be used to calculate a real volume of a droplet according to Equation 5.2 (Peng and Williams, 1998).

$$V_f = V_g + Q \times t_d \qquad \text{(Equation 5.2)}$$

where V_f is the final volume of a droplet (m^3); V_g is the initial volume of the droplet (m^3); Q is the actual flow rate of the dispersed phase through the pore ($m^3\ s^{-1}$) and t_d is the duration of detachment period (s).

PMMA microcapsules produced in this study had a narrow size distribution. However, their shell permeability is slightly higher than that of MF microcapsules, especially for the 1 h PMMA microcapsules. In the future, organic or inorganic material could be used together with PMMA to make double shell microcapsules to reduce the shell permeability, including silica (Hu *et al.*, 2004) , zinc oxide (Tang *et al.*, 2006), and methacrylic acid (MAA) (Tan *et al.*, 2009).

In this study, PMMA microcapsule shells was saturated with core perfume oil, which could influence their shell material mechanical properties. In order to compare PMMA shells with macroscopic PMMA, PMMA beads without perfume oil could be

prepared and determined using the micromanipulation rig. The intrinsic mechanical properties of macroscopic PMMA could then be determined using the methodology mentioned in Chapter 6, section 6.2.4.

In this study, release behaviours of PMMA microcapsules were studied, PMMA shell permeability and diffusivity were determined. Further research could focus on finding how formulation and reaction conditions affect the properties of microcapsules in order to reduce the oil release rate, including determination the release rate is sensitive to size and size distribution of PMMA microcapsules.

In this study, several novel approaches were applied to MF and PMMA microcapsules with different shell thickness, such as using CLSM to determine the shell thickness of microcapsules labelled with a florescence dye, using FEM simulation and micromanipulation measurements to determine the intrinsic mechanical properties of microcapsules, using a co-solvent and UV-Vis spectrophotometer to measure perfume oil release from microcapsules continuously in order determine intrinsic mass transfer parameters. These methodologies could be applied to microcapsules with various core and shell materials. They could provide further evidence of improvement in the quality of microcapsules by new formulation and processing conditions. For example, big molecular core material could be used in MF microcapsules to determine the impact of solute on relative permeability.

In this study, the properties of microcapsules were extensively studied, from their size and strength distributions to their intrinsic mechanical properties. However, further study could still be carried out on the release behaviour of microcapsules with external force. Some literature work determined the deposition of perfume microcapsules on fabric surface and their abrasion by friction (Mercadé-Prieto *et al.*, 2012b). To determine the release behaviour of microcapsules under friction force through a tribometer can be very interesting, since it is exact condition under which perfume microcapsules are expected to rupture and release oil.

Appendix A

Finite Element Modelling (FEM) of the compression of thick-shell microcapsules

The parallel compression of elastic microcapsules with thick shells was studied with finite element modelling (FEM) using Abaqus® 6.5. The top half of a core-shell sphere was simulated in 3D using S8R shell elements (about 38k elements) for thin shells (*h/r* < 10%), and C3D8R hexagonal solid elements (about 50-100k) for thicker shells. A rigid parallel plate was considered as the compressing probe, with frictionless contact with the shell. The capsule shell was assumed to be incompressible (Poisson ratio 0.5) and was modelled as a linear elastic material. Because only small compression displacements were simulated ($\varepsilon_m < 0.12$), the effect of the liquid core was found to be insignificant both from previous work (Fery and Weinkamer, 2007, Taber, 1982) and preliminary finite element simulations of 2D shells with and without a liquid core, see Figure A1.Therefore, the liquid core was not considered in further finite element modelling.

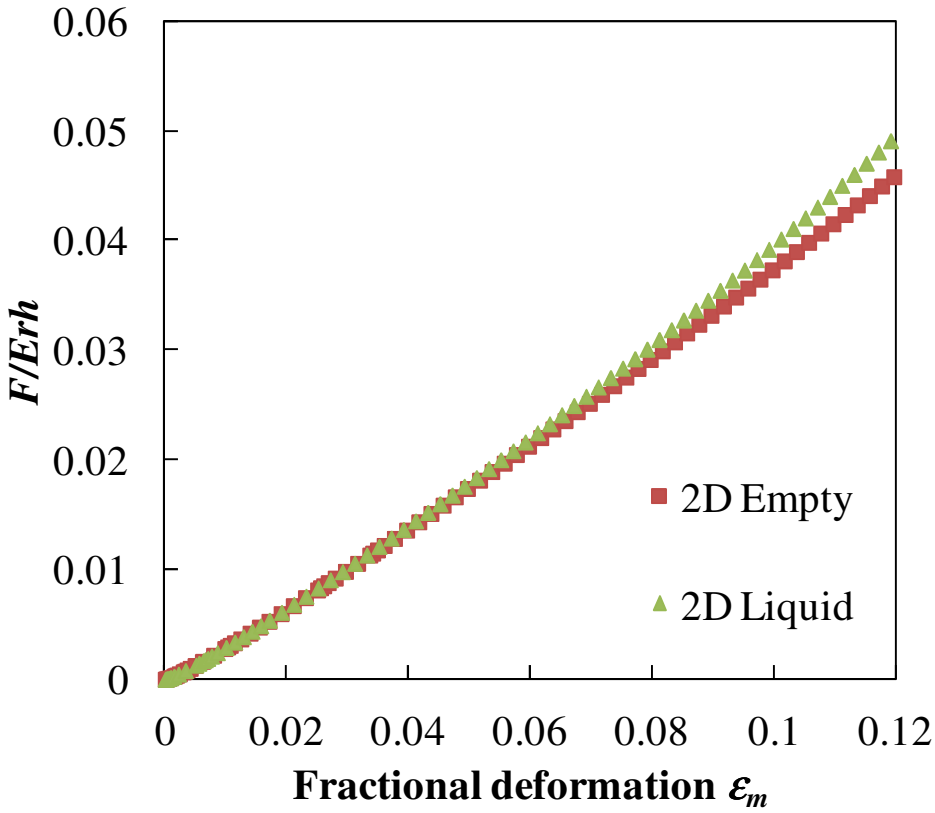

Figure A1. Simulation of 2D shells with and without a liquid core based on FEA (*h/r* = 0.15).

A.1 Estimation of the elastic modulus

The key parameter varied during the simulations was the shell thickness *h* to the capsule radius *r* ratio (h/r). At low h/r values, the dimensionless parameter F/Erh increases linearly with the displacement, ε_m ~0.5 h/r, as shown in Figure A2 (a). The linear slope *m* is calculated using

$$\frac{F}{Erh} = m\varepsilon_m \qquad \text{(Equation A1)}$$

The linearity of Equation A1 at small deformations is caused by the relevance of shell bending during the compression (Dubreuil *et al.*, 2003, Hutchinson, 2004). However, at large h/r values, for example at $h/r = 1$ when the microcapsule becomes a full homogenous sphere without a core, there is no or limited shell bending but compressive deformation. Under these conditions, the classic Hertz equation of a sphere between two parallel plates applies for small deformations (typically $\varepsilon_m < 0.1$) (Liu *et al.*, 1998).

$$\frac{F}{Er^2} = \frac{4}{3\left(1-\nu^2\right)}\varepsilon_m^{1.5} \qquad \text{(Equation A2)}$$

where ν is Poisson ratio. Thus, it is assumed that at large h/r values the compression force increases in a power law manner with the fractional deformation, such as

$$\frac{F}{Er^2} = a\varepsilon_m^{b} \qquad \text{(Equation A3)}$$

where a and b are fitting parameters. Hence, between low h/r (<20%) and full sphere behaviour ($h/r \approx 1$) there is an intermediate regime whereby the force increases with ε_m in a power law manner with b between ~1 (linear behaviour) and ~1.5 (Equ. A2); an example of the FEM results for $h/r = 44\%$ is given in Figure A2 (b).

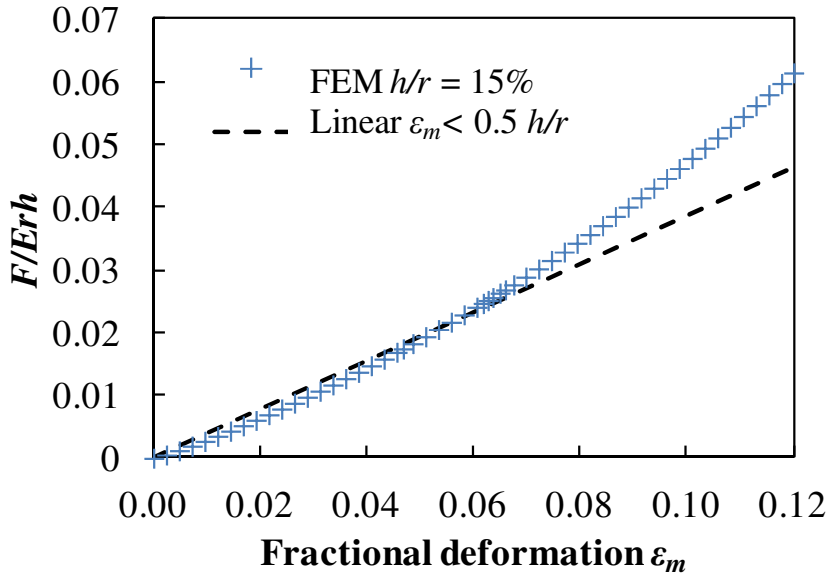

(a)

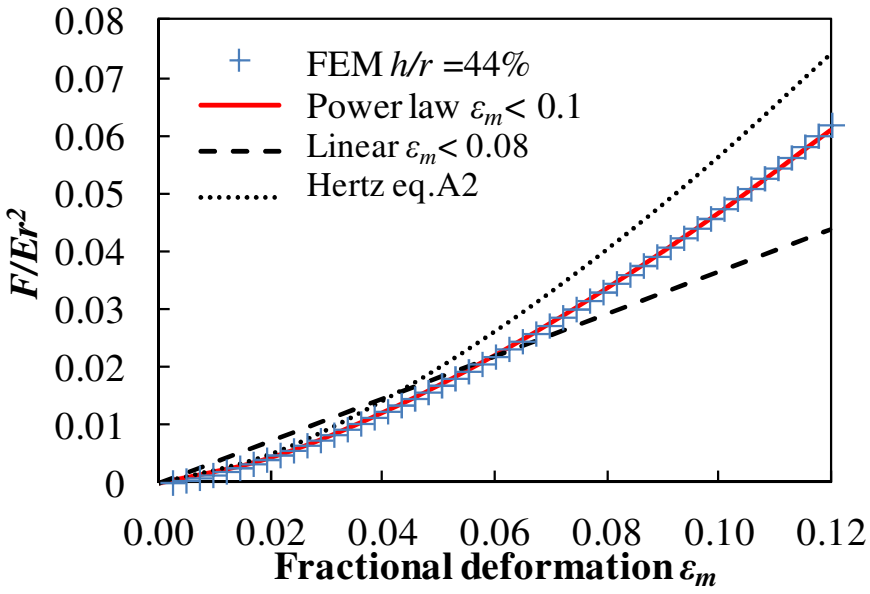

(b)

Figure A2. FEM results of parallel compression of core shell microcapsules with two different shell thickness to radius ratios: (a) $\boldsymbol{h/r = 15\%}$ and (b) $\boldsymbol{h/r = 44\%}$. Dashed lines are best fitting curves from the linear Equation A1, while the continuous line in (b) is the best fitting curve from Equation A3.

The determination of the elastic modulus of microcapsule shells is performed by comparing experimental and theoretical force curves (Mercade-Prieto *et al.*, 2011a, Mercade-Prieto *et al.*, 2012c). In the scenario of microcapsules with thick shells that break at small fractional deformations ($\varepsilon_{LE} < 0.15$ but mostly < 0.1), two different methodologies are proposed. The first one considers the linearity of Equation A1 up to $\varepsilon_m \approx 0.5\,h/r$, where the slope *m* increases linearly with h/r as shown in Figure A2(a). However, above $h/r \sim 20\%$ the system is no longer linear up to $\varepsilon_m \approx 0.5\,h/r$ (see Fery *et al*. (2004) for further discussion), thus fitting is only performed up to $\varepsilon_m = 0.08$ (a reasonable ε_{LE} value), shown in Figure A2 (b). The best fit *m* up to $\varepsilon_m = 0.5\ h/r$ or 0.08, whatever is lowest, are shown in Figure A3 for different h/r. For comparison, Reissner's solution for point-like indentation of thin shell spheres is also shown (2006), where $m = 4(3(1-\nu^2)^{0.5})^{-1} \times h/r$ (for an incompressible shell $m = 2.67 \times h/r$), which fits FEM results surprisingly well up to $h/r \sim 0.3$.

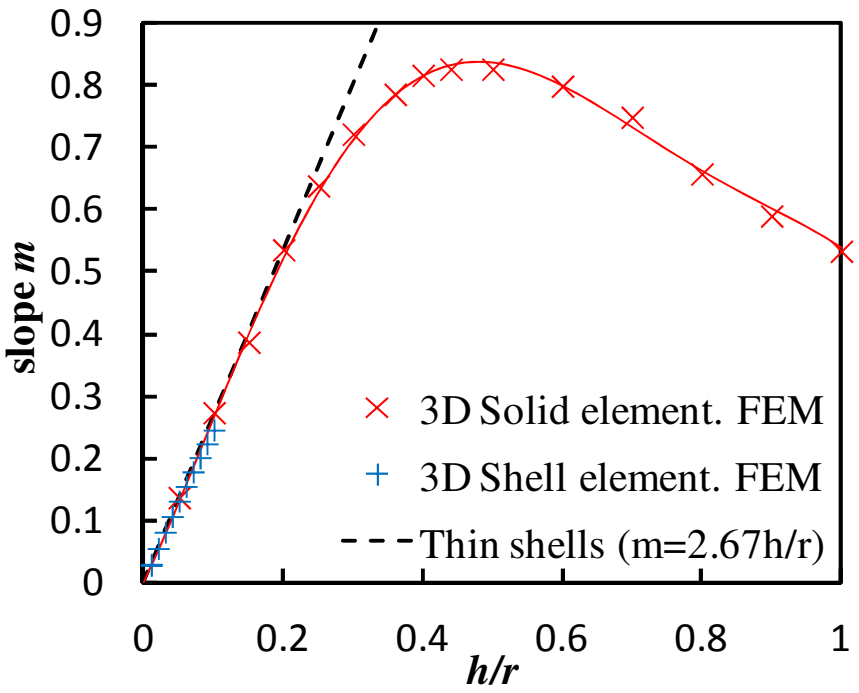

Figure A3. Correlation of the slope m with the shell thickness ratio h/r calculated up to the lowest ε_m between $\mathbf{0.5 \times h/r}$ and **0.08**. Continuous line shows the best fit:

$$\boldsymbol{m = -8.55 \times (h/r)^5 + 24.19 \times (h/r)^4 - 22.2 \times (h/r)^3 - 4.73 \times (h/r)^2 + 2.37 \times h/r}$$

The second method to determine E considers the power law behaviour of the compression force with ε_m. Equation B3 was used to fit the FEM results up to $\varepsilon_m = 0.1$, and an example is shown in Figure A2 (b). The best fit parameters a and b at different h/r values are given in Figure A4. Finally, the procedure to estimate the elastic modulus is as follows: (*i*) estimate the h/r ratio of the compressed microcapsule. (*ii*) Calculate the fitting parameters m (Equation A1) and a and b (Equation A3) using the polynomials given in the captions of Figure A3 and A4,

respectively, at the estimated h/r. (*iii*) Fit the experimental force profile up to ε_{LE} or ε_m~0.1, whatever is lowest, to the theoretical profiles (Equation A1 and A3) and obtain *E* with any suitable approach.

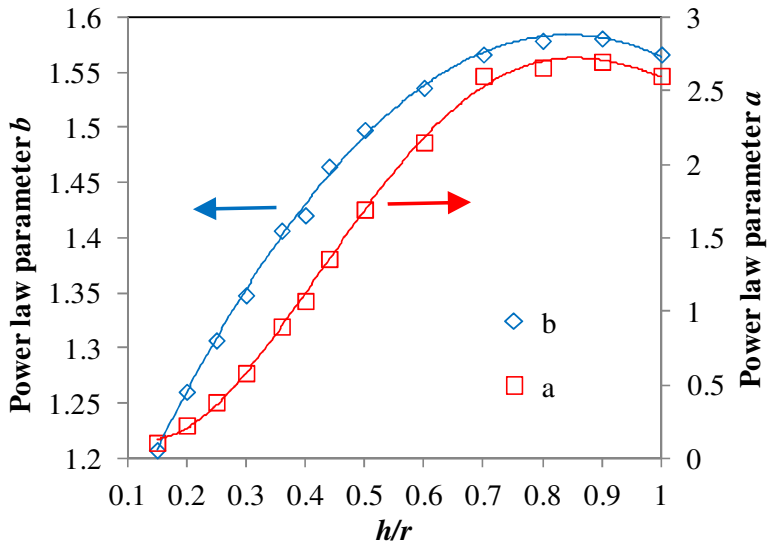

Figure A4. Best fit power parameters following a power law equation (Equation A3) for shell microcapsules of different thickness ratio $\boldsymbol{h/r}$. Lines are the best fit polynomials:

$\boldsymbol{a = 15.17 \times (h/r)^4 - 44.41 \times (h/r)^3 + 39.88 \times (h/r)^2 - 8.73 \times h/r + 0.686}$; and $\boldsymbol{b = -0.786 \times (h/r)^2 + 1.324 \times h/r + 1.026}$. The average relative error of the calculated $\boldsymbol{F/E\,r^2}$ using Equation A3 is of $\boldsymbol{1\%}$ up to $\boldsymbol{\varepsilon_m = 0.1}$.

A.2 Selection of the starting point in the elastic regime analysis

The linear model is highly unaffected by the starting point selected because it depends on the linear slope without considering the origin point. In the case of the power law model, the differences in the calculated *E* are usually less than 10%, with an average difference of 6 ± 3%. Figure A5 shows an example to determine the starting point using a log scale for the compression force. Changing the starting point about 0.1 µm, shown in the figure by dashed lines, which corresponds to a change of a fractional deformation of 0.002, results in a difference in *E* value by 8.9%.

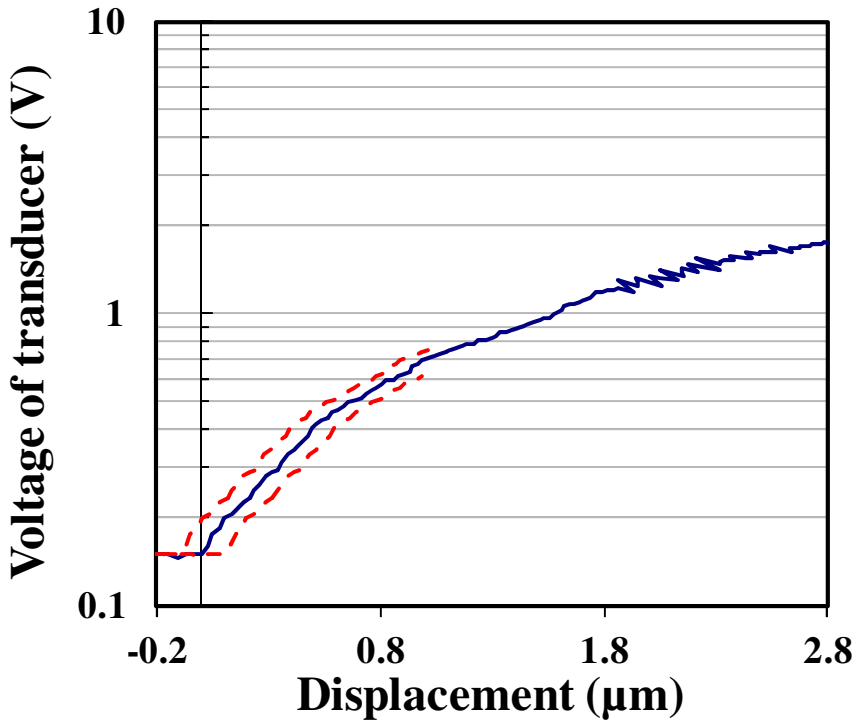

Figure A5. Compression profile of a single 4 h PMMA microcapsule (52µm) at small fractional deformations. Continuous line represents the computed experimental data with the selected starting point, at ε_m= 0. Dashed lines represent the profiles after changing the starting point plus or minus 0.1 µm.

A.3 Estimation of the rupture stress

When thick-shell microcapsules start rupturing under compression at very small ε_{LE}, the largest stressed area occurs in the shell area under the compressing planes, as discussed by Carlisle *et al.* (2007) for carbon micro-balloons. Figure A6 shows the 3D FEM distribution of the principal stress σ_p normalized with E at a fractional deformation ε_m of 0.06, around the ε_{LE} of the PMMA microcapsules. The rupture stress σ_B is found from such FEM results considering that rupture will start to occur at ε_{LE} at the position where the stress is largest (Mercade-Prieto *et al.*, 2012a). It is assumed, therefore, that the shell material exhibits fully elastic behaviour until rupture. The highest principal stresses σ_p can be of tensile (positive values) or compressive (negative) origin, which are found from Figure A6(a) and (b) respectively. The compressive stresses (negative σ_p) at the outer part of the shell are larger in magnitude than the tensile stresses of the inner part of the shell in contact with the liquid core.

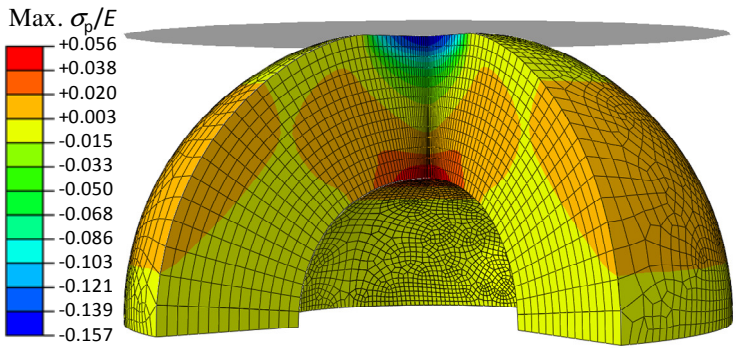

(a)

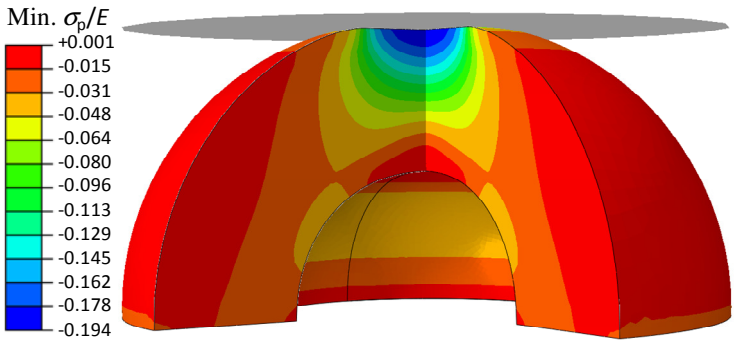

(b)

Figure A6. Distribution of the normalized (a) maximum and (b) minimum principal stresses with the elastic modulus ($\boldsymbol{\sigma_p/E}$) using FEM, for a $\boldsymbol{h/r = 50\%}$ microcapsule compressed at $\boldsymbol{\varepsilon_m = 0.06}$. The maximum tensile stress is obtained from (a) as the largest positive stress, whereas the maximum compressive stress is obtained from (b) as the largest negative stress. The mesh of elements is shown in (a).

The largest tensile and compressive stresses at different ε_m values were determined from the FEM results, shown in Figure A7. The thicker the shell, the more results resemble the full homogenous sphere scenario ($h/r = 1$), whereby stresses are mostly of a compressive nature. For the case of PMMA microcapsules, where h/r is

between 0.45 and 0.66, the compressive σ_p/E is about 2-4 times the tensile σ_p/E at ε_m values around ε_{LE}.

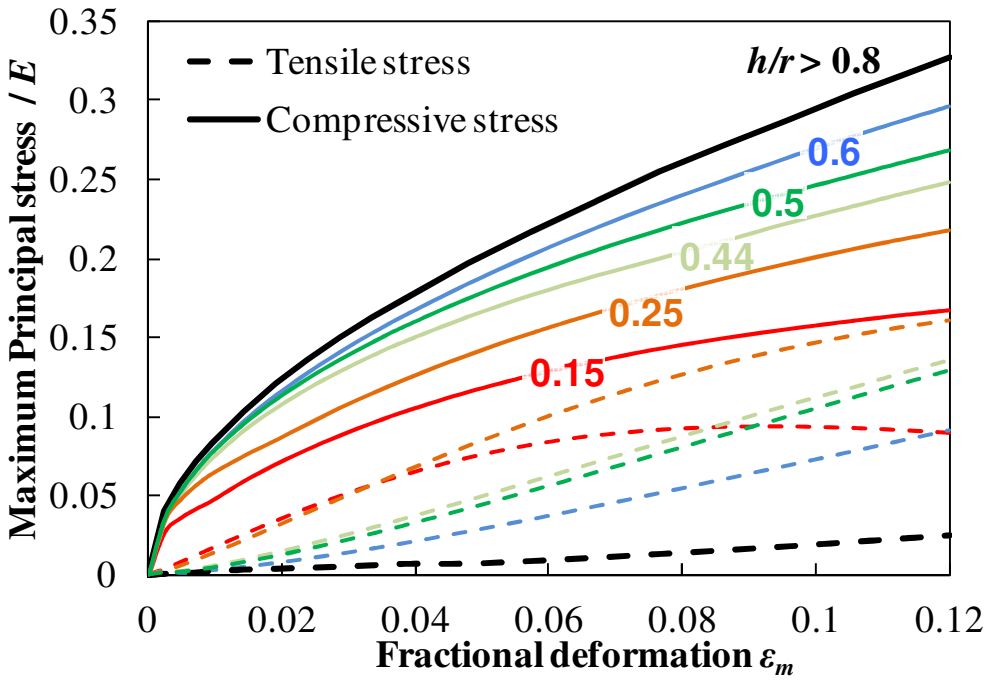

Figure A7. Determined $\boldsymbol{\sigma_p/E}$ from FEM simulations for different $\boldsymbol{h/r}$ values. Continuous lines are for the largest compressive stress values in the microcapsule, while dashed lines are for the largest tensile stresses, shown in Figure A6.

Appendix B

MATLAB code for calculating shell permeability for PMMA microcapsules

B.1 Oil release from a microsphere

The calculation of shell permeability for a 24 PMMA microsphere was based on Equation 7.11, which was described in Section 7.3.2.

$$\frac{C_{out}}{C_{out\infty}} = 1 - \sum_{n=1}^{\infty} \frac{6\alpha_r(1+\alpha_r)}{9+9\alpha_r+(\alpha_r q_n)^2} \exp\left(-\frac{Dq_n^2 t_r}{r^2}\right) \quad \text{(Equation 7.9)}$$

where $\alpha_r = V/V_S K_p$ represents the ratio of oil released to that remaining in the particle at equilibrium, and q_n are the non-zero positive roots of the transcendent equation

$q_n = \frac{3q_n}{3+\alpha q_n^2}$.

(c_{out}) is the concentration outside the particles during the release at a given time, *V* is the volume of co-solvent, *Vs* is total volume of the particle, *r* is the radius of the particle, *D* is the diffusivity, $K_p = \frac{C_{in\infty}}{C_{out\infty}}$ is the partition coefficient, the ratio of the concentration inside ($C_{in\infty}$) and outside ($C_{out\infty}$) the particle at the end of release, which are calculated using Equation 7.8 directly before using a Matlab code.

$$V_S C_{in0} = V C_{out\infty} + V_S C_{out\infty} K_p \qquad \text{(Equation 7.8)}$$

where C_{in0} is the initial concentration inside the particle, considered constant within the different particle. r is the distance from the centre of the particle to the location where the concentration of the oil is simulated.

MATLAB code:

A function "Qfunction" was defined based on equation $q_n = \frac{3q_n}{3+\alpha_r {q_n}^2}$:

```
function fx=Qfunction(x, alpha)

fx=tan(x)-(3*x)./(3+alpha.*x.^2);

 end
```

where, *x* represents q_n, *alpha* represents α_r and *fx* = $q_n - \frac{3q_n}{3+\alpha_r {q_n}^2}$ with roots

number *n*.

A function " findroot" was defined to find the root of function " Qfunction".

```
function [ rootsol ] = findroot( totalroot, alpha )
% defined a function

rootsol = zeros(totalroot,1);
 % create the root vector

x0=[2 5];
for m = 1:totalroot % defined a pivot number for " for" loop
      converge = false;
      while converge == false
           if Qfunction(x0(1),alpha)<0
                if Qfunction(x0(2),alpha)>0
                     rootsol(m)= fzero(@(x) Qfunction(x,alpha),x0);
                     converge = true;
                else
                     x0(2) = x0(2) - 0.5;
```

```
            end
        else
            x0(1) = x0(1) - 0.5;
        end
    end
    x0=[rootsol(m)+2 rootsol(m)+4];
end
 end
```

```
% using "for" and "if" loops to calculated the root one by one
```

Here, for a given α and a number of total roots *n* needed, the function will return the result roots.

A function "ReleaseFun " was defined based on equation 7.9:

```
function ConcRatio = ReleaseFun(alpha, qn,R, t, D)
% Equation 4 in the J.Controlled Release 60:169 paper (Polakovic et al., 1999)
   ConcRatio= 1 -
6*alpha*(1+alpha)*sum(1./(9+9*alpha+(alpha*qn).^2).*exp(-D*qn.^2.*t/(R^2)));
 end
```

where *ConcRatio* represents $\frac{C_{out}}{C_{out\infty}}$.

A function "ReleaseOptimeD " was defined to calculate value of diffusivity.

```
function [ Doptim ] = ReleaseOptimeD(    )

% Function to optimize the value of the diffusivity


ExcelFile = '0103-24-3.xlsx';

% define a excel file "ExcelFile" with release data inside, in order to use it later

ExpData = xlsread(ExcelFile);

% read the data from "ExcelFile", time (Minute), Fractional release (%)

ExpData(:,1) = ExpData(:,1)*60;

% changed release time from minutes to seconds


% start User variables

MaxRelease = 0.8;      %Maximum fractional release (%), below which diffusivity is

optimized

VolRatio = 5000;         %  V/V_S, Volume ratio between the amount of capsules and

solution solvent

Kp = 4225.4608;                  % Partition coefficient

Dinitial = 1.0e-013;

% estimated Diffusivity (m^2 s^-1), used in "fminsearch" function for more accurate

calculation;
```

```
r = 26e-6;                % radius of spheres (m)
% end User variables

alpha = VolRatio/Kp;  % α = V/V_S K_p

Doptim = fminsearch(@(D) ReleasePlot(D,ExpData, alpha, R, MaxRelease),Dinitial);
%    calculated diffusivity (m^2 s^-1 ) using "fminsearch" function, with estimated
diffusivity value "Dinitial".

 ReleasePlot(Doptim, ExpData, alpha, R, MaxRelease)
 % Plot release profile using "ReleasePlot" function, with optimized diffusivity value

 end
```

A function "ReleasePlot" was defined to plot the release profile of a microsphere.

```
function [ Res ] = ReleasePlot(D, ExpData, alpha, R, MaxRelease)
% defined a function to optimize the residual sum of squares of microsphere
fractional release
% Plot the release profile of a microsphere
% ExpData is the experimental data read from "ExcelFile", will be plotted later
% MaxRelease is the maximum percentage of release rate will be modeled in this case
```

```
close all
  % close all the figures
% start User variables
EndTime = ExpData(end,1);        % Final release time (seconds)
NumPoints = 1000;
% total number of roots for equation    q_n = 3q_n / (3+α_r q_n^2)
% end User variables

rootsol = findroot( 1000, alpha ); % returned "findroot" result into the vector "rootsol"

t = [0:EndTime/(NumPoints-1):EndTime]'; % created the vector for time

ConcRatio = zeros(size(t)); % created the fractional release (%) root vector

for j = 1:NumPoints    % defined a pivot number for "for" loop
      ConcRatio(j) = ReleaseFun(alpha, rootsol ,R, t(j), D);
% calculated fractional release (%), returned result into root vector

end
YCalc = spline(t,ConcRatio, ExpData(ExpData(:,2) < MaxRelease,1));
```

```
Res = sum((YCalc - ExpData(ExpData(:,2) < MaxRelease,2)).^2);
% calculated "Res" the residual sum of squares, which equals to
```

$$\text{Res} = \sum_{i=1}^{n}\left(y_i - f(x_i)\right)^2$$

```
figure1 = figure; % created a figure "figure1"
axes1 = axes('Parent',figure1,'FontSize',12,'FontName','Times New Roman');
box(axes1,'on');
hold(axes1,'all');
 % graph format
plot(ExpData(:,1), ExpData(:,2),'Parent',axes1,'Marker','+','LineStyle','none','Color',[1
0 0],'DisplayName','Experimental data')
% plot experimental data into "figure1"
hold on
plot(t, ConcRatio,'Parent',axes1,'LineWidth',3,'DisplayName','D = 3.2e-013 m^2/s')
 % plot modeling data in the same figure
 xlabel('Time (min)','FontSize',12,'FontName','Times New Roman');
ylabel('Relative release,"}c,'FontSize',12,'FontName','Times New Roman');
legend1 = legend(axes1,'show');
set(legend1,'EdgeColor',[1 1 1],'YColor',[1 1 1],'XColor',[1 1 1],...
      'Position',[0.5268215974333 0.324042111214441 0.332142857142857
```

```
0.126190476190476]);

ylim([0 1])

xlim([0 spline(ConcRatio, t, 0.9)])

 % graph format

end
```

Example of the result reported:

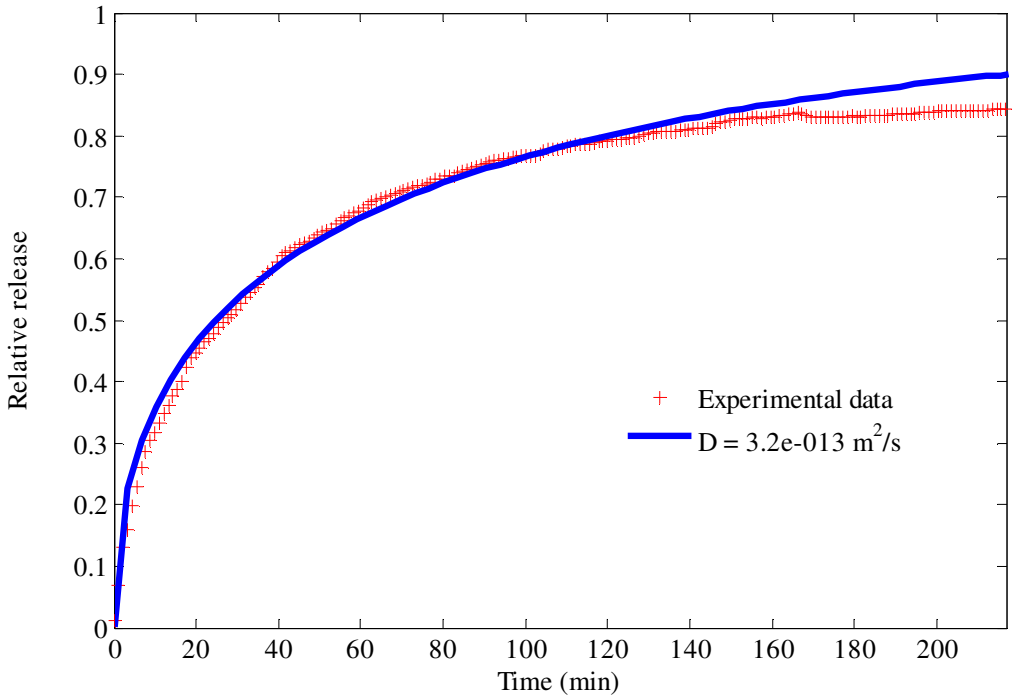

Figure B.1 Exported figure of experimental and fitted release profiles for PMMA microsphere. The result of diffusivity: $D = 3.2 \times 10^{-13} \mathrm{m}^2\ \mathrm{s}^{-1}$

B.2 Oil release from a thick shell microcapsule

The modelling of thick-shell microcapsules was based on two models: one is the model described in Section 7.3.2 for microspheres based on Equation 7.9, one is the

model mentioned in Section 7.3.3 as "hollow sphere" model, based on Equation 7.10. The first model used in this section was the same as the microsphere model, mentioned in Section B.1.

$$\frac{C_{out}}{C_{out\,\infty}}$$

$$= 1 - \frac{6}{\pi^2(r_{inner}^2 + r_{inner}r + r^2)} \sum_{n=1}^{\infty} \left(\frac{r\cos n\pi - r_{inner}}{n}\right)^2 \exp\left(-\frac{Dn^2\pi^2 t_r}{(r - r_{inner})^2}\right)$$

(Equation 7.10)

where r_{inner} is the radius of the hollow space in the microcapsule, r is radius of the microcapsule and n is the total root number of Equation 7.10.

MATLAB code is shown as follow:

A function "Releasefun4 h1" was defined based on equation 7.10 :

```
function ConcRatio = ReleaseFun4 h1(a, b, n, t, D)
% Equation 6.49 in crank's book p98 (Crank, 1975).
 ConcRatio= 1 -
6/(3.1415926^2*(a^2+a*b+b^2))*sum((((b*cos(3.1415926*n)-a)).^2./n.^2.).*exp(-D*
n.^2.*3.1415926^2*t/(b-a)^2));
 end
```

where *ConcRatio* represents $\frac{C_{out}}{C_{out\infty}}$.

A function "ReleaseoptimeD4 h1" was defined to optimize the value of the diffusivity.

```
function [ Doptim, Doptims] = ReleaseOptimeD4 h1(    )
% Function to optimize the value of the diffusivity


ExcelFile = '0103-4-3.xlsx';
% define a excel file "ExcelFile" with release data inside, in order to use it later
ExpData = xlsread(ExcelFile);
% read the data from "ExcelFile", time (Minute), Fractional release (%)
ExpData(:,1) = ExpData(:,1)*60;
% changed release time from minutes to seconds


% start User variables
MaxRelease = 0.8;      %Maximum fractional release (%), below which diffusivity is
optimized
Dinitial =    4e-013;            % estimated diffusivity (m^2 s^-1), used in "fminsearch"
function for more accurate calculation;
b = 26e-6;               % outer radius of the hollow spheres (m)
a = 11.8e-6;              % inner radius of the hollow spheres (m)
VolRatio = 5000;         %  V/V_S, volume ratio between the amount of capsules and
solution solvent
```

```
Kp = 2572.006936;                %Partition coefficient

R = 26e-6;                % radius of spheres (m)

% end User variables


alpha = VolRatio/Kp;  % α = V/V_S K_p

Doptim = fminsearch(@(D) ReleasePlot4 h1(D, ExpData, a, b, alpha, R,

MaxRelease),Dinitial);

% calculated diffusivity ( m^2 s^-1) using "fminsearch" function with estimated

diffusivity value "Dinitial" using "hollow sphere model" and " sphere model"


ReleasePlot4 h1(Doptim, ExpData, a, b, alpha, R, MaxRelease)

  % Plot release profile using "ReleasePlot4 h1" function, with optimized diffusivity

value


end
```

A function "ReleasePlot4 h1" was defined to plot the release profile of a thick shell microcapsule and the fitting with two models.

```
function [ Res ] = ReleasePlot4 h1(D, ExpData, a, b, alpha, R, MaxRelease)

% defined a function to optimize the residual sum of squares of microcapsule
```

```
fractional release

% Plot the release of a thick shell microcapsule

% ExpData is the experimental data read from "ExcelFile", will be plotted later

% MaxRelease is the maximum percentage of release rate will be modeled in this case

close all

   % close all the figures

%start User variables

EndTime = ExpData(end,1);        % Final release time (s)

NumPoints = 1000; % number of roots for equation 7.10.

%end User variables


rootsol = findroot( 1000, alpha ); % returned "findroot" result into the vector "rootsol"


n = [1:1:1000]'; % created a root vector


t = [0:EndTime/(NumPoints-1):EndTime]'; % created the vector for time


ConcRatio = zeros(size(t)); % created the fractional release (%) root vector for

"hollow sphere model"


ConcRatio1 = zeros(size(t)); % created the fractional release (%) root vector for "
```

```
sphere model"


for j = 1:NumPoints % defined a pivot number for "for" loop
        ConcRatio(j) = ReleaseFun4 h1(a, b, n ,t(j), D);
% calculated fractional release (%) using "hollow sphere model", returned result into
"hollow sphere model" root vector


        ConcRatio1(j) = ReleaseFun(alpha, rootsol ,R, t(j), D);
    % calculated fractional release (%) using "sphere model", returned result into
"sphere model" root vector


end
YCalc = spline(t,ConcRatio, ExpData(ExpData(:,2) < MaxRelease,1));
Res = sum((YCalc - ExpData(ExpData(:,2) < MaxRelease,2)).^2);
% calculated "Res" the residual sum of squares, which equals to
```

$$Res = \sum_{i=1}^{n} \left(y_i - f(x_i)\right)^2$$

```
figure1 = figure; % created a figure "figure1"
axes1 = axes('Parent',figure1,'FontSize',12,'FontName','Times New Roman');
% graph format
```

```
box(axes1,'on');

hold(axes1,'all');


plot(ExpData(:,1), ExpData(:,2),'Parent',axes1,'Marker','+','LineStyle','none','Color',[1

0 0],'DisplayName','Experimental data')

% plot experimental data into "figure1"

hold on

plot(t, ConcRatio,'Parent',axes1,'LineWidth',3,'DisplayName','hollow sphere D =

3.0e-013 m^2/s')

% plot "hollow sphere" modeling data in the same figure

hold on

plot(t, ConcRatio1,'Parent',axes1,'LineWidth',3,'Color',[0 0.498039215803146

0],'DisplayName','sphere D = 4.3e-013 m^2/s')

% plot "sphere" modeling data in the same figure


xlabel('Time (min)','FontSize',12,'FontName','Times New Roman');

ylabel({'Relative release',''},'FontSize',12,'FontName','Times New Roman');

legend1 = legend(axes1,'show');

set(legend1,'EdgeColor',[1 1 1],'YColor',[1 1 1],'XColor',[1 1 1],...

    'Position',[0.5268215974333 0.324042111214441 0.332142857142857

0.126190476190476]);
```

```
ylim([0 1])

xlim([0 spline(ConcRatio1, t, 0.9)])

% graph format

end
```

Example of the result reported:

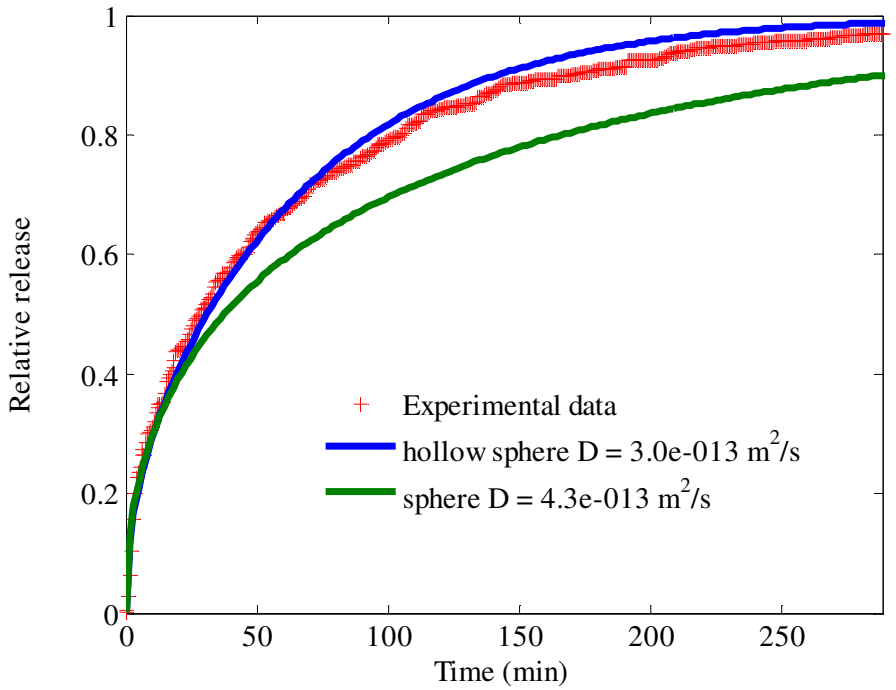

Figure B.2 Exported figure of experimental and fitted release profiles for thick-shell PMMA microcapsules ($0.47 < h/r < 0.62$). $D = 3.0 \times 10^{-13}\mathrm{m}^2\ \mathrm{s}^{-1}$ for the hollow sphere model; $D = 4.3 \times 10^{-13}\mathrm{m}^2\ \mathrm{s}^{-1}$ for the sphere model.

B.3 Oil release from a thin shell microcapsules

The modelling of thin-shell microcapsules was based on a thin-shell model

(Mercade-Prieto *et al.*, 2012b), which was described in Section 7.3.1. For comparison, the "hollow sphere" model was also used, which was described in Section 7.3.3, based on Equation 7.10. The details were explained in Section B.1, and the calculated data from "hollow sphere" model were exported. Data analysis was implemented using commercial software Excel®, Microsoft.

Example of the result reported:

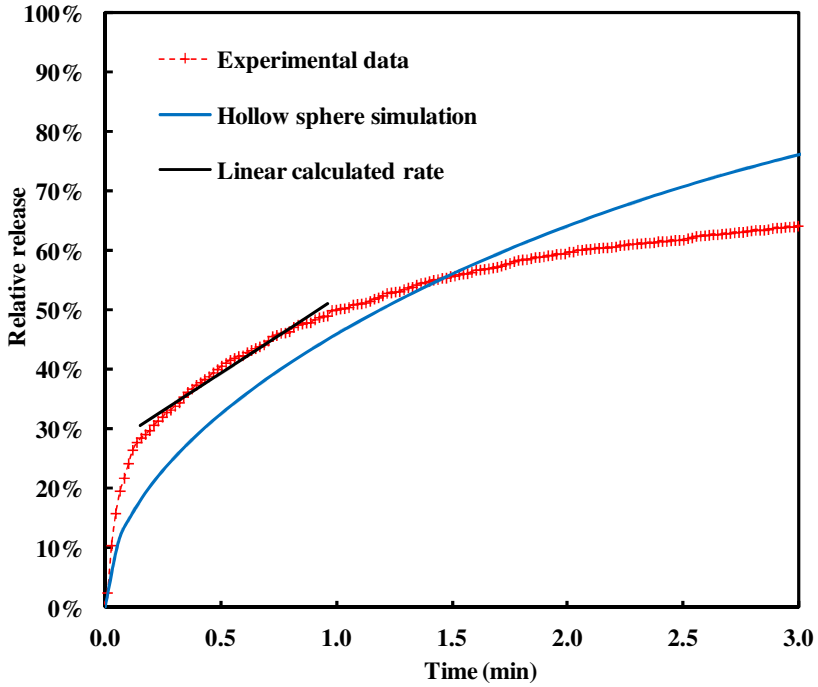

Figure B.3 Exported figure of experimental and fitted release profiles for thin-shell PMMA microcapsules ($h/r < 0.11$). $D = 1.3 \times 10^{-14} \mathrm{m}^2\ \mathrm{s}^{-1}$ for the thin-shell model;$D = 8.9 \times 10^{-15} \mathrm{m}^2\ \mathrm{s}^{-1}$ for the "hollow sphere" model.

References

Abrahamse, A. J., Van Der Padt, A., Boom, R. M. & De Heij, W. B. C. 2001. Process fundamentals of membrane emulsification: Simulation with CFD. *Aiche Journal,* 47**,** 1285-1291.

Abrahamse, A. J., Van Lierop, R., Van Der Sman, R. G. M., Van Der Padt, A. & Boom, R. M. 2002. Analysis of droplet formation and interactions during cross-flow membrane emulsification. *Journal of Membrane Science,* 204**,** 125-137.

Alay, S., Gode, F. & Alkan, C. 2011. Synthesis and Thermal Properties of Poly(n-butyl acrylate)/n-Hexadecane Microcapsules Using Different Cross-Linkers and Their Application to Textile Fabrics. *Journal of Applied Polymer Science,* 120**,** 2821-2829.

Alic, B., Sebenik, U. & Krajnc, M. 2012. Microencapsulation of butyl stearate with melamine-formaldehyde resin: Effect of decreasing the pH value on the composition and thermal stability of microcapsules. *Express Polymer Letters,* 6**,** 826-836.

An, P. Y., Ba, X. W. & Lu, S. A. 2010. Preparation and characterization of crosslinked poly(methylmethacrylate) heat sensitive color-developing nanocapsules. *Polymer Bulletin,* 64**,** 375-386.

Anastasiou, T. J., Lee, K. & Popplewell, L. M., inventors; International Flavors and Frangrances, Inc., assignee. Process for preparing a high stability microcapsule product and method for using same. The United Kingdom, patent EP1797946 A2. 2007a.

Anastasiou, T. J., Pluyter, J. G. L., Lei, Y., Lee, K. D. & Popplewell, L. M., inventors; International Flavors & Fragrances Inc., assignee. Encapsulated active material with reduced formaldehyde potential. USA, patent US 2007/0138674. 2007b.

Anna, S. L., Bontoux, N. & Stone, H. A. 2003. Formation of dispersions using "flow focusing" in microchannels. *Applied Physics Letters,* 82**,** 364-366.

Antipov, A. A., Sukhorukov, G. B. & Mohwald, H. 2003. Influence of the ionic strength on the polyelectrolyte multilayers' permeability. *Langmuir,* 19**,** 2444-2448.

Anton, N., Benoit, J. P. & Saulnier, P. 2008. Design and production of nanoparticles formulated from nano-emulsion templates - A review. *Journal of Controlled Release,* 128**,** 185-199.

Aouad, Y. G., inventor The Procter and Gamble Company, assignee. Laundry scent additive. USA, patent US 7871976. 2011a.

Aouad, Y. G., inventor The Procter and Gamble Company, assignee. Laundry scent additive. USA, patent US 7867968. 2011b.

Arellano, R. M. & Vazquez, E. P., inventors; Minnesota Mining & Manufacturing Innovative Properties Company, assignee. Abrasive item for cleaning wit scented abrasive fibres. USA, patent US 2004/0242133 A1. 2004.

Arshady, R. 1989. Preparation of Microspheres and Microcapsules by Interfacial Polycondensation Techniques. *Journal of Microencapsulation,* 6**,** 13-28.

Arshady, R. 1999. *Microspheres, Microcapsules & Liposomes, Volume 1: Preparation & Chemical Applications,* London, Citus Books.

Aryanti, N., Hou, R. Z. & Williams, R. A. 2009. Performance of a rotating membrane emulsifier for production of coarse droplets. *Journal of Membrane Science,* 326**,** 9-18.

Aryanti, N., Williams, R. A., Hou, R. Z. & Vladisavljevic, G. T. 2006. Performance of rotating membrane emulsification for o/w production. *Desalination,* 200**,** 572-574.

Aussant, E., Fraser, S., Unno, M. & Warr, J., inventors; Takasago International Corporation, assignee. Perfume for capsule composition. USA, patent US20070149424. 2007.

Aussant, E., Fraser, S., Unno, M. & Warr, J., inventors; Takasago International Corporation, assignee. Encapsulation of bulky fragrance molecules, patent EP 1894603 A1. 2008.

Aussant, E., Fraser, S. & Warr, J., inventors; Takasago International Corporation, assignee. Fragrance-containing core shell microcapsules, patent EP 2397120 A1. 2011.

Bakeine, G. J., Bertolotti, A., Latina, M., Congiu, T., Prati, U., Roveda, L., Trotta, F., Tormen, M., Di Fabrizio, E., Carlini, G., Facoetti, A. & Nano, R. 2007. Surface properties and implantation site affect the capsular fibrotic overgrowth. *Journal of Biomedical Materials Research Part A,* 83A**,** 965-969.

Balentine, D. A., Wiseman, S. A. & Bouwens, L. C. M. 1997. The chemistry of tea flavonoids. *Critical Reviews in Food Science and Nutrition,* 37**,** 693-704.

Barbosa-Cánovas, G. V., Ortega-Rivas, E., Juliano, P. & Yan, H. 2005. Food Powders: Physical Properties, Processing, and Functionality. Springer.

Bauer, D. R. 1986. Melamine/Formaldehyde Crosslinkers: Characterization, Network Formation and Crosslink Degradation. *Progress in Organic Coatings,* 14**,** 193-218.

Bauer, F., Garbe, D. & Surburg, H. 2001. *Common Fragrance and Flavor Materials,* Weinheim, New York, Chichester, Brisbane, Singapore, Toronto, Wiley-vch.

Baumgarten, N. 1989. Environmental Sem Premieres. *Nature,* 341**,** 81-82.

Bennett, S. W. & Brain, J., inventors; International Flavors & Fragrances Inc., assignee. Encapsulated fragrance chemicals. USA, patent US 2004/0072719 A1. 2004.

Berge, A., Gudmunds.S & Ugelstad, J. 1969. Melamine-Formaldehyde Compounds .I. Alkaline Decomposition of Methylol Melamines and Methoxymethyl Melamines. *European Polymer Journal,* 5**,** 171-&.

Berge, A., Kvaeven, B. & Ugelstad, J. 1970. Melamine-Formaldehyde Compounds .2. Acid Decomposition of Methylol Melamines and Methoxymethyl Melamines. *European Polymer Journal,* 6**,** 981-&.

Berry, G., Marynowski, J. M. & Kinne, K. W. 1995. Perfume-containing capsules with good flowability for laundry detergents. *Zeolites,* 15**,** 183.

Binks, B. P. & Fletcher, P. D. I. 2001. Particles adsorbed at the oil-water interface: A theoretical comparison between spheres of uniform wettability and "Janus" particles. *Langmuir,* 17**,** 4708-4710.

Bobnock, S. R., Debraal, C. J., Dihora, O. J., Druckrey, K. A., Hart, T. G., Kirksey, T. S. & Vanderveken, J. W. F., inventors; Appleton Papers Inc., assignee. Delivery particle. USA, patent WO2010014172. 2010.

Bodet, F. J., Carrara, G., Chung, H. A., Ditullio, J. D. D., Dykstra, R. R., Finley, M. K., Fossum, D. R., Ketcha, M. M., Liu, Z., Morgan, I. K. G. & Vinson, K. P., inventors; The Procter and Gamble Company, assignee. Perfuming method and product, patent WO2008111007A2. 2008a.

Bodet, J.-F., Dihora, O. J., Fossum, D. R., Jordan, I. T. G., Kirksey, J. T. S. & Waits, D. L., inventors; The Procter and Gamble Company, assignee. Fabric care compositions comprising formaldehyde scavengers. Belgium, patent EP 1991648. 2008b.

Bone, S., Vautrin, C., Barbesant, V., Truchon, S., Harrison, I. & Geffroy, C. 2011. Microencapsulated Fragrances in Melamine Formaldehyde Resins. *Chimia,* 65**,** 177-181.

Boom, R. M. 2003. *Membrane Emulsification: Process Principle.* PhD, wageningen university.

Brian, B. 2012. J&J to Remove 'Toxic' Chemicals from Products. *The Chemical Engineer* 6.

Bromley, A. J., Holdich, R. G. & Cumming, I. W. 2002. Particulate fouling of surface microfilters with slotted and circular pore geometry. *Journal of Membrane Science,* 196**,** 27-37.

Brown, E. N., Kessler, M. R., Sottos, N. R. & White, S. R. 2003. In situ poly(urea-formaldehyde) microencapsulation of dicyclopentadiene. *Journal of Microencapsulation,* 20**,** 719-730.

Calabrese, R. V., Chang, T. P. K. & Dang, P. T. 1986a. Drop Breakup in Turbulent Stirred-Tank Contactors .1. Effect of Dispersed-Phase Viscosity. *Aiche Journal,* 32**,** 657-666.

Calabrese, R. V., Wang, C. Y. & Bryner, N. P. 1986b. Drop Breakup in Turbulent Stirred-Tank Contactors .3. Correlations for Mean Size and Drop Size Distribution. *Aiche Journal,* 32**,** 677-681.

Capek, I. 1999. Microemulsion polymerization of styrene in the presence of anionic emulsifier. *Advances in Colloid and Interface Science,* 82**,** 253-273.

Capodagli, J. & Lakes, R. 2008. Isothermal viscoelastic properties of PMMA and LDPE over 11 decades of frequency and time: a test of time–temperature superposition. *Rheologica Acta,* 47**,** 777-786.

Carlisle, K. B., Lewis, M., Chawla, K. K., Koopman, M. & Gladysz, G. M. 2007. Finite element modeling of the uniaxial compression behavior of carbon microballoons. *Acta Materialia,* 55**,** 2301-2318.

Cavin, L., Geffroy, C., Harrison, I., Michael, Hotz, J., Matys, M. & Quellet, C., inventors; Givaudan SA assignee. Microcapsules, patent WO2008098387. 2008.

Chang, C. C., Tsai, Y. L., Chiu, J. J. & Chen, H. 2009. Preparation of Phase Change Materials Microcapsules by Using PMMA Network-Silica Hybrid Shell Via Sol-Gel Process. *Journal of Applied Polymer Science,* 112**,** 1850-1857.

Charcosset, C. 2009. Preparation of emulsions and particles by membrane emulsification for the food processing industry. *Journal of Food Engineering,* 92**,** 241-249.

Charcosset, C., Limayem, I. & Fessi, H. 2004. The membrane emulsification process - a review. *Journal of Chemical Technology and Biotechnology,* 79**,** 209-218.

Chen, F. T., Jiang, X. S., Liu, R. & Yin, J. 2011. Polymeric vesicles with well-defined poly(methyl methacrylate) (PMMA) brushes via surface-initiated photopolymerization (SIPP). *Polymer Chemistry,* 2**,** 614-618.

Chen, H. M., Ouyang, W., Lawuyi, B. & Prakash, S. 2006. Genipin cross-linked alginate-chitosan microcapsules: Membrane characterization and optimization of cross-linking reaction. *Biomacromolecules,* 7**,** 2091-2098.

Chen, W., Lu, F. & Cheng, M. 2002. Tension and compression tests of two polymers under quasistatic and dynamic loading. *Polymer Testing,* 21**,** 113-121.

Chevalier, V., Hurel, V. & Simon, P., inventors; L'Oreal, assignee. Cosmetic composition containing melamine-formaldehyde or urea-formaldehyde particles and its uses, patent EP 1046388. 2005.

Cho, S. A., Park, N. H., Kim, J. W. & Suh, K. D. 2002. Preparation of mono-sized PMMA/liquid crystal microcapsules by solute co-diffusion method. *Colloids and Surfaces a-Physicochemical and Engineering Aspects,* 196**,** 217-222.

Choi, J. K., Lee, J. G., Kim, J. H. & Yang, H. S. 2001. Preparation of microcapsules containing phase change materials as heat transfer media by in-situ polymerization. *Journal of Industrial and Engineering Chemistry,* 7**,** 358-362.

Choi, Y.-H. & Lee, W.-K. 2010. Effects of agitation in emulsion polymerization of vinyl acetate, ethylene, and N-methylol acrylamide. *Journal of Industrial and Engineering Chemistry,* 16**,** 431-436.

Christov, N. C., Ganchev, D. N., Vassileva, N. D., Denkov, N. D., Danov, K. D. & Kralchevsky, P. A. 2002. Capillary mechanisms in membrane emulsification: oil-in-water emulsions

stabilized by Tween 20 and milk proteins. *Colloids and Surfaces A: Physicochemical and Engineering Aspects,* 209**,** 83-104.

Clare, R. J., Cunningham, A. P., Denutte, R. G. H., Medina, J., Orlandini, L. & Smets, J., inventors; The Procter and Gamble Company, assignee. Perfumes and perfume encapsulates. Blegium, patent EP 2512406A1. 2012.

Clarke, A. R. & Eberhardt, C. N. 2000. *Microscopy Techniques for Materials Science,* Cambridge, Woodhead publishing limited.

Cole, P., Adami, H. O., Trichopoulos, D. & Mandel, J. 2010. Formaldehyde and lymphohematopoietic cancers: A review of two recent studies. *Regulatory Toxicology and Pharmacology,* 58**,** 161-166.

Colt, K. K., Fernandez, G. H. & Parekh, P. P., inventors; International Flavors & Fragrances Inc., assignee. Melamine-formaldehyde microcapsule slurries for fabric article freshening. The United Kingdom, patent EP1533415. 2007.

Corle, T. R. & Kino, G. S. 1996. *Confocal Scanning Optical Microscopy and Related Imaging Systems*, Elsevier Inc.

Crank, J. 1975. *The Mathematics of diffusion,* Oxford, Oxford University Press.

Curtis, R. V. & Juszczyk, A. S. 1998. Analysis of strength data using two- and three-parameter Weibull models. *Journal of Materials Science,* 33**,** 1151-1157.

Danilatos, G. D. 1993. Introduction to the Esem Instrument. *Microscopy Research and Technique,* 25**,** 354-361.

De Luca, G., Di Maio, F. P., Di Renzo, A. & Drioli, E. 2008. Droplet detachment in cross-flow membrane emulsification: Comparison among torque- and force-based models. *Chemical Engineering and Processing,* 47**,** 1150-1158.

De Luca, G., Di Renzo, A., Di Maio, F. P. & Drioli, E. 2006. Modelling droplet formation in cross-flow membrane emulsification. *Desalination,* 199**,** 177-179.

De Luca, G. & Drioli, E. 2006. Force balance conditions for droplet formation in cross-flow membrane emulsifications. *Journal of Colloid and Interface Science,* 294**,** 436-448.

De Luca, G., Sindona, A., Giorno, L. & Drioli, E. 2004. Quantitative analysis of coupling effects in cross-flow membrane emulsification. *Journal of Membrane Science,* 229**,** 199-209.

Denutte, H. R. G., Clare, R. J., Medina, J., Cunningham, A. P., Smets, J. & Orlandini, L., inventors; The Procter and Gamble Company, assignee. Encapsulates. USA, patent US 2011/0152146 A1. 2011.

Dorsey, N. E. 1940. PROPERTIES OF ORDINARY WATER-SUBSTANCE. *News Edition, American Chemical Society,* 18**,** 215.

Dragosavac, M. M., Holdich, R. G., Vladisavljevic, G. T. & Sovilj, M. N. 2012a. Stirred cell membrane emulsification for multiple emulsions containing unrefined pumpkin seed oil with uniform droplet size. *Journal of Membrane Science,* 392**,** 122-129.

Dragosavac, M. M., Sovilj, M. N., Kosvintsev, S. R., Holdich, R. G. & Vladisavljevic, G. T. 2008. Controlled production of oil-in-water emulsions containing unrefined pumpkin seed oil using stirred cell membrane emulsification. *Journal of Membrane Science,* 322**,** 178-188.

Dragosavac, M. M., Vladisavljevic, G. T., Holdich, R. G. & Stillwell, M. T. 2012b. Production of Porous Silica Microparticles by Membrane Emulsification. *Langmuir,* 28**,** 134-143.

Drelich, J., Fang, D. Y. & White, C. L. 2002. Measurement of interfacial tension in fluid-fluid systems. *In:* SOMASUNDARAN, P. (ed.) *Encyclopedia of Surface and Colloid Science.* New York: Taylor & Francis.

Dubey, R., Shami, T. C. & Rao, K. U. B. 2009. Microencapsulation Technology and Applications. *Defence Science Journal,* 59**,** 82-95.

Dubreuil, F., Elsner, N. & Fery, A. 2003. Elastic properties of polyelectrolyte capsules studied by atomic-force microscopy and RICM. *European Physical Journal E,* 12**,** 215-221.

Edwards, M. F. & Instone, T. 2001. Particulate products - their manufacture and use. *Powder Technology,* 119**,** 9-13.

Egidi, E., Gasparini, G., Holdich, R. G., Vladisavljevic, G. T. & Kosvintsev, S. R. 2008. Membrane emulsification using membranes of regular pore spacing: Droplet size and uniformity in the presence of surface shear. *Journal of Membrane Science,* 323**,** 414-420.

Environmental-Protection-Agency. Health and Environmental Effects Profile for Formaldehyde. Cincinnati: Environmental Criteria and Assessment Office.; 1985 oct.1985.

Erik, K. 1999. *Dispersions : Characterization, Testing, and Measurement,* New York, Marcel Dekker Inc.

Erkan, G., Sariisik, M. & Pazarlioglu, N. K. 2010. The Microencapsulation of Terbinafine via In Situ Polymerization of Melamine-Formaldehyde and Their Application to Cotton Fabric. *Journal of Applied Polymer Science,* 118**,** 3707-3714.

Ezendam, J., Te Biesebeek, J. D. & Wijnhoven, S. W. P. The presence of fragrance allergens in scented consumer products. Bilthoven: Rijksinstituut voor Volksgezondheid en Milieu RIVM; 2009 2010-03-08.

Fereidoon, S. 2005. Edible Oil and Fat Products: Edible Oils. *In:* FEREIDOON, S. (ed.) *Bailey's Industrial Oil and Fat Products.* Hoboken: John Wiley and Sons.

Ferguson, P. & Jones, C. C., inventors; Unilever NV & Unilever PLC, assignee. Laundry compositions, patent EP 2496676 A1. 2012.

Ferrando, M. & Spiess, W. E. L. 2000. Review: Confocal scanning laser microscopy. A powerful tool in food science. *Food Science and Technology International,* 6**,** 267-284.

Fery, A., Dubreuil, F. & Mohwald, H. 2004. Mechanics of artificial microcapsules. *New Journal of Physics,* 6.

Fery, A. & Weinkamer, R. 2007. Mechanical properties of micro- and nanocapsules: Single-capsule measurements. *Polymer,* 48**,** 7221-7235.

Fletcher, P. D. I., Binks, B. P., Holt, B. L., Parker, J., Beaussoubre, P. & Wong, K. 2010. Drop sizes and particle coverage in emulsions stabilised solely by silica nanoparticles of irregular shape. *Physical Chemistry Chemical Physics,* 12**,** 11967-11974.

Foris, P. L., Brown, R. W. & Phillips, J. P. S., inventors; National Cash Register Corporation, assignee. Capsule manufacture. USA, patent US 4100103. 1978.

Franck, A. Application of Rheology of Polymers: TA Instruments Germany; 2010.

Frank, G., Biastoch, R. & Kummer, M., inventors; BASF Aktiengesellschaft, assignee. Microcapsules of low-formaldehyde melamine/formaldehyde resins. USA, patent US 6261483B1. 2001.

Freiberg, S. & Zhu, X. 2004. Polymer microspheres for controlled drug release. *International Journal of Pharmaceutics,* 282**,** 1-18.

Fukumori, Y., Ichikawa, H., Yamaoka, Y., Akaho, E., Takeuchi, Y., Fukuda, T., Kanamori, R. & Osako, Y. 1991. Effect of Additives on Physical-Properties of Fine Ethyl Cellulose Microcapsules Prepared by the Wurster Process. *Chemical & Pharmaceutical Bulletin,* 39**,** 164-169.

Garrett, M. H., Hooper, M. A., Hooper, B. M., Rayment, P. R. & Abramson, M. J. 1999. Increased risk of allergy in children due to formaldehyde exposure in homes. *Allergy,* 54**,** 330-337.

Gasparini, G., Holdich, R. G. & Kosvintsev, S. R. 2010. PLGA particle production for water-soluble drug encapsulation: Degradation and release behaviour. *Colloids and Surfaces B-Biointerfaces,* 75**,** 557-564.

Gasparini, G., Kosvintsev, S. R., Stillwell, M. T. & Holdich, R. G. 2008. Preparation and characterization of PLGA particles for subcutaneous controlled drug release by membrane emulsification. *Colloids and Surfaces B-Biointerfaces,* 61**,** 199-207.

Gattner, H. & Ribka, J., inventors; Cassella Farbwerke Mainkur Aktiengesellschaft, assignee. Melamine resin and dye mixtures. USA. 1975.

Gaumann, A., Laudes, M., Jacob, B., Pommersheim, R., Laue, C., Vogt, W. & Schrezenmeir, J. 2000. Effect of media composition on long-term in vitro stability of barium alginate and polyacrylic acid multilayer microcapsules. *Biomaterials,* 21**,** 1911-1917.

Ghosh, S. K. 2006a. *Functional Coatings,* Weinheim, WILEY-VCH

Ghosh, S. K. 2006b. Functional Coatings and Microencapsulation: A General Perspective. *In:* GHOSH, S. K. (ed.) *Functional Coatings.* Weinheim: WILEY-VCH

Gimenez-Arnau, A., Gimenez-Arnau, E., Serra-Baldrich, E., Lepoittevin, J. P. & Camarasa, J. G. 2002. Principles and methodology for identification of fragrance allergens in consumer products. *Contact Dermatitis,* 47**,** 345-352.

Gindl, W., Zargar-Yaghubi, F. & Wimmer, R. 2003. Impregnation of softwood cell walls with melamine-formaldehyde resin. *Bioresource Technology,* 87**,** 325-330.

Gobel, H., Schmidt, G. & Soyka, D. 1994. Effect of Peppermint and Eucalyptus Oil Preparations on Neurophysiological and Experimental Algesimetric Headache Parameters. *Cephalalgia,* 14**,** 224-234.

Godderz, L. J., Peak, M. M. & Rodgers, K. K. 2005. Analysis of biological macromolecular assemblies using static light scattering methods. *Current Organic Chemistry,* 9**,** 899-908.

Gouin, S. 2004. Microencapsulation: industrial appraisal of existing technologies and trends. *Trends in Food Science & Technology,* 15**,** 330-347.

Green, B. K., inventor National Cash Register Corporation, assignee. Oil-contanting microscopic capsules and method of making them. USA, patent US2800458. 1957.

Haefliger, O. P., Jeckelmann, N., Ouali, L. & Leon, G. 2010. Real-Time Monitoring of Fragrance Release from Cotton Towels by Low Thermal Mass Gas Chromatography Using a Longitudinally Modulating Cryogenic System for Headspace Sampling and Injection. *Analytical Chemistry,* 82**,** 729-737.

Hao, D. X., Gong, F. L., Hu, G. H., Zhao, Y. J., Lian, G. P., Ma, G. H. & Su, Z. G. 2008. Controlling factors on droplets uniformity in membrane emulsification: Experiment and modeling analysis. *Industrial & Engineering Chemistry Research,* 47**,** 6418-6425.

Happi 2009. *Household & Personal Products Industry*, Rodman Publishing Corporation.

Harris, K. R. 2009. The fractional Stokes--Einstein equation: Application to Lennard-Jones, molecular, and ionic liquids. *The Journal of Chemical Physics,* 131**,** 054503.

Hayford, D. E., inventor Appleton Papers Inc., assignee. Capsules manufacture. USA, patent US 4444699. 1984.

Hernandez, O., Rhomberg, L., Hogan, K., Siegelscott, C., Lai, D., Grindstaff, G., Henry, M. & Cotruvo, J. A. 1994. Risk Assessment of Formaldehyde. *Journal of Hazardous Materials,* 39**,** 161-172.

Hertz, A., Sarrade, S., Guizard, C. & Julbe, A. 2006. Synthesis and encapsulation of yttria stabilized zirconia particles in supercritical carbon dioxide. *Journal of the European Ceramic Society,* 26**,** 1195-1203.

Hiramoto, Y. 1963. Mechanical Properties of Sea Urchin Eggs .1. Surface Force and Elastic Modulus of Cell Membrane. *Experimental Cell Research,* 32**,** 59-&.

Hiss, T. G. & Cussler, E. L. 1973. Diffusion in high viscosity liquids. *Aiche Journal,* 19**,** 698-703.

Ho, T. T. L. 2000. *Formulating Detergents and Personal Care Products: A Complete Guide to Product Development*.

Hoffman, D. & Eisermann, H., inventors; BASF Aktiengesellschaft, assignee. Low-viscosity, melamine-formaldehyde resin microcapsule dispersions with reduced formaldehyde. USA, patent US 2003/0004226 A1. 2003.

Holdich, R. G., Dragosavac, M. M., Vladisavljevic, G. T. & Kosvintsev, S. R. 2010. Membrane Emulsification with Oscillating and Stationary Membranes. *Industrial & Engineering Chemistry Research,* 49**,** 3810-3817.

Holdich, R. G., Dragosavac, M. M., Vladisavljević, G. T. & Piacentini, E. 2013. Continuous membrane emulsification with pulsed (oscillatory) flow. *Industrial and Engineering Chemistry Research,* 52**,** 507-515.

Holdich, R. G., Ipek, I. Y., Lazrigh, M. & Shama, G. 2012. Production and Evaluation of Floating Photocatalytic Composite Particles Formed Using Pickering Emulsions and Membrane Emulsification. *Industrial & Engineering Chemistry Research,* 51**,** 12509-12516.

Holzner, G. & Verhovnik, G., inventors; Firmenich S. A., assignee. Stabilized liquid rinse-off compositions comprising fragranced aminoplast capsules, patent WO2006018694A1. 2006.

Hong, K. & Park, S. 1999a. Melamine resin microcapsules containing fragrant oil: synthesis and characterization. *Materials Chemistry and Physics,* 58**,** 128-131.

Hong, K. & Park, S. 1999b. Preparation of polyurethane microcapsules with different soft segments and their characteristics. *Reactive & Functional Polymers,* 42**,** 193-200.

Horie, T., Nakatsune, K., Matsumoto, T., Tateishi, K. & Ohmura, N. 2011. Liquid-liquid two phase flow of millichannel with a dynamic mixer. *Chemical Engineering and Processing,* 50**,** 1-8.

Hsieh, W. C., Chang, C. P. & Gao, Y. L. 2006. Controlled release properties of Chitosan encapsulated volatile Citronella Oil microcapsules by thermal treatments. *Colloids and Surfaces B-Biointerfaces,* 53**,** 209-214.

Hu, J., Xiao, Z. B., Ma, S. S., Zhou, R. J., Wang, M. X. & Li, Z. 2012. Properties of osmanthus fragrance-loaded chitosan-sodium tripolyphosphate nanoparticles delivered through cotton fabrics. *Journal of Applied Polymer Science,* 123**,** 3748-3754.

Hu, J., Xiao, Z. B., Zhou, R. J., Ma, S. S., Li, Z. & Wang, M. X. 2011. Comparison of compounded fragrance and chitosan nanoparticles loaded with fragrance applied in cotton fabrics. *Textile Research Journal,* 81**,** 2056-2064.

Hu, J. F., Chen, H. Q. & Zhang, Z. B. 2009. Mechanical properties of melamine formaldehyde microcapsules for self-healing materials. *Materials Chemistry and Physics,* 118**,** 63-70.

Hu, Y.-H., Chen, C.-Y. & Wang, C.-C. 2004. Viscoelastic properties and thermal degradation kinetics of silica/PMMA nanocomposites. *Polymer Degradation and Stability,* 84**,** 545-553.

Huisman, S. G., Dennis P.M. Van Gils & Sun, C. 2012. Applying laser Doppler anemometry inside aTaylor–Couette geometry using aray-tracer to correct for curvatureeffects. *European Journal of Mechanics - B/Fluids*.

Hunt, A. & O' Neil, R. M., inventors; BASF Se, assignee. Process for the Preparation of Microcapsules. USA, patent US 7807076. 2004.

Hutchinson, I. H. 2004. Spin stability of asymmetrically charged plasma dust. *New Journal of Physics,* 6.

Hwang, J. S., Kim, J. N., Wee, Y. J., Jang, H. G., Kim, S. H. & Ryu, H. W. 2006a. Factors affecting the characteristics of melamine resin microcapsules containing fragrant oils. *Biotechnology and Bioprocess Engineering,* 11**,** 391-395.

Hwang, J. S., Kim, J. N., Wee, Y. J., Yun, J. S., Jang, H. G., Kim, S. H. & Ryu, H. W. 2006b. Preparation and characterization of melamine-formaidehyde resin microcapsules containing fragrant oil. *Biotechnology and Bioprocess Engineering,* 11**,** 332-336.

Ibrahim, S. & Nienow, A. W. 2004. Suspension of microcarriers for cell culture with axial flow impellers. *Chemical Engineering Research & Design,* 82**,** 1082-1088.

Ichikawa, H. & Fukumori, Y. 2000. A novel positively thermosensitive controlled-release microcapsule with membrane of nano-sized poly(N-isopropylacrylamide) gel dispersed in ethylcellulose matrix. *Journal of Controlled Release,* 63**,** 107-119.

Ichiura, H., Takayama, M., Nishida, N. & Otani, Y. 2012. Interfacial polymerization preparation of functional paper coated with polyamide film containing volatile essential oil. *Journal of Applied Polymer Science,* 124**,** 242-247.

Inomata, Y., Kasuya, Y., Fujimoto, K., Handa, H. & Kawaguchi, H. 1995. Purification of Membrane-Receptors with Peptide-Carrying Affinity Latex-Particles. *Colloids and Surfaces B-Biointerfaces,* 4**,** 231-241.

Ishiyama, C. & Higo, Y. 2002. Effects of humidity on Young's modulus in poly(methyl methacrylate). *Journal of Polymer Science Part B-Polymer Physics,* 40**,** 460-465.

Jafari, M. H. S., Parvinzadeh, M. & Najafi, F. Year. Preparation of Fragrant Microencapsules and Coating on Textiles. *In:* AIP Conference Proceedings, 2007. American Institute of Physics. .

Jahns, E., Boeckh, D., Bertleff, W. & Neumann, P., inventors; BASF Aktiengesellschaft, assignee. Microcapsule Preparations And Detergents And Cleaning Agents Containing Microcapsules. USA, patent US 20030125222. 2003.

Jellinek, J. S. 1975. *The Use of Fragrance in Consumer Products,* New York/London/Sydney/Toronto, John Wiley & Sons Inc.

Jo, Y. H., Song, Y. K., Yu, H. C., Cho, S. Y., Kumar, S. V., Ryu, B. C. & Chung, C. M. 2011. Microencapsulation of Phenyl Acetate with Poly(urea-formaldehyde). *Polymer-Korea,* 35**,** 152-156.

Jono, K., Ichikawa, H., Miyamoto, M. & Fukumori, Y. 2000. A review of particulate design for pharmaceutical powders and their production by spouted bed coating. *Powder Technology,* 113**,** 269-277.

Joseph, S. & Bunjes, H. 2012. Preparation of Nanoemulsions and Solid Lipid Nanoparticles by Premix Membrane Emulsification. *Journal of Pharmaceutical Sciences,* 101**,** 2479-2489.

Ju, H. K., Kim, J. W., Han, S. H., Chang, I. S., Kim, H. K., Kang, H. H., Lee, O. S. & Suh, K. D. 2002. Thermotropic liquid-crystal/polymer microcapsules prepared by in situ suspension polymerization. *Colloid and Polymer Science,* 280**,** 879-885.

Kamat, N. P., Lee, M. H., Lee, D. & Hammer, D. A. 2011. Micropipette aspiration of double emulsion-templated polymersomes. *Soft Matter,* 7**,** 9863-9866.

Kantor, M. L., Barantsevitch, E. & Milstein, S. J., inventors; Emisphere tech. Inc., assignee. Microencapsulated frangrances and method for preparation, patent WO9747288A1. 1997.

Karyakin, K., Lavrinenko, A. & Naydenov, I., inventors; Société anonyme NAICOM, assignee. Production method of urea-melamine-formaldehyde resin, patent EP 2402379 A1. 2012.

Katagiri, K., Imai, Y., Koumoto, K., Kaiden, T., Kono, K. & Aoshima, S. 2011. Magnetoresponsive On-Demand Release of Hybrid Liposomes Formed from Fe3O4 Nanoparticles and Thermosensitive Block Copolymers. *Small,* 7**,** 1683-1689.

Kawakatsu, T., Tragardh, G. & Tragardh, C. 2001. Production of W/O/W emulsions and S/O/W pectin microcapsules by microchannel emulsification. *Colloids and Surfaces a-Physicochemical and Engineering Aspects,* 189**,** 257-264.

Keh, H. J. & Chen, P. Y. 2001. Slow Motion of a Droplet between Two Parallel Plane Walls. *Chemical Engineering Science,* 56**,** 6863-6871.

Kelly, T. J., Smith, D. L. & Satola, J. 1999. Emission rates of formaldehyde from materials and consumer products found in California homes. *Environmental Science & Technology,* 33**,** 81-88.

Kentepozidou, A. & Kiparissides, C. 1995. Production of Water-Containing Polymer Microcapsules by the Complex Emulsion Solvent Evaporation Technique - Effect of Process Variables on the Microcapsule Size Distribution. *Journal of Microencapsulation,* 12**,** 627-638.

Kestin, J., Sokolov, M. & Wakeham, W. A. 1978. Viscosity of liquid water in the range -8 ºC to 150 ºC. *Journal of Physical and Chemical Reference Data,* 7**,** 941-948.

Kim, B. S., Lobaskin, V., Tsekov, R. & Vinogradova, O. I. 2007. Dynamics and stability of dispersions of polyelectrolyte-filled multilayer microcapsules. *Journal of Chemical Physics,* 126.

Kim, J. W., Ko, J. Y., Jun, J. B., Chang, I. S., Kang, H. H. & Suh, K. D. 2003. Multihollow polymer microcapsules by water-in-oil-in-water emulsion polymerization: morphological study and entrapment characteristics. *Colloid and Polymer Science,* 281**,** 157-163.

Kim, J. W., Lee, K. S., Ju, H. K., Ryu, J. H., Han, S. H., Chang, I. S., Kang, H. H., Oh, S. G. & Suh, K. D. 2004. Microencapsulation of cholesteryl alkanoate by polymerization-induced

phase separation and its association with drugs. *Journal of Polymer Science Part a-Polymer Chemistry,* 42**,** 2202-2213.

Kobayashi, I., Uemura, K. & Nakajima, M. 2007. CFD analysis of generation of soybean oil-in-water emulsion droplets using rectangular straight-through microchannels. *Food Science and Technology Research,* 13**,** 187-192.

Kosaraju, S. L., D'ath, L. & Lawrence, A. 2006. Preparation and characterisation of chitosan microspheres for antioxidant delivery. *Carbohydrate Polymers,* 64**,** 163-167.

Kosvintsev, S. R., Gasparini, G. & Holdich, R. G. 2008. Membrane emulsification: Droplet size and uniformity in the absence of surface shear. *Journal of Membrane Science,* 313**,** 182-189.

Kosvintsev, S. R., Gasparini, G., Holdich, R. G., Cumming, I. W. & Stillwell, M. T. 2005. Liquid-liquid membrane dispersion in a stirred cell with and without controlled shear. *Industrial & Engineering Chemistry Research,* 44**,** 9323-9330.

Kou, X., Li, Q., Lei, J. D., Geng, L. Y., Deng, H. Q., Zhang, G. F., Ma, G. H., Su, Z. G. & Jiang, Q. Y. 2012. Preparation of molecularly imprinted nanospheres by premix membrane emulsification technique. *Journal of Membrane Science,* 417**,** 87-95.

Kukizaki, M. 2009. Shirasu porous glass (SPG) membrane emulsification in the absence of shear flow at the membrane surface: Influence of surfactant type and concentration, viscosities of dispersed and continuous phases, and transmembrane pressure. *Journal of Membrane Science,* 327**,** 234-243.

Kukovič, M. & Knez, E., inventors; Aero, Kemicna, Graficna in Papirna Industrija, D.O.O., assignee. Process for preparing carriers saturated or coated with microencapsulated scents, patent WO 96/09114. 1996.

Kumar, A. & Katiyar, V. 1990. Modeling and Experimental Investigation of Melamine Formaldehyde Polymerization. *Macromolecules,* 23**,** 3729-3736.

Kuroiwa, T., Kiuchi, H., Noda, K., Kobayashi, I., Nakajima, M., Uemura, K., Sato, S., Mukataka, S. & Ichikawa, S. 2009. Controlled preparation of giant vesicles from uniform water droplets obtained by microchannel emulsification with bilayer-forming lipids as emulsifiers. *Microfluidics and Nanofluidics,* 6**,** 811-821.

Kusy, R. P., Whitley, J. Q. & Kalachandra, S. 2001. Mechanical properties and interrelationships of poly(methyl methacrylate) following hydration over saturated salts. *Polymer,* 42**,** 2585-2595.

Lan, C. W., Niu, G. C. C., Chang, S. J., Yao, C. H. & Kuo, S. M. 2011. Chitosan in Applications of Biomedical Devices. *Biomedical Engineering-Applications Basis Communications,* 23**,** 51-62.

Lazenby, V., Hinwood, A., Callan, A. & Franklin, P. 2012. Formaldehyde personal exposure measurements and time weighted exposure estimates in children. *Chemosphere,* 88**,** 966-973.

Leal-Calderon, F., Thivilliers, F. & Schmitt, V. 2007. Structured emulsions. *Current Opinion in Colloid & Interface Science,* 12**,** 206-212.

Lebedeva, O. V., Kim, B. S. & Vinogradova, O. I. 2004. Mechanical properties of polyelectrolyte-filled multilayer microcapsules studied by atomic force and confocal microscopy. *Langmuir,* 20**,** 10685-10690.

Leblond, F. A., Tessier, J. & Halle, J. P. 1996. Quantitative method for the evaluation of biomicrocapsule resistance to mechanical stress. *Biomaterials,* 17**,** 2097-2102.

Lee, D. H., Sim, G. S., Kim, J. H., Lee, G. S., Pyo, H. B. & Lee, B. C. 2007a. Preparation and characterization of quercetin-loaded polymethyl methacrylate microcapsules using a polyol-in-oil-in-polyol emulsion solvent evaporation method. *Journal of Pharmacy and Pharmacology,* 59**,** 1611-1620.

Lee, K. & Popplewell, L. M., inventors; International Flavors & Fragrances Inc., assignee. Stable fragrance microcapsule suspension and process for using same. USA, patent US 2005/0227907 A1. 2005.

Lee, K. D., Popplewell, L. M. & Anastasiou, T. J., inventors; International Flavors & Fragrances Inc., assignee. Process for preparing a high stability microcapsule product and method for using same. USA, patent US 2007/0138673 A1. 2007b.

Lee, Y. H., Kim, C. A., Jang, W. H., Choi, H. J. & Jhon, M. S. 2001. Synthesis and electrorheological characteristics of microencapsulated polyaniline particles with melamine-formaldehyde resins. *Polymer,* 42**,** 8277-8283.

Li, J. H., Guan, Y. X., Wang, H. Q. & Yao, S. J. 2009. Dehydrogenation of 11 alpha-hydroxy-16 alpha, 17-epoxyprogesterone by encapsulated Arthrobacter simplex cells in an aqueous/organic solvent two-liquid-phase system. *Journal of Chemical Technology and Biotechnology,* 84**,** 208-214.

Li, W. 2010. *Integrated Droplet-Based Microfluidics for Chemical Reactions and Processes* Doctor of Philosophy, University of Toronto.

Li, W., Wang, J., Wang, X., Wu, S. & Zhang, X. 2007a. Effects of ammonium chloride and heat treatment on residual formaldehyde contents of melamine-formaldehyde microcapsules. *Colloid and Polymer Science,* 285**,** 1691-1697.

Li, W., Wang, J. P., Wang, X. C., Wu, S. Z. & Zhang, X. X. 2007b. Effects of ammonium chloride and heat treatment on residual formaldehyde contents of melamine-formaldehyde microcapsules. *Colloid and Polymer Science,* 285**,** 1691-1697.

Li, W., Zhang, X. X., Wang, X. C. & Niu, J. J. 2007c. Preparation and characterization of microencapsulated phase change material with low remnant formaldehyde content. *Materials Chemistry and Physics,* 106**,** 437-442.

Liu, F., Wen, L. X., Li, Z. Z., Yu, W., Sun, H. Y. & Chen, J. F. 2006. Porous hollow silica nanoparticles as controlled delivery system for water-soluble pesticide. *Materials Research Bulletin,* 41**,** 2268-2275.

Liu, K. K., Williams, D. R. & Briscoe, B. J. 1998. The large deformation of a single micro-elastomeric sphere. *Journal of Physics D-Applied Physics,* 31**,** 294-303.

Liu, M. 2010. *Understanding the Mechanical Strength of Microcapsules and Their Adhesion on Fabric Surfaces.* DOCTOR OF PHILOSOPHY, University of Birmingham.

Liu, R., Ma, G. H., Meng, F. T. & Su, Z. G. 2005a. Preparation of uniform-sized PLA microcapsules by combining Shirasu Porous Glass membrane emulsification technique and multiple emulsion-solvent evaporation method. *Journal of Controlled Release,* 103**,** 31-43.

Liu, T., Donald, A. M. & Zhang, Z. 2005b. Novel manipulation in environmental scanning electron microscope for measuring mechanical properties of single nanoparticles. *Materials Science and Technology,* 21**,** 289-294.

Long, Y., Vincent, B., York, D., Zhang, Z. B. & Preece, J. A. 2010. Organic-inorganic double shell composite microcapsules. *Chemical Communications,* 46**,** 1718-1720.

Long, Y., York, D., Zhang, Z. B. & Preece, J. A. 2009. Microcapsules with low content of formaldehyde: preparation and characterization. *Journal of Materials Chemistry,* 19**,** 6882-6887.

Loxley, A. & Vincent, B. 1998. Preparation of poly(methylmethacrylate) microcapsules with liquid cores. *Journal of Colloid and Interface Science,* 208**,** 49-62.

Luo, W. J., Yang, W., Jiang, S., Feng, J. M. & Yang, M. B. 2007. Microencapsulation of decabromodiphenyl ether by in situ polymerization: Preparation and characterization. *Polymer Degradation and Stability,* 92**,** 1359-1364.

Ma, G. 2003. Control of polymer particle size using porous glass membrane emulsification: A review. *China Particuology,* 1**,** 105-114.

Ma, L. W., Liu, M. Z. & Shi, X. 2012. pH- and temperature-sensitive self-assembly microcapsules/microparticles: Synthesis, characterization, in vitro cytotoxicity, and drug release properties. *Journal of Biomedical Materials Research Part B-Applied Biomaterials,* 100B**,** 305-313.

Madene, A., Jacquot, M., Scher, J. & Desobry, S. 2006. Flavour encapsulation and controlled release - a review. *International Journal of Food Science and Technology,* 41**,** 1-21.

Malvern Instruments Limited. A Basic Guide to Particle Characterization. Worcestershire: Malvern instruments limited; 2012.

Malvern Instruments Ltd. Optical property validation: Comparing laser diffraction and image analysis measurements Worcestershire; 2007.

Manga, M. S., Cayre, O. J., Williams, R. A., Biggs, S. & York, D. W. 2012. Production of solid-stabilised emulsions through rotational membrane emulsification: influence of particle adsorption kinetics. *Soft Matter,* 8**,** 1532-1538.

Martin-Banderas, L., Flores-Mosquera, M., Riesco-Chueca, P., Rodriguez-Gil, A., Cebolla, A., Chavez, S. & Ganan-Calvo, A. M. 2005. Flow focusing: A versatile technology to produce size-controlled and specific-morphology microparticles. *Small,* 1**,** 688-692.

Masataka, K. & Yasuhiro, O., inventors; Fuji photo fim, assignee. Process for preparing microcapsules. USA, patent US 3981821. 1976.

Mashmoushy, H., Zhang, Z. & Thomas, C. R. 1998. Micromanipulation measurement of the mechanical properties of baker's yeast cells. *Biotechnology Techniques,* 12**,** 925-929.

Mercade-Prieto, R., Allen, R., York, D., Preece, J. A., Goodwin, T. E. & Zhang, Z. 2012a. Determination of the Failure Stresses for Fluid-filled Microcapsules that Rupture Near the Elastic Regime. *Experimental Mechanics,* 52**,** 1435-1445.

Mercade-Prieto, R., Allen, R., York, D., Preece, J. A., Goodwin, T. E. & Zhang, Z. B. 2011a. Compression of elastic-perfectly plastic microcapsules using micromanipulation and finite element modelling: Determination of the yield stress. *Chemical Engineering Science,* 66**,** 1835-1843.

Mercade-Prieto, R., Allen, R., York, D., Preece, J. A., Goodwin, T. E. & Zhang, Z. B. 2012b. Determination of the shell permeability of microcapsules with a core of oil-based active ingredient. *Journal of Microencapsulation,* 29**,** 463-474.

Mercade-Prieto, R., Allen, R., Zhang, Z. B., York, D., Preece, J. A. & Goodwin, T. E. 2012c. Failure of elastic-plastic core-shell microcapsules under compression. *Aiche Journal,* 58**,** 2674-2681.

Mercade-Prieto, R., Nguyen, B., Allen, R., York, D., Preece, J. A., Goodwin, T. E. & Zhang, Z. B. 2011b. Determination of the elastic properties of single microcapsules using micromanipulation and finite element modeling. *Chemical Engineering Science,* 66**,** 2042-2049.

Mercadé-Prieto, R., Pan, X., Fernández-González, A., Zhang, Z. & Bakalis, S. 2012a. Quantification of Microcapsules Deposited in Cotton Fabrics before and after Abrasion Using Fluorescence Microscopy. *Industrial & Engineering Chemistry Research,* 51**,** 16741-16749.

Mercadé-Prieto, R., Pan, X., Fernández-González, A., Zhang, Z. & Bakalis, S. 2012b. Quantification of Microcapsules Deposited in Cotton Fabrics before and after Abrasion Using Fluorescence Microscopy. *Industrial & Engineering Chemistry Research,* 51**,** 16741–16749.

Mercade-Prieto, R. & Zhang, Z. B. 2012. Mechanical characterization of microspheres - capsules, cells and beads: a review. *Journal of Microencapsulation,* 29**,** 277-285.

Mihranyan, A., Ferraz, N. & Stromme, M. 2012. Current status and future prospects of nanotechnology in cosmetics. *Progress in Materials Science,* 57**,** 875-910.

Moira, P. P. D., inventor The Wiggins Teape Group Limited, assignee. Self-contained pressure sensitive copying material and its production. USA, patent US 4612556. 1986.

Monllor, P., Bonet, M. A. & Cases, F. 2007. Characterization of the behaviour of flavour microcapsules in cotton fabrics. *European Polymer Journal,* 43**,** 2481-2490.

Mulqueen, M. & Huibers, P. D. T. 2002. Measuring Equilibrium Surface Tensions. *Analysis and characterization in surface chemistry.* Cambridge, USA: John Wiley and Sons.

Murua, A., Portero, A., Orive, G., Hernandez, R. M., De Castro, M. & Pedraz, J. L. 2008. Cell microencapsulation technology: Towards clinical application. *Journal of Controlled Release,* 132**,** 76-83.

Nagata, S. 1975. *Mixing: Principles and Applications and Research in Food Processing,* Tokyo, Halsted Press.

Nakashima, T. & Shimizu, M. 1988. Porous glass from calcium alumino borosilicate glass. *Ceramics,* 21**,** 408.

Nakashima, T., Shimizu, M. & Kukizaki, M. Membrane Emulsification, Operation Manual. Miyazaki, Japan: Industrial Research Institute of Miyazaki Prefecture; 1991.

Nakashima, T., Shimizu, M. & Kukizaki, M. 2000. Particle control of emulsion by membrane emulsification and its applications. *Advanced Drug Delivery Reviews,* 45**,** 47-56.

Nazir, A., Schroen, K. & Boom, R. 2010. Premix emulsification: A review. *Journal of Membrane Science,* 362**,** 1-11.

Nazir, H., Lv, P. P., Wang, L. Y., Lian, G. P., Zhu, S. P. & Ma, G. H. 2011. Uniform-sized silicone oil microemulsions: Preparation, investigation of stability and deposition on hair surface. *Journal of Colloid and Interface Science,* 364**,** 56-64.

Nelson, G. 2002. Application of microencapsulation in textiles. *International Journal of Pharmaceutics,* 242**,** 55-62.

Nesic, V., Sipetic, S., Vlajinac, H., Stosic-Divjak, S. & Jesic, S. 2010. Risk Factors for the Occurrence of Undifferentiated Carcinoma of Nasopharyngeal Type: A Case-Control Study. *Srpski Arhiv Za Celokupno Lekarstvo,* 138**,** 6-10.

Ness, N. J., inventor Quest International B.V., assignee. Perfume encapsulates. The United Kingdom, patent EP1368115 A1. 2003.

Ness, N. J., inventor Quest International Services B.V. , assignee. Perfume encapsulates USA, patent US 7238655. 2007.

Nordstierna, L., Abdalla, A. A., Nordin, M. & Nyden, M. 2010. Comparison of release behaviour from microcapsules and microspheres. *Progress in Organic Coatings,* 69**,** 49-51.

O'sullivan, M., Zhang, Z. B. & Vincent, B. 2009. Silica-Shell/Oil-Core Microcapsules with Controlled Shell Thickness and Their Breakage Stress. *Langmuir,* 25**,** 7962-7966.

Ohtsubo, T., Tsuda, S. & Tsuji, K. 1991. A Study of the Physical Strength of Fenitrothion Microcapsules. *Polymer,* 32**,** 2395-2399.

Okada, Y. & Igarashi, Y., inventors; Kureha Kagaku Kogyo Kabushiki Kaisha, assignee. Process for producing a microcapsule. USA, patent US 4460722. 1984.

Okada, Y. & Igarashi, Y., inventors; Kureha Kagaku Kogyo Kabushiki Kaisha, assignee. Microcapsule for pressure-sensitive recording paper and process for producing the same. USA, patent US 4562116. 1985.

Okano, M. & Ogata, Y. 1952. Kinetics of the Condensation of Melamine with Formaldehyde. 74**,** 5728-5731.

Okubo, M. & Hattori, H. 1993. Studies on Suspension and Emulsion .138. Competitive Adsorption of Fibrinogen and Albumin onto Polymer Microspheres Having Hydrophilic/Hydrophobic Heterogeneous Surface-Structures. *Colloid and Polymer Science,* 271**,** 1157-1164.

Omi, S., Kanetaka, A., Shimamori, Y., Supsakulchai, A., Nagai, M. & Ma, G. H. 2001. Magnetite (Fe3O4) microcapsules prepared using a glass membrane and solvent removal. *Journal of Microencapsulation,* 18**,** 749-765.

Paramita, V., Iida, K., Yoshii, H. & Furuta, T. 2010. Effect of Feed Liquid Temperature on the Structural Morphologies of d-Limonene Microencapsulated Powder and Its Preservation. *Journal of Food Science,* 75**,** E39-E45.

Parekh, P. P., Fernandez, G. H. & Colt, K. K., inventors; International Flavors & Fragrances Inc., assignee. Melamine-formaldehyde microcapsule slurries for fabric article freshening. USA, patent US 2005/0113282. 2005.

Park, S.-J., Kim, K.-S. & Kim, S.-H. 2005. Effect of poly(ethylene oxide) on the release behaviors of poly(ε-caprolactone) microcapsules containing erythromycin. *Colloids and Surfaces B: Biointerfaces,* 43**,** 238-244.

Park, S. I., Park, N. H. & Suh, K. D. 2002. The effect of mono-sized liquid crystal domains on electro-optical properties in a polymer dispersed liquid crystal prepared by using monodisperse poly(methylmethacrylate)/liquid crystal microcapsules. *Liquid Crystals,* 29**,** 783-787.

Peirone, M. A., Delaney, K., Kwiecin, J., Fletch, A. & Chang, P. L. 1998. Delivery of recombinant gene product to canines with nonautologous microencapsulated cells. *Human Gene Therapy,* 9**,** 195-206.

Pena, B., De Menorval, L. C., Garcia-Valls, R. & Gumi, T. 2011. Characterization of Polysulfone and Polysulfone/Vanillin Microcapsules by H-1 NMR Spectroscopy, Solid-State C-13 CP/MAS-NMR Spectroscopy, and N-2 Adsorption Desorption Analyses. *Acs Applied Materials & Interfaces,* 3**,** 4420-4430.

Pena, B., Panisello, C., Areste, G., Garcia-Valls, R. & Gumi, T. 2012. Preparation and characterization of polysulfone microcapsules for perfume release. *Chemical Engineering Journal,* 179**,** 394-403.

Peng, S. J. & Williams, R. A. 1998a. Controlled production of emulsions using a crossflow membrane. *Particle & Particle Systems Characterization,* 15**,** 21-25.

Peng, S. J. & Williams, R. A. 1998b. Controlled production of emulsions using a crossflow membrane part I: Droplet formation from a single pore. *Chemical Engineering Research & Design,* 76**,** 894-901.

Piacentini, E., Giorno, L., Dragosavac, M. M., Vladisavljević, G. T. & Holdich, R. G. 2013. Microencapsulation of oil droplets using cold water fish gelatine/gum arabic complex coacervation by membrane emulsification. *Food Research International,* 53**,** 362-372.

Pluyter, J. G. L. & Anastasiou, T. J., inventors; International flavors & fragrances., assignee. Encapsulated Fragrance Materials and Methods for Making Same. The United Kingdom, patent EP 1719554. 2006.

Polakovic, M., Gorner, T., Gref, R. & Dellacherie, E. 1999. Lidocaine loaded biodegradable nanospheres II. Modelling of drug release. *Journal of Controlled Release,* 60**,** 169-177.

Popplewell, L. M., Brain, J., Pluyter, J. G. L., Zhen, Y. & Lee, K. D., inventors; International Flavors & Fragrances Inc., assignee. Encapsulated materials. USA, patent US 20050112152. 2005.

Popplewell, L. M., Guerry, R., Zhen, Y. & Joyce, C., inventors; International Flavors & Fragrances Inc., assignee. Hard surface cleaning compositions and methods for making same. USA, patent US 2006/0258557. 2006.

Popplewell, L. M., Lee, K. & Pluyter, J. G. L., inventors; International Flavors & Fragrances Inc., assignee. Encapsulated fragrance chemicals. USA, patent US 2004/0071742 A1. 2004.

Poux, S. & Meier, W. 2005. Synthesis and characterization of new polymer nanocontainers. *Macromolecular Symposia,* 222**,** 157-162.

Pranzetti, A., Salaun, S., Mieszkin, S., Callow, M. E., Callow, J. A., Preece, J. A. & Mendes, P. M. 2012. Model Organic Surfaces to Probe Marine Bacterial Adhesion Kinetics by Surface Plasmon Resonance. *Advanced Functional Materials,* 22**,** 3672-3681.

Pretzl, M., Neubauer, M., Tekaat, M., Kunert, C., Kuttner, C., Leon, G., Berthier, D., Erni, P., Ouali, L. & Fery, A. 2012. Formation and Mechanical Characterization of Aminoplast Core/Shell Microcapsules. *Acs Applied Materials & Interfaces,* 4**,** 2940-2948.

Pugh, R. J. 2005. Experimental techniques for studying the structure of foams and froths. *Advances in Colloid and Interface Science,* 114**,** 239-251.

Quellet, C. & Hotz, J., inventors; Givaudan SA, assignee. Product, patent WO 2009100553. 2009.

Ramelow, U. S. & Pingili, S. 2010. Synthesis of Ethylene Glycol Dimethacrylate-Methyl Methacrylate Copolymers, Determination of their Reactivity Ratios, and a Study of Dopant and Temperature Effects on their Conductivities *Polymers,* 2**,** 265-285.

Rasmussen, W. L. C. 2001. *Novel Carbazole Based Methacrylates, Acrylates, and Dimethacrylates to Produce High Refractive Index Polymers.* Doctor of Philosophy, Virginia Polytechnic Institute and State University.

Rayner, M., Tragardh, G. & Tragardh, C. 2005. The impact of mass transfer and interfacial expansion rate on droplet size in membrane emulsification processes. *Colloids and Surfaces a-Physicochemical and Engineering Aspects,* 266**,** 1-17.

Rayner, M., Tragardh, G., Tragardh, C. & Dejmek, P. 2004. Using the Surface Evolver to model droplet formation processes in membrane emulsification. *Journal of Colloid and Interface Science,* 279**,** 175-185.

Rehor, A., Canaple, L., Zhang, Z. B. & Hunkeler, D. 2001. The compressive deformation of multicomponent microcapsules: Influence of size, membrane thickness, and compression speed. *Journal of Biomaterials Science-Polymer Edition,* 12**,** 157-170.

Reissner 2006. *Elsner Progr Colloid Polym Sci,* 132**,** 117-123.

Ren, Y. L., Donald, A. M. & Zhang, Z. B. 2007. Investigation of radiation damage to microcapsules in environmental SEM. *Materials Science and Technology,* 23**,** 857-864.

Renken, A. & Hunkeler, D. 1998. Microencapsulation: a review of polymers and technologies with a focus on bioartificial organs. *Polimery,* 43**,** 530-539.

Retiveau, A. The Role of Fragrance in Personal Care Products; 2012.

Ribeiro, H. S., Rico, L. G., Badolato, G. G. & Schubert, H. 2005. Production of O/W emulsions containing astaxanthin by repeated Premix membrane emulsification. *Journal of Food Science,* 70**,** E117-E123.

Rodrigues, S. N., Fernandes, I., Martins, I. M., Mata, V. G., Barreiro, F. & Rodrigues, A. I. 2008. Microencapsulation of limonene for textile application. *Industrial & Engineering Chemistry Research,* 47**,** 4142-4147.

Rodrigues, S. N., Martins, I. M., Fernandes, I. P., Gomes, P. B., Mata, V. G., Barreiro, M. F. & Rodrigues, A. E. 2009. Scentfashion (R): Microencapsulated perfumes for textile application. *Chemical Engineering Journal,* 149**,** 463-472.

Rueger, P. E. & Calabrese, R. V. Dispersion of water into oil in a rotor–stator mixer. Part 1: Drop breakup in dilute systems. *Chemical Engineering Research and Design*.

Ryu, J. H., Lee, S. G. & Suh, K. D. 2004. The influence of nematic liquid crystal content on the electrooptical properties of a polymer dispersed liquid crystal prepared with monodisperse liquid crystal microcapsules. *Liquid Crystals,* 31**,** 1587-1593.

Saeki, K., Matsukawa, H. & Satomura, M., inventors; Fuji Photo Film Co., Ltd., assignee. Method for preparing microcapsules. USA, patent US 4251386. 1981.

Sakai, S., Ito, S., Inagaki, H., Hirose, K., Matsuyama, T., Taya, M. & Kawakami, K. 2011. Cell-enclosing gelatin-based microcapsule production for tissue engineering using a microfluidic flow-focusing system. *Biomicrofluidics,* 5.

Salari, J. W. O., Leermakers, F. A. M. & Klumperman, B. 2011. Pickering Emulsions: Wetting and Colloidal Stability of Hairy Particles-A Self-Consistent Field Theory. *Langmuir,* 27**,** 6574-6583.

Salari, M. H., Amine, G., Shirazi, M. H., Hafezi, R. & Mohammadypour, M. 2006. Antibacterial effects of Eucalyptus globulus leaf extract on pathogenic bacteria isolated from specimens of patients with respiratory tract disorders. *Clinical Microbiology and Infection,* 12**,** 194-196.

Salentinig, S., Yaghmur, A., Guillot, S. & Glatter, O. 2008. Preparation of highly concentrated nanostructured dispersions of controlled size. *Journal of Colloid and Interface Science,* 326**,** 211-220.

Salgi, P. & Rajagopalan, R. 1993. Polydispersity in Colloids - Implications to Static Structure and Scattering. *Advances in Colloid and Interface Science,* 43**,** 169-288.

Sari, A., Alkan, C., Karaipekli, A. & Uzun, O. 2009. Microencapsulated n-octacosane as phase change material for thermal energy storage. *Solar Energy,* 83**,** 1757-1763.

Sato, K. 1968. Condensation of Methylolmelamine. *Bulletin of the chemical society of Japan,* 41**,** 7-17.

Sato, K., Nakajima, T. & Anzai, J. 2012. Preparation of poly(methyl methacrylate) microcapsules by in situ polymerization on the surface of calcium carbonate particles. *Journal of Colloid and Interface Science,* 387**,** 123-126.

Sawalha, H., Fan, Y. X., Schroen, K. & Boom, R. 2008. Preparation of hollow polylactide microcapsules through premix membrane emulsification-Effects of nonsolvent properties. *Journal of Membrane Science,* 325**,** 665-671.

Schaab, C. K. & Tararuj, C., inventors; Webcraft Technologies, Inc., assignee. Powder and microcapsule fragrance enhanced sampler. USA, patent US 4952400 A. 1988.

Schibler, L., inventor Ciba, Limited., assignee. Process for the Encapsulation of Dispersible Materials USA, patent US 3594328. 1971.

Schmidt, C. J., Tebbett, I. R. & Couch, M. W. 2000. Carbonless copy paper: A review of its chemical components and health hazards. *American Industrial Hygiene Association Journal,* 61**,** 214-222.

Schroder, V., Behrend, O. & Schubert, H. 1998. Effect of dynamic interfacial tension on the emulsification process using microporous, ceramic membranes. *Journal of Colloid and Interface Science,* 202**,** 334-340.

Schroder, V. & Schubert, H. 1999. Production of emulsions using microporous, ceramic membranes. *Colloids and Surfaces a-Physicochemical and Engineering Aspects,* 152**,** 103-109.

Schwarb, F., Imanidis, G., Smith, E., Haigh, J. & Surber, C. 1999. Effect of Concentration and Degree of Saturation of Topical Fluocinonide Formulations on In Vitro Membrane Transport and In Vivo Availability on Human Skin. *Pharmaceutical Research,* 16**,** 909-915.

Seitz, M. E., inventor The Standard Register Company, assignee. Melamine-formaldehyde microencapsulation in aqueous solutions containing high concentrations of organic solvent. USA, patent US 5268130. 1990.

Seitz, M. E., inventor The Standard Register Company, assignee. Microencapsulation process using melamine-formaldehyde and microcapsules producted thereby. USA, patent US 5204185. 1993.

Sgraja, M., Blomer, J., Bertling, J. & Jansens, P. J. 2008. In Situ Encapsulation of Tetradecane Droplets in Oil-in-Water Emulsions Using Amino Resins. *Journal of Applied Polymer Science,* 110**,** 2366-2373.

Shen, J., Chen, C. C. & Sauer, J. A. 1985. Effects of Sorbed Water on Properties of Low and High Molecular-Weight Pmma .1. Deformation and Fracture-Behavior. *Polymer,* 26**,** 511-518.

Shen, J., Qin, Y., Wang, G. X., Fu, X., Wei, C. & Lei, B. 2011. Relative permeabilities of gas and water for different rank coals. *International Journal of Coal Geology,* 86**,** 266-275.

Sinclair, P., inventor The Wiggins Teape Group Limited, assignee. Production of microcapsules. The United Kingdom, patent GB2073132. 1981.

Skoog, D. A., West, D. M., Holler, F. J. & Crouch, S. R. 1999. *Analytical Chemistry: An Introduction* Thomson Learning.

Smets, J., Nair, R. J., Pintens, A., Yasuhara, T. & Iwasaki, T., inventors; The Procter and Gamble Company, assignee. Microcapsule and method of producing same. USA, patent US 7901772. 2011a.

Smets, J., Vansteenwinckel, P. C. A., Gizaw, Y., Hulskotter, F., Boechh, D. & Haehnle, H.-J., inventors; The Procter and Gamble Company, assignee. High-efficiency perfume capsules. USA, patent US 2011/0111999. 2011b.

Smith, A. E., Zhang, Z. & Thomas, C. R. 2000. Wall material properties of yeast cells: Part 1. Cell measurements and compression experiments. *Chemical Engineering Science,* 55**,** 2031-2041.

Soderholm, K. J. & Calvert, P. D. 1983. Effects of Water on Glass-Filled Methacrylate Resins. *Journal of Materials Science,* 18**,** 2957-2962.

Sohn, S. O., Lee, S. M., Kim, Y. M., Yeum, J. H., Choi, J. H. & Do Ghim, H. 2007. Aroma finishing of PET fabrics with PVAc nanoparticles containing lavender oil. *Fibers and Polymers,* 8**,** 163-167.

Soliman, K. & Marschall, E. 1990. Viscosity of selected binary, ternary, and quaternary liquid mixtures. *Journal of Chemical & Engineering Data,* 35**,** 375-381.

Song, Y. C., Tong, W. J. & Gao, C. Y. 2012. Regulation of Free Carboxylate Groups of Alginate Microspheres with Nacl Solution and Its Effect in Doxorubicin Loading and Release. *Acta Polymerica Sinica***,** 771-777.

Sotoyama, K., Asano, Y., Ihara, K., Takahashi, K. & Doi, K. 1999. Water oil emulsions prepared by the membrane emulsification method and their stability. *Journal of Food Science,* 64**,** 211-215.

Specos, M. M. M., Escobar, G., Marino, P., Puggia, C., Tesoriero, M. V. D. & Hermida, L. 2010. Aroma Finishing of Cotton Fabrics by Means of Microencapsulation Techniques. *Journal of Industrial Textiles,* 40**,** 13-32.

St. Laurent, C. T. R. J. B., Carrara, G., Denutte, G. R. H., D'hardemare, R., Gray, G. P., Mariani, M., Merere, I., Orchard, J. A., Topkara, H. S. & Smets, J., inventors; The Procter and Gamble Company, assignee. Perfuming method and product, patent WO2007030511A1. 2007.

Stachurski, Z. H. 2003. Strength and deformation of rigid polymers: the stress-strain curve in amorphous PMMA. *Polymer,* 44**,** 6067-6076.

Stenekes, R. J. H., De Smedt, S. C., Demeester, J., Sun, G. Z., Zhang, Z. B. & Hennink, W. E. 2000. Pore sizes in hydrated dextran microspheres. *Biomacromolecules,* 1**,** 696-703.

Stillwell, M. T., Holdich, R. G., Kosvintsev, S. R., Gasparini, G. & Cumming, I. W. 2007. Stirred cell membrane emulsification and factors influencing dispersion drop size and uniformity. *Industrial & Engineering Chemistry Research,* 46**,** 965-972.

Stoffel, M., Wahl, S., Lorenceau, E., Hohler, R., Mercier, B. & Angelescu, D. 2012. Study of a new multi channel foam and emulsion generator. *MRS Proceedings,* 1425.

Su, J. F., Wang, L. X., Ren, L. & Huang, Z. 2007. Mechanical properties and thermal stability of double-shell thermal-energy-storage microcapsules. *Journal of Applied Polymer Science,* 103**,** 1295-1302.

Su, J. F., Wang, S. B., Zhang, Y. Y. & Huang, Z. 2011. Physicochemical properties and mechanical characters of methanol-modified melamine-formaldehyde (MMF) shell microPCMs containing paraffin. *Colloid and Polymer Science,* 289**,** 111-119.

Su, J. F., Wang, X. Y. & Dong, H. 2012. Influence of temperature on the deformation behaviors of melamine-formaldehyde microcapsules containing phase change material. *Materials Letters,* 84**,** 158-161.

Sumiga, B., Knez, E., Vrtacnik, M., Savec, V. F., Staresinic, M. & Boh, B. 2011. Production of Melamine-Formaldehyde PCM Microcapsules with Ammonia Scavenger used for Residual Formaldehyde Reduction. *Acta Chimica Slovenica,* 58**,** 14-25.

Sun, G. & Zhang, Z. 2001. Mechanical properties of melamine-formaldehyde microcapsules. *Journal of Microencapsulation,* 18**,** 593-602.

Sun, G. & Zhang, Z. 2002. Mechanical strength of microcapsules made of different wall materials. *International Journal of Pharmaceutics,* 242**,** 307-311.

Sympatec. Image Analysis; 2012.

Taber, L. A. 1982. Large Deflection of a Fluid-Filled Spherical-Shell under a Point Load. *Journal of Applied Mechanics-Transactions of the Asme,* 49**,** 121-128.

Taguchi, Y. & Tanaka, M. 2001. Preparation of microcapsules composed of waste-expanded polystyrene and paper fiber by semichemical recycle. *Journal of Applied Polymer Science,* 80**,** 2662-2669.

Taguchi, Y., Yokoyama, H., Kado, H. & Tanaka, M. 2007. Preparation of PCM microcapsules by using oil absorbable polymer particles. *Colloids and Surfaces a-Physicochemical and Engineering Aspects,* 301**,** 41-47.

Takeuchi, S., Garstecki, P., Weibel, D. B. & Whitesides, G. M. 2005. An axisymmetric flow-focusing microfluidic device. *Advanced Materials,* 17**,** 1067-+.

Tan, T. F., Wang, S. R., Li, X. G., Wang, C. Y. & An, Y. 2009. Facile preparation and characterization of hollow poly(St-co-MMA-co-BA-co-MAA) core-double shell latex nanoparticles for electrophoretic displays. *Current Applied Physics,* 9**,** 989-992.

Tang, E., Cheng, G. & Ma, X. 2006. Preparation of nano-ZnO/PMMA composite particles via grafting of the copolymer onto the surface of zinc oxide nanoparticles. *Powder Technology,* 161**,** 209-214.

Tavera, E. M., Kadali, S. B., Bagaria, H. G., Liu, A. W. & Wong, M. S. 2009. Experimental and modeling analysis of diffusive release from single-shell microcapsules. *Aiche Journal,* 55**,** 2950-2965.

Teixeira, C. S. N. R., Martins, I. M. D., Mata, V. L. G., Barreiro, M. F. F. & Rodrigues, A. E. 2012a. Characterization and evaluation of commercial fragrance microcapsules for textile application. *Journal of the Textile Institute,* 103**,** 269-282.

Teixeira, M. A., Rodriguez, O., Rodrigues, S., Martins, I. & Rodrigues, A. E. 2012b. A case study of product engineering: Performance of microencapsulated perfumes on textile applications. *Aiche Journal,* 58**,** 1939-1950.

Thomas, C. R., Zhang, Z. & Cowen, C. 2000. Micromanipulation measurements of biological materials. *Biotechnology Letters,* 22**,** 531-537.

Timgren, A., Tragardh, G. & Tragardh, C. 2010. A model for drop size prediction during cross-flow emulsification. *Chemical Engineering Research & Design,* 88**,** 229-238.

Turchiuli, C., Lemarié, N., Cuvelier, M.-E. & Dumoulin, E. 2013. Production of fine emulsions at pilot scale for oil compounds encapsulation. *Journal of Food Engineering,* 115**,** 452-458.

Tzhayik, O., Cavaco-Paulo, A. & Gedanken, A. 2012. Fragrance release profile from sonochemically prepared protein microsphere containers. *Ultrasonics Sonochemistry,* 19**,** 858-863.

Uchiyama, H., Cetti, J. R., Alonso, M., Montezinos, D. L. & Cobb, D. S., inventors; The Procter and Gamble Company, assignee. Compositions comprising a dispersant and microcapsules containing an active material. USA, patent US 2003/0216488 A1. 2003a.

Uchiyama, H., Cetti, J. R., Alonso, M., Montezinos, D. L. & Cobb, D. S., inventors; The Procter and Gamble Company, assignee. Malodor-controlling compositions comprising odor control agents and microcapsules containing an active material. USA, patent US 2003/0215417 A1. 2003b.

Ullah, A., Holdich, R. G., Naeem, M. & Starov, V. M. 2012a. Shear enhanced microfiltration and rejection of crude oil drops through a slotted pore membrane including migration velocities. *Journal of Membrane Science,* 421**,** 69-74.

Ullah, A., Holdich, R. G., Naeem, M. & Starov, V. M. 2012b. Stability and deformation of oil droplets during microfiltration on a slotted pore membrane. *Journal of Membrane Science,* 401**,** 118-124.

Umer, H., Nigam, H., Tamboli, A. M. & Nainar, M. S. M. 2011. Microencapsulation: Process, Techniques and Applications. *International Journal of Research in Pharmaceutical and Biomedical Sciences,* 2**,** 474-481.

Van Der Graaf, S., Nisisako, T., Schroen, C. G. P. H., Van Der Sman, R. G. M. & Boom, R. M. 2006. Lattice Boltzmann simulations of droplet formation in a T-shaped microchannel. *Langmuir,* 22**,** 4144-4152.

Van Dijke, K. C., Schroen, K., Van Der Padt, A. & Boom, R. 2010. EDGE emulsification for food-grade dispersions. *Journal of Food Engineering,* 97**,** 348-354.

Vincent, P. I. 1972. Correlation between Critical Tensile-Strength and Polymer Cross-Sectional Area. *Polymer,* 13**,** 558-&.

Vinogradova, O. I. 2004. Mechanical properties of polyelectrolyte multilayer microcapsules. *Journal of Physics-Condensed Matter,* 16**,** R1105-R1134.

Vladisavljevic, G. T., Kobayashi, I. & Nakajima, M. 2008. Generation of highly uniform droplets using asymmetric microchannels fabricated on a single crystal silicon plate: Effect of emulsifier and oil types. *Powder Technology,* 183**,** 37-45.

Vladisavljevic, G. T., Shimizu, M. & Nakashima, T. 2004. Preparation of monodisperse multiple emulsions at high production rates by multi-stage premix membrane emulsification. *Journal of Membrane Science,* 244**,** 97-106.

Vladisavljevic, G. T. & Williams, R. A. 2005. Recent developments in manufacturing emulsions and particulate products using membranes. *Advances in Colloid and Interface Science,* 113**,** 1-20.

Vo, T. D. T., Himmelsbach, M., Haunschmidt, M., Buchberger, W., Schwarzinger, C. & Klampfl, C. W. 2008. Improved analysis of melamine-formaldehyde resins by capillary zone electrophoresis-mass spectrometry using ion-trap and quadrupole-time-of-flight mass spectrometers. *Journal of Chromatography A,* 1213**,** 83-87.

Volodkin, D. V., Delcea, M., Mohwald, H. & Skirtach, A. G. 2009. Remote Near-IR Light Activation of a Hyaluronic Acid/Poly(L-lysine) Multilayered Film and Film-Entrapped Microcapsules. *Acs Applied Materials & Interfaces,* 1**,** 1705-1710.

Walley, D. R., Buttery, H. J., Norbury, R. J., Schmidt, D. G. & Michael, W. R., inventors; The Procter and Gamble Company and Minnesota Mining & Manufacturing Innovative Properties Company, assignee. Coated perfume particles. USA, patent US 5066419. 1991.

Wang, C. X. & Chen, S. L. 2005. Aromachology and its application in the textile field. *Fibres & Textiles in Eastern Europe,* 13**,** 41-44.

Wang, H. P., Yuan, Y. C., Rong, M. Z. & Zhang, M. Q. 2009. Microencapsulation of styrene with melamine-formaldehyde resin. *Colloid and Polymer Science,* 287**,** 1089-1097.

Wang, L. Y., Gu, Y. H., Zhou, Q. Z., Ma, G. H., Wan, Y. H. & Su, Z. G. 2006. Preparation and characterization of uniform-sized chitosan microspheres containing insulin by membrane emulsification and a two-step solidification process. *Colloids and Surfaces B-Biointerfaces,* 50**,** 126-135.

Wang, L. Y., Ma, G. H. & Su, Z. G. 2005. Preparation of uniform sized chitosan microspheres by membrane emulsification technique and application as a carrier of protein drug. *Journal of Controlled Release,* 106**,** 62-75.

Ward, T., Faivre, M., Abkarian, M. & Stone, H. A. 2005. Microfluidic flow focusing: Drop size and scaling in pressure versus flow-rate-driven pumping. *Electrophoresis,* 26**,** 3716-3724.

Webb, P. A. A Primer on Particle Sizing by Static Laser Light Scattering: Micromeritics Instrument Corp.; 2000 01.2000.

Weckhuysen, B. M. 2004. Ultraviolet-Visible Spectroscopy. *In:* WECKHUYSEN, B. M. (ed.) *In-situ Spectroscopy of Catalysts.* American Scientific Publishers.

Wijmans, J. G. & Baker, R. W. 1995. The Solution-Diffusion Model - a Review. *Journal of Membrane Science,* 107**,** 1-21.

Williams, R. A., Peng, S. J., Wheeler, D. A., Morley, N. C., Taylor, D., Whalley, M. & Houldsworth, D. W. 1998. Controlled production of emulsions using a crossflow membrane part II: Industrial scale manufacture. *Chemical Engineering Research & Design,* 76**,** 902-910.

Wohlfarth, C. 2009. Viscosity of propan-1-ol. *In:* LECHNER, M. D. (ed.) *Supplement to IV/18.* Springer Berlin Heidelberg.

Xie, J. W., Ng, W. J., Lee, L. Y. & Wang, C. H. 2008. Encapsulation of protein drugs in biodegradable microparticles by co-axial electrospray. *Journal of Colloid and Interface Science,* 317**,** 469-476.

Xu, H. X., Fang, Z. P. & Tong, L. F. 2008. Effect of microencapsulated curing agents on the curing behavior for diglycidyl ether of bisphenot a epoxy resin systems. *Journal of Applied Polymer Science,* 107**,** 1661-1669.

Xu, J. H., Luo, G. S., Chen, G. G. & Wang, J. D. 2005. Experimental and theoretical approaches on droplet formation from a micrometer screen hole. *Journal of Membrane Science,* 266**,** 121-131.

Xu, R. 2000. *Particle Characterization: Light Scattering Methods,* Norwell, Kluwer Academic Publishers.

Xu, S., Zhang, X., Xia, S. & Zhang, W. 2006. *Principle and Application of Microencapsulation Technique,* Beijing, Chemical industry Press.

Xue, J. & Zhang, Z. B. 2009. Physical, Structural, and Mechanical Characterization of Calcium-Shellac Microspheres as a Carrier of Carbamide Peroxide. *Journal of Applied Polymer Science,* 113**,** 1619-1625.

Yan, Y., Zhang, Z. B., Stokes, J. R., Zhou, Q. Z., Ma, G. H. & Adams, M. J. 2009. Mechanical characterization of agarose micro-particles with a narrow size distribution. *Powder Technology,* 192**,** 122-130.

Yang, G. H., Tan, Y. S., Han, Y. Z., Qiu, J. S. & Tsubaki, N. 2008. Increasing the shell thickness by controlling the core size of zeolite capsule catalyst: Application in iso-paraffin direct synthesis. *Catalysis Communications,* 9**,** 2520-2524.

Yap, S. F., Adams, M. J., Seville, J. P. K. & Zhang, Z. B. 2008. Single and bulk compression of pharmaceutical excipients: Evaluation of mechanical properties. *Powder Technology,* 185**,** 1-10.

Yepes, M. E. G. & Cremades, L. V. 2011. Characterization of Wood Dust from Furniture by Scanning Electron Microscopy and Energy-dispersive X-ray Analysis. *Industrial Health,* 49**,** 492-500.

Yin, C., Chia, S. M., Quek, C. H., Yu, H. R., Zhuo, R. X., Leong, K. W. & Mao, H. Q. 2003. Microcapsules with improved mechanical stability for hepatocyte culture. *Biomaterials,* 24**,** 1771-1780.

Yuan, L., Liang, G. Z., Xie, J. Q. & He, S. B. 2007. Synthesis and characterization of microencapsulated dicyclopentadiene with melamine-formaldehyde resins. *Colloid and Polymer Science,* 285**,** 781-791.

Yuan, Q. C., Aryanti, N., Gutierrez, G. & Williams, R. A. 2009a. Enhancing the Throughput of Membrane Emulsification Techniques To Manufacture Functional Particles. *Industrial & Engineering Chemistry Research,* 48**,** 8872-8880.

Yuan, Q. C., Aryanti, N., Hou, R. Z. & Williams, R. A. 2009b. Performance of slotted pores in particle manufacture using rotating membrane emulsification. *Particuology,* 7**,** 114-120.

Yuan, Q. C., Cayre, O. J., Fujii, S., Armes, S. P., Williams, R. A. & Biggs, S. 2010a. Responsive Core-Shell Latex Particles as Colloidosome Microcapsule Membranes. *Langmuir,* 26**,** 18408-18414.

Yuan, Q. C., Cayre, O. J., Manga, M., Williams, R. A. & Biggs, S. 2010b. Preparation of particle-stabilized emulsions using membrane emulsification. *Soft Matter,* 6**,** 1580-1588.

Yuan, Q. C., Hou, R. Z., Aryanti, N., Williams, R. A., Biggs, S., Lawson, S., Silgram, H., Sarkar, M. & Birch, R. 2008a. Manufacture of controlled emulsions and particulates using membrane emulsification. *Desalination,* 224**,** 215-220.

Yuan, Q. C., Williams, R. A. & Biggs, S. 2009c. Surfactant selection for accurate size control of microcapsules using membrane emulsification. *Colloids and Surfaces a-Physicochemical and Engineering Aspects,* 347**,** 97-103.

Yuan, Y. C., Rong, M. Z. & Zhang, M. Q. 2008b. Preparation and characterization of poly (melamine-formaldehyde) walled microcapsules containing epoxy. *Acta Polymerica Sinica***,** 472-480.

Zhang, H. Z. & Wang, X. D. 2009. Fabrication and performances of microencapsulated phase change materials based on n-octadecane core and resorcinol-modified melamine-formaldehyde shell. *Colloids and Surfaces a-Physicochemical and Engineering Aspects,* 332**,** 129-138.

Zhang, Y. & Rochefort, D. 2012. Characterisation and applications of microcapsules obtained by interfacial polycondensation. *Journal of Microencapsulation***,** 1-14.

Zhang, Y. J., Lu, Y. B., Guo, F., Peng, C., Li, M. M. & Xu, W. J. 2012. Preparation of microencapsulated ammonium polyphosphate with montmorillonite-melamine formaldehyde resin and its flame retardancy in EVM. *Polymers for Advanced Technologies,* 23**,** 166-170.

Zhang, Y. L., Lian, G. P., Zhu, S. P., Wang, L. Y., Wei, W. & Ma, G. H. 2008. Investigation on the uniformity and stability of sunflower oil/water emulsions prepared by a shirasu porous glass membrane. *Industrial & Engineering Chemistry Research,* 47**,** 6412-6417.

Zhang, Z., Blewett, J. M. & Thomas, C. R. 1999a. Modelling the effect of osmolality on the bursting strength of yeast cells. *Journal of Biotechnology,* 71**,** 17-24.

Zhang, Z., Ferenczi, M. A., Lush, A. C. & Thomas, C. R. 1991. A Novel Micromanipulation Technique for Measuring the Bursting Strength of Single Mammalian-Cells. *Applied Microbiology and Biotechnology,* 36**,** 208-210.

Zhang, Z., Ferenczi, M. A. & Thomas, C. R. 1992. A Micromanipulation Technique with a Theoretical Cell Model for Determining Mechanical-Properties of Single Mammalian-Cells. *Chemical Engineering Science,* 47**,** 1347-1354.

Zhang, Z., Law, D. & Lian, G. 2010. Characterization Methods of Encapsulates. *In:* ZUIDAM, N. J. & NEDOVIC, V. (eds.) *Encapsulation Technologies for Active Food Ingredients and Food Processing.* New York: Springer

Zhang, Z., Saunders, R. & Thomas, C. R. 1999b. Mechanical strength of single microcapsules determined by a novel micromanipulation technique. *Journal of Microencapsulation,* 16**,** 117-124.

Zhang, Z., Stenson, J. D. & Thomas, C. R. 2009a. Chapter 2 Micromanipulation in Mechanical Characterisation of Single Particles. *In:* JINGHAI, L. (ed.) *Advances in Chemical Engineering.* Academic Press.

Zhang, Z., Stenson, J. D. & Thomas, C. R. 2009b. Micromanipulation in Mechanical Characterisation of Single Particles. *In:* LI, J. (ed.) *Advances in Chemical Engineering.* Elsevier Inc.

Zhao, C. X. & Middelberg, A. P. J. 2011. Two-phase microfluidic flows. *Chemical Engineering Science,* 66**,** 1394-1411.

Zhou, Q. Z., Ma, G. H. & Su, Z. G. 2009. Effect of membrane parameters on the size and uniformity in preparing agarose beads by premix membrane emulsification. *Journal of Membrane Science,* 326**,** 694-700.

Zhou, Q. Z., Wang, L. Y., Ma, G. H. & Su, Z. G. 2007. Preparation of uniform-sized agarose beads by microporous membrane emulsification technique. *Journal of Colloid and Interface Science,* 311**,** 118-127.

Zhu, J. & Barrow, D. 2005. Analysis of droplet size during crossflow membrane emulsification using stationary and vibrating micromachined silicon nitride membranes. *Journal of Membrane Science,* 261**,** 136-144.

Zhu, K. Y., Qi, H. Z., Wang, S., Zhou, J. W., Zhao, Y. H., Su, J. F. & Yuan, X. Y. 2012. Preparation and Characterization of Melamine-Formaldehyde Resin Micro- and Nanocapsules Filled with n-Dodecane. *Journal of Macromolecular Science Part B-Physics,* 51**,** 1976-1990.

Zuckerman, J. L., Pushaw, R. J., Perry, B. T. & Wyner, D. M., inventors; Outlast Technologies, Inc., assignee. Frbric coating containing energy absorbing phase chage meterial and method of manufacturing same. USA, patent US 6514362 B1. 2003.

Zuidam, N. J. & Shimoni, E. 2010. Overview of Microencapsulates for Use in Food Products or Processes and Methods to Make Them. *In:* ZUIDAM, N. J. & NEDOVIC, V. (eds.) *Encapsulation Technologies for Active Food Ingredients and Food Processing.* Springer.

Zydowicz, N., Nzimba-Ganyanad, E. & Zydowicz, N. 2002. PMMA microcapsules containing water-soluble dyes obtained by double emulsion/solvent evaporation technique. *Polymer Bulletin,* 47**,** 457-463.